SYNTHESES OF FUNCTIONAL BODIPY MOLECULES FOR MULTIPLE APPLICATIONS

By

NEELAM SHIVRAN

(CHEM01200804026)

Bhabha Atomic Research Centre, Mumbai

A thesis submitted to the
Board of Studies in Chemical Sciences
In partial fulfillment of requirements
For the Degree of

DOCTOR OF PHILOSOPHY
Of
HOMI BHABHA NATIONAL INSTITUTE

September, 2013

Homi Bhabha National Institute

Recommendations of the Viva Voce Board

As members of the Viva Voce Board, we certify that we have read the dissertation prepared by **NEELAM SHIVRAN** entitled **"SYNTHESES OF FUNCTIONAL BODIPY MOLECULES FOR MULTIPLE APPLICATIONS"** and recommend that it may be accepted as fulfilling the dissertation requirement for the Degree of Doctor of Philosophy.

Chairman- Prof. Kamlesh Dasgupta — Date: 10/5/2014

Guide/Convener- Prof. Subrata Chattopadhyay — Date: 10/5/2014

External Examiner- Prof. Dilip Dhavale — Date: 10/5/2014

Co-Guide/Member 1- Prof. Alok K. Ray — Date: 10/5/2014

Member 2- Prof. S. K. Nayak — Date: 10/5/2014

Member 3- Prof. H. Pal — Date: 10/5/2014

Final approval and acceptance of this dissertation is contingent upon the candidate's submission of the final copies of the dissertation to HBNI.

I hereby certify that we have read this dissertation prepared under our direction and recommend that it may be accepted as fulfilling the dissertation requirement.

Date: 10/5/2014

Place: HBNI, Mumbai

Guide: Dr. S. Chattopadhyay

STATEMENT BY AUTHOR

This dissertation has been submitted in partial fulfillment of requirements for an advanced degree at Homi Bhabha National Institute (HBNI) and is deposited in the Library to be made available to borrowers under rules of the HBNI.

Brief quotations from this dissertation are allowable without special permission, provided that accurate acknowledgement of source is made. Requests for permission for extended quotation from or reproduction of this manuscript in whole or in part may be granted by the Competent Authority of HBNI when in his or her judgment the proposed use of the material is in the interests of scholarship. In all other instances, however, permission must be obtained from the author.

Neelam Shivran

DECLARATION

I, hereby declare that the investigation presented in the thesis has been carried out by me. The work is original and has not been submitted earlier as a whole or in part for a degree/ diploma at this or any other Institution / University.

Neelam Shivran

Dedicated to…

…my beloved parents

ACKNOWLEGEMENT

I would like to express my sincere appreciation to my doctoral supervisor **Dr. S. Chattopadhyay, Head, Bio-Organic Division (BOD), BARC, Mumbai**, for his encouragement, patience, valuable guidance and never-ending support during entire span of this research. His extensive knowledge of the subject, vision, and creative thinking has been the source of motivation for me throughout this work. His individual characteristics like dedication, determination and selfless hard work have helped me to improve myself as a better human being. His encouraging words and motivating thoughts will be a source of inspiration for me for the rest of my life.

I am grateful to **Dr. Alok Ray**, co-guide for his guidance, valuable suggestions and help in doing the laser experiments. I would also like to extend my gratitude to all my doctoral committee members **Dr. K. Dasgupta**, **Dr. T. Mukherjee, Dr. S.K. Nayak** and **Dr. H. Pal** for reviewing my project and suggestions.

I am especially indebted to **Dr. S. Mula** for his cheerful co-operation and support in the lab. Many detailed and in-depth discussions with him have invaluably shaped the course of this work. I gratefully acknowledge the help and support provided by **Dr. (Mrs) Anubha Sharma, Dr. S. K. Ghosh and Dr. A. Chattopadhyay** throughout the period of my research work.

I am thankful to **Dr. T. K. Ghanty, Dr. C. Majumder, Dr. D. K. Maity** for their help in doing the theoretical calculations. I am sincerely thankful to **Dr. S. P. Koiry** and **Dr. D. K. Aswal** for learning experimental set ups of electronics and understanding the concept of electronics, **Dr. V. Sudarshan** for helping me in AFM studies, **Dr. K. Bhushan** for his help in SIMS analysis. I am grateful to **Dr. Debarati** and **Dr. S. Basu** for their kind help in doing XRR experiments and analysis. Special thanks to **Mrityunjay Tyagi** for carrying out biological experiments.

I must thank all the members of the BOD family (**Bioorganic Division**), including the staffs and students for their support and good wishes. I thank **Dr. A. K. Bauri, Mrs. Abha N. Kumar, Mrs. Kshama Roy Kundu, Mr. Mrunesh Koli, Mr. Manoj Choudhary** and **Ms. Monika** for their cooperation, unconditional help and wholehearted support in the lab. The friendship, enlightening discussions, and the overall good spirit have made my stay at this place pleasant and enjoyable.

Speaking of friendships, I am forever grateful to my close friends **Dr. Rohit Singh Chauhan, Dr. Prerana Gupt, Parashiva Prabhu, Rakesh Kumar Sharma, Suman Bakshi, Meenakshi K. and Abha** for their moral support, motivation and being a part of my life. Thank you for your precious friendship, constructive criticism, inspiring advice and positive viewpoint that played a crucial role in shaping my life during these past five years. Thank you so much for laughing with me, sharing my pains and caring for me.

Finally I convey my heartfelt gratitude to my family. The phrase "Thank you" can never capture the gratitude I want to express to my **Mumma** and **Papa** who always supported me to pursue my dreams, stood by me during all ups and downs of my life and took the pain of separation. Their faith in me, encouragement and good wishes made me to achieve this goal of my life. I thank my **Mamaji** and **grandparents** specially **Nanaji** (*whom I lost during this journey*) for their long waited patience and blessings.

I know I am the luckiest person on earth and feel extremely blessed to have my dearly loved siblings **Komal, Poonam, Rajesh, Aditya** and **Diksha**. I thank them for their love, support, encouragement and patience. Specially, I am thankful to my adorable little sister **Diksha** who always have been a source of energy, happiness and love. She made me feel so at home with her liveliness and chirpy voice over the phone during these years.

Last but not least I thank Almighty for adding this beautiful chapter to my life. It's been an incredible journey and I am so grateful to all the amazing people that have helped me along the way.

…Neelam Shivran

CONTENTS

Chapter-2: Rational Design and Synthesis of Some Photstable Bodipy Laser Dyes

Chapter-3: Meso-Functionalization of Bodipy Molecules

Chapter-4: Development of Water-Soluble Bodipys for Biological Applications

Chapter-5: Formulation of Bodipy-Si-Based Molecular Electronics Devices

LIST OF FIGURES

LIST OF SCHEMES

LIST OF TABLES

List of Abbreviation

Å	Angstrom(s)
Ar	Aryl
BODIPY	Borondipyrromethene, 4,4-difluoro-4-bora-3a,4a-diaza-*s*-indacene
δ	Chemical shift
DABCO	1,4-Diazabicyclo[2.2.2]octane
DCM	Dichloromethane
DDQ	2,3-Dichloro-5,6-Dicyano-1,4-benzoquinone
DMEM	Dulbecco's Modified Eagle Medium
DMSO	Dimethylsulfoxide $(CH_3)_2SO$
DSSC	Dye-sensitized solar cell
Et	Ethyl
EtOAc	Ethyl acetate
EtOH	Ethanol
eq	equivalents
g	gram(s)
HOMO	Highest occupied molecular orbital
HPLC	High Performance Liquid Chromatography
Hz	Hertz
J	Coupling constant (in NMR spectroscopy)
LUMO	Lowest unoccupied molecular orbital
MeOH	Methanol
NDR	Negative Differential Resistance
NIR	Near-infrared

NMR	Nuclear Magnetic Resonance
PBS	Phosphate buffered saline
PDT	Photodynamic therapy
PEG	Polyethylene glycol
PM	Pyrromethene
ppm	Parts per million
SIMS	Secondary ion mass spectrometry
^{t}Bu	*tert*-Butyl
TBAP	Tertrabutylammoniumperchlorate
TFA	Trifluoroacetic acid
THF	Tetrahydrofuran
TMS	Trimethylsilyl
XRR	X-ray reflectometry

SYNOPSIS

Despite existing for almost a century, fluorescent dyes continue to attract the attention of scientists from an ever flourishing multidisciplinary arena. Recent developments in the field of personal diagnostics and in the area of organic electroluminescent devices have boosted interest in the development of next-generation emissive dyes. Countless classes of highly fluorescent organic compounds are now known, but the difluoro-boraindacene family (4,4-difluoro-4-borata-3a-azonia-4a-aza-s-indacene, abbreviated hereafter as Bodipy) has gained recognition as one of the more versatile fluorophores. Earlier, the potential use of these dyes as biological labels was recognized[1] and several new Bodipy dyes were designed, and these dyes were recognized as photostable substitutes for fluorescein. The use of Bodipy as an effective biological label has been complemented by its known propensity to function as a tunable laser dye.[2] In parallel, more fundamental studies on the chemical reactivity and the photophysical properties of the new dyes emerged.

The Bodipy derivatives are strongly UV-absorbing small molecules with outstanding photophysical characteristics when compared with classical fluorophores, such as fluorescein and rhodamines dyes, and show fluorescence emissions in the visible region. These are neutral compounds with intense absorption and emission profiles (λ_{max} between 500-545 nm), high molar absorption coefficients (~40,000 to 80,000 M^{-1} cm^{-1}), high fluorescence quantum yields (normally $\Phi_f > 0.60$), reasonably long fluorescence lifetimes (τ in the nanosecond range) and relatively small Stokes' shift (~10 nm). In the BODIPY-based dyes phosphorescence is a rare phenomenon, due to negligible triplet energy state and a slow rate of intersystem crossing (ISC), except for a diiodo Bodipy which showed high ISC rate due to the heavy-atom effect.[3] In addition, Bodipy dyes have excellent thermal stability both in

solution and solid states, good solubility in most organic solvents, resistance towards self-aggregation in solution, and insensitivity to changes in pH and solvent polarity.

The stability of Bodipy core is partially due to the first row elements (B, N, and F) which allow efficient orbital overlap to promote delocalisation of the π-system. Slightly polarized heteroatoms generate various electron-rich and electron-deficient reaction sites at different positions on the internally zwitterionic Bodipy framework that favour both nucleophilic and electrophilic substitution reactions on the Bodipy core. The absorption bands of Bodipy dyes can be further shifted to the red or NIR region by facile derivatization of the Bodipy core. The photophysical characteristics of synthetically modified Bodipys vary with respect to the number, nature, as well as the position of the attached substituents.[4] Additionally, the emission behaviour of Bodipy fluorophores are greatly affected by the steric interactions between their components and intramolecular rotations of their chromophoric units.[5]

Given the importance of the Bodipy molecules, the present work was aimed at (i) formulation of some photo-stable Bodipy laser dyes, (ii) development of red Bodipy dyes, preferably with good water solubility for their biological applications, (iii) development of new Bodipy chemistry for regioselective functionalization, and (iv) exploration of their redox property for molecular electronics applications. The content of the thesis is presented in five chapters, which are briefly summarized in the following.

Chapter 1: Introduction to Bodipy Compounds

This chapter deals with the chemical structures and nomenclature of the Bodipy core, their general photophysical attributes, as well as their importance in advanced technology and various applications. This is followed by a discussion on the reported synthetic methods of the Bodipy core. Next, this chemistry of Bodipy *e. g.* electrophilic substitution and condensation reactions at different positions, used for structural modifications is presented.

Finally, the major inherent limitations such as small Stokes' shifts and photochemical instability of the Bodipy dyes are mechanistically analysed to highlight the objectives and importance of the present work.

Chapter 2: Rational Design and Synthesis of Some Photo-stable Bodipy Laser Dyes

The photochemical instability of the Bodipy dyes is due the generation of singlet oxygen during their excitation, which reacts at the *meso*-olefinic group, inducing dye degradation.[6a,b] Presently, two different approaches *viz*. substitution of the F atoms at the B-centre with alkyl groups as such, and in combination with incorporation of a bulky group at the *meso*-position were adopted to improve the photo-stability. Earlier, presence of an electron-rich *meso*-aryl group was found to improve the photo-stability without compromising the lasing efficiency of the dyes.[7]

To this end, the alkyne diethylene glycol derivative **1** was synthesized by a base-catalyzed alkylation of the glycol with propargyl bromide. This on conversion to the corresponding Grignard reagent, followed by reaction with the commercially available PM567 dye **2a** afforded the new dye **3a**. In another case, the known Bodipy compound **2b**, synthesized as reported earlier,[7] was coupled with the Grignard reagent of **1** to obtain the new dye **3b** (**Scheme 1.**).

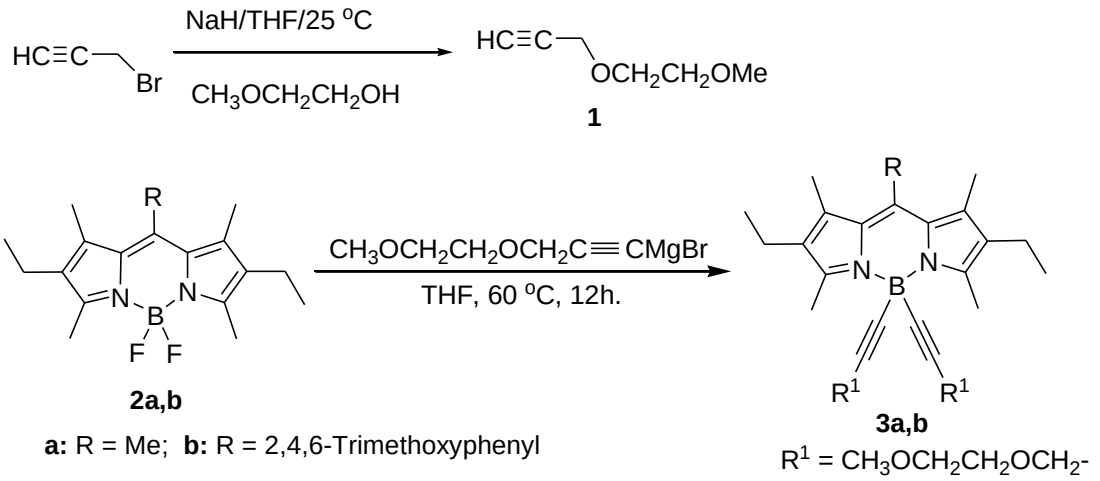

Scheme 1.

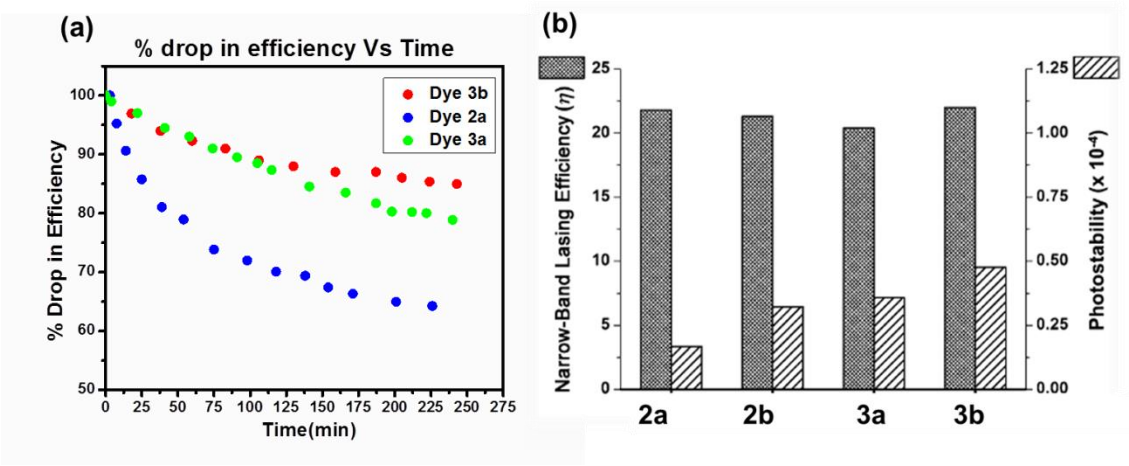

Fig. 1. (a) Normalised decay profiles of the lasing efficiencies of the Bodipy dyes **2a**, **3a** and **3b** as a function of irradiation time. **(b)** Narrow band lasing efficiencies (η) and photostabilities (Φ_f) of the Bodipy dyes in ethanol.

Examination of the photo-physical and lasing properties, as well as photochemical stabilities (**Fig. 1.**) revealed improved photostability of the dyes **3a** and **3b**, compared to their precursors. The lasing performance of the dye **3b** was also excellent, although a higher concentration was required for the optimum output. The photostability and lasing results were rationalised by analysing their redox potentials (cyclic voltammetry), and triplet state life times and absorption spectra (pulse radiolysis) as well as quantum chemical calculations.

Chapter 3: *Meso*-Functionalization of Bodipy Molecules

Functionalization of the Bodipy core is an important synthetic goal as it helps in tuning their light- and electron transfer-induced processes, improving hydrophilicity, and anchoring to various mattrices for wider applications.[8a,b] Most of the previous research, directed to this end were targeted to functionalization of the pyrrole moieties of the Bodipy core. This results in undesirable changes in the photo-physical properties and restrict the targeted applications.[9] Instead, *meso*-functionalization of the Bodipy moiety with alkyl/arylalkyl moiety would provide new Bodipy-based functional molecules without perturbing the photo-electronic properties. Direct synthesis of these types of Bodipy molecules *via* the condensation of substituted pyrroles with aliphatic aldehydes/acid chlorides

has inherent limitations due to the instability of the required acid chlorides, and non-reactivity of the aldehydes.

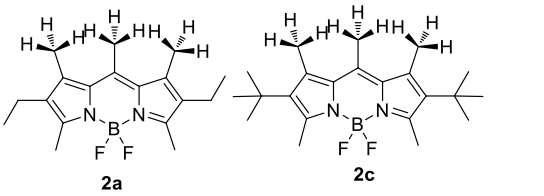

Fig. 2.

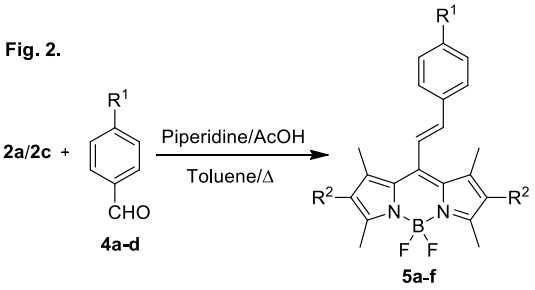

Scheme 2.

Table 1:

Bodipy	Aldehyde, R^1	Product, R^1, R^2	% yield[a]
2a	**4a**, OMe	**5d**, OMe, Et	10[b]
2a	**4c**, NO_2	**5e**, NO_2, Et	55
2a	**4d**, Br	**5f**, Br, Et	61
2c	**4a**, OMe	**5a**, OMe, *t*-Bu	65
2c	**4b**, OH	**5b**, OH, *t*-Bu	50
2c	**4c**, NO_2	**5c**, NO_2, *t*-Bu	67

[a]based on isolation; [b]13% 3-styryl analogue was also isolated.

Given that the Bodipy molecules with a *meso*-alkyl group is highly twisted due to spatial crowding of the C-1/ C-7 hydrogen atoms and the *meso*-alkyl group (**Fig. 2.**), it was envisaged that a Knoevenagel-type condensation of the Bodipy molecules at the *meso*-alkyl (Me) group would alleviate such an unfavourable steric interaction. Costela *et al*. showed that the *meso*-H analogue of **2c** is planner.[10a,b] Thus, the release of steric strain may drive the condensation selectively at the *meso*-position, overriding the least acidity of the *meso*-methyl protons. Using such a strategy, a novel method of selective *meso*-functionalization of the Bodipy dyes **2a** and **2c** using readily available and inexpensive reagents was developed (**Scheme 2** and **Table 1**). The steric strain release hypothesis was proved from the single crystal X-ray data that showed reduced torsional angle and increased dihedral angle on introduction of a *meso*-styryl moiety in the dyes **2a** and **2c**. Identification of the isolated intermediate of the Knoevenagel condensation also established the reaction mechanism.

Chapter 4: Development of Water-soluble Bodipys for Biological Applications

As a bright fluorophore, Bodipys are well suited for biological analysis,[11] and other biomedical applications including imaging and photo-dynamic therapy (PDT).[12,13a-c] Their electrical neutrality would avoid potential nonspecific binding through electrostatic

interactions between the dye and the targeted molecule.[14] However, this requires the Bodipys to be water soluble, and absorb in the red or NIR region. Because carbohydrates are known ligands of various cell surface lectins,[15] a carbohydrate-attached Bodipy with red fluorescence appeared attractive for biological applications particularly for PDT.

Towards these objectives, two strategies were adopted. In one approach, the Bodipy molecule **6**, containing a meso-phenol group was synthesized by standard reactions. Its acid catalyzed reaction with glucose pentaacetate furnished the intermediate **7**, which on alkaline hydrolysis afforded the dye **8**. For the synthesis of the Bodipy molecule **11** with red fluorescence, the known dye **2a** was subjected to classical Knoevenagel condensation with the aldehyde **4b**, and the resultant styryl-Bodipy compound **9** was glycosylated as above (**Scheme 3**.).

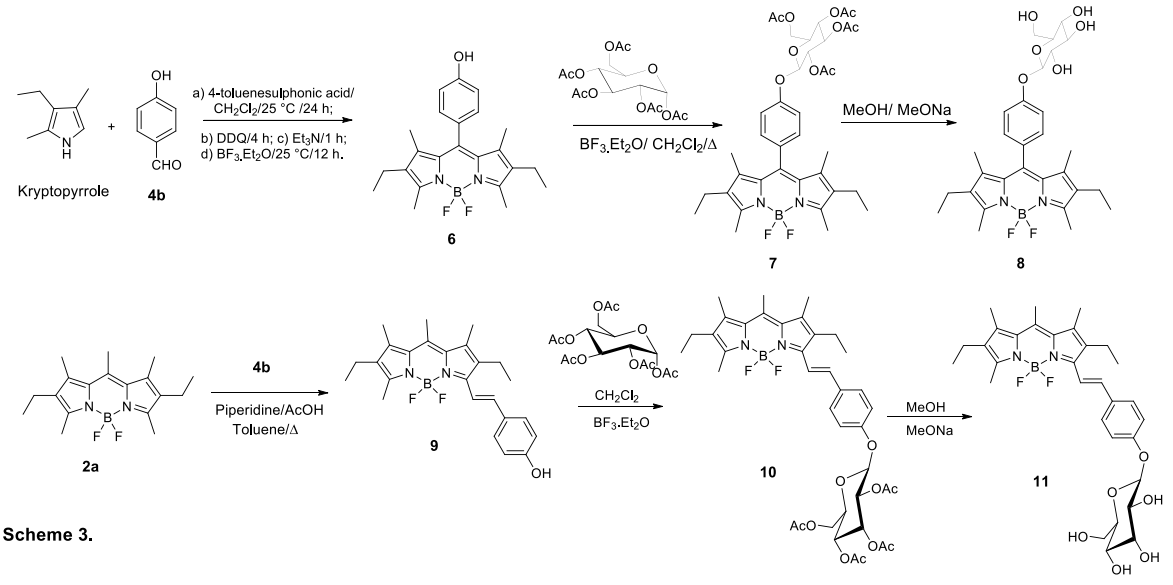

Scheme 3.

The compounds **8** and **11** showed groove binding with calf-thymus DNA through ionic interactions as revealed from the binding constants 1.2×10^4 M^{-1} and 8.3×10^4 M^{-1} respectively. Both the compounds showed toxicity to the human lung cancer A549 cells, compound **11** being more potent (IC_{50} = ~30 μM). The potency could be augmented

significantly in presence of light. The better cytotoxicity of **11** was attributed to its ability to cross cell surface and accumulate in the cytoplasm, while **8** was located on the cell surface as evident by fluorescence microscopy.

Chapter 5: Formulation of Bodipy-Si-based Molecular Electronics Devices

While the Bodipy compounds are appraised for opto-electronic applications, the tunable reversible redox properties are also promising for application in molecular electronics, but remains unprecedented.[16] The prototype σ–π systems grafted on Si wafers through an alkyl spacer (σ) are known to show current rectification behavior.[17] On the other hand, the negative differential resistance (NDR) characteristic *i.e.* decreasing current with increasing voltage in a particular voltage range with high peak to valley ratio (PVR) along with hysteresis is important because of its potential application in the realization of logic devices and memory circuits. [16,18] Molecules having redox properties and bias-induced conformational changes are potential candidates for NDR effect with hysteresis. However, molecules, chemically bonded to Si surface would be too rigid. Instead, the required conformational changes can be easily achieved by forming a bi-layer on it by physical interaction with another redox molecule.[17]

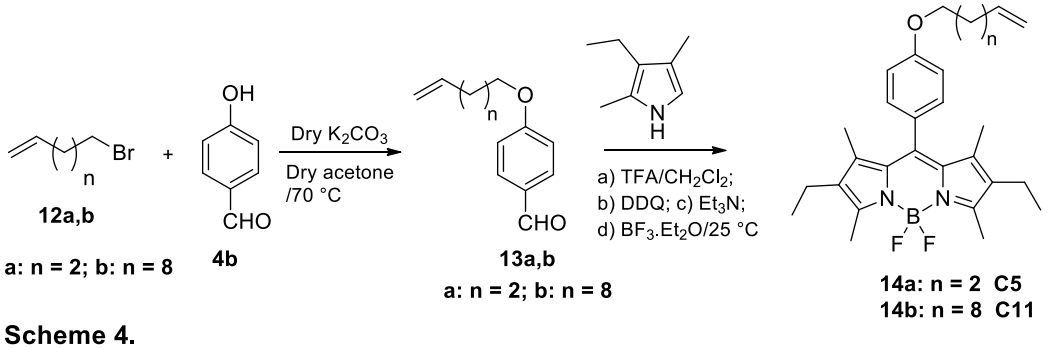

Scheme 4.

To explore these possibilities, the Bodipy compounds **14a/b** were synthesized as the required σ (alkyl)–π (Bodipy) systems (**Scheme 4.**). For this, the phenol **4b** was *O*-alkylated with bromides **12a/b** in the presence of a base, and the resultant compounds **13a/b** were coupled with kryptopyrrole following a standard route. Taking advantage of the terminal

alkene groups of **14a/b**, the molecules were electro-grafted on Si wafers to obtain the monolayered Si-organic hybrids. These were used to fabricate the metal/molecule/Si (n++) devices where a tiny Hg drop served as the counter electrode. The devices made of **14a** and **14b** showed current rectification at 1.5 V with rectification ratios ($| J_{-1.5V} | / J_{1.5V}$) of 37 and 500 respectively. Next, the bilayers were constructed by dipping the above mono-layered Si wafers into a CH_2Cl_2 solution of the planar Bodipy molecule **2a**. The devices constructed (**Fig. 3.**) using the bilayers showed NDR property with the PVR values ranging between 10 and 1000 (**Fig. 4.**), and the NDR effect can be repeated by short-circuiting the electrodes to the neutral state.

The mono and bilayers were characterized by electrochemical characterization, contact angle measurements, ellipsometry, secondary ion mass-spectrometry (SIMS), X-ray reflectivity (XRR) and atomic force microscopy (AFM). Each mono- and bi-layers exhibited granular surface morphology with an average grain size of 8 and 14 nm, respectively. The thicknesses (ellipsometery) of the mono- and bilayers were 1.3±0.2 and 2.1±0.2 nm for **14a**, and 2.2±0.2 and 3.1±0.2 nm respectively for **14b**. These data corroborated with the XRR-derived values, and correlated with the SIMS depth profiles of the bilayers.

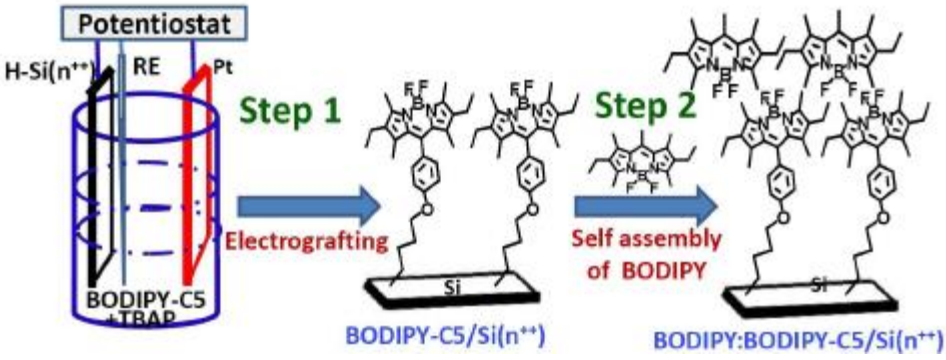

Fig. 3. Schematic showing two step formation process of the bilayers with the Bodipy dyes **14a**/**b**. In Step 1 monolayers of **14a**/**b** were electrografted to H-Si(n++), and in Step 2, dye **2a** was deposited on the monolayers by weak interactions to form **2a**:**14a** or **14b**/Si(n++).

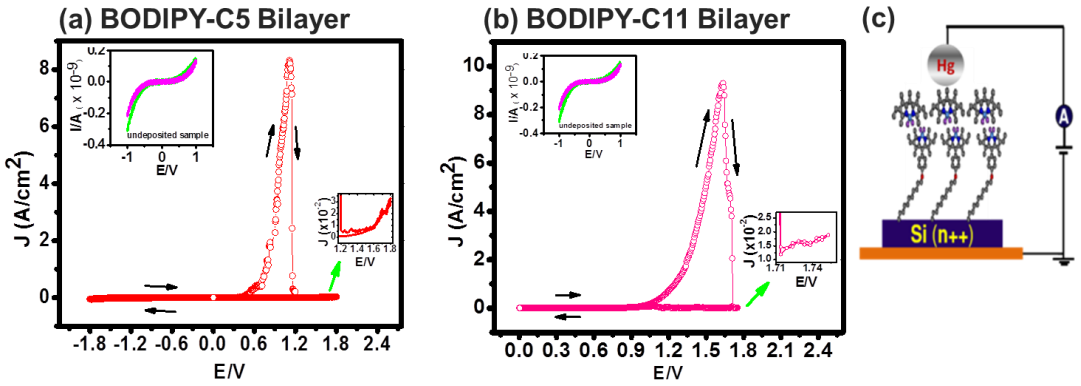

Fig. 4. Room temperature *J-V* characteristic recorded for the Bodipy bilayers by scanning the bias in the sequence -1.8 V → 0 V → +1.8 V→ 0 V → -1.8 V at a scan speed of 5 mV/s. (a) **2a**:**14a**/Si(n++), (b) **2a**:**14b**/Si(n++), (c) Schematic of the structures employed for the measurements.

Summary

The ever-growing importance of the Bodipy dyes has motivated a large amount of research into the design, synthetic modifications, and spectroscopic/photophysical characterization of these bright small fluorophores. In the present work, new Bodipy chemistry was developed to generate several new Bodipy molecules with altered photophysical and photochemical properties. These molecules were subsequently used as novel functional materials as photo-stable laser dyes, anti-cancer PDT agents, and nano-rectifiers/ memory devices.

CHAPTER-1

INTRODUCTION TO BODIPY COMPOUNDS

Chapter 1: Table of Contents

1.1. Preamble

Despite existing for almost a century, fluorescent dyes continue to attract the attention of scientists from an ever flourishing multidisciplinary arena. Recent developments in the field of personal diagnostics and in the area of organic electroluminescent devices have boosted interest in the development of next-generation emissive dyes. Countless classes of highly fluorescent organic compounds are now known, but the difluoro-boraindacene family (4,4-difluoro-4-borata-3a-azonia-4a-aza-s-indacene, abbreviated as Bodipy) has gained recognition as one of the more versatile fluorophores. Since the potential use of these dyes as biological labels was recognized,[1,2] several new Bodipy dyes were designed and synthesized. Subsequently these dyes are considered as photostable substitutes of fluorescein. The use of Bodipy as effective biological labels has been complemented by their known propensity to function as tunable laser dyes.[3] In parallel, more fundamental studies on the chemical reactivity and the photophysical properties of the new dyes emerged. Increasing versatile use of the Bodipys as organic photo-voltaic materials, and in emerging nanotechnological applications make the future extremely bright for the "porphyrin's little sisters".

1.2. Chemical Structures of Bodipy Dyes

The Bodipy framework consists of a dipyrromethene (PM) ligand complexed with a disubstituted boron atom, generally a BF_2 moiety. The PM ligand is formed by joining of two pyrrole units via an interpyrrolic methine bridge. Due to the complexation with BF_2, the Bodipy fluorophore can be considered as an example of a "rigidified" monomethine cyanine dye (**Figure 1.2.1**) with fixed planarity of the chromophoric π-electron system.[4] The rigidity, introduced by the boron complexation further prevents the *cis-trans* isomerization and interpyrrolic methine chain-twisting, eventually leading to unusual high fluorescence yields from the

dipyrromethene boron framework, comparated to the flexible cyanine dyes. Conjugation of the π-electrons runs along the organic backbone, and can be extended further by attachment of suitable groups onto the periphery or to one or both the pyrrole fragments. The IUPAC numbering system for the Bodipy dyes (**Figure 1.2.1**) is different to that used for dipyrromethenes.[5] However, the terms *α*-, *β*-, and *meso*-positions are used in just the same way for both systems.

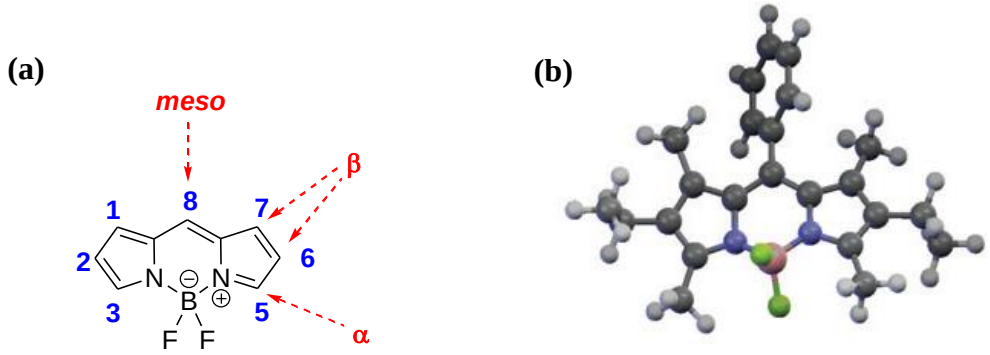

Figure 1.2.1 (a) Chemical structure of the Bodipy core; (b) Molecular model of a representative Bodipy derivative functionalized on the Bodipy backbone and *meso* position.

The Bodipy derivatives are strongly UV-absorbing small neutral molecules with outstanding photophysical characteristics when compared to the classical fluorophores, such as fluorescein and rhodamines dyes, and show fluorescence emissions in the visible region. They have intense, nearly superimposable absorption and emission profiles (λ_{max} between 500-545 nm), large molar absorption coefficients (~40,000 to 80,000 M^{-1} cm^{-1}), high fluorescence quantum yields (Φ_f normally > 0.60), reasonably long fluorescence lifetimes (τ in ~ 1 to 10 ns range) and relatively small Stokes' shift (~10 nm). The absorption spectra, recorded in solution or plastic films exhibit intense transitions that correspond to the $S_0 \rightarrow S_1$ process, together with clear vibrational fine structures, and a more modest set of transitions owing to the $S_0 \rightarrow S_2$ process. Both transitions usually show vibrational fine structures ranging from 1200 to 1400 cm^{-1}, typical of the molecular C=C framework of the Bodipy core. Owing to the strong

absorption transitions, the radiative rate constants of the Bodipys are usually quite high (*ca*. 10^8 s^{-1}). Phosphorescence is generally a rare phenomenon with these dyes, due to negligible triplet energy state and a slow rate of intersystem crossing (ISC), except for some diiodo Bodipys where ISC is promoted due to the heavy-atom effect.[6] In addition, a Bodipy with ancillary Ru(II)-polypyridine complex showed triplet emission.[7] The Bodipy dyes have excellent thermal stability both in solution and in solid states, good solubility in many organic solvents; are resistant towards self-aggregation in polar solvents, and insensitive to changes in pH and solvent polarity.

The stability of Bodipy core is partially due to the first row elements (B, N, and F), which allow efficient orbital overlap to promote delocalisation of the π-system. Slightly polarized heteroatoms generate various electron-rich and electron-deficient reaction sites at different positions on the internally zwitterionic Bodipy framework that favour both nucleophilic and electrophilic substitution reactions on the Bodipy core, and have been used for their functionalization (*vide infra*).

1.3. Synthetic Methodologies of Bodipys

Several methods for the synthesis of Bodipy have been developed since their accidental discovery in 1968 by Treibs and Kreuzer by reaction of 2,4-dimethylpyrrole with acetic anhydride in the presence of $BF_3.OEt_2$.[8] The basic route of constructing the Bodipy core generally involves an acid-catalyzed condensation of two molecules of a 2-substituted pyrrole with an electrophilic carbonyl compound, *e. g*. aldehyde, acid anhydride, and acyl chloride, followed by oxidation and complexation with $BF_3.OEt_2$. However, the oxidation step is not required when an acyl chloride is used as the electrophile. The synthyses using (i) pyrroles and

acid chlorides/ anhydrides or aldehydes, and (iii) from ketopyrroles are adequately discussed in an excellent review, and brifley described below.[1]

1.3.1. *Condensation of pyrroles with acid chlorides or anhydrides*

In general, synthesis of the 8-substituted Bodipy dyes (*i. e.*, those with substituents in the *meso* position) is relatively easy, and is accomplished via condensation of aromatic and aliphatic acyl chlorides with suitable pyrroles (**Scheme 1.3.1**).[2e,3d,9a] These conversions involve formation of unstable dipyrromethene hydrochloride salt intermediates. Although, the intermediate salts are easier to handle and purify as the C-substitution increases, these are not generally isolated during the syntheses of the Bodipy dyes. In the particular case where the intermediate salt was isolated and purified by flash chromatography, the intermediate was treated with Et_3N in toluene before adding $BF_3.OEt_2$.[9b]

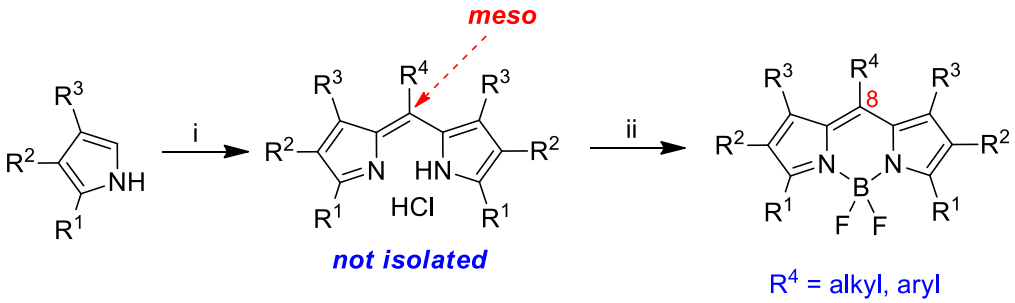

Scheme 1.3.1 Reagents and conditions: (i) (a) R^4COCl/CH_2Cl_2/40 °C/1 h; (ii) (a) Et_3N or $^iPr_2EtN$/toluene/25 °C/15 min; (b) $BF_3{\cdot}OEt_2$/80 °C/15 min.

Besides acid chlorides, other activated carboxylic acid derivatives can also be used in this strategy. In particular, use of acid anhydrides produces a free carboxylic acid that may be used later to attach the probes to obtain various target molecules. One such approach using glutaric anhydride as the condensing agent helped in subsequent attachment of cholesterol to construct model florescent-labeled membranes (**Scheme 1.3.2**).[9a]

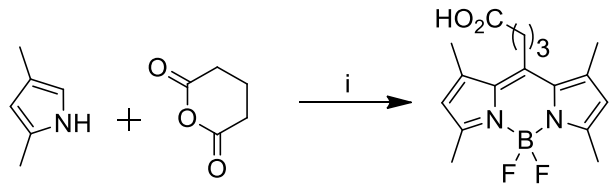

Scheme 1.3.2 Reagents and conditions: (i) (a) $BF_3{\cdot}OEt_2$/reflux/5 h; (b) $BF_3{\cdot}OEt_2/Et_3N$/25 ^oC/12 h.

1.3.2. *Condensation of pyrroles with aldehydes*

This method, involving condensation of aromatic aldehydes with pyrroles requires an additional oxidation step to form the dipyrromethene intermediates (**Scheme 1.3.3**).[2e] Generally DDQ and *p*-chloranil are used for the oxidation. However, the oxidizing reagents can introduce experimental complications, needing removal of the undesired byproducts. Also, use of aliphatic aldehydes has not been reported so far in this approach.

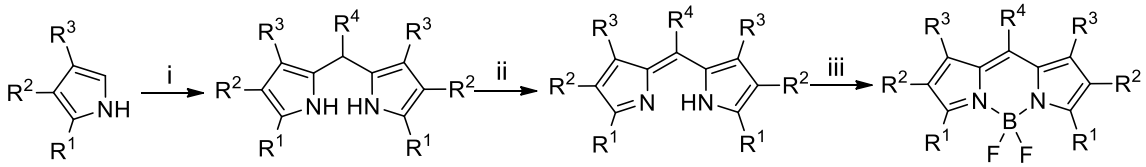

Scheme 1.3.3 Reagents and conditions: (i) R^4CHO/H^+; (ii) oxidation; (iii) base/ $BF_3{\cdot}OEt_2$.

1.3.3. *From ketopyrroles*

The previous two synthetic strategies are extensively used to construct symmetrically substituted Bodipy dyes only. A slight modification of the method wherein a carbonyl-containing pyrrole is condensed with a C2-unsubstituted pyrrole molecule is useful in the syntheses of unsymmetrical Bodipy dyes,[10] and has been used to prepare several Bodipy-based biological labels (**Scheme 1.3.4**).[2a,b] An active carboxylate group can be introduced at the 8-position by following a similar procedure. This route is useful for the preparation of reasonably large batches of dyestuffs, although it tends to be expensive in terms of solvent wastage. In general, these materials separate well on a chromatography column and can be purified to a high degree by

recrystallization. The main advantage of this method is its application to incorporate diverse substituents on the pyrrole rings.

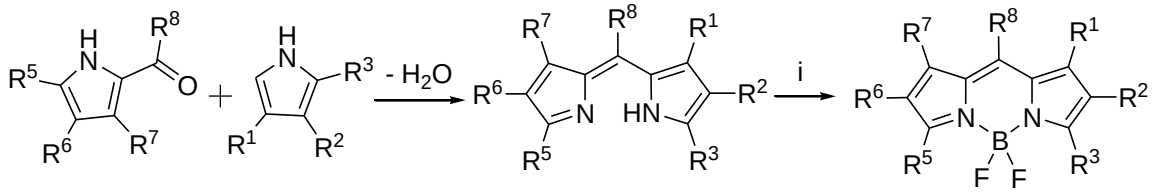

Scheme 1.3.4 Reagents and conditions: (i) base/ $BF_3{\cdot}OEt_2$.

1.4. Derivatization of the Bodipy Framework

Usually the Bodipy dyes have certain problems, such as small Stokes' shifts, poor solubility in aqueous media, and lack of functional groups for conjugation to biological materials.[11] These restrict complete utilization of the Bodipy fluorophores for various biomedical and bioanalytical applications, and warrants efficient synthetic strategies for functionalization of the Bodipy core. To this end, the intrinsic electron-rich character of the Bodipy chromophore has been conveniently used for its derivatization at various positions to synthesize a range of new compounds covering the entire visible spectrum and beyond. In particular, the optoelectronic properties of the Bodipy molecules can be fine-tuned by functionalization of the core framework at the 8- (*meso*-), 2,6- and 3,5- positions, the B-center, as well as by rigidification of the Bodipy core. Some of these are demonstrated during the present investigation, as illustrated in the subsequent chapters.

1.4.1. *Functionalization at the meso- or 8-position*

Compared to the substitutions at the pyrrolic positions, the C-8 (*meso*)-functionalization is usually accomplished by direct acid-catalyzed condensation of suitable pyrroles with appropriately substituted aryl aldehydes or acyl chlorides.[12] The *meso*-substitution does not change the spectral characteristics of the parent dye significantly due to the orthogonal geometry

of the *meso* substituent and the Bodipy fluorophore, which results in poor electronic conjugation between the two moieties. Hence this strategy offers the most versatile method for introducing various "functionalities" on the Bodipy core for specific application such as selective sensors of redox active molecules,[13,14] metal-chelators,[15] and pH probes,[16] light-harvesting arrays and biological labels[17] (**Figure 1.4.1**).

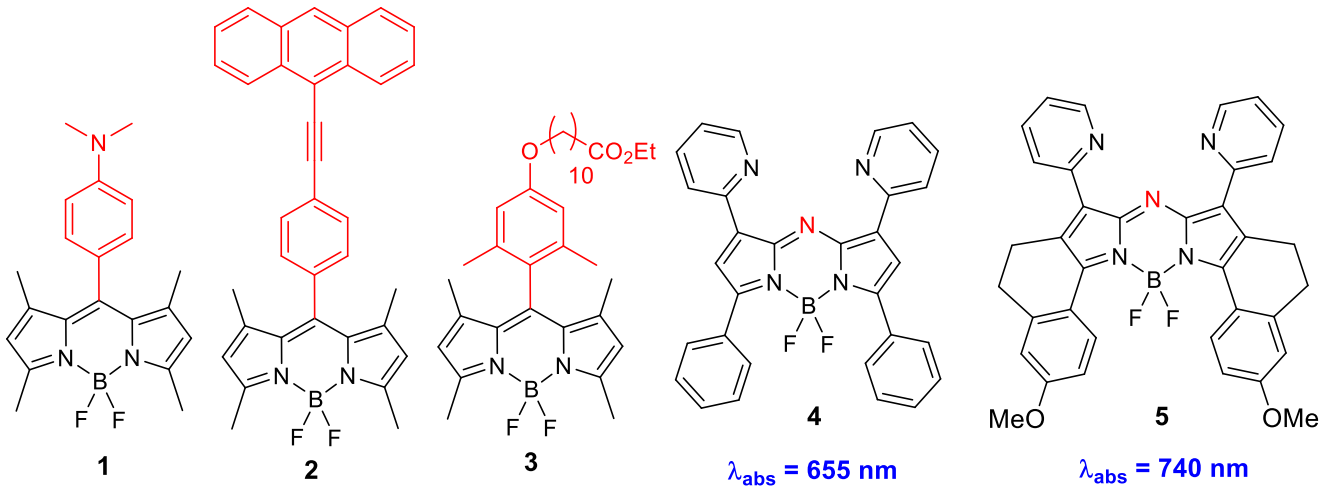

Figure 1.4.1 Chemical structures of some *meso*-substituted Bodipys.

A sub-class of the Bodipy dyes commonly known as ˝aza-Bodipys˝ possesses a nitrogen atom at the *meso*-site in place of the carbon atom.[18] These dyes exhibit intense absorption and emission profiles in the 650-850 range with high molar extinction coefficient, but moderate fluorescence quantum yields (0.23-0.36), and are insensitive to the solvent polarity. The lone pair of electrons on the *meso*-nitrogen reduce the HOMO-LUMO energy gap, resulting in red shifts in their absorption and emission maxima.[19] Although the aza-Bodipy dyes are mostly important as photodynamic therapy (PDT) agents, several chemosensors have also been made using these compounds. For example, compound **4** show high selectivity in sensing Hg^{2+} ions.[20] The spectra of these dyes can be easily pushed to the near-IR region by rigidifying the structure, or incorporation of electron-donating groups as shown with compound **10**.

1.4.2. *Functionalization at the 2,6-positions*

The 2 and/or 6-positions of the Bodipy core are most susceptible to electrophilic attack since they bear the least positive charge. However, electrophilic substitution reactions at the designated positions of the Bodipys are limited only to sulfonation,[21] halogenation,[6] nitration,[22] and formylation[14] (**Figure 1.4.2**). Introduction of the sulfonate groups impart water-solubility to the hydrophobic Bodipy core without affecting the absorption and emission maxima significantly, while the introduction of electron withdrawing groups like nitro or halo groups drastically decrease the fluorescence quantum yields with respect to the parent dyes. The reduced fluorescence quantum yields of the bromo and iodo substituted Bodipy is attributed to the internal heavy-atom effect.[6] Recently, the 2,6-diiodo Bodipys have been exploited to generate a myriad of diphenylethynyl-Bodipy oligomers as potential building blocks in the construction of several light-emitting conjugated polymers and functional supramolecular assemblies.[23] It should be noted that this approach leaves the B-F bonds unscathed; the substitution reactions occur exclusively at the 2,6-positions, and is therefore a valuable route for selective substitution.

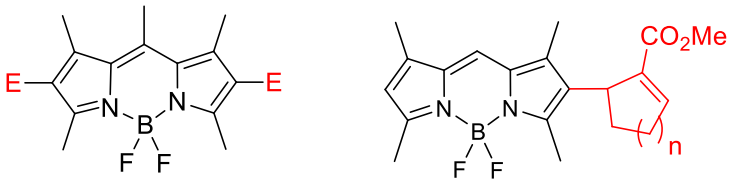

6 E = Br; **7** E = I; **8** E = SO_3H **9**

Figure 1.4.2 Chemical structures of some 2- and/or 6-substituted Bodipys.

1.4.3. *Functionalization at the 3,5-positions*

The higher acidity of the methyl groups at the 3,5-positions of the Bodipys is utilized for functionalization by a base-catalyzed Knoevenagel-type condensations to generate a styryl group.[2a,b,24]

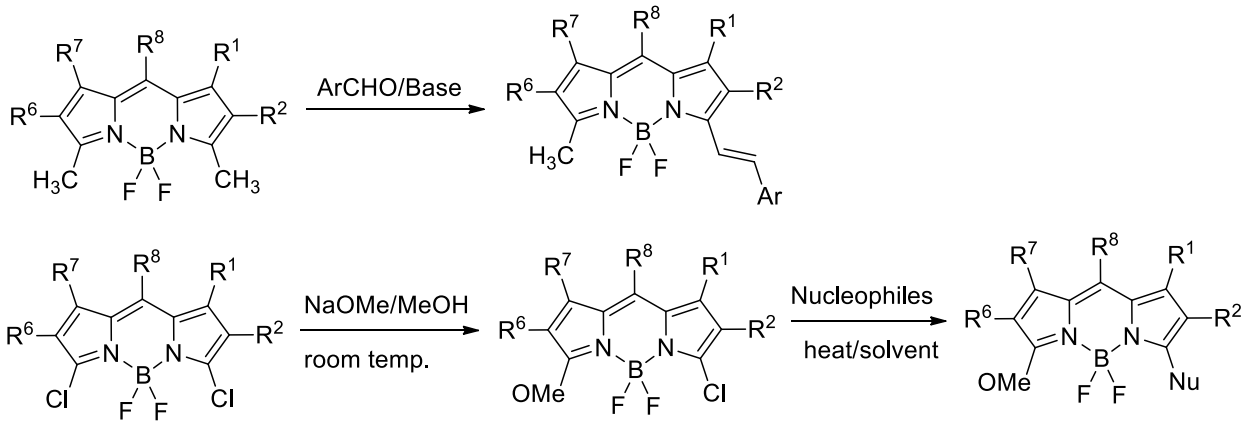

Scheme 1.4.1 Substitutions at C-3 and C-5

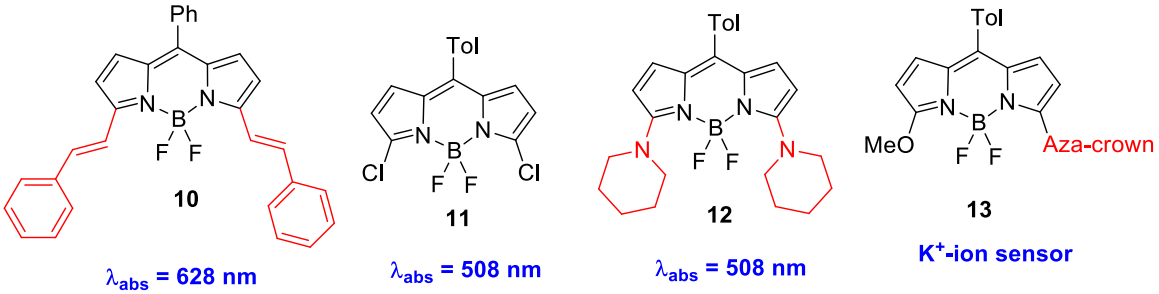

Figure 1.4.3 Chemical structures of various 3- and/or 5-substituted Bodipys.

A number of electron-donating, and recently even electron-withdrawing aromatic aldehydes have been used to introduce different styryl moieties at the 3- and/or 5-positions, in order to bring significant red-shifts in the absorption and emission spectra of the parent chromophore. This method offers a convenient route for generating highly functionalized Bodipy derivatives such as 1,3,5,7-tetrastyryl Bodipys in a single step by controlling the reaction conditions.[25] Furthermore, the intermediate carbenium ion can be oxidized *in situ* to obtain the corresponding 3-formyl derivatives in respectable yields.[24b] The novel nucleophilic addition-elimination substitution reactions of the 3,5-dichloro-Bodipys with various O-, N-, S- and C-nucleophiles including heterocycles and even aza-18-crown-6 ethers have been carried out under forcing condition to obtain a variety of symmetrical and unsymmetrical Bodipys with substitution patterns that are

difficult to realize otherwise.[26,27] These synthetic strategies and the type of compounds synthesized by these are shown in **Scheme 1.4.1** and **Figure 1.4.3** respectively.

1.4.4. *Modification at the boron center*

Murase *et al.* reported first compound of this kind wherein the F atom was replaced with aryl groups using PhMgCl.[28a] The organometallic approach has been further developed by Ziessel's group[28b,c] and used to introduce aryl,[28d] ethynylaryl,[28e] ethynyl[28f] and alkoxide subunits in place of the F atoms to generate a new family of highly luminescent, redox-active and photostable dyes called C-Bodipys, E-Bodipys and O-Bodipys, respectively (**Scheme 1.4.2**).

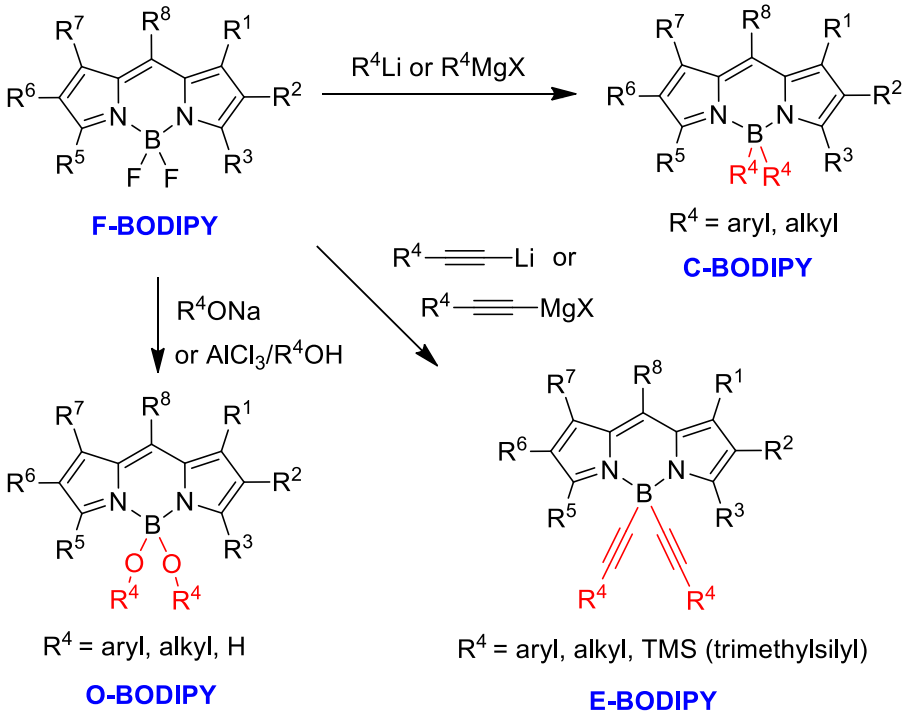

Scheme 1.4.2 Different methods for the substitution at the boron centre.

This strategy widens the area of Bodipy compounds as the limitations such as small Stokes' sifts and fluorescence quenching can be overcome. Interestingly, unlike the BF_2-Bodipy dyes, where the substituent alteration can be used for tuning the absorption and fluorescence spectral profiles over a wide range, the substituents in the E-Bodipy dyes do not affect the photophysical

properties. The asymmetric derivative **15** (**Figure 1.4.4**) is an attractive dye, as it collects photons across most of the accessible spectral range. Several groups are currently exploring such Bodipy-based scaffolds to construct molecular dyads, photovoltaics, electroluminescent devices, energy transfer cassettes and supramolecular assemblies.[28e,29]

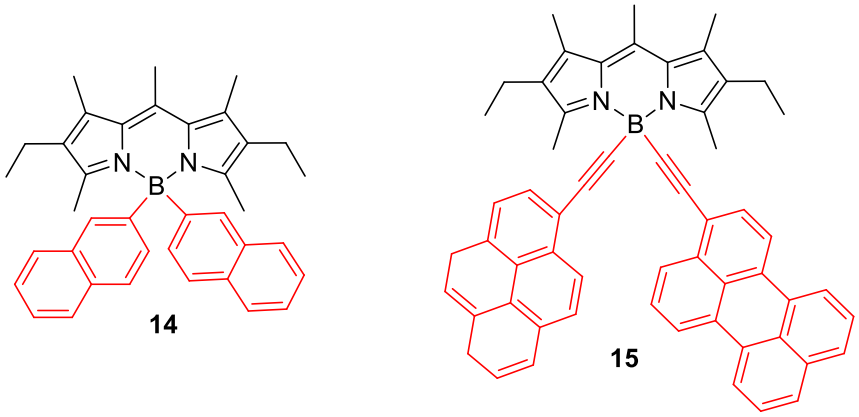

Figure 1.4.4 Chemical structures of some B-substituted Bodipys.

1.5. Variation of Properties by Structural Modifications

1.5.1. *Spectral properties*

The photophysical characteristics of the synthetically modified Bodipys vary with respect to the number, nature, as well as the position of the attached substituents.[30] Additionally, the emission behaviour of the Bodipy fluorophore is greatly influenced by the steric interactions between their components and intramolecular rotations of their chromophoric units.[31] The changes in the absorption/emission characteristics of the Bodipy dyes *vis-à-vis* the substituent pattern is presented below.

***Meso*-substitution:** Apart from the effect on quantum yield, substitution at the *meso*-site does not significantly change the absorption and emission wavelengths of the Bodipy core. In certain molecules, the reduction in the quantum yields results due to free rotation of the *meso*-substituents. For example, compared to compound **16**, its 1,7-H-analogue, **17** shows a much

reduced quantum yield. In compound **16**, the 1,7-substituents inhibit free rotation of the *meso*-phenyl group, and thus, prevents the non-radiative energy loss from the excited state (**Figure 1.5.1**).

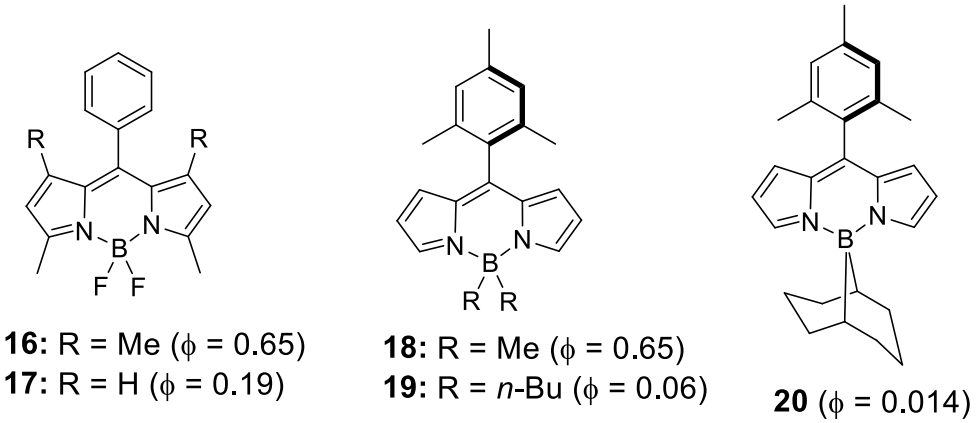

Figure 1.5.1 The effect *meso*- and B-substitutions on the emission of some Bodipy dyes.

F-substitution: Substitution of F atoms with alkyl groups reduces the fluorescence quantum yield of the parent dye significantly, and the effect is more drastic with larger and bulkyl alkyl groups (**Figure 1.5.1**). On the other hand, substitution with an aryl or an ethynylaryl group augments fluorescence quantum yield. The commercially available BF_2–containing Bodipy **21** (**Figure 1.5.2**) is widely used for laser applications. Replacement of one or both of its F atoms with the phenyl or ethynylpyrenyl groups as in **22-24** make them highly fluorescent in solution. Further, while the absorption and fluorescence maxima of **21** are insensitive to the solvent polarity, the same for the *B*-Ar Bodipys **22-24** show small red shifts in more polar solvents. This suggests minimium interactions of the *B*-aryl groups with more polar media. But most importantly, due to the presence of the UV-absorbing aryl substituents, these compounds can be regarded as energy transfer cassettes, especially when the *B*-Ar groups have good extinction coefficients. The Bodipy system **24** absorbs in the range 230-317 nm corresponding to the $\pi \rightarrow \pi^*$ transition of the pyrene units, and emits exclusively from the Bodipy part, ascertaining total

energy transfer.[28d] The cascade effect of these systems is very attractive for designing advanced optical materials because of the large virtual Stokes shifts (can also exceed 13000 cm^{-1}) of these dyes.

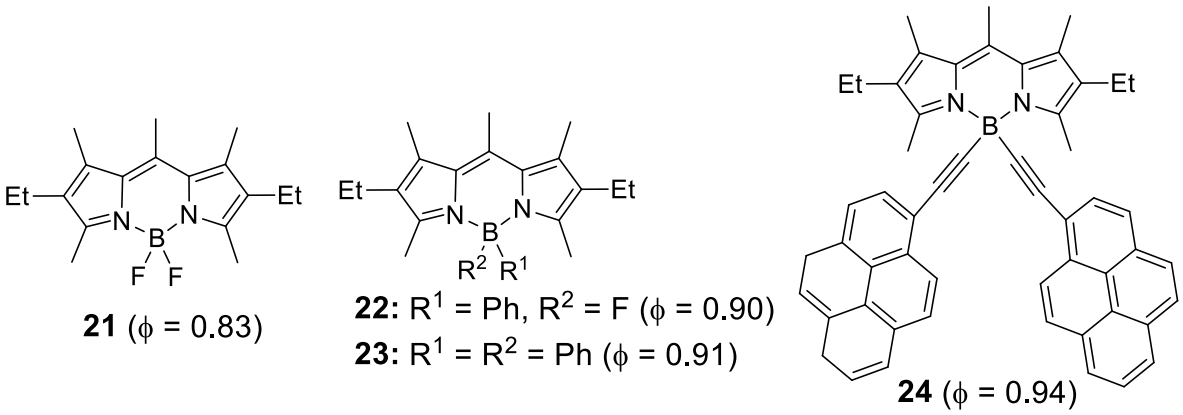

Figure 1.5.2 Spectral changes in the F-containing and F-replaced Bodipys.

3,5-substitution: There are opportunities to shift the emission wavelength of the Bodipy-based fluorophore towards lower energy using different synthetic methods. A relatively facile method involves extending the degree of π conjugation running through the central core. Thus, introduction of electron donating substituents at the 3,5-positions of BF_2-Bodipy can push the emission wavelengths to the red region by increasing the π-electron conjugation. Thus, compared to **25**, the emission of the 3,5-diaryl substituted Bodipys **26-28** (**Figure 1.5.3**) are shifted to longer wavelengths (545-626 nm), with a gradual drop in their fluorescence quantum yields from 49% to 20%.[32] However, in accord with the exponential energy-gap law, this is associated with a decrease in the fluorescence quantum yield. The distyrylboradiazaindacenes **30**, synthesized from the corresponding 3,5-dimethyl derivative showed pronounced charge-transfer character, with much reduced fluorescence quantum yields in polar solvents.[33] Water-soluble dyes were subsequently obtained by functionalization with oligo(ethyleneglycol) residues, which can be used for biological applications.

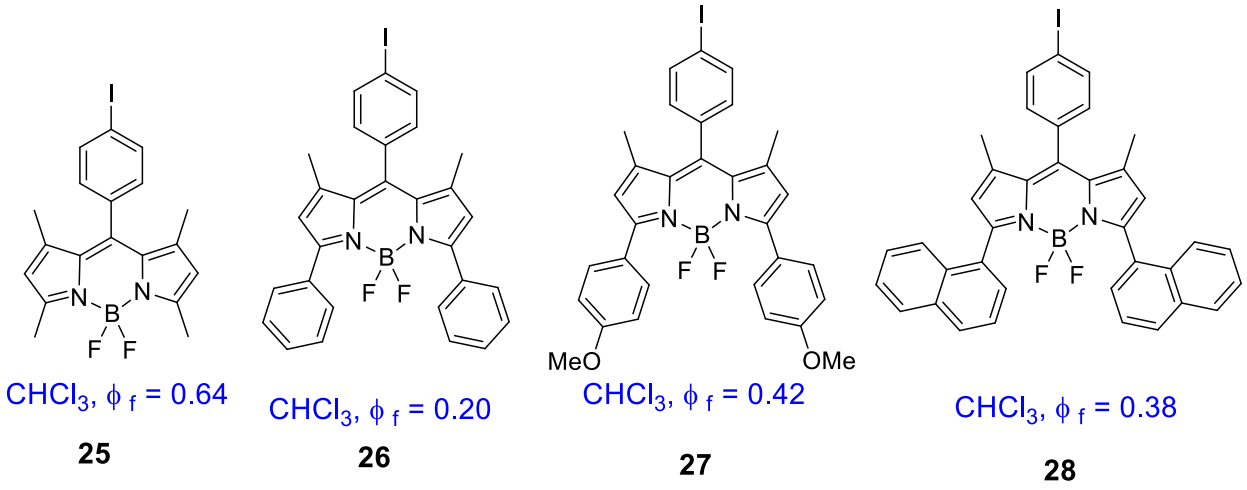

Figure 1.5.3 Modified Bodipy dyes showing different spectral properties.

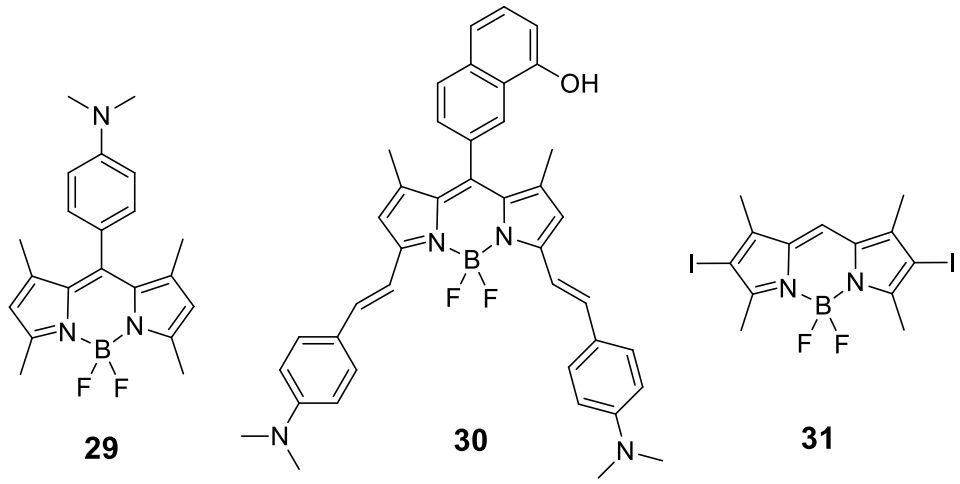

Figure 1.5.4 Spectral changes of the Bodipys due to substitutions at different positions.

2,6-substitution. Using the facile electrophilic reaction at their 2,6-positions, heavy atoms, such as iodine are often attached to the Bodipy framework. Such a substitution favors intersystem crossing to increase triplet states yields, which are otherwise very poor in the Bodipy dyes. Although this reduced the fluorescence efficiency, the iodinated dyes such as **31** (**Figure 1.5.4**) are capable of generating significant amount of $^1O_2$ under aerobic conditions. This property is used in developing photodynamic agents for the treatment of cancers.[6a] Introduction of other

electron withdrawing groups such as NO_2 and SO_3H at 2,6-position(s) also decreases the fluorescence quantum yields of the Bodipys.[3a,3d]

1.5.2. *Redox Properties*

The level of substitution of Bodipy core decides their redox chemistry.[34] Cyclic voltammograms (CVs) of derivatives lacking functionalities at the 2-, 6-, and meso-positions display irreversible oxidation and reduction, because of the high reactivity of the electrogenerated radical ions. The process of oxidative polymerization is a specific side reaction that leads to the irreversible redox behaviour. The redox process becomes more reversible with the addition of substituents, very often leading to the observation of clean looking cyclic voltammograms. In general, the removal of an electron from the Bodipy core to create the radical cation, *i. e*. oxidation of Bodipy takes place around 1.0 V *vs* saturated Calomel electrode (SCE). The reduction segments in the CV take place around -1.4 V *vs* SCE, corresponding to the radical anion generation. This difference ΔE of ~2.4 eV between the first oxidation and reduction waves is remarkably similar for most of the simple Bodipy derivatives. The well behaved electrochemical behavior of the Bodipy compounds has been exploited by Bard *et al*. to demonstrate electrochemically-generated chemiluminescence.[35] In general, the instability behavior of the oxidized Bodipys resembles that of pyrroles and thiophenes, but greater steric protection in these compounds prevents their fast dimerization and polymerization.[36]

The electrochemical behavior can qualitatively and quantitatively explain phenomena like fluorescence quenching by photo-induced electron transfer (PET), aggregation-induced emission (AIE), and metal ion sensing behaviors of the Bodipys, attached to ligands, such as crown ethers. Of late, the azabodipys have aroused specific interest for biological applications

for their efficient far-red and near-IR fluorescence. Like the cyanine framework, the nitrogen lone pair of electrons at the 8-position reduce the HOMO–LUMO energy gap.

1.6. Various applications of BODIPY dyes

1.6.1. *Laser dyes*

The Bodipys dyes are very useful for laser applications since they have low ISC rates and low triplet excitation coefficients over the entire laser spectral region,[3a,b,e,37] and often possess a triplet-triplet absorption coefficient about one-fifth that of the rhodamine dyes.[38] Some of the Bodipys dyes outperform the widely used laser dye, rhodamine 6G (Rh6G), considered as the benchmark in lasing efficiency and photochemical stability. Boyer and Pavlopoulos are the pioneers in exploring the lasing properties of the Bodipys dyes.[3] Various Bodipys dyes have been synthesized by changing the substituents in 2, 6 and 8-positions (**Figure 1.6.1**). Among these, the dyes **21** (**PM567**) and **32** (**PM597**) are commercially available, and extensively used for tunable dye laser applications. The reported[3d] efficiencies of some the dyes compared to the dye **34** are shown in **Table 1.6.1**. The popularity of the dye **32** is primarily due to its uncharacteristically high Stokes' shift (30-38 nm) that drastically reduces self absorption to enhance the lasing efficiencies.[39]

Despite several advantages, there are two major limitations of the Bodipy dyes *viz*. small Stokes' shifts and photochemical instability that need to be overcome for their wider application as laser dyes. The former reduces the lasing efficiency of the dyes due to the ground state absorption (GSA). The problem has been partially resolved by incorporating simple or bicyclic rigid aryl substituents at the C-3 center or the boron atom of the Bodipy moiety.[28b,9b,40] However, the photochemical degradation continues to be a hurdle in the long-term operation of the Bodipy -based liquid dye lasers, especially for high power and high-repetition rate operation.[41]

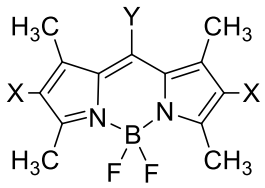

32. X = *t*-Bu, Y = Me; **33**. X = Y = H; **34**. X = H, Y = CH_3;
35. X = H, Y = C_2H_5; **36**. X = Y = CH_3; **37**. X = $CO_2C_2H_5$, Y = C_2H_5;
38. X = NO_2, Y = CH_3; **39**. X = Br, Y = CH_3

Figure 1.6.1 Various analogues of Bodipy dyes.

Table 1.6.1: Photophysical properties of the Bodipy Dyes[a]

No	λ_{max} (nm)	Log ε	λ_{fl} (nm)	Φ	λ_{las} (nm)	RE (%)[b]
33	505	4.92	516	0.80	533	30
34	493	4.90	519	0.99	542	100
35	495	4.99	517	1.00	546	90
36	518	4.67	543	0.70[c]	570	75
21	517	4.81	546	0.83[c]	570	100
37	493[d]	4.97[d]	531	0.38[c]	556	50
38	493	4.62	533	[g]	[g]	[g]
39	516[e]	4.81	546[e]	0.45[f]		

[a]MeOH was used as the solvent unless mentioned otherwise. [b]Relative Efficiency (RE) in laser power output, compared to that of **34** assigned as 100.[32] [c]In EtOH. [d]λ_{max} = 495 nm (log *E* 5.26).[42] [e]In 10% CH_2Cl_2 in MeOH. [f]In CH_2Cl_2. [g]Unreproducible data due to photoinstability.

The photo-degradation of the Bodipys is believed to be due to their reaction at the C-8 olefin moiety with singlet oxygen ($^1O_2$), generated from their triplet states during photo-excitation (**Scheme 1.6.1**).[43] Prevention of the dye decomposition with a triplet quencher like benzoquinone as well as trace amounts (1 wt% doping level) of $^1O_2$ quenchers, such as 1,4-diazobicyclo[2.2.2]octane (DABCO), bis(3,3,5,5-tetramethylpiperidin-4-yl)decanedioate (Tin770), and N-*tert*-butyl-α-phenylnitrone (TBP) supported the proposed mechanism.

Especially the highest efficacy of the $^1O_2$-quencher, DABCO, amongst the additives strongly suggested $^1O_2$ as the major causative agent for the dye decomposition. The modest effect of changing solvents (EtOH *vs* MeCN) can be attributed to the longer lifetime (30 μs) of $^1O_2$ in MeCN as opposed to that (10 μs) in EtOH.[49b] Some solid-state dye laser materials containing dispersed Bodipy dyes, developed with the primary aim of improving the laser energy output also showed better photostability compared to the liquid dye lasers.[44] Possibly, polymerization of the suitable monomer containing the dispersed dyes provides the polymeric solid matrix free of oxygen to increase the photochemical half-lives of dyes.

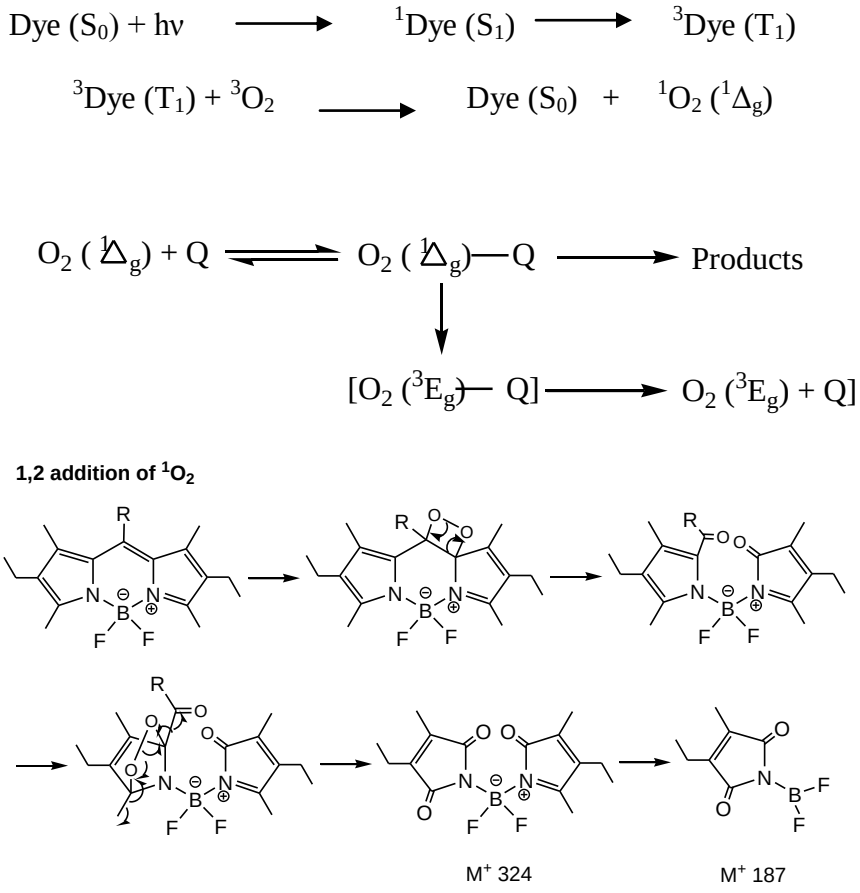

Scheme 1.6.1 Mechanism of photochemical decomposition of the Bodipy dyes.

1.6.2. *Energy cassette*

Optimum usage of the organic dyes, including the Bodipy molecules in flow cytometry and fluorescence microscopy is impeded due to their small Stokes' shift.[28c,45] Covalent attachment of an ancillary light absorber to the Bodipy core to form a cassette provides an opportunity to overcome this problem. The aim is to channel all the photons absorbed by the secondary chromophore, usually an aromatic polycycle, to the Bodipy emitter. Thus, there is a large inequality in excitation and emission wavelengths, and the full benefits of the Bodipy emitter are retained.[9b,40] An important feature of these systems is that the two chromophores remain electronically isolated because of the orthogonal arrangement around the attaching sites. The structure of the dual-dye system is the determining factor for the rate of energy transfer, which decreases with increasing center-to-center separation, in line with a dipole–dipole transfer mechanism. The overall energy-transfer efficiency exceeds 90%, even in the most extended system.[40] A number of BF_2-Bodipys **40-43**, bonded with secondary polycycle chromophore *e. g.*, anthracene or pyrene as ancillary light absorbers has been developed (**Figure 1.6.2**).[9b,40] In another type of dual chromophore dyes such as compounds **14** and **15**, or the aromatic polycycles (pyrene, perylene), or a mixture of both are attached to the B-atom. Although the absorption spectral profiles contain important contributions from each of the subunits, fluorescence occurs exclusively from the Bodipy fragment.[17]

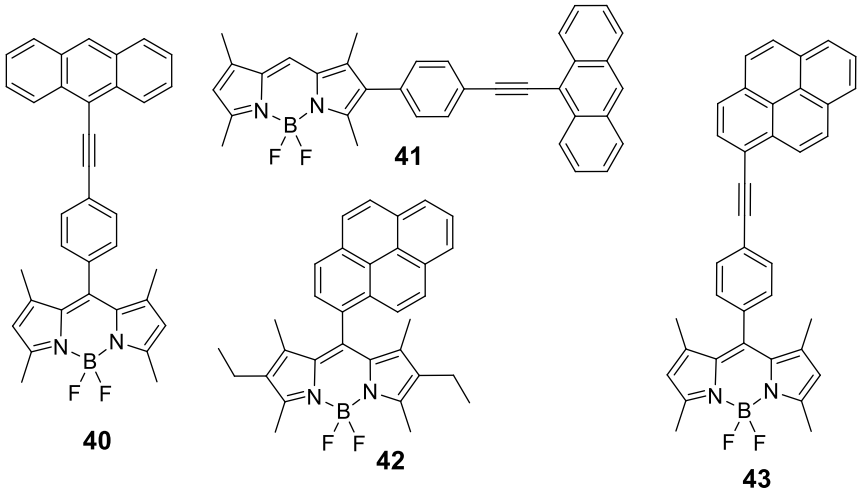

Figure 1.6.2 Examples of BF_2-Bodipys attached to some ancillary light absorbers.

1.6.3. *Biological applications*

Due to their excellent physicochemical properties and low dark toxicities,[46] the Bodipy dyes are among the most promising candidates as fluorescent labels and probes. Also, these dyes do not significantly influence the biological functions, on account of their small molecular size. Numerous Bodipy-based fluorescent labels are widely used to target important biological markers such as DNAs, RNAs, amino acids, lipids, dextran, and proteins.[47,48] In general, for effective bio-conjugation, the Bodipy-based probes are functionalized with reactive ligand/anchor groups (such as carboxylic acids, sulphonic acids, polyethylene glycol, polysaccharides and oligonucleotides) at the terminus.[49]

More recently, some Bodipy derivatives have been evaluated as a totally new class of potent PDT agents, an application more commonly associated with porphyrins and phthalocyanines.[6,50] To prove the possibility of spin–orbit perturbation, O'Shea and co-workers designed three aza-Bodipys according to the following modules relying on: i) the inherent spin–orbit coupling of the aza-Bodipy without heavy atoms; ii) intramolecular external heavy-atom effect[51] in which bromine atoms are positioned on the aryl rings and not on the aza-Bodipy core,

giving rise to moderate $^1O_2$ generation; and iii) internal heavy atom effect[52] in the bromo-substituted aza-Bodipys, yielding the $^1O_2$ efficiently (**Figure 1.6.3a**). Introduction of functionalized styryl and distyryl groups with water-soluble moieties, such as PEG-ylated structures enhanced biocompatibility, hydrophilicity and cellular uptake. Based on these concepts, a few aza-Bodipy **44-46** and styryl/distyryl Bodipy **47-49** photosensitizers (PSs) (**Figure 1.6.3b**) have been developed, and some of the water-soluble and symmetrical distyryl Bodipy showed the in vitro localization and photocytotoxicity.[49,53] However, the hydrophobic nature of Bodipy core restricts their application in biological labelling. On the other hand, a high water-solubility, required for the biological applications often leads to the aggregation and self-quenching of these dyes. These warrant design of the Bodipys with proper balance in their hydrophobicity and hydrophilicity for their use as biolabel and as PDT agents.

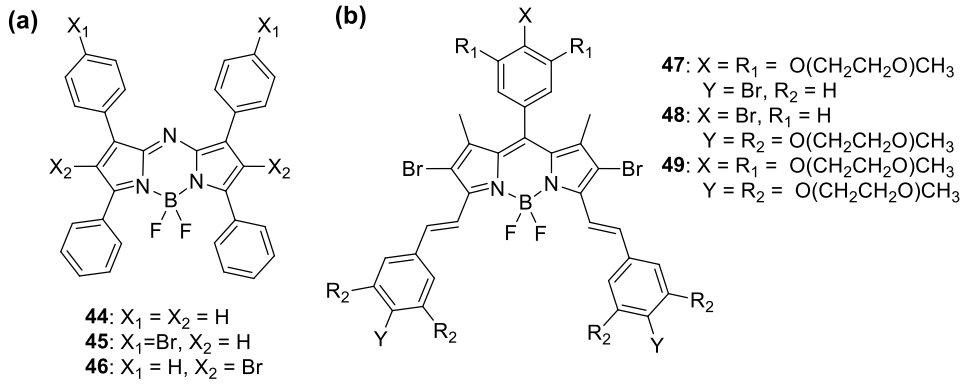

Figure 1.6.3 Some Bodipy photosensitizers (a) aza-Bodipys; (b) distyryl-Bodipys.

1.6.4. *Use in microelectronics*

The redox property of the Bodipys coupled with the unique combination of their facile synthesis, high absorption coefficient, and high photoluminescence efficiency make them attractive molecules for application in optoelectronics. The reversible (amphoteric) redox behavior of the Bodipy molecules makes them suitable as electron donors as well as acceptors. In

particular, due to the presence of a tetrahedral boron atom in the structure, the Bodipys can provide the platform for developing isotropic active materials for (opto)electronic devices and solar cells. Indeed, the Bodipy derivatives have been recently employed as p-type donor materials in conjunction with methanofullerene ~phenyl C61-butyric acid methyl ester (PCBM) as acceptors in bulk heterojunction (BHJ) solar cells.[54] The introduction of one or two styryl units in the Bodipy structure permits modulation of the HOMO-LUMO gap, while the solubility and film-forming properties of the molecules are brought by the oligooxyethylene chains.

Thayumanavan *et al*. used the Sonogashira polymerization technique to synthesize novel π-conjugated copolymers incorporating Bodipy core as the "donor" and quinoxaline (**Qx**), 2,1,3-benzothiadiazole (**BzT**), *N,N'*-di(2'-ethyl)hexyl-3,4,7,8-naphthalenetetracarboxylic diimide (**NDI**), and *N,N'*-di(2'-ethyl)hexyl-3,4,9,10-perylene tetracarboxylic diimide (**PDI**) as the acceptors (**Figure 1.6.4**). The charge transport measurements of the polymers indicated that the Qx, and BzT-conjugated Bodipy polymers act as p-type semiconductors, while the PDI and NDI-conjugated Bodipy polymers function as n-type semiconductors, and the switch between p-type and n-type can be accomplished by a choice of suitable comonomers.[55]

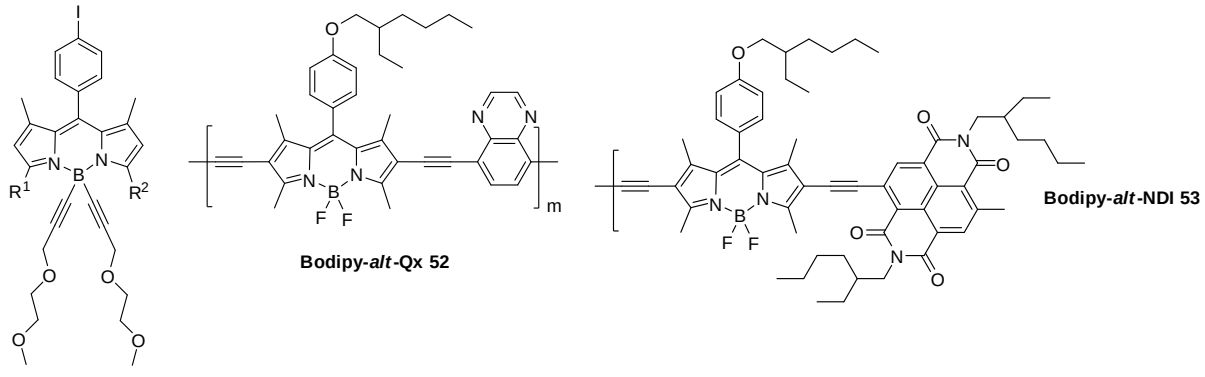

50 R^1 = H, R^2 =CH=CC$_6$H$_4$-O(CH$_2$O)$_2$Me
51 R^1 = R^2 = CH=CC$_6$H$_4$-O(CH$_2$O)$_2$Me

Figure 1.6.4 Chemical structures of some Bodipy-based BHJ solar cells.

1.7. Conclusion and Rationale of the Present Work

From the foregoing, the adaptability of the Bodipy molecules for various synthetic transformations in developing a diverse array of novel functional molecules is evident. It is now possible to produce derivatives having attachments placed at the *meso*, pyrrole, or boron sites of the Bodipy moiety, each providing distinct advantages for this purpose. The *meso*-site favors orthogonal geometries for the attached aromatic residues, which can minimize electronic coupling. Substitutions at the pyrrole sites allow coplanar geometries that maximize electronic communication between the subunits, while that at the boron center provides free rotation without any electronic coupling. Thus, the same appendage can exert different properties according to the site of its attachment.

Against the above backdrop, the objectives of the present work can be broadly classified as the following

(i) formulation of some Bodipy dyes with improved photo-stability, evaluation of their lasing performance as well as photo-stability under lasing conditions, and mechanistic rationalization of the results by theoretical calculations and triplet state studies;

(ii) development of red Bodipy dyes, preferably with good water solubility for their biological and other applications;

(iii) development of new Bodipy chemistry for regioselective functionalization, especially at the *meso*-position; and

(iv) exploration of their redox property for molecular electronics applications.

The results of these studies are discussed in Chapters-2-5, while the bibliography is listed in Chapter-6. Initially the work was focused on improving the photostability of the Bodipy dyes without compromising their lasing abilities. To this end, several new efficient Bodipy laser dyes

were rationally designed, synthesized, and their lasing property as well as photostability assessed. These, together with mechanistic rationalization of the results constitute the Chapter 2.

In the next part (Chapter-3), the study was extended towards development of new Bodipy chemistry for regioselective Knoevenagel condensation with aromatic aldehydes for introducing stryryl-moieties at the pyrrole rings and/ or *meso*-position. The Knoevenagel condensation, carried out at the pyrrole rings was used for extending the π-conjugation of the Bodipy core for an easy access to some red Bodipy dyes. Most interestingly, a novel concept of steric strain release (SSR) was invoked to override the relative acidity factor of the C-3, C-7, and *meso*-methyl protons to direct the Knoevenagel condensation exclusively at the *meso*-methyl group. Further, fine tuning of the *meso*-functionalization protocol was achieved by increasing the electrophilicity of the aromatic aldehydes. The SSR hypothesis and the reaction mechanism were unequivocally proved by single crystal X-ray analyses of the parent and product Bodipys as well as the intermediate of the reaction.

Extending the studies towards biological applications some Bodipy-*O*-glycosides were developed by attaching glucose moiety to the Bodipy molecules. All the compounds showed *in vitro* toxicity to the human lung cancer A549 cells and the toxicity of few compounds could be attributed to their ability to cross cell surface and accumulate in the cytoplasm (Chapter-4). Finally, the study was extended towards development of new Bodipy based organic material for nanoelectronics (Chapter-5). The required novel materials were constructed by synthesizing a (σ–π) system comprising of an alkyl spacer (σ-moiety) and a suitable Bodipy molecule (π-moiety) followed by its grafting on Si wafers. Measurement of the charge transport properties of these materials showed current rectification behavior. The rectification characteristic was modulated to negative differential resistance (NDR) behavior by forming a supra-molecular

assembly of another Bodipy molecule. The bilayer formation allowed the supra-molecular assembly to undergo bias induced conformational changes, to exhibit the NDR behavior.

CHAPTER-2

RATIONAL DESIGN AND SYNTHESIS OF SOME PHOTSTABLE BODIPY LASER DYES

Chapter 2: Table of Contents

2.1. Preamble

As discussed in the previous chapter (**1.6.1**) improvement of the photochemical stability of the Bodipy dyes is a central theme in dye laser research for their commercial applications. It is well established the photodegradation of the Bodipy dyes is primarily mediated by their reaction with singlet oxygen ($^1O_2$), generated *in situ* from the excited states of the dye molecules.[38b,42a,b,43c,56b] The methods adopted to enhance the lasing operating lifetimes of these dyes, such as the use of deoxygenated dye solutions[43c] or the addition of a high concentration (*ca*. 100 mm) of $^1O_2$ quenchers, such as Tin770, TBP,[56b] or DABCO,[38b,42a] are practically non-viable for the large scale operations, where large amounts (several L) of dye solutions are used. Also, high concentrations of the $^1O_2$ quenchers reduce the laser efficiency by quenching the dye fluorescence significantly.

It was anticipated that a systematic variation in the substitution pattern of the Bodipy dyes might provide a photostable laser dye with better spectral and lasing properties. In this regard, several efforts by structural modification such as alteration of the pyrrole rings-alkyl substituents or incorporation of different substituents at C-8 and/or C-2 + C-6 positions of the pyrromethene moiety have been attempted. But their long term photostability in liquid dye lasers has neither been clearly established nor rationalized.[42b,56b] The most stable Bodipy dye, PM650 (with a C-8 CN substitution instead of the Me group of PM567, **21**), reported so far is unsuitable for lasing due to its low fluorescence yield.[42b] Previously incorporation of an electron-rich aryl substituent at the C-8 (*meso*-) position improved the photostability of the dyes without compromising their lasing efficiency.[56a] For example, the photostability of the meso-(2,4,6-trimethoxyphenyl)-substituted congener (**54a**, **Figure 2.1.1**) was twice that of **21**.[56a] The substituent prevented photochemical degradation by reducing the generation of $^1O_2$ as well as the

reaction probability of the dye with $^1O_2$, but had no electronic interaction with the Bodipy chromophore.

The boron centre in the Bodipy core offers another option for substitution with no electronic effect on the dye core because the changes in the π-electron density on the fluorine atoms in the S_0 and S_1 states are very low.[56c] The substitution at the boron centre has been used to increase Stokes' shift,[28d,29] solubility and chemical stability of the Bodipy dyes.[58] However, the lasing performance of the B-substituted Bodipy dyes has not been tested so far. Presently, two different approaches *viz*. substitution of the F atoms at the B-centre with an oxygenated alkyl group as such, and in combination with incorporation of a bulky group at the *meso*-position were adopted to improve the photo-stability. To this end, in this study, two B-substituted Bodipy dyes (**54b** and **54c**, **Scheme 2.2.1.1**) were synthesized, and examined for their photophysical and lasing properties, as well as their photochemical stabilities. The results were rationalized by analyzing their redox potentials (using cyclic voltammetry, CV), and triplet state life times and absorption spectra (by pulse radiolysis) as well as quantum chemical calculations.

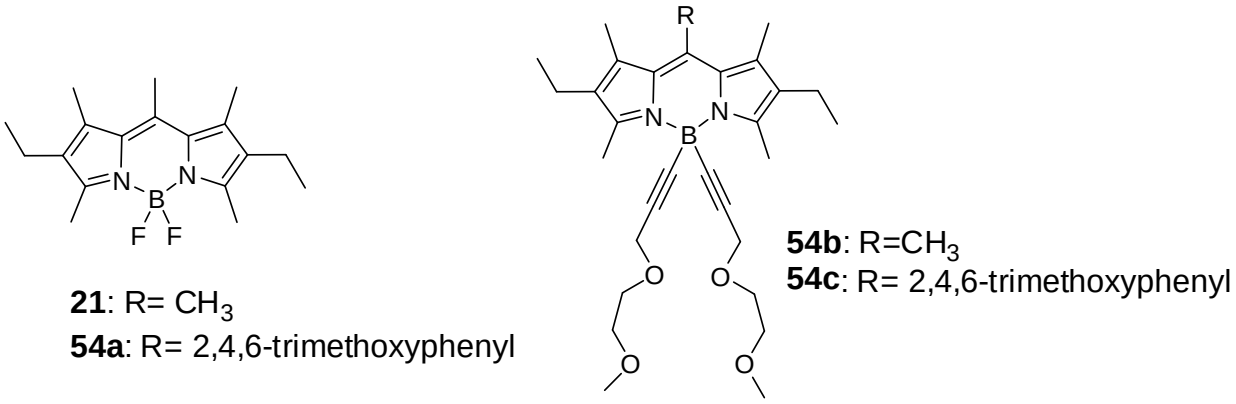

Figure 2.1.1 Chemical structures of Bodipy dyes

2.2. Studies on the B-Substituted Bodipy Dyes

2.2.1. Synthesis

The low solubility of the Bodipy dyes restricts their use especially in polar solvents like methanol, ethanol and water. Previously, laser experiments on different B-aryl- and B-alkyl-substituted Bodipy dyes could not be performed from this laboratory because of the poor solubility of the dyes in these solvents. Hence, in this study the 2,5-dioxaoct-7-yne moiety was judiciously chosen for substituting the B-fluoro atoms of the Bodipy dyes **21** and **54a**.[56a] Such a replacement was envisaged to improve the solubility of the resultant dyes in polar solvents. Previously, the Bodipy dye **54a** was found to be an efficient and photochemically stable laser dye.[56] Hence, it was envisaged that a new dye possessing the structural combinations of the dyes **21** and **54a**, namely substitutions at the meso position and the boron centre, might have improved lasing performance.

For the formulation of boron substituted dyes first, the alkyne diethylene glycol derivative **55** was synthesized by a base-catalyzed alkylation of the glycol with propargyl bromide (**Scheme 2.2.1.1**).[58] Appearance of a triplet at δ 2.41 for the alkyne proton and a doublet at δ 4.18 for the propargylic protons confirmed the propargylation (**Figures 2.2.1.1 a-b**). This

was converted to the corresponding Grignard reagent by reaction with EtMgBr and subsequently reacted with **21** to afford the new dye **54b**. The ^{1}H NMR of compound **54b** showed characteristic peak of propargylic –OCH_2 protons at δ 4.16. Appearance of a singlet at δ -13.4 in place of the triplets at δ 3.87 for the BF_2 group in the ^{11}B NMR spectrum confirmed its formation (**Figures 2.2.1.2 a–b** and **2.2.1.3**).

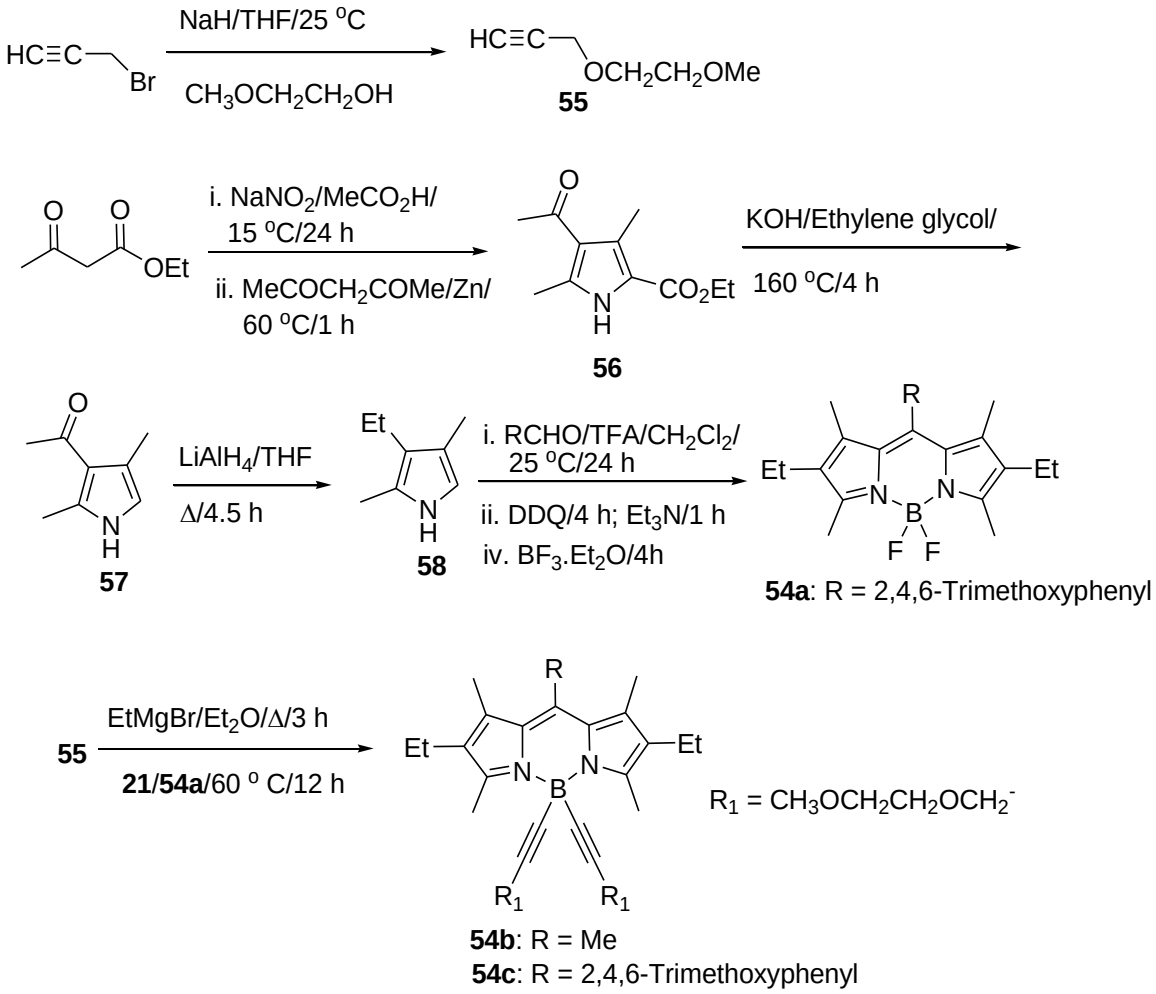

Scheme 2.2.1.1 Synthesis of the compounds **54b** and **54c**

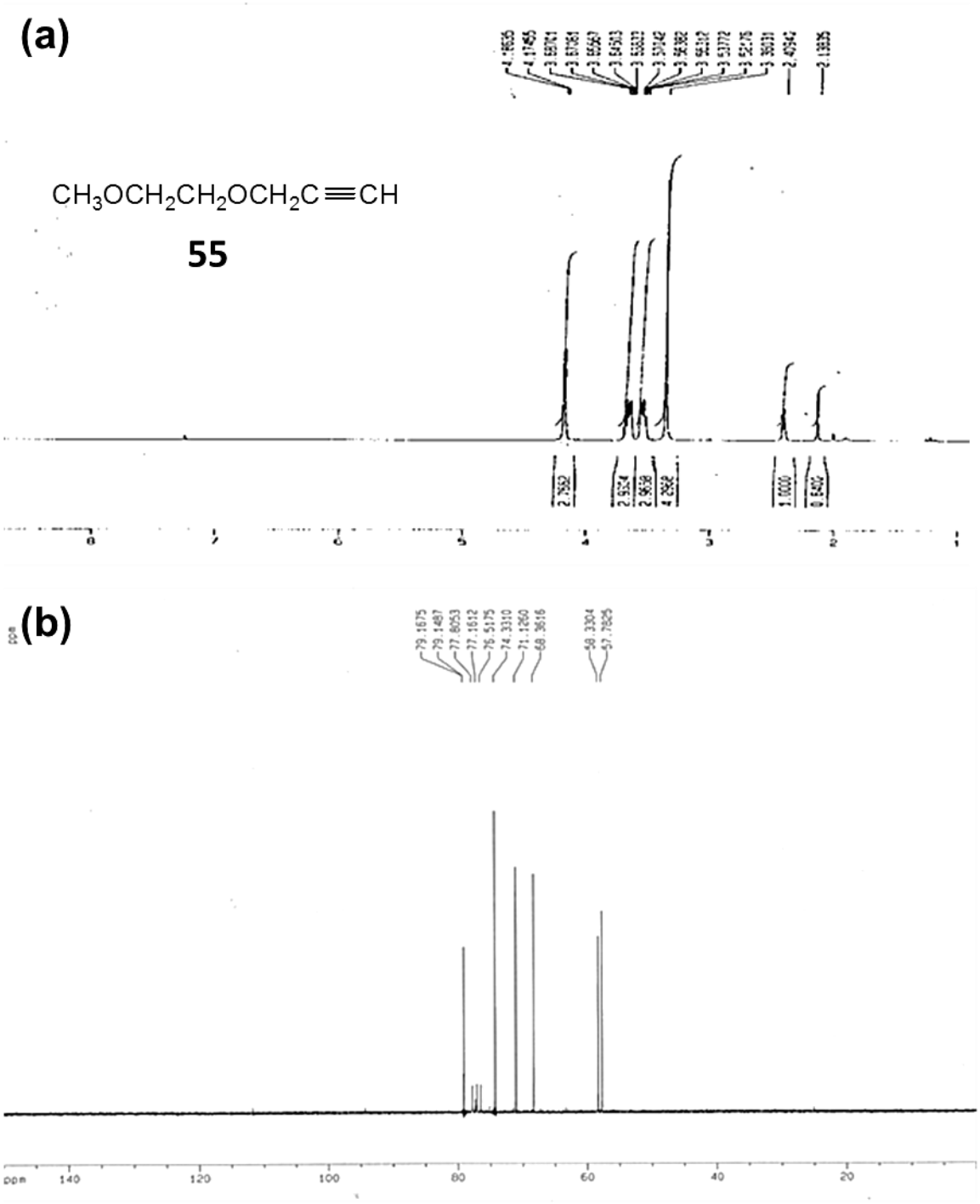

Figure 2.2.1.1 The NMR spectrum of **55** (a) ^{1}H NMR, (b) ^{13}C NMR.

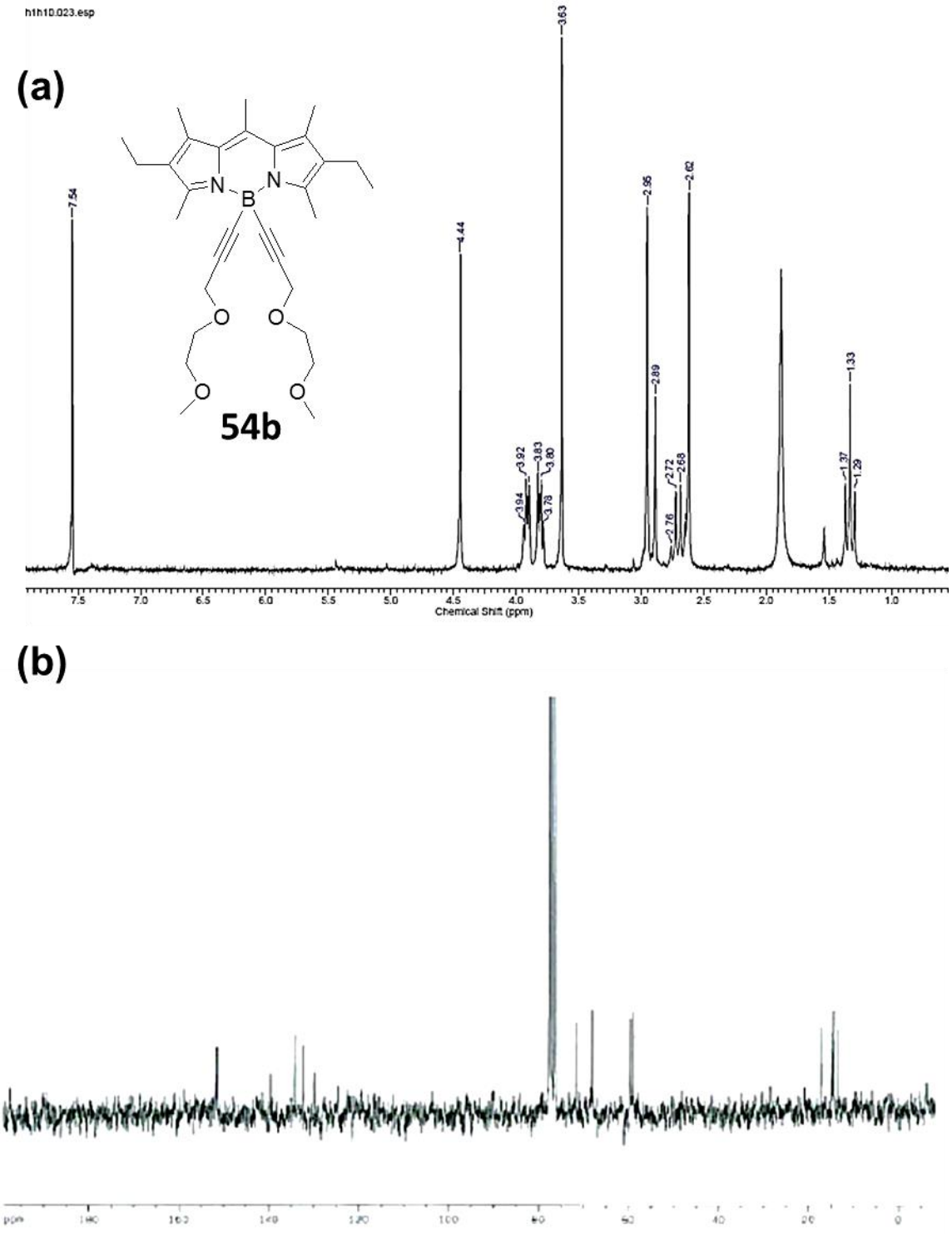

Figure 2.2.1.2 The NMR spectrum of **54b** (a) ^{1}H NMR, (b) ^{13}C NMR.

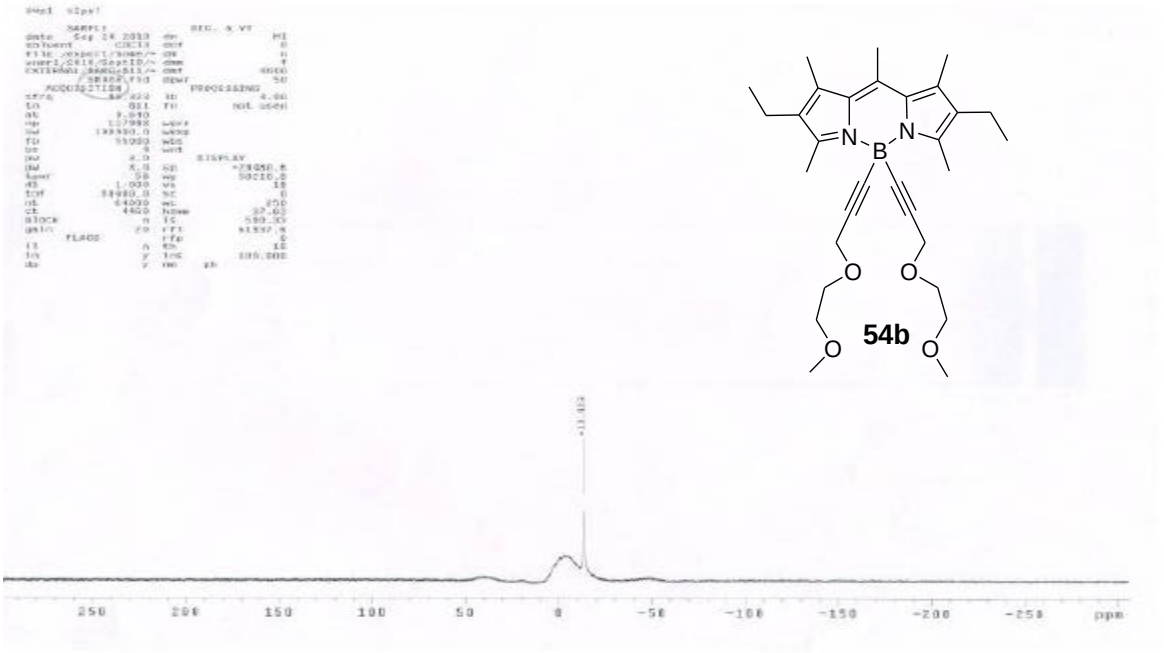

Figure 2.2.1.3 ^{11}B NMR spectrum of compound **54b**

The synthesis of compound **54c** started by nitrosation of ethyl acetoacetate at low temperature with $NaNO_2$/$MeCO_2H$ followed by *in situ* tandem reduction of the resultant product with Zn-dust and condensation with acetyl acetone to furnish the pyrrole **56**. Its alkaline hydrolysis under heating directly furnished the ketone **57**. This was subjected to reduction with $LiAlH_4$ to furnish **58** via direct conversion of its CO functionality to the CH_2 moiety. A trifluoroacetic acid (TFA)-catalyzed condensation of the pyrrole derivative **58** with 2,4,6-trimethoxybenzaldehyde, followed by 2,3-dichloro-5,6-dicyano-1,4-benzoquinone (DDQ) oxidation and subsequent reaction with $BF_3.Et_2O$ furnished **54a**.[56a] All the intermediates and compound **54a** were characterized from their known ^{1}H and ^{13}C NMR spectra. **Figures 2.2.1.4 a-b** show the NMR patterns of **54a**.

The dye **54c** was obtained by nucleophilic substitution of the F atoms of **54a** with the Grignard reagent prepared from **55** as above (**Scheme 2.2.1.1**). Formation of compound **54c** was also confirmed from the disappearance of the ^{11}B NMR triplets at δ 3.87 (BF_2) and appearance of

a ^{11}B NMR singlet at δ -13.2. Besides, the characteristic ^{1}H and ^{13}C NMR resonances due to the Bodipy core and $–OCH_2/–OCH_3$ apendages, the peaks for the alkyne–CH_2–O moieties at δ 4.19 in the ^{1}H NMR and at δ 90.6 in ^{13}C NMR were also observed (**Figures 2.2.1.5 a-b**).

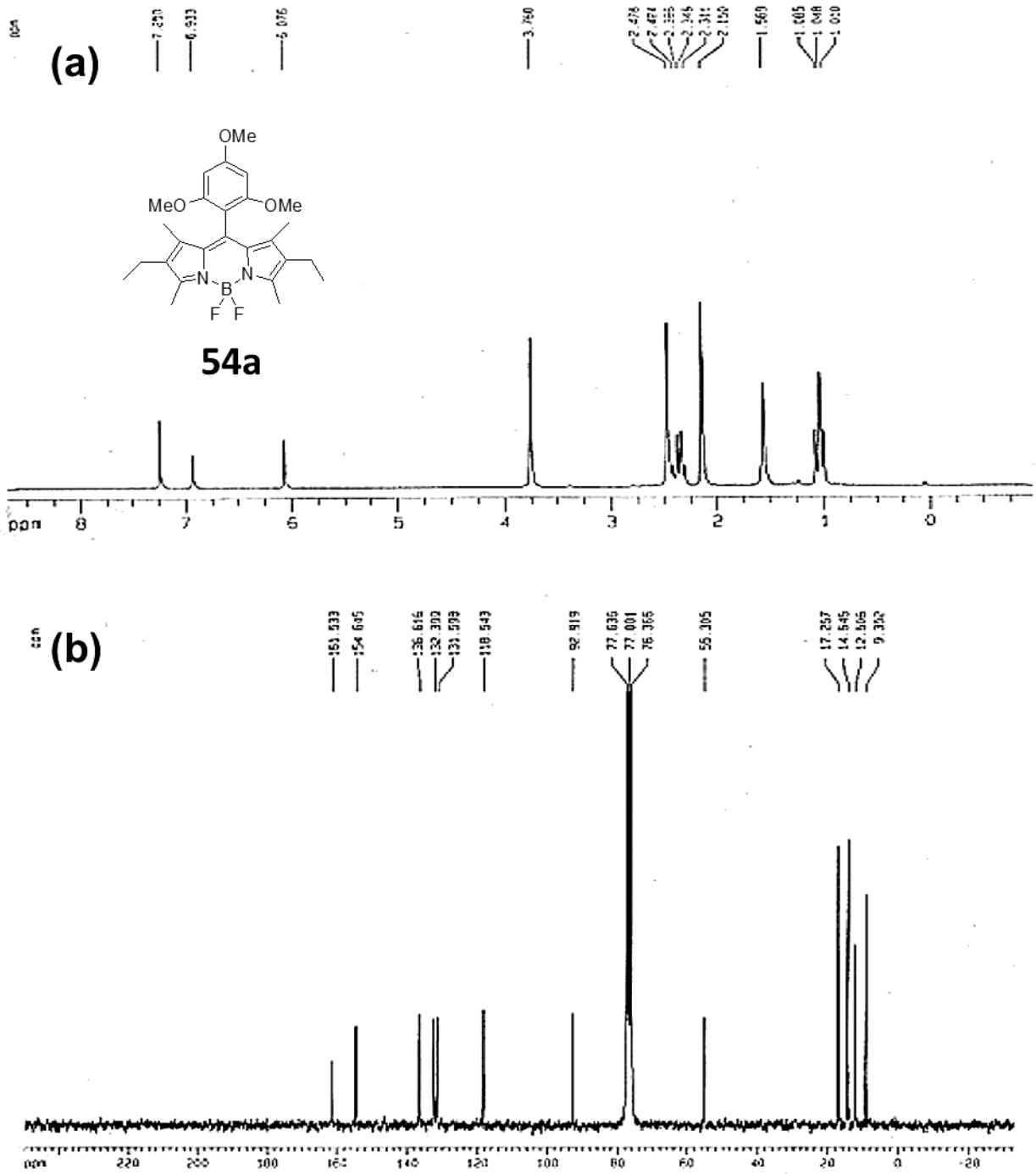

Figure 2.2.1.4 The NMR spectrum of **54a** (a) ^{1}H NMR, (b) ^{13}C NMR.

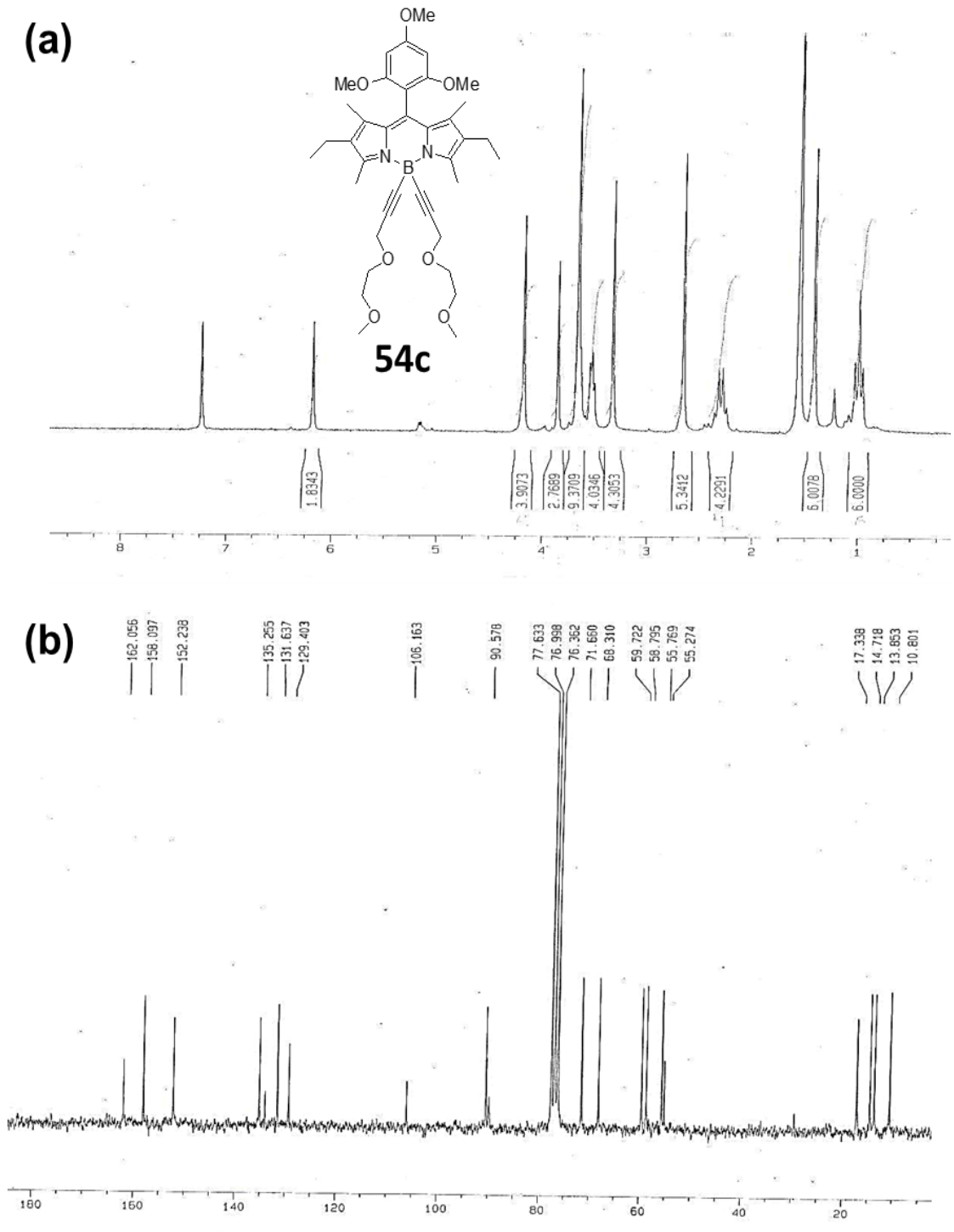

Figure 2.2.1.5 The NMR spectrum of **54c** (a) ^{1}H NMR, (b) ^{13}C NMR.

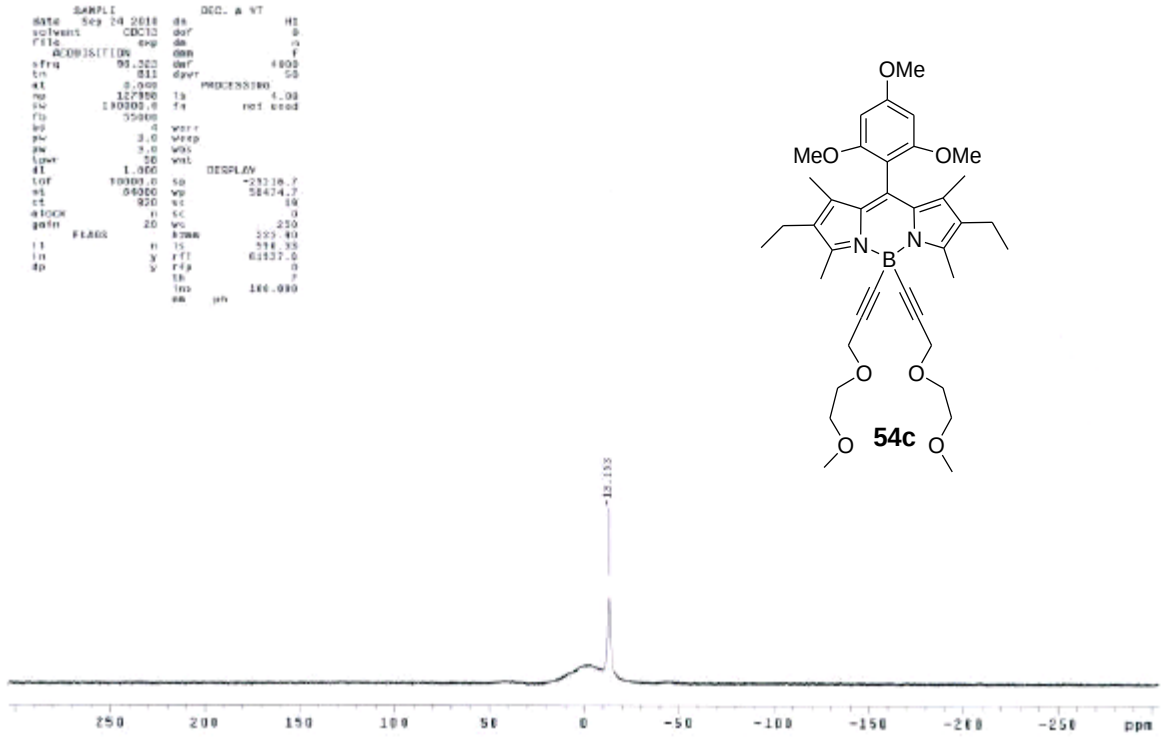

Figure 2.2.1.6 ^{11}B NMR spectrum of compound **54c**

2.2.2. Photophysical characteristics

The measured photophysical parameters (longest-wavelength absorption maxima (λ_{abs}), emission maxima (λ_{em}), fluorescence quantum yields (Φ_{fl}), fluorescent lifetimes (τ), maximum molar absorptivities (ε_{max}) along with the calculated Stokes' shifts (ν) and the radiative (k_r) and non-radiative (k_{nr}) decay constants of the dyes **54a**–**c** relative to those of the dye **21** in EtOH solvent are presented in **Table 2.2.2.1**. The normalized absorption and emission spectra of the dyes in EtOH solvent are also shown in **Figure 2.2.2.1** for comparison. All the compounds showed similar absorption spectra with features typical of the Bodipy dyes, such as strong $S_0 \rightarrow S_1$ transitions with clear maxima (λ_{max}) between 510 and 530 along with vibronic transitions on the higher-energy side evident as a shoulder, and ill-defined, weak bands corresponding to the $S_0 \rightarrow S_2$ transitions at about 420 nm.[59] Each dye showed small fwhm that is characteristic of the

cyanine type of chromophores. The $S_0 \rightarrow S_1$ absorption band of the dye **54c** was red shifted by 10 nm relative to that of the corresponding meso-methyl dye **54b**.

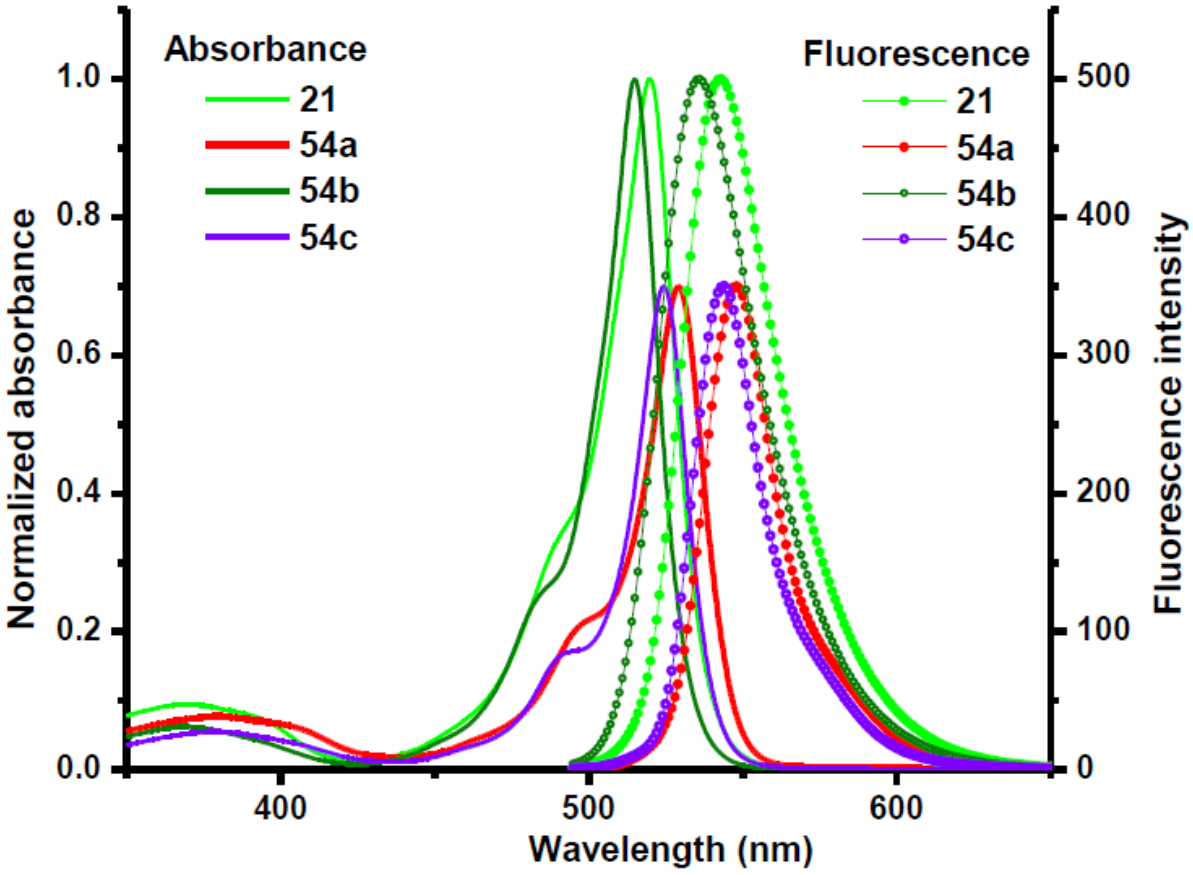

Figure 2.2.2.1 Normalized absorption and fluorescence spectra of dyes **21** and **54a**–**c** in EtOH.

Table 2.2.2.1: Photophysical parameters of the dyes **21** and **54a**–**c** in EtOH

Dye	λ_{abs}[a]	ε_{max}[b]	λ_{em}[c]	V	Φ_{fl}[d]	τ[e]	k_r[f]	k_{nr}[g]
	[nm]	**[10^4 $M^{-1}cm^{-1}$]**	**[nm]**	**[cm^{-1}]**		**[ns]**	**[10^{-8} s^{-1}]**	**[10^{-8} s^{-1}]**
21	517	8.3	534	616.0	0.84[d]	6.43	1.31	0.25
54a	528	10.4	537	317.4	0.85	6.98	1.22	0.21
54b	513	8.4	529	589.6	0.84	6.22	1.35	0.26
54c	523	9.4	533	358.7	0.81	6.61	1.22	0.29

[a]Error: ± 0.2 nm. [b]Extinction coefficients for the corresponding λ_{max}. [c]Error: ± 0.3 nm. [d]The fluorescence of all the dyes was measured at the excitation wavelength 490 nm. The fluorescence quantum yields of **54a**–**c** are reported relative to that of **21** (Φ_{fl} = 0.84).[59] [e]Fluorescence lifetime. [f,g]Radiative and non-radiative decay rates.

The fluorescence spectra of the dyes were almost mirror images of the respective absorption spectra, with minimum energy loss. All the dyes were found to be highly fluorescent (Φ_{fl} >0.8) but the absorption and emission spectra of the compounds **54a** and **54c** were relatively sharper and stronger compared to that of the meso-methyl dyes **21** and **54b**, reflecting a significantly higher polarizability of those dye chromophores due to the increased π electron clouds. Also, the absorption and emission spectra of the B-substituted new dyes **54b** and **54c** showed a smaller blue shift (~5 nm) compared to the corresponding parent dyes **21** and **54a**. The dye **54c** had a higher ε_{max}, but smaller Stokes' shift relative to those of **21** and **54b**. The photophysical data clearly revealed that substitution of the F-atoms at the boron centre had insignificant effect on the spectral properties of the Bodipy chromophore. Overall, the photophysical properties of the two new Bodipy dyes **54b** and **54c** appear favorable for use as laser dyes.

2.2.3. Lasing characteristics

The narrow-band lasing data of all the Bodipy dyes in EtOH are presented in **Table 2.2.3.1** and their lasing characteristics shown in **Figures 2.2.3.1** and **2.2.3.2**. The narrow-band lasing profiles of all the dyes followed an expected pattern, showing a maximum efficiency at a particular wavelength (λ_L), characteristic of the dye (**Figure 2.2.3.1**). The maximum lasing efficiency values (η) of the dyes **21** (21.8%) and **54b** (20.4%) at their respective λ_Ls (**Table 2.2.3.1**) revealed a marginal reduction on replacing the F-atoms at the boron atom with the 2,5-dioxaoct-7-yne moiety. The lasing efficiency of dye **54b** in the highly viscous diethylene glycol dimethyl ether solvent was comparable to that in EtOH, when the chosen dye concentrations had similar optical density (O. D. = 1.2) at the pump wavelength (532 nm). This suggested that the torsional motion of the flexible 2,5-dioxaoct-7-yne moieties at the boron centre do not contribute to the non-radiative processes for energy dissipation. Thus, the marginal loss of the lasing efficiency of **54b** compared to that of **21** may be due to its slightly higher triplet extinction coefficient (**Table 2.2.7.1**). The excited S_1–S_n absorption process may also contribute to this, although the excited-state absorption cross-sections for the Bodipy derivatives are very low.[60] It is noteworthy that the loss of the lasing efficiency on going from the dye **21** to **54b** was more than compensated by incorporating the electron rich aryl substitution at the *meso*-position of the Bodipy chromphore. Thus, consistent with the expectation, the maximum lasing efficiency of the dye **54c** (22.0%) was found to be even higher than that of **21** at their respective λ_Ls (**Table 2.2.3.1**). The spatial profile of the lasing output for each dye was circular at the respective maximum lasing efficiency. This would ensure uniform propagation of the laser light over a longer distance, which is beneficial for different types of laser applications.

Table 2.2.3.1: Lasing characteristics of the Bodipy dyes **21** and **54a–c** in EtOH

Dye	λ_L [nm]	$\eta^{[a]}$ [%]	η_s [%]	GSA [10^{-18} cm^2] at λ_L	Φ_{pd}	Φ_{pd}^{-1} of **54b** and **54c** /Φ_{pd}^{-1} of **21**
21	552	21.8	24	5.1	6.0×10^{-4}	--
54b	552	20.4	21	1.1	2.8×10^{-4}	2.1
54c	546	22.0	30	10.0	2.1×10^{-4}	2.9

[a]Error: ±1.0%.

The comparative laser slope efficiencies (**Figure 2.2.3.2**) of the Bodipy dyes clearly demonstrated an enhanced laser performance of dye **54c** compared to the dyes **21** and **54b**, irrespective of the pump energy. The threshold pump energy values (L_T) of the dyes **54b** (0.19 mJ) and **54c** (0.26 mJ) are also much smaller than that of dye **21** (0.36 mJ). The laser tuning range of **54c** was similar to those of **21** and **54b**, but its λ_L (546 nm) was blue-shifted by 6 nm relative to those (552 nm) of **21** and **54b**.

Despite these positive attributes, the maximum lasing efficiency of **54c** was achieved at a higher O. D. (1.8) than that (O. D. 0.7) with the dyes **21** and **54b**. This implied that a higher concentration of dye **54c** is required for its optimum performance as a laser dye, and suggested higher ground state absorption (GSA) of **54c** at the lasing wavelength that would reduce the laser photons. This was confirmed by the triplet states studies carried out by pulse radiolysis (PR) experiments. Since the results of PR studies were also importane in explaining the relative photostabilities of the Bodipy dyes, these will be discussed later.

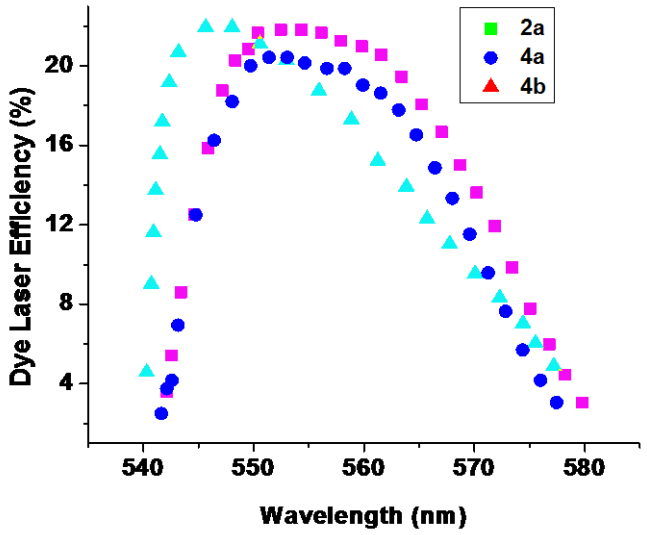

Figure 2.2.3.1 Narrow band lasing efficiencies of the Bodipy dyes **21**, **54b** and **54c** in EtOH, determined by pumping at 532 nm radiation of a Q-switched pulsed Nd-YAG laser.

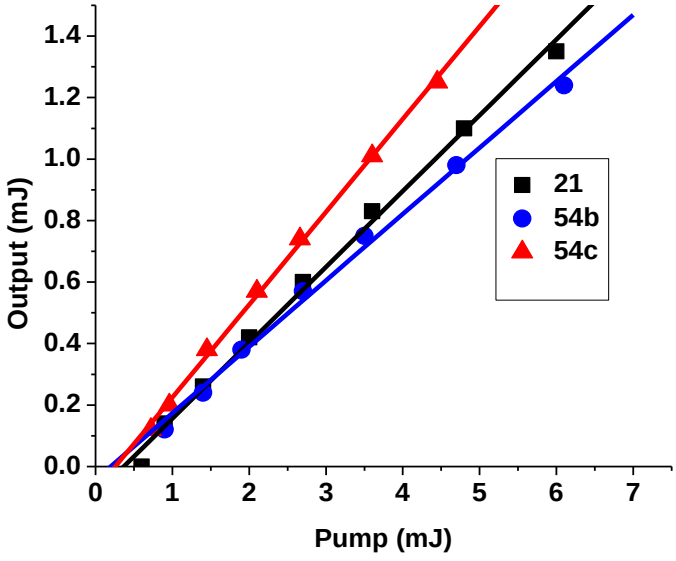

Figure 2.2.3.2 Comparative slope efficiencies of Bodipy dyes **21**, **54b** and **54b** at their respective λ_Ls in EtOH solutions, determined by pumping at 532 nm radiation of a Q-switched pulsed Nd-YAG laser.

2.2.4. Photostability characteristics

Initially, the quantum yields of photodegradation (Φ_{pd}) of the dyes **21**, **54b** and **54c** in air-equilibrated EtOH solutions were measured under non-lasing conditions. Consistent with the fact that the degradation of the dyes at the olefinic site would produce non-fluorescent products,[56a] the longest wavelength absorption bands ($S_0 \rightarrow S_1$) of the dye solutions did not show any shape change, but the peak heights were reduced after photoexposure. Analyses of the absorption intensities, from the peak area (**Table 2.2.3.1**, higher Φ_{pd}^{-1}) clearly revealed impact of the substitutions at boron on the enhanced photostabilities of the new dyes in EtOH solution. The meso-(2,4,6-trimethoxyphenyl) substitution increased the photostability further,[56a] rendering dye **54c** as the most photostable of the four dyes. The increased stabilities of the dyes **54b** and **54c** after irradiation at 532 nm for 4 h under non-lasing conditions were also confirmed by HPLC analyses (**Table 2.2.4.1**).

Table 2.2.4.1: Quantification of photodecomposition of Bodipy dyes **21**, **54b** and **54c**.[a]

Dye	% Photo-decomposition
21	85
54b	45
54c	35

[a]The individual dyes were irradiated under non-lasing conditions by the 532 nm output of a pulsed Nd:YAG laser for a period of 4 h. The extents of degradation were quantified from the integrated area of the respective HPLC chromatogram using a standard graph, prepared separately with the individual dyes. The values are mean of three independent similar experiments.

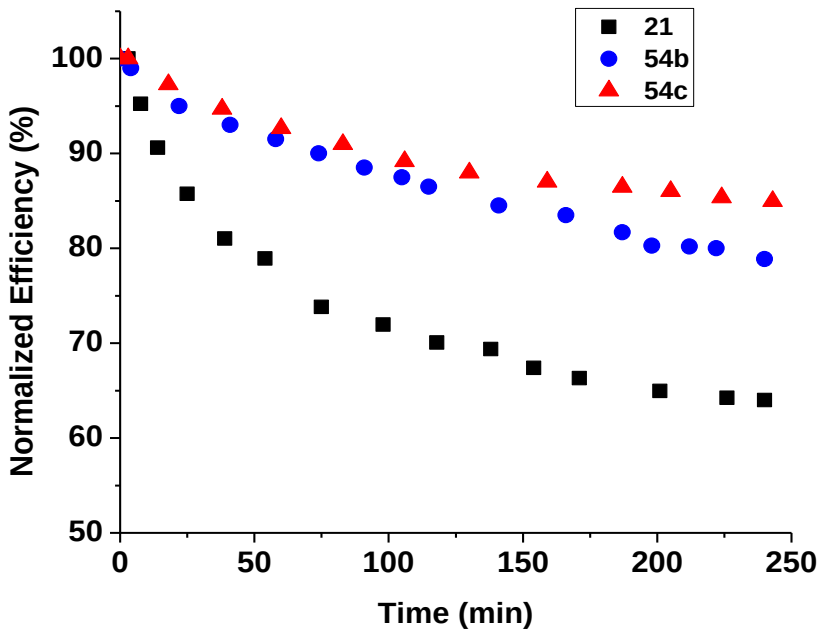

Figure 2.2.4.1 Normalized profiles of the lasing efficiencies of the Bodipy dyes **21**, **54b** and **54c** as a function of irradiation time.

In separate experiments, the photostabilities of the dyes **21** and **54b** and **54c** under lasing conditions were evaluated by assessing their respective lasing efficiencies in EtOH solution a function of irradiation time. A time-dependent decrease in the lasing efficiencies (**Figure 2.2.4.1**) was observed with all the dyes. However, the decrease was very rapid for **21** compared to that of **54b** and **54c**, confirming better photostabilities of the new B-substituted dyes even under lasing conditions. Typically after exposure for 4 h, the lasing efficiencies of **54b** and **54c** decreased by 21 and 15%, respectively, whereas that of **21** was reduced by 36% of its initial value. Overall, the comparative results of the lasing efficiencies and photostabilities of the Bodipy dyes (**Figure 2.2.4.2**) clearly showed the supremacy of the new B-substituted dyes, especially **54c** over the commercial dye **21**.

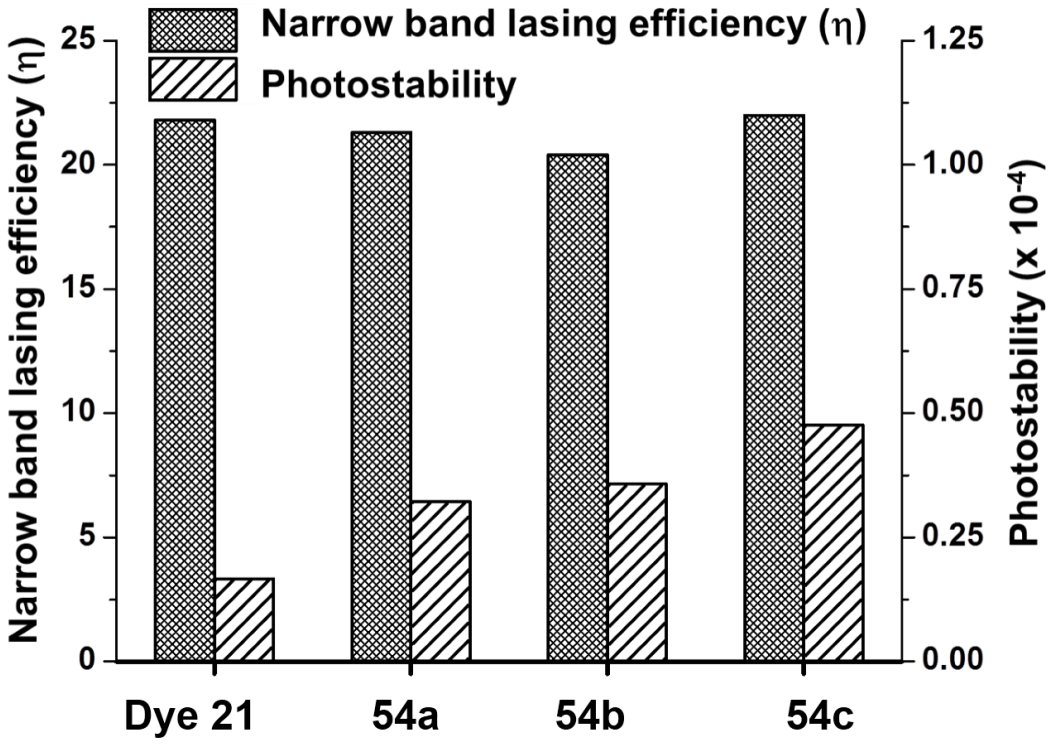

Figure 2.2.4.2 Narrow band lasing efficiencies (η) and photostabilities (Φ^{-1}) of the Bodipy dyes **21** and **54a**–**c** in EtOH.

Given that the *in situ* generated $^1O_2$ is responsible for the photodegradation of the dyes, the higher stabilities of **54b** and **54c** may be due to their lower 1) reaction rates with $^1O_2$ and/ or 2) $^1O_2$ generation capacities. Hence, these factors were investigated in comparison with dye **21** and the results are discussed below.

2.2.5. Electrochemical characteristics

Cyclic voltammetric analysis of Bodipy dyes **21**, **54b** and **54c** showed a reversible peak in each case in the anodic portion of the cyclic voltammograms (**Figure 2.2.5.1**), which was assigned to one-electron oxidation of the Bodipy unit.[61] The corresponding oxidation potentials ($E_{ox}°$) reveal that the boron substitution has a negative effect on the oxidation potentials. Dye

54b (E_{ox}° = 0.95 V) was more easily oxidised than **21** (E_{ox}° = 1.02 V) by 70 mV and the presence of the electron-donating aryl group at the meso position further reduced the E_{ox}° of dye **54c** (E_{ox}°= 0.83 V), making it more prone to oxidation than **54b** by 120 mV. The above data suggest the trend in probability of oxidation of the dyes increases in the order **21** < **54b** < **54c**, which is opposite to that observed experimentally. Other factors, like the rate of reaction with $^1O_2$ and the $^1O_2$ generation capacity of the dyes might play a predominant role in the relative photostabilities of the dyes. To investigate these, we carried out theoretical calculations on the ground and excited states of the dyes as well as $^1O_2$, and characterised the triplet states of the dyes by pulse radiolysis.

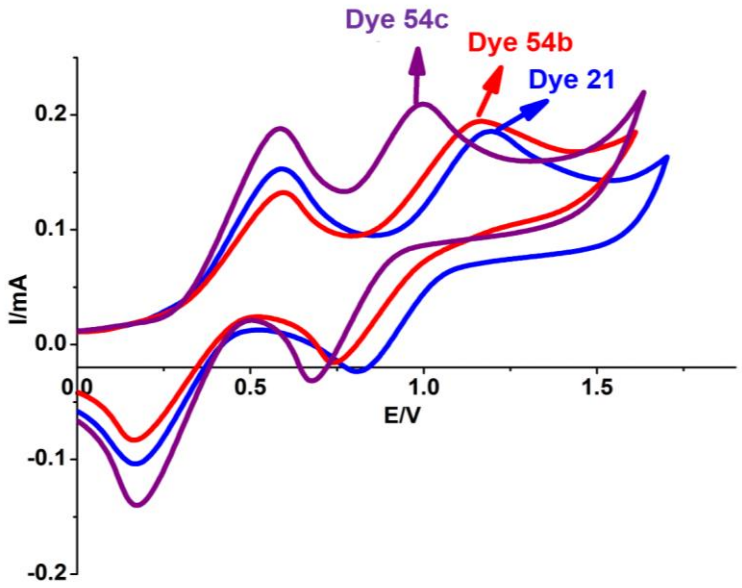

Figure 2.2.5.1 Cyclic voltammograms of the Bodipy dyes **21**, **54b** and **54c** in CH_2Cl_2 at room temperature.

2.2.6. Theoretical interpretations

The ground-state (S_0) minimum- energy structures **21-R**, **54b-R** and **54c-R** (**Figure 2.2.6.1**) of the Bodipy dyes **21**, **54b** and **54c**, respectively, were optimised by carrying out DFT

calculations. These conformers were subsequently used to study the excited-state structures and properties of the dyes in the lowest singlet (S_1) and triplet (T_1) states. After characterising all the ground-state features, the reaction course of the dyes with $^1O_2$ was investigated by placing the $^1O_2$ in the proximity of the most vulnerable position, the C7'=C8 double bond, of each dye (**Figure 2.2.6.1**). The transition-state (TS) structures were identified as **21-TS**, **54b-TS** and **54c-TS**, and the peroxides **21-P**, **54b-P** and **54c-P** were identified as the reaction products obtained from **21**, **54b** and **54c**, respectively (**Figure 2.2.6.1**). In all the reactions, the TSs are formed by partial cleavage of the C7'=C8 π bond and formation of the C7'–O2 bond as the initial events, as supported by the bond lengths (**Table 2.2.6.1**). With dye **21**, the C8=C7' (1.41 Å) and O1O2 (1.21 Å) bond lengths increase to 1.53 and 1.41 Å, respectively, in the TS. The distance between C7' and O2 (1.46 Å) indicated formation of a σ bond between them. The C8 and O1 atoms are too far apart (2.64 Å) to form a stable bond, but gradually move closer for bond formation (bond length = 1.51 Å), furnishing the peroxide compound **21a-P**. Charge density calculations further established the mechanism. According to the calculations, in the TS, the electron density at O1 is more than that at O2, whereas the electron density at C8 is less than that in **21a-R**. This is consistent with the proposed mechanism (**Figure 2.2.6.1**). After the formation of the C8–O1 bond, O1 and O2 become electronically similar, as is evident from the charge densities on the two atoms. However, most importantly, the model suggests a much higher (more than two-fold) activation energy for the reaction between $^1O_2$ with **54b** (5.86 kcal mol^{-1}) or **54c** (5.35 $kcalmol^{-1}$) than for **21** (2.45 kcal mol^{-1}) (**Figure 2.2.6.2**). This would make dye **1a** the most vulnerable to oxidation by singlet oxygen, which explains the observed trend in the photostabilities of the dyes: **21** << **54b** ≈ **54c**.

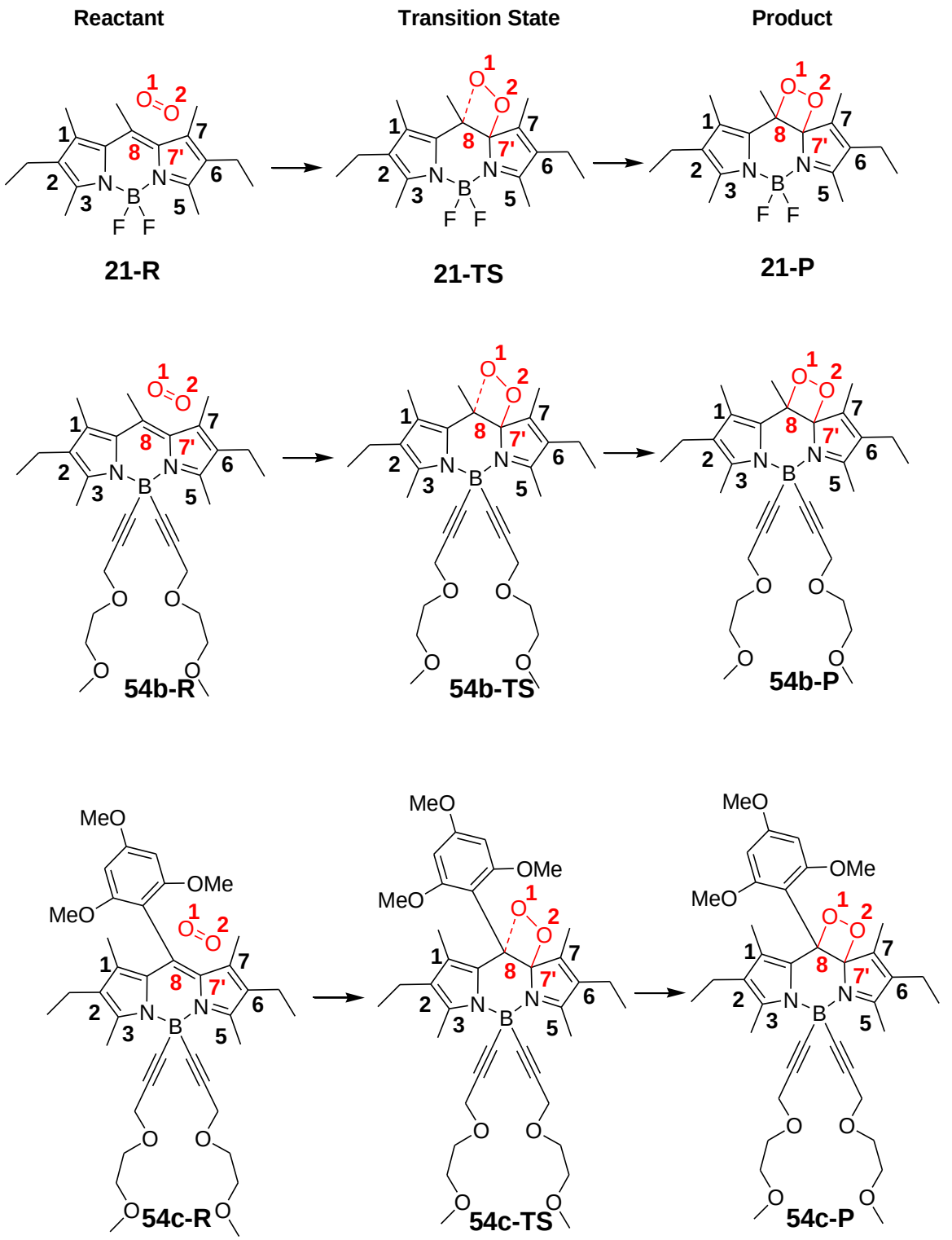

Figure 2.2.6.1 Reaction mechanism of the Bodipy dyes **21**, **54b** and **54c** with $^1O_2$.

Table 2.2.6.1: Changes of bond lengths and atomic charges during the reaction of the dye **21** with $^1O_2$.

	Bond length				**Atomic charge**			
Dye	r (Å) (C8-O1)	r (Å) (C7'-O2)	r (Å) (C8-C7')	r (Å) (1O-2O)	C-7' (a.u.)	C-8 (a.u.)	O-1 (a.u.)	O-2 (a.u.)
21-R	-	-	1.41	1.21	0.104	-0.193	-	-
21-TS	2.64	1.46	1.53	1.41	0.087	-0.111	-0.430	-0.209
21-P	1.51	1.44	1.55	1.49	0.187	-0.144	-0.204	-0.193

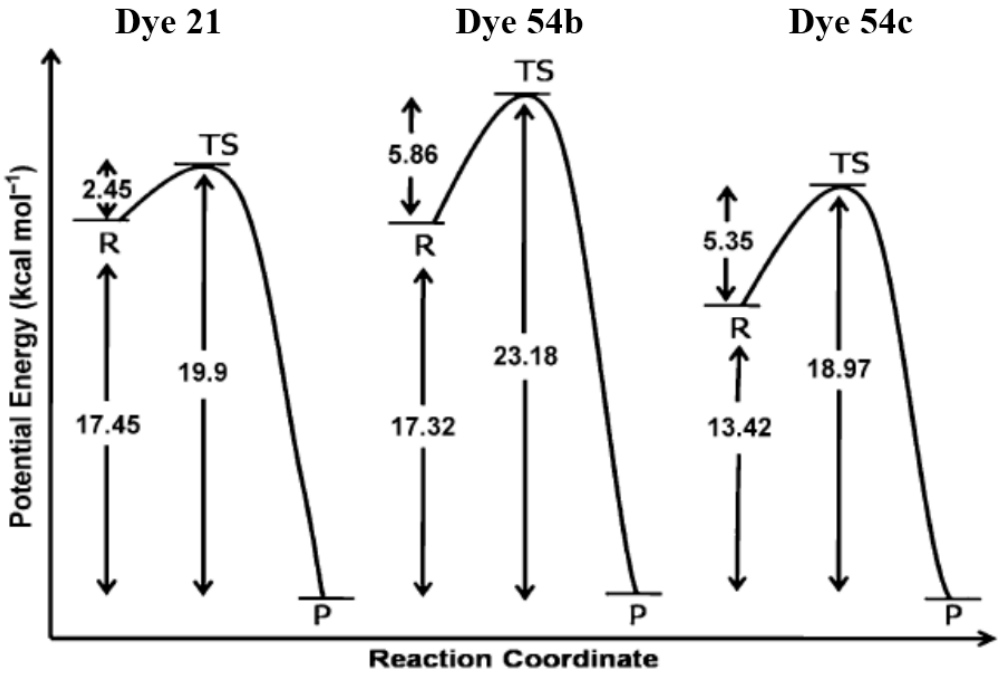

Figure 2.2.6.2 Change of potential energies during the reaction of the Bodipy dyes **21**, **54b** and **54c** with $^1O_2$.

2.2.7. Pulse radiolysis studies

The triplet states determine 1) the amount of $^1O_2$ generated by the dyes through energy transfer to dissolved O_2 and also 2) the reduction in the lasing efficiency by absorbing the lasing

photons. Hence, triplet-state studies can provide valuable information on the lasing characteristics and photostabilities of the Bodipy dyes. Triplet state spectroscopy and the energy-transfer processes of the dyes **21**, **54b** and **54c** were investigated by pulse radiolysis in benzene solutions. Radiolysis of benzene gives a high yield of the triplet state (G = 4.2/100 eV) with an energy of 82 kcal mol^{-1}, which can generate dye triplets by energy transfer. However, owing to the low lifetime (τ = 3 ns) of the benzene triplet, a high concentration of solute is required. This limitation can be overcome by using a triplet sensitizer such as biphenyl (E_T = 65 kcal mol^{-1}) along with the solute. The triplet states of the laser dyes **21**, **54b** and **54c** in benzene solution were generated by pulse radiolysis in the presence of biphenyl. Under these conditions, biphenyl triplets are initially formed, which, in turn, transfer energy to generate the triplet states of the Bodipy dyes. The triplet states of the dyes show absorption at 550–750 nm. The spectra consist of a single peak with the λ_{max} at around 720 nm for **21** and **54b**, however, the λ_{max} (640 nm) of the triplet species of **54c** was blueshifted by 80 nm (**Table 2.2.7.1**). Thus, the T–T absorption spectrum of dye **54c** overlaps considerably with its fluorescence spectrum. This would increase the reabsorption loss of the lasing photons, which explains the requirement of dye **54c** to have a higher optical density for an equivalent lasing efficiency to that of dye **21**. The other noticeable feature of the spectra is the appearance of a bleaching signal (negative signal) immediately after the pulse. The bleaching signal obeys a first-order decay law (at low doses) at wavelengths at which light absorption by the ground state is much higher than the transient absorption. The triplet-state extinction coefficients at λ_{max} and the rate constants for energy transfer from the biphenyl triplet to the dye (k_{et}) and from the dye (**21**, **54b** and **54c**) to $^1O_2$ k (^{3}Dye → O_2) were calculated from experimental data and are presented in **Table 2.2.7.1**. Interestingly, the value of k (^{3}Dye → O_2) decreases gradually from **21** to **54c**. The values of k (^{3}Dye → O_2) for the dyes

54b and **54c** are two- and four-fold less than that of **21**. This suggests that relative to dye **21**, dyes **54b** and **54c** generated two and four times less $^1O_2$. Thus, according to the $^1O_2$ generation capacity, the stabilities of the dyes would be as follows: **21** < **54b** < **54c**. Taken together, the above data reveal that despite being more prone to oxidation, dyes **54b** and **54c** are more photostable than **21** due to their lower reaction rates with $^1O_2$ and lower $^1O_2$ generation capacity.

Table 2.2.7.1: Triplet state data of Bodipy dyes **21**, **54b** and **54c**.

Dye	**λ_{max} (nm)**	**ε_{max} ($LM^{-1}cm^{-1}$)**	**k_{et} (^{3}B.P→Dye) ($LM^{-1}s^{-1}$)**	**k (^{3}Dye→O_2) ($LM^{-1}s^{-1}$)**
21	720	7880	4.1×10^9	1.9×10^{-9}
54b	720	8020	7.7×10^9	1.0×10^{-9}
54c	640	8900	2.8×10^9	0.5×10^{-9}

2.3. Red-shifted BODIPY dyes

In this part, we aimed to design and synthesize a new series of dyes emitting in the red spectral region for lasing application. There are few red emitting fluorescent dyes are commercially available such as, Rhodamine dyes, Texas Red (λ_{em} = 615 nm), Alexa 594 (λ_{em} = 617 nm) and Alexa 663 (λ_{em} = 647 nm) etc. But a very few red emitting dyes are available from Bodipy class of fluorophores for lasing application. The research is aimed to shift emission of the dyes to the red region while keeping their suitable properties for lasing application. There are reports, to shift the emission band of green emitting dye to longer wavelengths by attaching electron-donating groups to the Bodipy core,[9b] by rigidifying the structure,[40,62] and by extending the conjugation of the chromophore.[6b,63] But there are no any solid reports whether their fluorescence emission is of utility for the generation of laser emission. Also, these structural changes can lead to sometimes to molecules with undesired photo-physical properties. To this end, a new red shifted Bodipy dye was synthesized by incorporating a mono-styryl group at the C-3 position of the commercially available PM567 dye **21** followed by appending an ethyleneglycol moiety at the B-centre and their lasing action as well as photostability were studied. The structures of the dyes are shown in **Figure 2.3.1**.

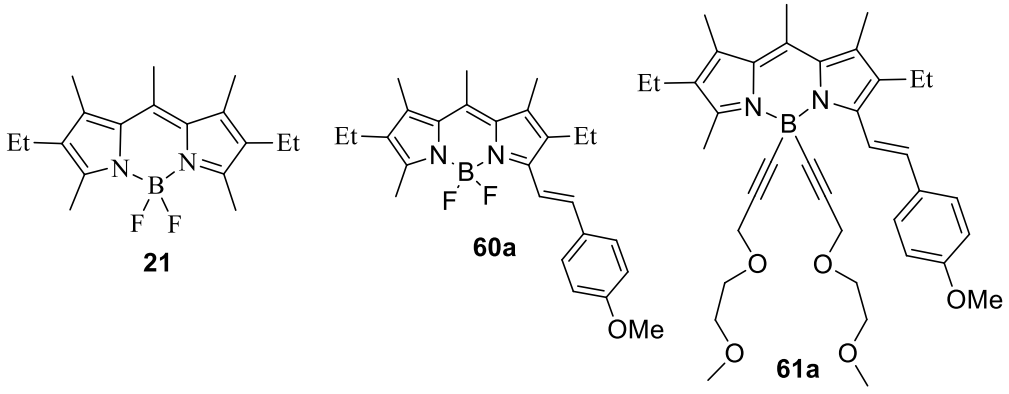

Figure 2.3.1 Chemical structures of dyes **21**, **60a** and **61a**.

2.3.1. Synthesis

The 3-styryl substituted dye **60a** was synthesized from PM567 dye **21** via the Knoevenagel-type condensation with *p*-anisaldehyde in a mixture of toluene and piperidine (**Scheme 2.3.1.1**). Since, 3,5-methyl protons are equally prone for the reaction leading to formation of distyryl **60b** derivative along with monostyryl derivative **60a**. Therefore, to improve the yield of monostyryl product, the effects of reaction time and aldehyde concentrations were studied, and the results are shown in **Table 2.3.1.1**. Introduction of one styryl group at C-3 as in the dye **60a** reduced its solubility in EtOH. Hence its lasing efficacy could not be studied. To overcome the problem, dye **61** was synthesized by subjecting the dye **60a** for nucleophilic substitution of the fluorine atoms by reaction with the Grignard reagent prepared from 2,5-dioxaoct-7-yne (**Scheme 2.3.1.2**). The ^{1}H NMR of compound **61a** showed characteristic peak of propargylic protons at δ 4.10 (**Figure 2.3.1.1 a-b**). The Bodipy dyes with such modifications at B-centre are known to be chemically more stable than the corresponding BF_2 congeners.

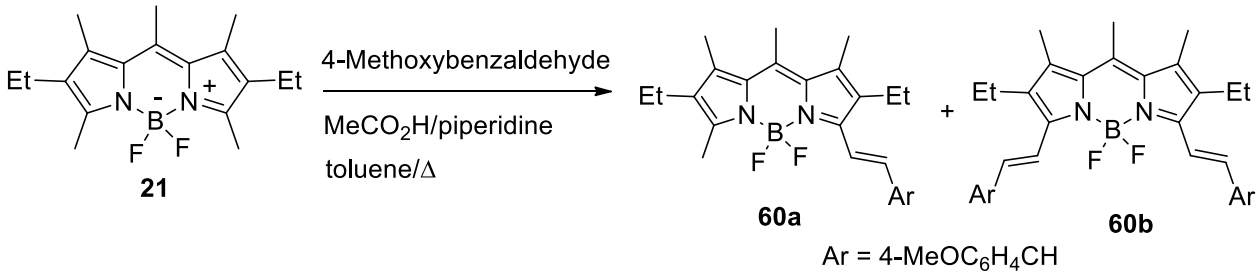

Scheme 2.3.1.1 Synthesis of compounds **60a** and **60b**.

Table 2.3.1.1: Effect of concentration of corresponding aldehyde in the reaction

Sr. no.	Amount of PM567	Equivalent PM 567 : MeOPhCHO	Time	% Yield of 60a
1	100 mg	1:1	3 h	4.3
2	100 mg	1:1	5 h	Degraded
3	100 mg	1:1.5	3 h	7.0
4	100 mg	1:1.8	3 h	14.7
5	100 mg	1:2	3 h	13.1
6	100 mg	1:2.5	3 h	11.9

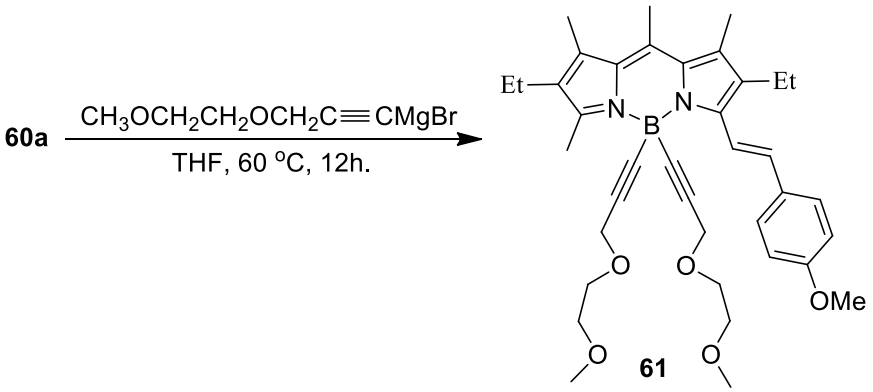

Scheme 2.3.1.2 Synthesis of compound **61**

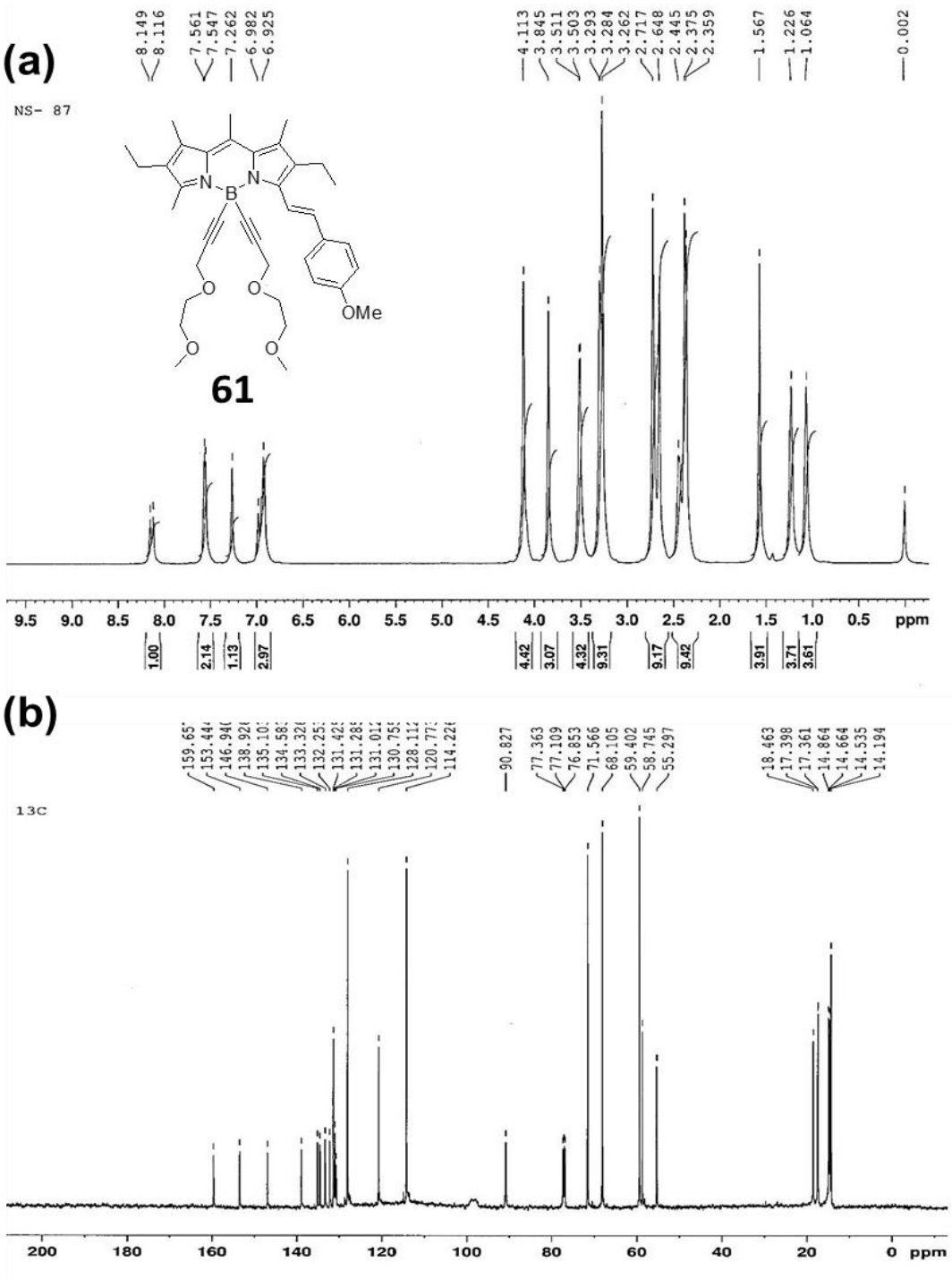

Figure 2.3.1.1 The NMR spectrum of **61** (a) ^{1}H NMR, (b) ^{13}C NMR.

2.3.2. Photophysical characteristics

The photophysical parameters of all the dyes are listed in **Table 2.3.2.1**. The shapes of the absorption spectra of the dyes **60a**, **60b** and **61a** were similar to that of the commercially available dye **21** but the maxima were bathochromically shifted by 56.5 nm, 56 nm (for **60a** and **61a** respectively) and much higher 122 nm (for **60b**) with extension of conjugation (**Figure 2.3.2.1**). The fluorescence spectra of the dyes were also identical throughout the series, and entirely consistent with fluorescence from the Bodipy subunit. The spectral shifts to higher wavelengths are a result of the extension of the delocalized electronic π-system to the styryl group. The non-conjugating effect of substitution at B-centre was evident from the similarities of the absorption and fluorescence spectra of the dyes **60a** and **61**. For compound **60a**, **60b** and **61** the strong absorption band centered near 350 nm can probably be assigned to the π→π* transition of the styryl moieties and the overlapped $S_0 \rightarrow S_2$ (π→π*) transition band of the Bodipy core.

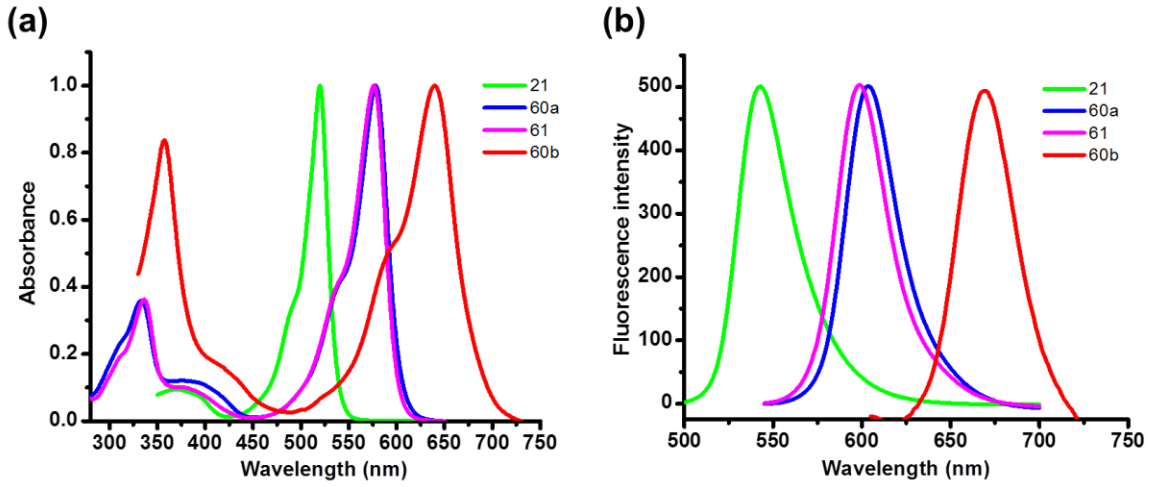

Figure 2.3.2.1 (a) Normalized absorption spectra, (b) Fluorescence spectra of dyes **21**, **60a**, **60b** and **61** in CH_2Cl_2.

Table 2.3.2.1: Photo-physical properties and photo-degradation data in ethanol

Dye	λ_{abs} (nm)	λ_{fl} (nm)	ε_{max} ($M^{-1}cm^{-1}$)	Φ_{fl}[a]	$\Delta\lambda$ (nm)	Max. laser Efficiency η (%)	Degradation Rate, (Q_{pd})
21	518.0	532	8.1×10^4	0.84	14.0	47	6.8×10^{-4}
60a	574.5	592	8.0×10^4	0.66	17.5	--	--
60b	640.0	669	9.4×10^4	0.60[a]		--	--
61	574.0	590	9.5×10^4	0.67	16.0	5	3.8×10^{-4}

[a]The fluorescence quantum yields of the dyes refer relative to that of the dye Rh101 (Φ_{fl} = 1 in EtOH).

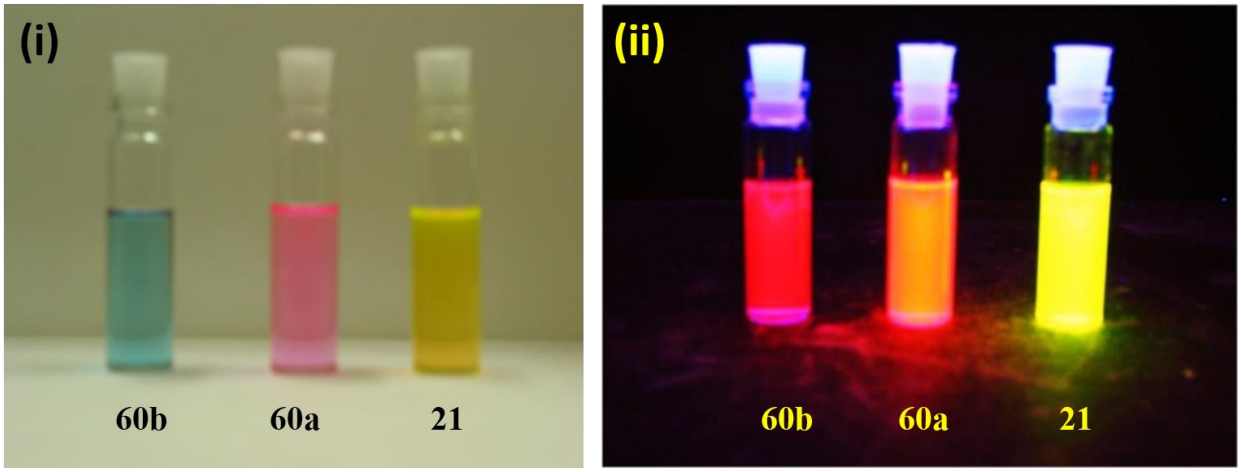

Figure 2.3.2.3 Dyes **21**, **60a** and **60b** (i) under visible light, (ii) under UV light.

2.3.3. Lasing characteristics and photo-degradation

The comparative lasing performances of dyes **21** and **61** were studied in ethanol. The lasing efficiencies of the dyes **21** and **61** were determined under an optically matched condition (O. D. = 0.24 at 532 nm with 1 mm cell). The lasing efficiency of dye **61** was significantly less than that of the dye **21**. This was surprising, given the fluorescence quantum yield of **61** was not

appreciably less than that of **21**. It is possible that the pumping wavelength (532 nm) was far from the λ_{max} (574 nm) of **61** to excite the dye efficiently. This may reduce the lasing efficiency. However, it was gratifying to note that dye **61** was much photostable than the dye **21** (**Figure 2.3.3.1**).

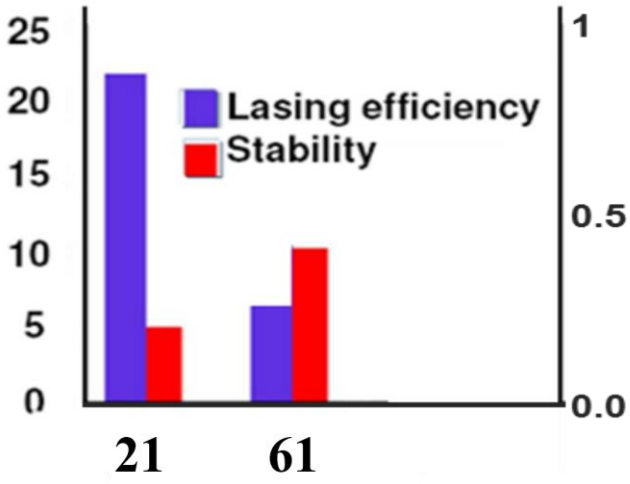

Figure 2.3.3.1 Comparative lasing efficiency and photostability of dyes **21** and **61**.

2.4. Summary

We have designed and synthesised two different congeners of the commercially available Bodipy dye PM567 by substitution at the boron centre and/or at both the boron centre and the meso position. The two congeners show high lasing efficiencies and increased photostability. The better photostabilities of the boron-substituted dyes **54b** and **54c** have been rationalised by theoretical calculations and pulse radiolysis studies. The substitution at the boron centre reduced the $^1O_2$ generation capacity of the dyes and their reaction rates with $^1O_2$, enhancing the lifetimes of these dyes under lasing conditions. These findings will be helpful for the future development of photostable Bodipy dyes. The lasing efficiency of the new red shifted dye **61** was very less, although its photostability was better than that of the precursor dye.

2.5. Experimental

2.5.1. General details

Laser grade PM567 (Exciton), rhodamines 101 and 6G (Lambda Physik) were used without any further purification. Spectroscopic and chromatographic analyses revealed their purities to be >99%. All other chemicals and spectroscopic grade solvents were purchased from Aldrich, Merck or Sigma, and used without any further purification. The IR spectra were recorded as thin films with a JASCO Model A-202 FT-IR spectrophotometer. Unless otherwise mentioned, the ^{1}H NMR (200 MHz) and ^{13}C NMR (50 MHz) spectra were recorded in $CDCl_3$ with a Bruker AC-200 instrument and the data are presented in terms of chemical shift in δ (ppm), coupling constant (J in Hz) and multiplicities. The mass spectra (70 eV) were recorded with a MD-80 Fission instrument. The electrochemical analysis was done in Autolab PGSTAT 302N instrument. CHN analyses were carried out using Thermo Finnigan Flash EA1112 series. The spectrophotometric analyses were carried out at 25 ^{o}C with a Jasco V-550 UV-vis spectrophotometer and a Jasco FP 6500 spectrofluorometer using quartz cells of 1 cm path length. All anhydrous reactions were carried out under Ar using freshly dried solvents. The column chromatography and thin layer chromatography (TLC) were performed using column grade silica gel (40-63 μm) and silica gel-coated aluminum plates with fluorescent indicator respectively.

2.5.2. Synthesis

4,7-Dioxaoct-1-yne (55). To a stirred suspension of NaH (0.288 g, 12.0 mmol) in THF (100 mL) was added ethyleneglycol monomethyl ether (0.760 g, 10.0 mmol) in THF (50 mL). After stirring the mixture for 3 h, propargyl bromide (1.19 g, 10.0 mmol) was added into it and the mixture stirred for another 12 h. The mixture was diluted with H_2O (50 mL) and extracted with CH_2Cl_2 (50 mL). The organic layer was dried, concentrated, and the residue distilled (60 ^{o}C/ 30

mm) to furnish **55**. Yield: 0.855 g (75%); colorless liquid; IR: 2925, 2175 cm^{-1}; ^{1}H NMR: δ 2.41 (t, *J* = 2.4 Hz, 1H), 3.38 (s, 3H), 3.52-3.59 (m, 2H), 3.64-3.73 (m, 2H), 4.18 (d, *J* = 2.4 Hz, 2H); ^{13}C NMR: δ 57.8, 58.3, 68.4, 71.1, 74.3, 79.2; EI-MS (m/z): 114 $[M]^{+}$. Anal. Calcd. for $C_6H_{10}O_2$: C, 63.14; H, 8.83%. Found: C, 63.25; H, 8.79%.

Ethyl 4-Acetyl-3,5-dimethyl-1H-pyrrole-2-carboxylate (56). To a stirred cooled (0 °C) solution of ethyl acetoacetate (4.9 g, 0.038 mol) in acetic acid (10 mL) was added a cold solution of $NaNO_2$ (2.8 g, 0.041 mol) in H_2O (10 mL). After stirring the mixture for 24 h at 25 °C, acetyl acetone (3.8 g, 0.038 mol) and zinc dust (5.3 g) were added, and the mixture was stirred at 60 °C for 1 h. The mixture was brought to room temperature and extracted with $CHCl_3$ (3 × 10 mL) Concentration of the extract in vacuo followed by crystallization from $CHCl_3$ gave **56**. Yield: 6.35 g (80%); white solid; mp: 142 °C (lit.[64] mp: 143-144 °C); IR: 3302, 1678, 1646 cm^{-1}; ^{1}H NMR: δ 1.36 (t, *J* = 7.1 Hz, 3H), 2.43 (s, 3H), 2.51 (s, 3H), 2.57 (s, 3H), 4.34 (q, *J* = 7.1 Hz, 2H), 9.41 (broad s, 1H, NH); ^{13}C NMR: δ 12.5, 14.1, 14.6, 30.9, 60.2, 117.8, 123.1, 129.3, 138.9, 162.0, 195.4; MS (m/z): 209 $[M]^{+}$.

2,4-Dimethyl-3-acetyl-1H-pyrrole (57). A mixture of **56** (3.0 g, 0.014 mol) and KOH (1.5 g, 0.027 mol) in ethylene glycol (10 mL) was heated at 160 °C for 4 h. After cooling, the mixture was extracted with $CHCl_3$ (3 × 10 mL), and the extract was washed with H_2O (2 × 10 mL) and brine (1 × 5 mL) and dried. Removal of solvent gave pure **57**. Yield: 1.86 g (97%); white solid; mp: 96 °C; IR: 3300, 1680 cm^{-1}; ^{1}H NMR: δ 2.26 (s, 3H), 2.43 (s, 3H), 2.50 (s, 3H), 6.36 (s, 1H), 8.52 (broad s 1H, NH); ^{13}C NMR: δ 13.7, 15.2, 30.7, 115.0, 120.5, 120.7, 136.2, 195.9; MS (m/z): 137 $[M]^{+}$. Anal. Calcd. for $C_8H_{11}NO$: C, 70.04; H, 8.08; N, 10.21%. Found: C, 70.10; H, 8.02; N, 10.17%.

2,4-Dimethyl-3-ethyl-1H-pyrrole (58). To a stirred suspension of $LiAlH_4$ (0.333 g, 8.76 mmol) in dry THF (20 mL) was added **57** (1.0 g, 7.30 mmol) in THF (10 mL). The mixture was refluxed for 4.5 h and brought to room temperature, and the excess hydride was decomposed with aqueous saturated Na_2SO_4. The mixture was extracted with $CHCl_3$ (2 × 10 mL), and the extract was concentrated in vacuo. The residue was subjected to column chromatography (neutral Al_2O_3, hexane-EtOAc) to furnish **58**. Yield: 0.673 g (75%); brown liquid; IR: 3377, 1689, 1644 cm^{-1}; ^1H NMR: δ 1.23 (t, *J* = 7.4 Hz, 3H), 2.18 (s, 3H), 2.28 (s, 3H), 2.54 (q, *J* = 7.4 Hz, 2H), 6.48 (s, 1H), 7.51 (broad s, 1H, NH); ^{13}C NMR: δ 10.1, 10.9, 15.5, 17.3, 112.8, 117.4, 120.1, 123.1; MS (m/z): 123 $[M]^+$.

2,6-Diethyl-4,4-difluoro-1,3,5,7-tetramethyl-8-(2',4',6'-trimethoxyphenyl)-4-bora-3a,4a-diaza-s-indecene (54a). A mixture of **58** (0.450 g, 3.7 mmol), 2,4,6-trimethoxybenzaldehyde (0.363 g, 1.85 mmol) and TFA (0.012 g, 0.10 mmol) in CH_2Cl_2 (20 mL) was stirred at room temperature for 24 h. DDQ (0.420 mg, 1.85 mmol) was added to the resulting deep-red solution and stirring continued for 4 h. The mixture was treated with Et_3N (0.5 mL), stirred for another h, $BF_3.Et_2O$ (0.762 mL, 4.6 mmol) was added in portions over 4 h and stirred at room temperature overnight. The resulting dark mixture was washed successively with aqueous saturated $NaHCO_3$ (2 × 10 mL), H_2O (2 × 10 mL) and brine (5 mL), and dried. Removal of the solvent in vacuo followed by column chromatography of the residue (silica gel, hexane/EtOAc) furnished **54a**. Yield: 0.19 g (22%); orange needles (hexane); mp: 157 °C; ^1H NMR: δ 1.05 (t, *J* = 7.6 Hz, 6H), 1.57 (s, 6H), 2.15 (s, 6H), 2.37 (q, 4H, J) 7.6 Hz), 2.48 (s, 6H), 3.76 (s, 3H), 6.08 (s, 1H), 6.93 (s, 1H); ^{13}C NMR: δ 9.4, 12.5, 14.6, 17.3, 55.3, 92.9, 118.5, 131.6, 132.4, 136.6, 154.7,161.5; EI-MS: (m/z): 470 $[M]^+$.

General procedure of synthesis of 54b, 54c and 61a. To a solution of 2,5-dioxaoctyne (4.08 mM) in THF (10 mL) was added EtMgBr (4.08 mM, 4.08 mL 1 M in Et_2O). The mixture was heated at 60 °C for 2 h followed by addition of the suitable Bodipy dye (0.82 mM) and further for 18 h at 60 °C. The resulted dark mixture was thoroughly washed successively with aqueous saturated NH_4Cl (1 X 20 mL), H_2O (1 × 20 mL), brine (1 × 20 mL) and dried. Removal of solvent in vacuo followed by column chromatography of the residue (silica gel, hexane-EtOAc) furnished the respective B-substituted dyes. **54b**. Yield: 62%; red squares (benzene/hexane); mp : 154 °C; IR: 2927, 2167 cm^{-1}; ^1H NMR: δ 1.00 (t, *J* = 7.6 Hz, 6H), 2.18 (s, 6H), 2.35 (q, *J* = 7.6 Hz, 4H), 2.59 (s, 3H), 2.66 (s, 6H), 3.34 (s, 6H), 3.49-3.55 (m, 4H), 3.59-3.65 (m, 4H) 4.16 (s, 4H); ^{13}C NMR: δ 13.8, 14.5, 14.9, 17.1, 17.3, 58.8, 59.5, 68.4, 71.6, 90.7, 129.9, 132.3, 134.2, 139.5, 151.5; ^{11}B NMR (96 MHz): δ -13.4 (s); EI-MS (m/z): 506 $[M]^+$; Anal. Calcd. for $C_{30}H_{43}BN_2O_4$:C, 71.14; H, 8.56; N, 5.53%. Found: C, 71.11; H, 8.52; N, 5.51%.

54c. Yield: 70%; red needle (CH_2Cl_2/cyclohexane); mp: 149 °C; IR: 2948, 2835, 1632 cm^{-1}; ^1H NMR: δ 1.01 (t, *J* = 7.5 Hz, 6H), 1.44 (s, 6H), 2.30 (q, *J* = 7.5 Hz, 4H), 2.68 (s, 6H), 3.35 (s, 6H), 3.49-3.56 (m, 4H), 3.62-3.68 (m, 10H), 3.87 (s, 3H), 4.19 (s, 4H) 6.19 (s, 2H); ^{13}C NMR: δ 10.8, 13.8, 14.7, 17.3, 55.3, 55.8, 58.8, 59.7, 68.3, 71.7, 90.6, 106.2, 129.4, 131.6, 135.3, 152.2, 158.1, 162.1; ^{11}B NMR (96 MHz): δ -13.2 (s); EI-MS (m/z): 659 $[M+1]^+$, 658 $[M]^+$; Anal. Calcd. for $C_{38}H_{51}BN_2O_7$: C, 69.30; H, 7.80; N, 4.25%. Found: C, 70.00; H, 7.65; N, 4.44%.

61a. Yield: 60%; mp: 225 °C; IR: 2959, 1636 cm^{-1}; ^1H NMR (500 MHz, $CDCl_3$): δ 1.05 (t, *J* = 7.5 Hz, 3H), 1.22 (t, *J* = 7.5 Hz, 3H), 2.35-2.43 (m, 8H), 2.64-2.70 (m, 8H), 3.25-3.28 (m, 10H), 3.49-3.50 (m, 4H), 3.83 (s, 3H), 4.10 (s, 4H), 6.91-6.97 (m, 3H), 7.54 (d, *J* = 7.0 Hz, 2H), 8.10 (d, *J* = 16.5 Hz, 1H); ^{13}C NMR (125 MHz): δ 14.2, 14.5, 14.7, 14.9, 17.3, 17.4, 18.5, 55.3, 58.7, 59.4, 68.1, 71.6, 90.8, 114.2, 120.7, 128.1, 130.8, 131.0, 131.3, 131.4, 132.2, 133.3, 134.6, 135.1,

138.9, 146.9, 153.4, 159.6. EI-MS (m/z): 625 $[M+1]^+$; Anal. Calcd. for $C_{26}H_{31}BF_2N_2O$: C, 73.01; H, 7.92; N, 4.29%. Found: C, 73.07; H, 7.91; N, 4.48%.

2,6-Diethyl-4,4-difluoro-3-*p*-methoxystyryl-1,5,7,8-tetramethyl-4-bora-3a,4a-diaza-s-indecene 60a. A mixture of **21** (1.0 mmol), *p*-anisaldehyde (1.1 mmol), glacial acetic acid (0.5 mL) and piperidine (3.5 mL) was refluxed in toluene (35 mL) with simultaneous azeotropic removal of water formed during the reaction. After the consumption of **21**, H_2O (100 mL) was added into the reaction mixture, which was extracted with $CHCl_3$ (3 × 20 mL). The organic layer was dried and concentrated in vacuo to give a residue, which on column chromatography (silica gel, hexane-EtOAc) furnished the respective styryl derivatives. pink cuboidals (CH_2Cl_2/cyclohexane). Yield: 13%; mp: 235 °C; IR: 2961, 1635, 1606, 1478 cm^{-1}; ^1H NMR: δ 1.05 (t, *J* = 7.5 Hz, 3H), 1.20 (t, *J* = 7.5 Hz, 3H), 2.32-2.47 (m, 8H), 2.53 (s, 3H), 2.57-2.74 (m, 8H), 3.83 (s, 3H), 6.87 (d, *J* = 8.7 Hz, 2H), 7.07 (d, *J* = 16.8 Hz, 1H), 7.48-7.62 (m, 3H); ^{13}C NMR: δ 12.5, 14.0, 14.4, 14.7, 17.1, 18.3, 55.3, 114.2, 118.1, 128.4, 130.5, 132.4, 132.7, 133.1, 134.2, 136.5, 136.7, 138.8, 148.0, 153.2, 159.9. EI-MS (m/z): 437 $[M+1]^+$, 417 $[M-19]^+$. Anal. Calcd. for $C_{26}H_{31}BF_2N_2O$: C, 71.57; H, 7.16; N, 6.42%. Found: C, 71.10; H, 7.21; N, 6.18%.

2.5.3. Photophysical studies

The absorption and emission spectra of the dyes (~10^{-6} M) in various solvents were measured using a 1 cm quartz cuvette. The fluorescence quantum yields (Φ_{fl}) of the dyes **21, 54b** and **54c** relative to that of the reference dye **21** and the molar extinction coefficients (ε_{max}) were determined in ethanol. The excited state (S_1) lifetimes of **21, 54b** and **54c** in ethanol were determined by the time-resolved fluorescence measurements, carried out using an LED based time-correlated single-photon-counting (TCSPC) spectrometer. The fluorescence decays were measured with a 490 nm LED (1 MHz) excitation source and a TBX4 detection module coupled

with a special Hamamatsu PMT. The instrument response function was 1.2 ns at fwhm. Following deconvolution analysis of the fluorescence decays, the time resolution of the present setup was ~50 ps. All the measurements were carried out at ambient room temperature (298 ± 1 K) using a microprocessor based temperature controller.

2.5.4. Lasing studies

The lasing studies of the dyes **21**, **54b** and **54c** in ethanol were carried out using a constructed narrow band dye laser set up, transversely pumped by the second harmonic (at 532 nm) output of a Q-switched pulsed Nd:YAG laser at a repetition rate of 10 Hz with ~7 mJ pulse energy and 5-7 ns FWHM pulses. All laser data for the dyes in ethanol were measured using the indigenously made dye laser set up, schematically shown in **Figure 2.4.1**. The dye laser was constructed in grazing-incidence-grating configuration (with a grating of 2400 lines/mm), with a 25X 4-prisms pre-expander. The pump and dye laser powers were measured by the same power meter (OPHIR). The tuning curve of each dye solution was obtained by scanning the wavelength of dye laser through the gain profile of dyes and measuring the average pump and dye laser powers with the power meter. For determining the pump laser threshold (L_T) and slope efficiency (η_s) of each dye solution, the input pump energy was varied and the lasing output of each of the dyes at peak of respective gain curves was plotted as a function of pump energy.

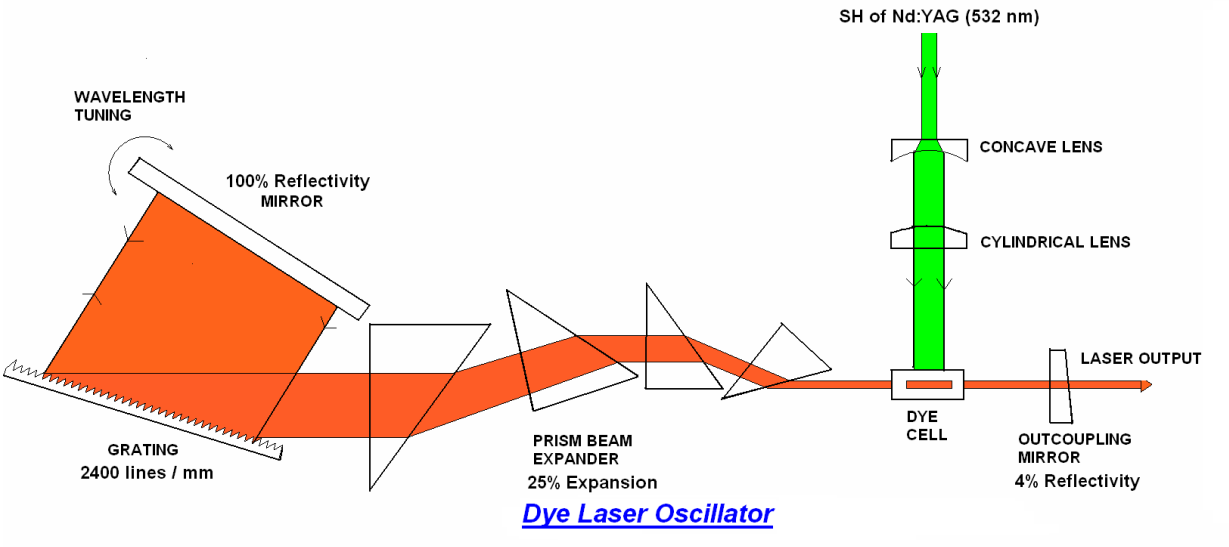

Figure 2.4.1 A schematic of the narrow band dye laser set up used for experiments.

2.5.5. Photostability studies

The quantum yield of photo-degradation (Φ_{pd}) of the dyes is defined as probability of decomposition of the dye molecules by the absorbed pump photons. Photostability is inverse of the Φ_{pd} value. A known quantity of dye solution (2 mL) in a dye laser cuvette was exposed to pump energy of 4 mJ at 532 nm. The concentration of the dye solution was chosen such that the pump beam was totally absorbed within the dye solution in the cuvette during the excitation of 4 h. The solution was stirred constantly by a teflon-coated magnetic stirrer to avoid local heating. The number of photo-degraded dye molecules in the exposed volume of the dye solutions was quantitatively estimated from the absorbances at the respective λ_{max} before and after photo-exposure for a set period of time. The reflection loss of pump beam on incident surfaces of dye cell was considered in calculating the absorbed cumulative pump photons. The extent of photo-degradation of the dye molecules was also determined by HPLC analyses.

2.5.6. Electrochemical studies

Cyclic voltammetry was done at 25 °C in deoxygenated CH_2Cl_2 containing Bu_4NClO_4 (TBAP) (0.1 M), and a solute concentration of 1-5 × 10^{-3} M. The redox potentials were standardized with ferrocene (Fc) as the internal reference, and converted to saturated Calomel electrode (SCE) assuming that $E_{1/2}$ (Fc/Fc^+) = +0.38 V SCE. The error in half-wave potentials was ±10 mV. All waves were monoelectronic.

2.5.7. Pulse radiolysis

The triplet states studies of the dyes were carried out using the nanosecond pulse radiolysis technique.[65a] The dose absorbed per pulse was determined using an aerated 0.01 mol dm^{-3} KSCN solution, taking the value of $G\varepsilon$ of $(SCN)_2$ as 2.59 × 10^{-4} m^2 J^{-1} at 475 nm.[65b] The dose was kept at 15 Gray per pulse. The dye solutions (1 × 10^{-4} M) were prepared in spectroscopy grade benzene and purged with high purity N_2 to remove dissolved oxygen. The pulse radiolysis experiments were carried out using biphenyl (5 × 10^{-3} M) as the triplet sensitizer. Formation of the dye triplets and their extinction coefficients were determined by energy transfer from the biphenyl triplet to the dyes. For studying the reactions of the dyes at triplet state with O_2, the experiments were carried using a high concentration of the dye (5 × 10^{-3} M) in the absence of a triplet sensitizer. The decay of the triplet states of the dyes were monitored at their respective λ_{max}. Concentration of oxygen in solutions was adjusted by mixing appropriate volumes of nitrogen purged dye solutions in benzene with aerated dye solutions in benzene.

2.5.8. Theoretical calculations

The minimum-energy structures of all the Bodipy dyes (**21**, **54b** and **54c**) in the ground state (S_0) were established by applying a correlated hybrid density function (B3LYP) using a Dunningtype correlation consistent atomic basis set (cc-pVDZ) for all the atoms. The quasi-

Newton–Raphson-based algorithm was used to carry out geometry optimisation on each of the dyes with various possible conformers as the initial structures. Time-dependent density functional theory (TDDFT) was used with the B3LYP density function to study the excited- state structures and the properties of the dyes in the lowest singlet (S_1) and triplet states (T_1) with the most stable ground-state (S_0) conformer as the starting structure. The same atomic basis set, cc-pVDZ, was used for all the excited-state calculations. The minimum-energy structures of these dyes taking the effect of medium into account were calculated by using the PCM model of macroscopic solvation. Excited state calculations were also carried out on these solvent-modified geometries to determine the effect of solvent by using TDDFT (B3LYP) coupled with the PCM solvent model. The minimum-energy structures of the transition states (TS) and products for the reaction of $^1O_2$ and the dyes were calculated by applying the GAMESS suite of program for ab initio electronic structure calculations.[11] The calculated TS structures were confirmed by Hessian calculations having only one imaginary frequency. Single point energy calculations were also carried out with long-range corrections added to B3LYP functional adopting a smaller size basis function (6-31G**) and the reaction barriers were observed to be in the same order.

CHAPTER-3

MESO-FUNCTIONALIZATION OF BODIPY MOLECULES

Chapter 3: Table of Contents

3.1. Preamble

The Bodipy-BF_2 compounds have not only gained recognition for their laser applications but are also valued for making opto-electronic devices.[19,67] Functionalization of the Bodipy core is an important synthetic goal as it helps in tuning their property to light- and electron transfer-induced processes, improving hydrophilicity, and anchoring to various matrices. All these widen the scope of their applications. Most of the previous research, directed to this end were targeted to functionalize the pyrrole moieties of the Bodipy core by (i) halogenation followed by organometallic coupling to introduce alkene/alkyne/arene substitutions;[39a,68a] ii) direct neucleophilic substitution;[2b,28a,68b] and (iii) *de novo* syntheses of the Bodipy core from modified pyrroles.[4a,9b] However, substitution at the pyrrole moiety may bring about undesirable changes in the physical properties, affecting the targeted function adversely. For example, presence of electron-donating groups in the pyrrole ring would reduce the fluorescence quantum yields of the Bodipy molecules especially in polar solvents.[69]

Instead, *meso*-functionalization of the Bodipy moiety with alkyl/arylalkyl moiety would provide new Bodipy-based functional molecules without perturbing the photo-electronic properties. Presence of sp/sp^2-hybridized carbon at the *meso*-position adversly affects the fluorescence and lasing efficiency of the Bodipy molecules.[42b,56a] Earlier, Liebeskind-Srogl cross-coupling of 8-thiomethylbodipy with various boronic acids has been used for *meso*-functionalization of the Bodipy moiety.[70] However, this requires reagents that are expensive and/ or have to be synthesized by multi-step routes. Direct synthesis of these types of Bodipy molecules *via* the condensation of substituted pyrroles with aliphatic aldehydes/acid chlorides has inherent limitations due to the instability of the required acid chlorides, and non-reactivity of the aldehydes.[1, 19,67a]

3.2. Meso-Substituted Bodipy Dyes

The commercially available Bodipy dyes, PM567 (**21**) and PM597 (**32**) (**Figure 3.2.1**) contain CH_3 substitutions at the pyrrole rings and at the C-8 (*meso*-) position. Mulliken-charge analysis of the 1,3,5,7,8-pentamethyl Bodipy dye showed that the electron density on the core carbon atoms follows the order: C-8> C-1/7> C-3/5. Thus, the CH_3 groups at those positions can undergo the base-catalyzed Knoevenagel-type condensation with various aryl aldehydes according to their realtive acidities C-3/C-5> C-2/C-7> C-8. This strategy provides a simpler avenue for functionalization of the Bodipy moiety, and has been exploited extensively to develop C-3/C-5 styryl Bodipy derivatives with red-shifted fluorescence.[33a,58,61,63a,71] In all these studies, the chosen Bodipy substrates had an aryl substituent at the *meso*-position, ensuring the reaction to proceed regioselectively at the C-3 and C-5 methyl groups. More recently, syntheses of tri- and tetrastyryl Bodipys by this route are also reported under specific conditions.[25a,72] However, this strategy has never been used for *meso*-functionalization. In the present studies, a conceptually new strategy is developed to drive the reaction selectively at the *meso*-position. The rationalle of the synthetic design and the efficacy of the protocol is described in this chapter.

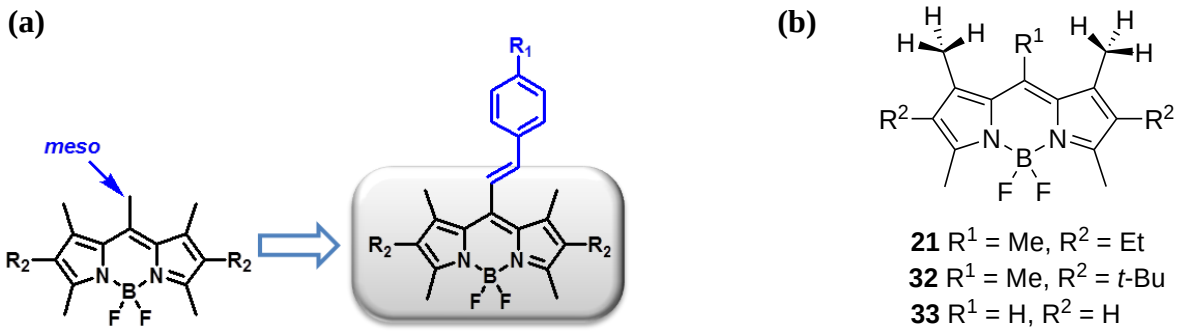

Figure 3.2.1 (a) *Meso*-substitution, (b) Chemical structures of the Bodipy dyes

3.2.1. Synthesis

As mentioned previously, the acidity factor of the Me groups of the Bodipy compounds **21** and **32** predicts that their Knoevenagel-type condensation with aldehydes would take place at those Me groups, attached to the pyrrole rings. Our previous conformational analysis revealed that in the planer form of **21**, the van der Waals radii of even the hydrogen atoms of the C-1/ C-7 and the *meso*-Me groups can overlap. This makes the *meso*-site spatially crowded to force the Me group out of the Bodipy plane. As a result, the highly twisted *meso*-substituents are largely decoupled from the Bodipy core.[73] Consistent with this, Costela *et al*. showed that compound **33**, the *meso*-H analogue of **21** is planner.[74a,b] It was envisaged that a Knoevenagel-type condensation of the Bodipy molecules at the *meso*-Me groups of the dyes **21** and **33** would alleviate such an unfavourable steric interaction. Thus, the release of steric strain may drive the condensation selectively at the *meso*-position, overriding the least acidity of the *meso*-methyl protons. In this study, we proved the hypothesis by selective *meso*-functionalization of the Bodipy dyes **21** and **32** using readily available and inexpensive reagents (**Scheme 3.2.1.1**). To this end, the steric and acidity factors were separately addressed, and discussed below.

3.2.1.1. Steric factor

Initially, following a known procedure,[33a] the condensation between **32** and **62a** was carried out in the presence of piperidine and AcOH. The dye **32** is highly twisted due to a strong co-axial steric repulsion between the 2- (and 6-) *tert*-butyl and other methyl groups at the pyrrole moieties. The steric distortion in **32** is even more in the excited state, resulting in an uncharacteristically high stokes shift (~1350 cm^{-1}), compared to other Bodipy dyes.[75] Hence, its condensation was expected to take place regio-selectively at the *meso*-position to reduce the steric strain. True to our expectation, the reaction proceeded uneventfully to furnish compound

63a, the *meso*-styryl analogue of **32** as the single product within 30 min. Due to its C_2-symmetry, the ^{1}H NMR spectrum of **63a** was much simpler, and also showed disappearance of the singlet for the C-8 methyl protons of **32** along with the appearance of an one-proton olefinic doublets at δ 6.51 (J = 16.3 Hz) as well as resonances at δ 6.92-7.02 (3H) and δ 7.41 (3H) for the other olefinic and four aryl protons, confirming the formation of vinyl bond at the *meso*-site (**Figure 3.2.1.2 a**). Appearance of the triplet at δ 1.13 in the ^{11}B NMR spectrum also confirmed that F-atoms were retained in the product (**Figure 3.2.1.2 b**). Earlier, condensation of **21** with benzaldehyde, under similar conditions furnished the 3-styryl derivative in a very low yield (<3%) along with a large number of unidentified products.[76] Thus, the present result with **32** indicated steric factor as the major driving force for the regioslelectivity of the reaction, which was also confirmed by analyzing the X-ray crystal structure of **63a** (**Figure 3.2.1.3**). The degree of steric relaxation in forming **63a** was evident from dihedral angle between the two pyrrole units (C4-C5-C6-C3) and the torsion angles of the pyrrole rings (C1-C2-C3-C4 and C6-C7-C8-C9) in **32** and **63a**. The crystallographic data revealed that the torsion angles of the pyrrole rings and the C4-C5-C6-C3 dihedral angle of **63a** was significantly less than those *viz*. 3.8^o and 172.8^o respectively of **32**.[75] These suggested that the Bodipy chromophore of **63a** was comparatively more planner than that in **32**. With these encouraging results, the synthetic strategy was extended for the condensation of **32** with **62b** as well as **62c** to obtain the *meso*-styryl Bodipy compounds **63b** and **63c** respectively. The results are shown in **Table 3.2.1.1**.

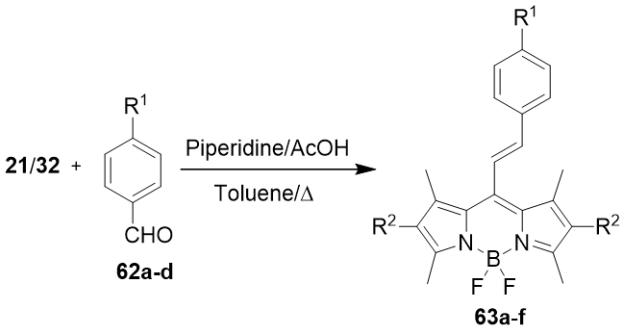

Scheme 3.2.1.1 Synthesis of the compounds 63a-f.

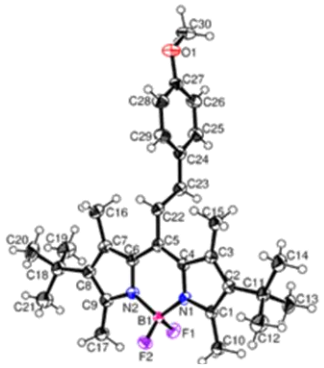

Figure 3.2.1.1 X-ray crystal structure of **63a**

Table 3.2.1.1: Synthesis of compounds **63a-f.**

Bodipy	Aldehyde, R^1	Product, R^1, R^2	% yield[a]
32	**62a**, OMe	**63a**, OMe, *t*-Bu	65
32	**62b**, OH	**63b**, OH, *t*-Bu	50
32	**62c**, NO_2	**63c**, NO_2, *t*-Bu	67
21	**62a**, OMe	**63d**, OMe, Et	10[b]
21	**62c**, NO_2	**63e**, NO_2, Et	55
21	**62d**, Br	**63f**, Br, Et	61

[a]based on isolation; [b]3% 3-styryl analogue was also isolated.

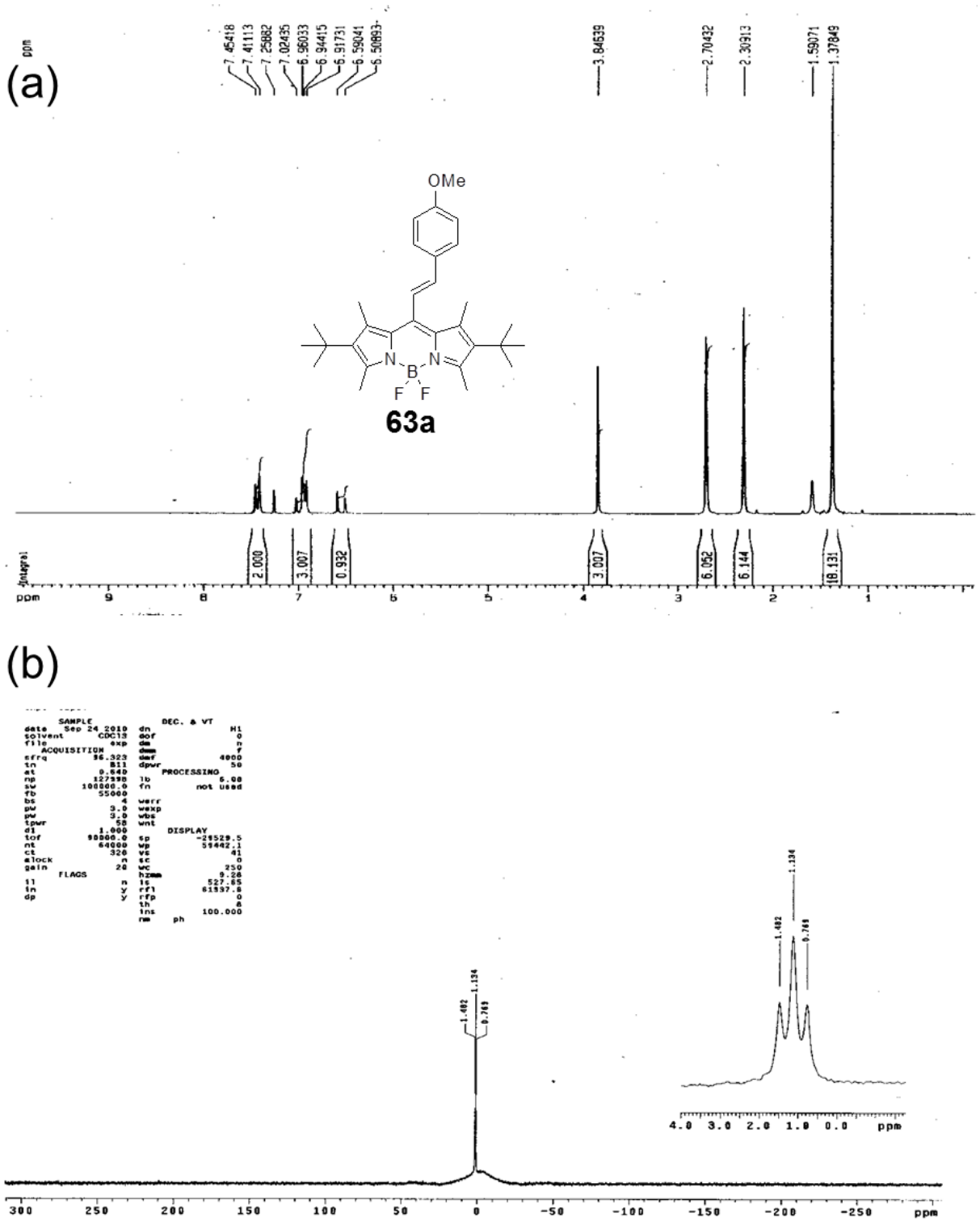

Figure 3.2.1.2 The NMR spectrum of **63a** (a) ^{1}H NMR, (b) ^{11}B NMR.

3.2.1.2. Acidity factor

To address the acidity issue, the condensation between the dye **21** and **62a**, under the same conditions was attempted. Unlike the dye **32** that has two bulky *tert*-Bu groups at C-2/ C-6, the dye **21** contains the much smaller Me groups at those positions. Hence its *meso*-position is sterically less crowded, and the acidity factor was expected to contribute to the reaction course. True to the hypothesis, the reaction afforded the *meso*-styryl (**63d**) and C-3 styryl (**63d'**) analogues of **21** in 10% and 13% yields respectively as the major isolated compounds along with some unanalyzed products (possibly poly-styryl and degradation products) (**Scheme 3.2.1.2**). Nevertheless, the formation of the compound **63d** supported the steric factor hypothesis. Formation of compound **63d** was confirmed from the ^{1}H NMR and ^{11}B NMR spectra (**Figures 3.2.1.3 a-b**). The main diagnostic features of the ^{1}H NMR spectrum (**Figure 3.2.1.4**) of **63d'** were the appearances of two triplets and two quartets for the $-CH_3$ and $-CH_2$ protons of the ethyl groups, consistent with its lack of the C_2-symmetry unlike compound **63d**. Based on the available X-ray crystallography data, the torsion angle (0.8^{o}) of the pyrrole rings in **21** is known to be much less than that in **32**.[75] Hence, the release of steric strain on condensation at the *meso*-position of the dye **21** will be less than that with **32**, explaining the distribution of the products.

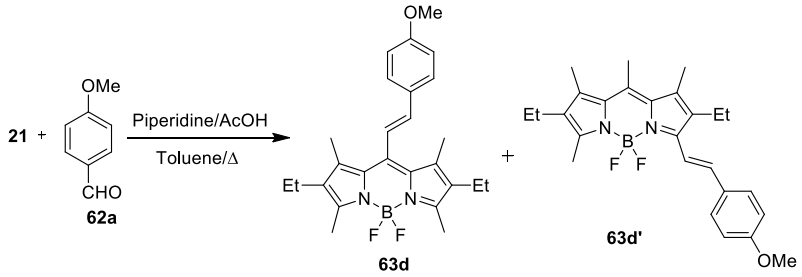

Scheme 3.2.1.2 Synthesis of the compounds **63d** and **63d'**.

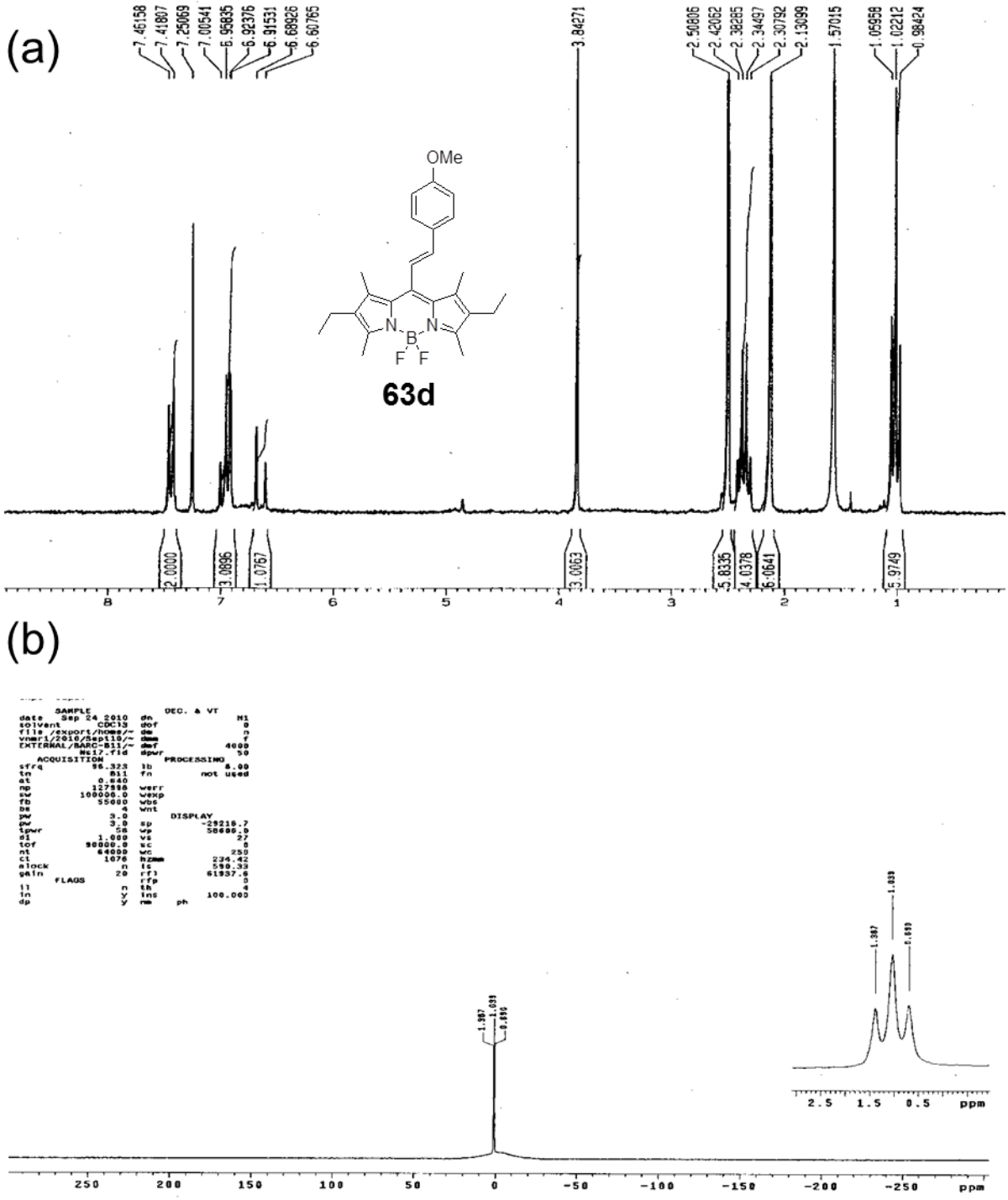

Figure 3.2.1.3 The NMR spectrum of **63d** (a) ^{1}H NMR, (b) ^{11}B NMR.

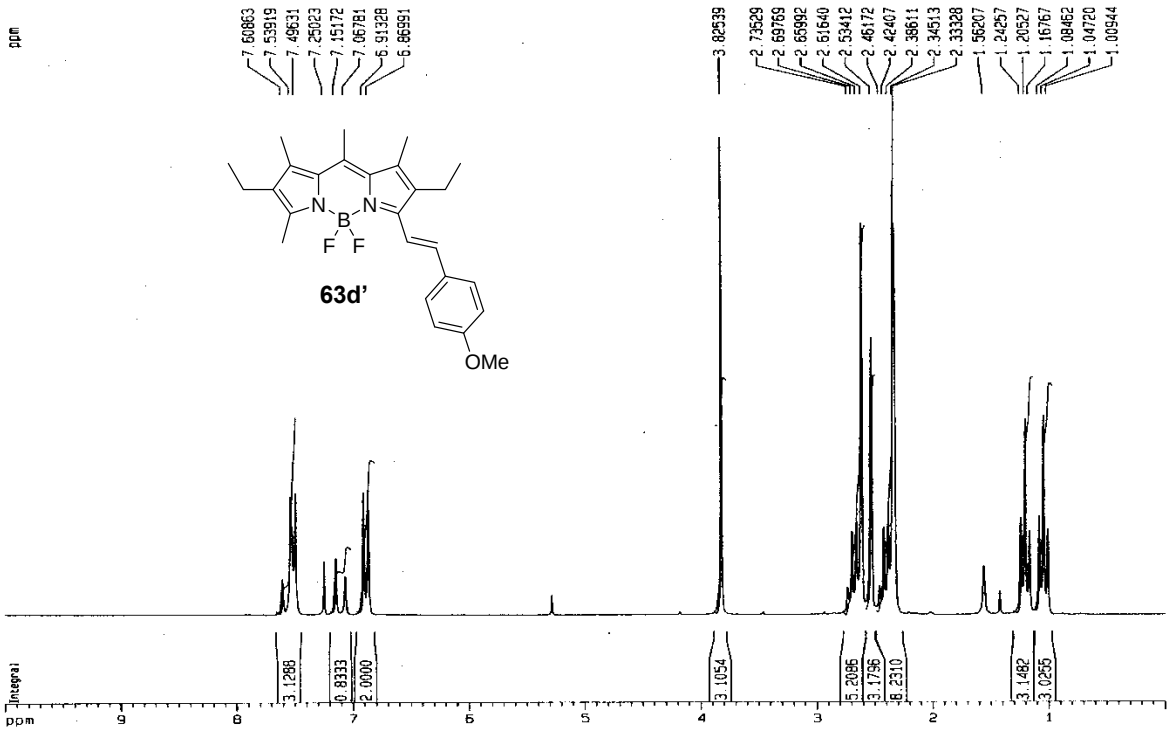

Figure 3.2.1.4 ^{1}H NMR spectrum of compound **63d'**

It was reasoned that use of more electrophilic aldehydes might negate the acidity factor of the *meso* and pyrrole Me protons to direct the condensation at the *meso*-position even with the less strained molecule **21**. To confirm this, compound **21** was subjected to condensation with **62c**. The reaction was slow and attained an equilibrium at 4 h to furnish the *meso*-styryl analogue **63e** along with the recovered dye **21** (40%). Formation of the C-3 and/or C-5 styryl derivatives was not noticed, despite the higher acidities of the designated Me protons. This also established that relaxation of steric strain was the major determinant of the reaction. The reaction proceeded through the intermediacy of a pink colored stable product that could be isolated (30% yield at 2 h) and characterized as **64** by spectroscopy, CHN analysis and X-ray crystallography (**Figure 3.2.1.5**). To the best of our knowledge, this is the first report of isolation and characterization of the intermediate in a Knovenagel type condensation with the Bodipy dyes. The intermediacy of compound **64** in the reaction was confirmed by its conversion to **63e** along with some amount of

21 on heating in the presence of piperidine and AcOH. The partial recovery of **21** also explained the sluggishness of the reaction and lesser yield due to the attainment of an equilibrium. The mechaism of the formation of **63e** can be represented as shown in **Scheme 3.2.1.3**.

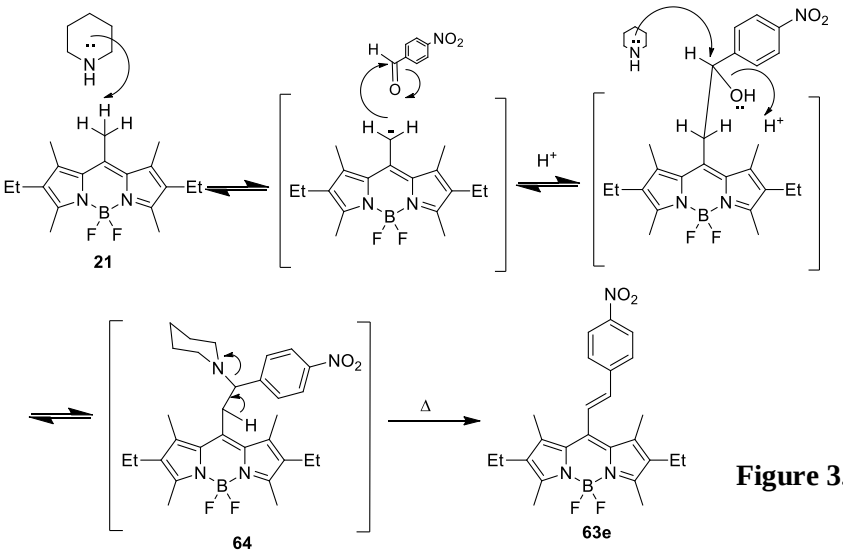

Scheme 3.2.1.3 Mechanism of formation of **63e**

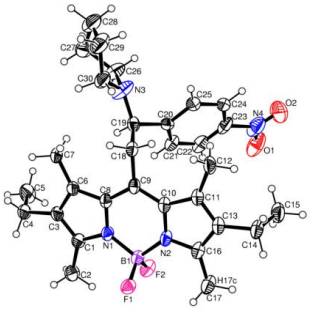

Figure 3.2.1.5 X-ray crystal structures of **64**

The ^{1}H NMR showed three multiplates between δ 3.18-3.73 ppm related with the C-8 protons (–CH_2, –CH). The twelve protons multiplets at δ 2.37-2.48 in its ^{1}H NMR spectrum (**Figure 3.2.1.7**) corresponded to the five –CH_2 groups of piperidine ring and two protons of –CH_2 group of pyrrole at C-2 position. Its LCMS molecular ion peak [M^+] at m/e 536.3 and the fragment peaks at m/z 452.2, 219.1 and 173.12 etc. further established the formation of compound **64**. In a similar manner, the styryl derivative **63f** could also be synthesized in 61% yield (**Table 3.2.1.1**) by condensing the dye **21** with **62d**.

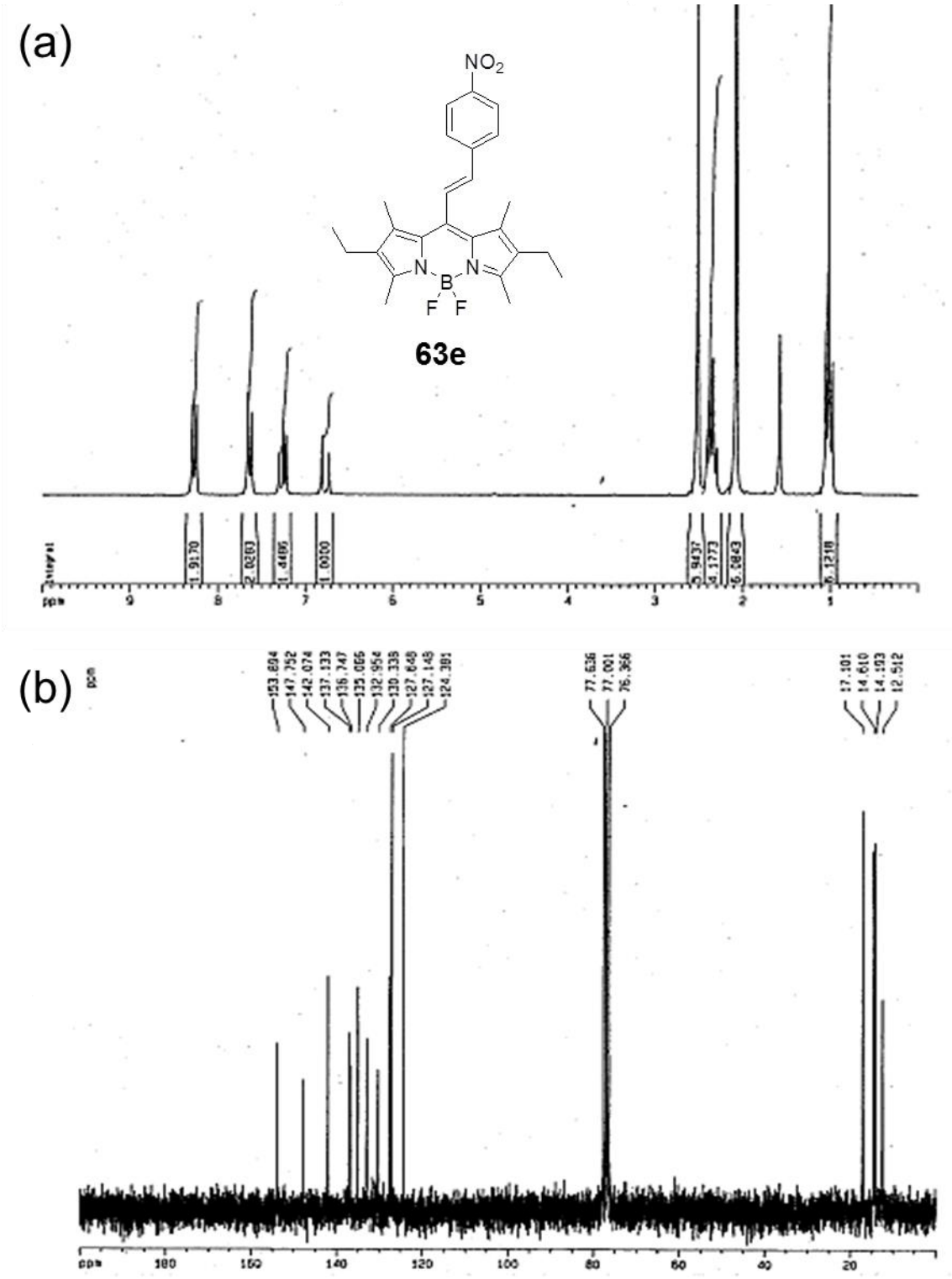

Figure 3.2.1.6 The NMR spectrum of compound **63e** (a) ^{1}H NMR, (b) ^{13}C NMR.

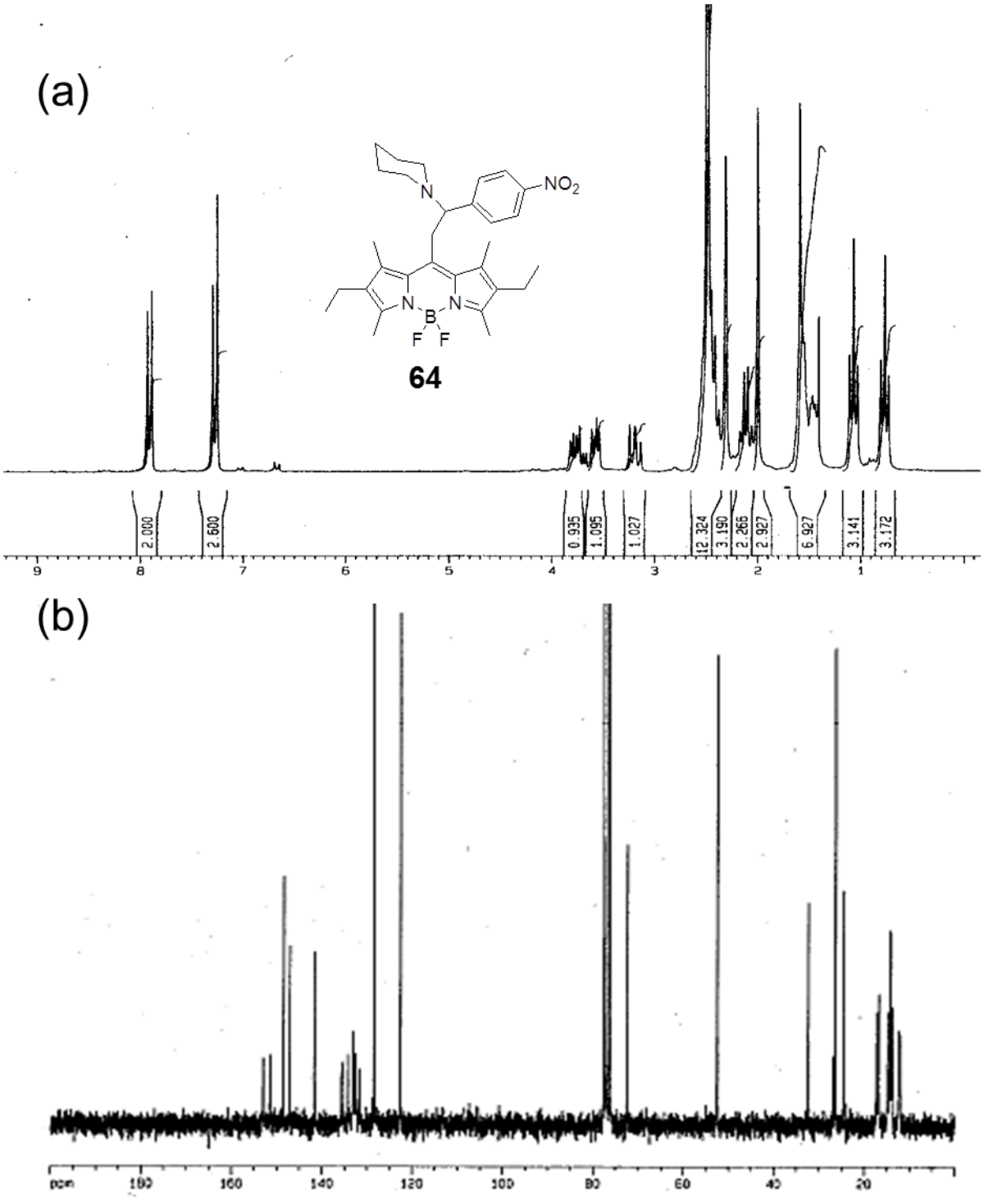

Figure 3.2.1.7 The NMR spectrum of compound **64** (a) ^{1}H NMR, (b) ^{13}C NMR.

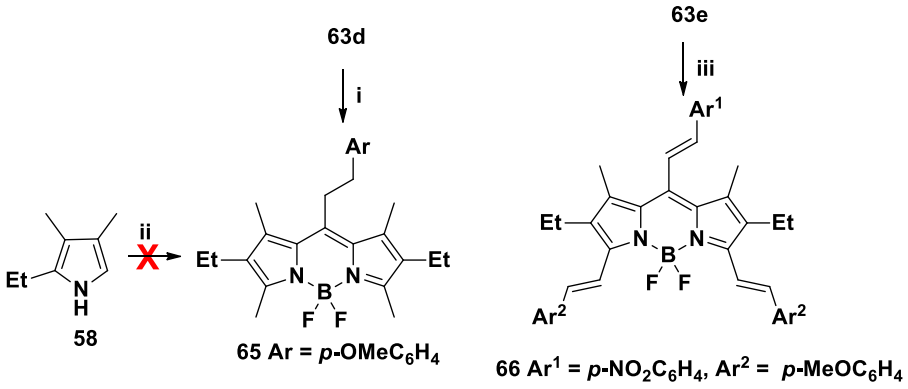

(i) H_2/10% Pd-C/CH_2Cl_2-EtOH. ii) a. *p*-$OMeC_6H_4(CH_2)_2CHO$ /TFA/CH_2Cl_2/25 ^oC/1 h; b. DDQ/4 h; c. Et_3N/1 h; d. $BF_3.Et_2O$ /25 ^oC/ 4 h. iii) **9a**/piperidine/AcOH/Toluene/Δ.

Scheme 3.2.1.4 Synthesis of the compounds **65** and **66**.

3.2.1.3. Applications

To illustrate the utility of the new *meso*-functionalization method, a few new Bodipy compounds were synthesized (**Scheme 3.2.1.4**) using some of the above *meso*-styryl Bodipy compounds. For example, the highly fluorescent dye **65** was synthesized by catalytic hydrogenation of **63d** that showed a very weak fluorescence (*vide infra*). The ^1H NMR spectrum of **65** showed two new multiplets at δ 2.84-2.93 and 3.27-3.36, each accounting for two protons for the vinylic and benzylic CH_2 groups in place of the olefenic resonances, confirming its formation (**Figure 3.2.1.8**). It is worth mentioning that compound **65** could not be synthesized via the conventional route of condensing kryptopyrrole (**58**) with *p*-methoxydihydrocinnamaldehyde, due to low reactivity of the arylalkyl aldehydes.[19]

The polystyryl Bodipys are useful functional molecules. Previously, Akkaya *et al*. synthesized a tetrastyryl Bodipy (A_4 system),[25a] while Ziessel *et al*. synthesized AB, A_2B_2 and ABCD types of polystyryl Bodipy dyes.[73] In the present work, the Bodipy compound **63e** was condensed with the aldehyde **62a** to furnish the 3,5,8-tristyryl substituted Bodipy dye **66**, belonging to a new AB_2 system of polystyryl Bodipy dye. The ^1H-NMR spectrum (**Figure**

3.2.1.9) of **66** exhibited all the characteristic signals of the tristyryl-Bodipy unit. For example, the eighteen-protons resonances between δ 6.74-8.29 corresponded to the three phenyl subunits and six vinyl protons on the tristyryl arms, while the six-protons singlet at δ 2.50 due to the 3,5-methyls disappeared.

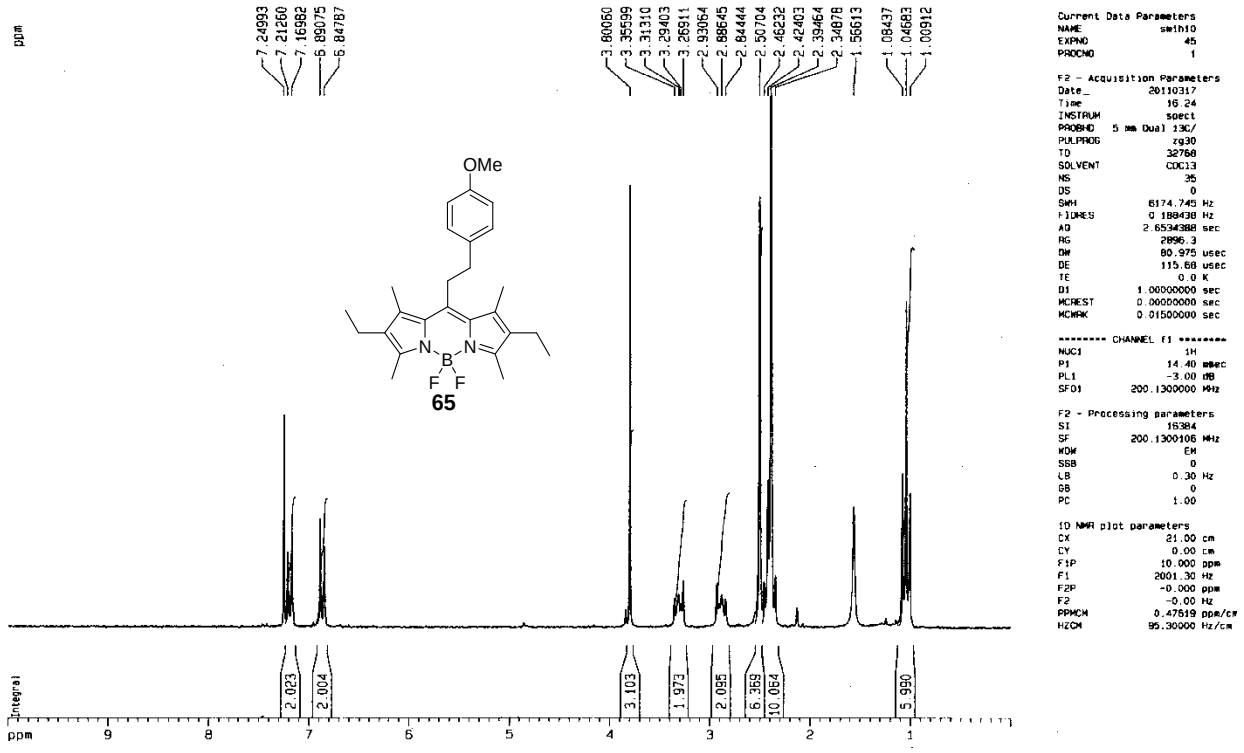

Figure 3.2.1.8 ^{1}H NMR spectrum of compound **65**.

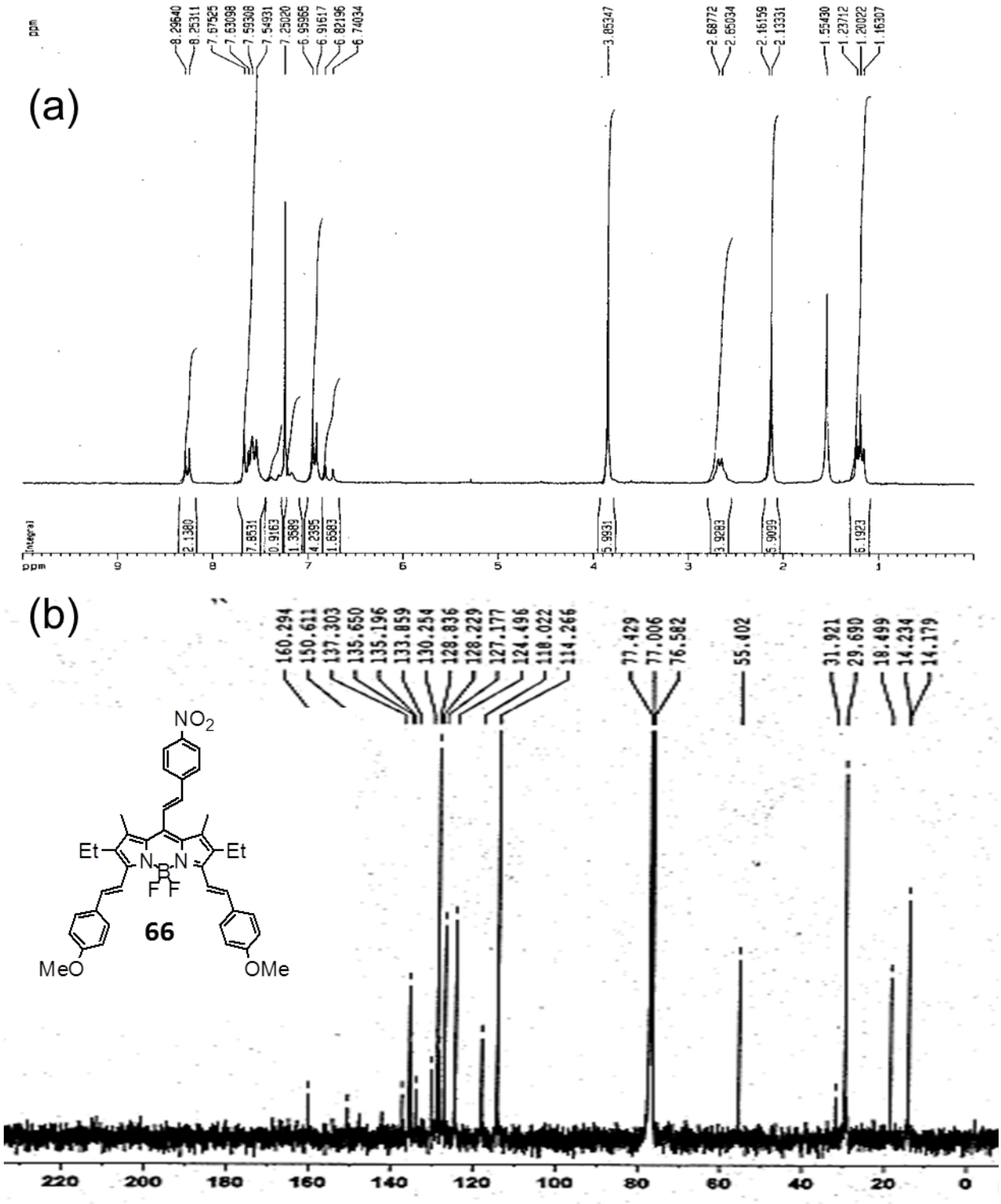

Figure 3.2.1.9 The NMR spectrum of compound **66** (a) ^{1}H NMR, (b) ^{13}C NMR.

3.2.2. Photophysical characteristics

The spectroscopic properties (**Table 3.2.2.1**) of all the compounds, recorded in CH_2Cl_2 revealed that that the *meso*-styryl Bodipys (**63a-e**) were significantly less fluorescent ($\Phi_{fl} < 0.01$) and showed reduced Stokes' shifts, compared to the corresponding precursor Bodipys. The results were consistent with the previous report[75b] and provided direct evidence of the steric relaxation after *meso*-styryl modification. Interestingly, saturation of the styryl double bond as in **63d** augmented the fluorescence ($\Phi_{fl} = 0.76$) significantly, offering the possibility of constructing on/off chemical sensors. The rather large red shifts (8-13 nm) of the absorption λ_{max} *vis-à-vis* excitation λ_{max} of **63a-e** indicated complex excited state transition.

Table 3.2.2.1: Photophysical parameters of the dyes in CH_2Cl_2

Compound	λ_{abs} (nm)	ε ($M^{-1}cm^{-1}$)	λ_{ext} (nm)	λ_{fl} (nm)	Φ_{fl}
32	525.0	81000	531.0	556.0	0.34[a]
63a	533.0	59000	522.0	529.0	< 0.01
63b	533.0	60000	521.0	529.0	0.01
63c	536.2	54000	524.0	532.0	< 0.01
21	520.0	71000	525.0	534.0	0.79[b]
63d	528.5	58000	520.0	542.0	< 0.01
63e	531.5	51000	518.0	532.0	< 0.01
63f	529.6	61000	520.0	537.0	< 0.01
63d'	577.5	84000	581.0	593.0	0.66
64	534.2	56000	536.0	559.0	0.02
65	523.2	75000	526.0	537.0	0.72
66	666.0	89000	-	-	-

[a]Relative to that (0.43) in EtOH; [b]Relative to that (0.84) in EtOH.

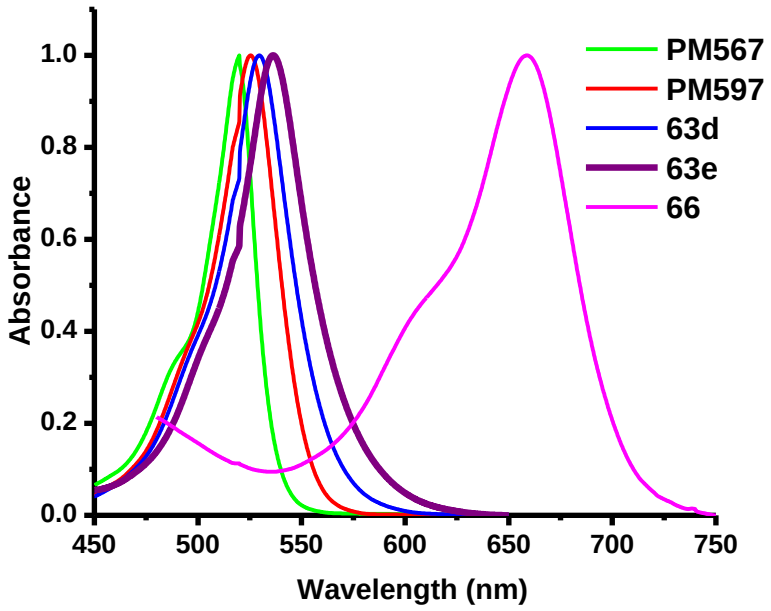

Figure 3.2.2.1 Absorption spectra of the dyes in CH_2Cl_2

3.2.3. Electrochemical Studies

Functional fluorescent dyes are of central importance as active components for light and electron transfer induced processes, mainly in the field of materials science and analysis.[77] A combination of reversible electron transfer and of efficient light absorption/emission is essential for constructing photovoltaic/photoelectrochemical devices.[78] Due to their high absorption coefficients and quantum yields of emission, the Bodipy compounds have favorable photonic qualities.[79] However, for photovoltaic applications, the radical cations and anions formed during electron transfer need to be fairly stable. The meso-position of the indacene framework is of crucial importance in stabilizing the radical anions. The cyclic voltammograms of some selected Bodipy compounds (**21**, **63d**, **63d'** and **66**) are shown in **Figures 3.2.3.1a-d**. The CV results (**Table 3.2.3.1**) revealed reversible cathodic waves, assigned to the one-electron reduction of the Bodipy units.[61] Compound **63d** (E_{red}^{o} = -1.36 V) was easily reducible by ~220 mV than **21** (E_{red}^{o} = -1.58 V), while reduction of the tri-styryl compound **66** was even easier by ~600 mV than **21**.

These suggested better stability of the radical anions due to *meso*-styryl modification. However, this alone did not alter the oxidation potential, as is reflected from the same E_{ox}^{o} values (1.02 V) of **21** and **66**. In case of **66**, two anodic waves were observed, the first oxidation step (E_{ox}^{o} = 0.75 V) was assigned to the removal of one electron from the Bodipy core, while the higher potential could be due to the oxidation of the styryl residue (E_{ox}^{o} = 1.23 V).[61] Similarly, two anodic waves were observed in case of **63d'** showing the oxidation of Bodipy core (E_{ox}^{o} = 0.83 V) and styryl residue (E_{ox}^{o} = 1.26 V). Compound **63e** (E_{red}^{o} = -1.02 V)was easily reducible by ~560 mV than **21**.

Table 3.2.3.1: Electrochemical data of various compounds

Compound	E_{ox}°/V	(ΔE)	E_{red}°/V	(ΔE)
21	1.02	0.437	-1.58	0.416
63d	1.02	0.332	-1.36	0.429
63d'	0.83, 1.26	0.428	-1.43	0.410
63e	1.06	0.344	-1.02	0.379
66	0.75, 1.23	0.253	-0.98	0.474

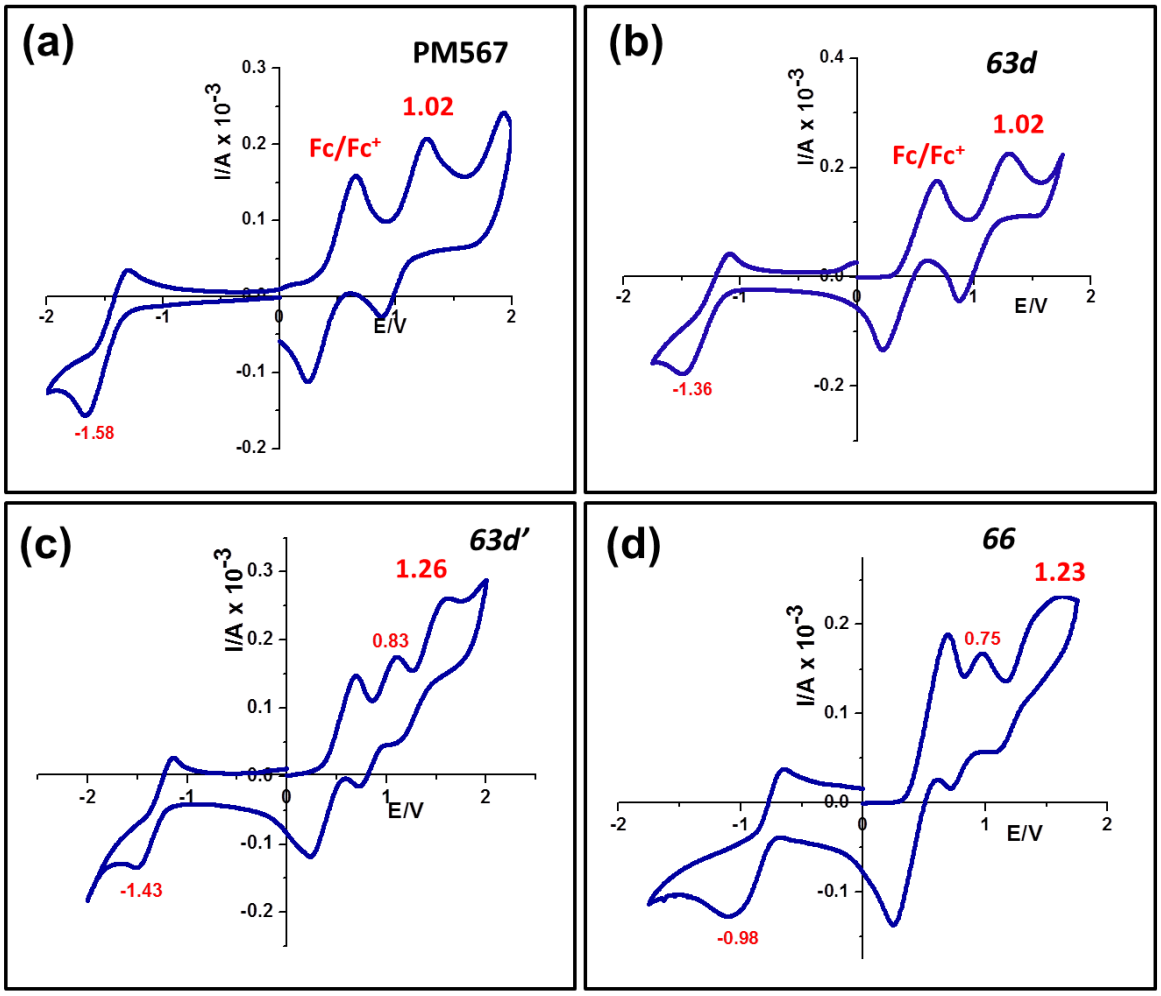

Figure 3.2.3.1 Cyclic voltammogram of the *meso*-methyl and *meso*-functionalized Bodipys. (a): **21**; (b): **63d**; (c): **63d'**; (d): **66**. The experiments were carried out in CH_2Cl_2 at 25 ^oC using 0.1 M Bu_4NClO_4 (TBAP) as the supporting electrolyte and ferrocene (Fc) as internal reference at +0.38V.

3.2.4. Theoretical interpretation

The excited state of the Bodipy core has inherent charge redistribution towards the *meso*-position.[67c] Presence of the electron withdrawing *meso*-styryl group would facilitate it further and may alter the localization of the LUMO and HOMO. For example, our theoretical calculation revealed maximum electron densities of the LUMO and HOMO of **66** on the *meso*-styryl and Bodipy moieties respectively (**Figure 3.2.4.1** and **3.2.4.2**). Hence the emision process

with the *meso*-styryl Bodipys would be symmetry forbidden, explaining their low/ non-fluorescence. However, such a charge distribution may be important in using the *meso*-styryl compounds as potential sensitizers for rapid electron injection into the conduction band of TiO_2 in dye sensitized solar cells (DSSCs).[67c]

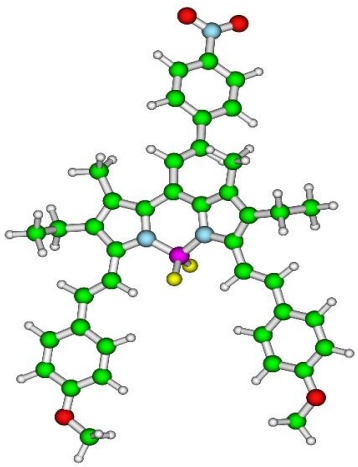

Figure 3.2.4.1: Optimized structure of **66**.

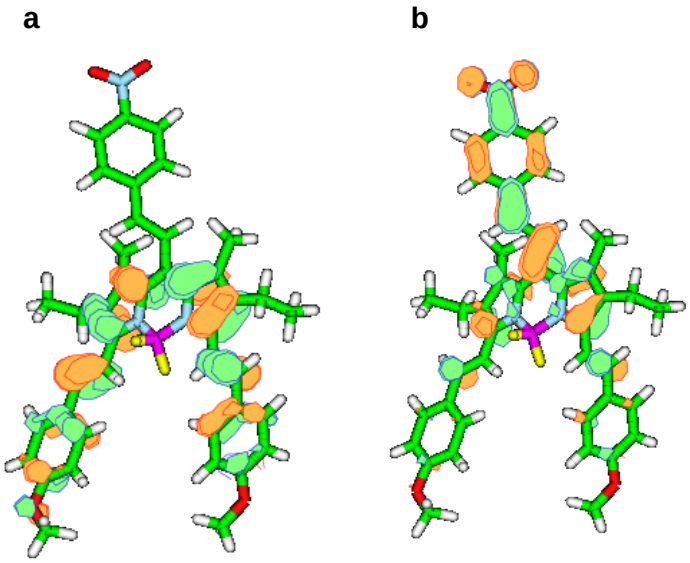

Figure 3.2.4.2: Geometriies of the HOMO (a) and LUMO orbitals (b) of **66**.

3.3. Summary

In conclusion, we have tactically used the inherent steric strain of the Bodipy moieties to functionalize them at the *meso*-position. The styryl substitutions at the *meso*-position alleviate the steric strain of the parent Bodipys. Also, the steric strain release hypothesis was proved from the single crystal X-ray data that showed reduced torsional angle and increased dihedral angle on introduction of a *meso*-styryl moiety in the dyes **32** and **21**. The strain release was more for **32**, to furnish the products in higher yields compared to that with **21**. For the less strained Bodipy **21**, the *meso*-selectivity could be achieved by increasing the electrophilicity of the aldehyde. Identification of the isolated intermediate **64** of the Knoevenagel condensation also established the reaction mechanism. This method allows for the preparation of a rich variety of 8-substituted

Bodipys using readily available aromatic aldehydes. The new *meso*-styryl Bodipys could be useful for development of chemical sensors and DSSCs.

3.4. Experimental

3.4.1. General Methods

The general details of the synthetic methodologies and spectroscopic studies have already been discussed in Chapter-2.

3.4.2. Synthesis

Typical process for the Knoevenagel-type condensation. A mixture of **21/32** (1.0 mmol), **62a-d** (1.1 mmol), glacial acetic acid (0.5 mL) and piperidine (3.5 mL) was refluxed in toluene (35 mL) with simultaneous azeotropic removal of water formed during the reaction. After the consumption of **21/32**, H_2O (100 mL) was added into the reaction mixture, which was extracted with $CHCl_3$ (3 × 20 mL). The organic layer was dried and concentrated in vacuo to give a residue, which on column chromatography (silica gel, hexane-EtOAc) furnished the respective styryl derivatives.

2,6-Di-*tert*-butyl-4,4-difluoro-8-*p*-methoxystyryl-1,3,5,7-tetramethyl-4-bora-3a,4a-diaza-s-indecene 63a. red needles (CH_2Cl_2/cyclohexane); mp: 249 °C; IR: 2948, 2835, 1632, 1603, 1439 cm^{-1}; ^1H NMR: δ 1.38 (s, 18H), 2.31 (s, 6H), 2.70 (s, 6H), 3.85 (s, 3H), 6.51 (d, J = 16.3 Hz, 1H), 6.92-7.02 (m, 3H), 7.41 (d, J = 8.6 Hz, 2H); ^{13}C NMR (50 MHz): δ 16.7, 18.2, 31.9, 33.2, 55.3, 114.5, 122.3, 127.9, 129.3, 131.6, 136.6, 137.1, 138.1, 138.8, 153.1, 160.3; ^{11}B NMR (96 MHz): δ 1.13 (t, J = 34.0 Hz); EI-MS (m/z): 493 $[M+1]^+$, 492 $[M]^+$. Anal. Calcd. for $C_{30}H_{39}BF_2N_2O$: C, 73.17; H, 7.98; N, 5.69%; Found: C, 73.13; H, 7.67; N, 5.56%.

2,6-Di-*tert*-butyl-4,4-difluoro-8-*p*-hydroxystyryl-1,3,5,7-tetramethyl-4-bora-3a,4a-diaza-s-indecene 63b. red solid; mp: >250 °C; IR: 3501, 2989, 1737, 1510 cm^{-1}; ^1H NMR (500 MHz): δ

1.38 (s, 18H), 2.31 (s, 6H), 2.70 (s, 6H), 6.52 (d, *J* = 16.5 Hz, 1H), 6.86 (d, *J* = 8.5 Hz, 2H), 6.95 (d, *J* = 16.5 Hz, 1H), 7.37 (d, *J* = 8.5 Hz, 2H); ^{13}C NMR (125 MHz): δ 16.8, 18.2, 31.9, 33.2, 115.9, 122.1, 128.1, 136.5, 137.1, 138.2, 153.0, 156.1; EI-MS (m/z): 478 $[M]^+$, 477 $[M-1]^+$. Anal. Calcd. for $C_{29}H_{37}BF_2N_2O$: C, 72.80; H, 7.80; N, 5.86%; Found: C, 72.99; H, 7.80; N, 5.56%.

2,6-Di-*tert*-butyl-4,4-difluoro-1,3,5,7-tetramethyl-8-*p*-nitrostyryl-4-bora-3a,4a-diaza-s-indecene 63c. red needles (CH_2Cl_2/cyclohexane); mp: >250 °C; IR: 2965, 1745, 1513 cm^{-1}; ^{1}H NMR (500 MHz): δ 1.38 (s, 18H), 2.27 (s, 6H), 2.72 (s, 6H), 6.67 (d, *J* = 16.5 Hz, 1H), 7.31 (d, *J* = 16.5 Hz, 1H), 7.62 (d, *J* = 8 Hz, 2H), 8.27 (d, *J* = 8 Hz, 2H); ^{13}C NMR (125 MHz): δ 16.8, 18.2, 31.8, 33.2, 124.4, 127.0, 129.4, 131.3, 133.9, 136.0, 137.6, 137.8, 142.3, 147.8, 154.3; EI-MS (m/z): 507 $[M]^+$, 506 $[M-1]^+$. Anal. Calcd. for $C_{29}H_{36}BF_2N_3O_2$: C, 68.64; H, 7.15; N, 8.28%; Found: C, 68.78; H, 7.31; N, 8.66%.

2,6-Diethyl-4,4-difluoro-8-*p*-methoxystyryl-1,3,5,7-tetramethyl-4-bora-3a,4a-diaza-s-indecene 63d. red cuboidals (CH_2Cl_2/cyclohexane); mp: 185 °C; IR: 2963, 1637, 1604, 1477 cm^{-1}; ^{1}H NMR: δ 1.02 (t, *J* = 7.6 Hz, 6H), 2.13 (s, 6H), 2.35 (q, *J* = 7.6 Hz, 4H), 2.51 (s, 6H), 3.84 (s, 3H), 6.61 (d, *J* = 16.3 Hz, 1H), 6.87-7.01 (m, 3H), 7.42 (d, *J* = 8.7 Hz, 2H); ^{13}C NMR: δ 12.4, 14.3, 14.7, 17.1, 55.3, 114.5, 120.5, 128.0, 129.0, 130.8, 132.5, 137.3, 137.4, 139.1, 152.8, 160.3; ^{11}B NMR (96 MHz): δ 1.04 (t, *J* = 33.4 Hz); EI-MS (m/z): 437 $[M+1]^+$, 417 $[M-19]^+$. Anal. Calcd. for $C_{26}H_{31}BF_2N_2O$: C, 71.57; H, 7.16; N, 6.42%; Found: C, 71.17; H, 6.95; N, 6.32%.

2,6-Diethyl-4,4-difluoro-3-*p*-methoxystyryl-1,5,7,8-tetramethyl-4-bora-3a,4a-diaza-s-indecene 63d'. pink cuboidals (CH_2Cl_2/cyclohexane); mp: 235 °C; IR: 2961, 1635, 1606, 1478 cm^{-1}; ^{1}H NMR: δ 1.05 (t, *J* = 7.5 Hz, 3H), 1.20 (t, *J* = 7.5 Hz, 3H), 2.32-2.47 (m, 8H), 2.53 (s,

3H), 2.57-2.74 (m, 8H), 3.83 (s, 3H), 6.87 (d, *J* = 8.7 Hz, 2H), 7.07 (d, *J* = 16.8 Hz, 1H), 7.48-7.62 (m, 3H); ^{13}C NMR: δ 12.5, 14.0, 14.4, 14.7, 17.1, 18.3, 55.3, 114.2, 118.1, 128.4, 130.5, 132.4, 132.7, 133.1, 134.2, 136.5, 136.7, 138.8, 148.0, 153.2, 159.9. EI-MS (m/z): 437 $[M+1]^+$, 417 $[M-19]^+$. Anal. Calcd. for $C_{26}H_{31}BF_2N_2O$: C, 71.57; H, 7.16; N, 6.42%; Found: C, 71.10; H, 7.21; N, 6.18%.

2,6-Diethyl-4,4-difluoro-1,3,5,7-tetramethyl-8-*p*-nitrostyryl-4-bora-3a,4a-diaza-s-indecene

63e. red needles (CH_2Cl_2/cyclohexane); mp: >250 °C; IR: 2930, 2868, 1634, 1597, 1478 cm^1; ^{1}H NMR: δ 1.02 (t, *J* = 7.5 Hz, 6H), 2.08 (s, 6H), 2.34 (q, *J* = 7.5 Hz, 4H), 2.51 (s, 6H), 6.73 (d, *J* = 16.4 Hz, 1H), 7.22 (d, *J* = 16.4 Hz, 1H), 7.61 (d, *J* = 8.6 Hz, 2H), 8.25 (d, *J* = 8.6 Hz, 2H); ^{13}C NMR: δ 12.5, 14.2, 14.6, 17.1, 124.4, 127.1, 127.7, 130.3, 133.0, 135.1, 136.7, 137.1, 142.1, 147.8, 153.9; EI-MS (m/z): 451 $[M]^+$, 432 $[M-19]^+$. Anal. Calcd. for $C_{25}H_{28}BF_2N_3O_2$: C, 66.53; H, 6.25; N, 9.31%; Found: C, 66.12; H, 6.02; N, 9.36%.

8-*p*-Bromostyryl-2,6-diethyl-4,4-difluoro-1,3,5,7-tetramethyl-4-bora-3a,4a-diaza-s-indecene

63f. red needles (CH_2Cl_2/cyclohexane); mp: 223 °C; IR: 2965, 1538, 1472 cm^{-1}; ^{1}H NMR (500 MHz): δ 1.03 (t, *J* = 7.5 Hz, 6H), 2.11 (s, 6H), 2.36 (q, *J* = 7.5 Hz, 4H), 2.52 (s, 6H), 6.64 (d, *J* = 16.0 Hz, 1H), 7.08 (d, *J* = 16.0 Hz, 1H), 7.36 (d, *J* = 8.0 Hz, 2H), 7.54 (d, *J* = 8.0 Hz, 2H); ^{13}C NMR (125 MHz): δ 12.5, 14.3, 14.7, 17.1, 122.8, 123.6, 128.0, 130.5, 132.2, 132.7, 134.9, 136.2, 137.2, 137.9, 153.3; EI-MS (m/z): 485 $[M]^+$, 483 $[M-2]^+$. Anal. Calcd. for $C_{25}H_{28}BBrF_2N_2$: C, 61.88; H, 5.82; N, 5.77%; Found: C, 61.86; H, 5.50; N, 6.04%.

Compound 64. A mixture of **21** (100 mg, 0.32 mmol), *p*-nitrobenzaldehyde (71 mg, 0.47 mmol), glacial acetic acid (0.2 mL) and piperidine (1 mL) was refluxed in toluene (10 mL) for 2 h. Water formed during the reaction was removed azeotropically by heating in a Dean–Stark apparatus. After that, water (100 mL) was added into it and the reaction mixture was extracted

with $CHCl_3$ (3 × 50 mL). The organic layer was then dried over Na_2SO_4 and the solvent was removed under reduced pressure. Column chromatography of the residue (silica gel, hexane-EtOAc) furnished **64** as a red solid. Yield: 51 mg (30%); red needles (CH_2Cl_2/cyclohexane); mp: 162 °C; IR: 2932, 2864, 1478 cm^{-1}; ^1H NMR: δ 0.77 (t, *J* = 7.5 Hz, 3H), 1.07 (t, *J* = 7.5 Hz, 3H), 1.40-1.61 (m, 6H), 2.00 (s, 3H), 2.10 (q, *J* = 7.5 Hz, 2H), 2.31 (s, 3H), 2.35-2.49 (m, 12H), 3.14-2.24 (m, 1H), 3.52-3.62 (m, 1H), 3.72-3.85 (m, 1H), 7.30 (d, *J* = 8.7 Hz, 2H), 7.89 (d, *J* = 8.7 Hz, 2H); ^{13}C NMR: δ 12.3, 13.8, 14.2, 14.8, 16.8, 17.2, 24.6, 26.4, 26.9, 32.4, 52.5, 72.5, 122.6, 128.5, 131.6, 132.6, 133.1, 134.2, 135.6, 141.6, 147.1, 148.5, 151.5, 153.0; EI-MS (m/z): 537 $[M+1]^+$, 452, 219, 174. Anal. Calcd. for $C_{30}H_{39}BF_2N_4O_2$: C, 67.17; H, 7.33; N, 10.44%; Found: C, 66.82; H, 7.41; N, 10.07%.

Compound 65. To a stirred degassed solution of **63d** (60 mg, 0.19 mmol) in CH_2Cl_2/EtOH (10 mL/10 mL) under Ar was added 10% Pd/C (6 mg, 10% mol.), and the mixture stirred at 25 ^oC under H_2 (atmospheric pressure). After complete consumption of the starting material (*cf*. TLC, 48 h), the mixture was filtered through celite, concentrated in vacuo and the crude product purified by flash column chromatography (silica gel, hexane/EtOAc, 80:20) to get **65**. Yield: 36 mg (60%); red powder; mp: 157 °C; IR: 2963, 1477 cm^{-1}; ^1H NMR: δ 1.05 (t, *J* = 7.5 Hz, 6H), 2.33-2.47 (m, 10H), 2.51 (s, 6H), 2.84-2.93 (m, 2H), 3.27-3.36 (m, 2H), 3.80 (s, 3H), 6.85 (d, *J* = 8.6 Hz, 2H), 7.17 (d, *J* = 8.6 Hz, 2H); ^{13}C NMR (75 MHz): δ 12.5, 13.7, 14.9, 17.2, 29.8, 36.5, 55.3, 114.1, 114.4, 128.1, 128.8, 130.9, 132.4, 132.7, 135.6, 143.6, 152.4, 158.3; EI-MS (m/z): 438 $[M]^+$, 437 $[M-1]^+$. Anal. Calcd. for $C_{26}H_{33}BF_2N_2O$: C, 71.24; H, 7.59; N, 6.39%; Found: C, 71.11; H, 7.95; N, 6.18%.

Compound 66: A mixture of **63e** (120 mg, 0.267 mmol), **62a** (72.6 mg, 0.534 mmol), glacial acetic acid (0.150 mL) and piperidine (1 mL) was refluxed in toluene (10 mL) for 4 h. Water

formed during the reaction was removed azeotropically by heating in a Dean–Stark apparatus. After the total consumption of the starting material, water (100 mL) was added into it and the reaction mixture was extracted with $CHCl_3$ (3 × 50 mL). The organic layer was dried and the solvent removed under reduced pressure. Column chromatography of the residue (silica gel, hexane-EtOAc) furnished **13**. Yield: 125 mg (82%); green needles (CH_2Cl_2/cyclohexane); mp: > 250 °C; IR: 2929, 2871, 1630, 1479 cm^{-1}; ^1H NMR: δ 1.20 (t, *J* = 7.44 Hz, 6H), 2.16 (s, 6H), 2.67 (q, *J* = 7.47 Hz, 4H), 3.85 (s, 6H), 6.74 (d, *J* = 16.3 Hz, 1H), 6.92 (d, *J* = 8.7 Hz, 4H), 7.18-7.39 (m, 3H), 7.55-7.77 (m, 8H), 8.25 (d, *J* = 8.7 Hz, 2H); ^{13}C NMR (75 MHz): δ 14.1, 14.2, 18.5, 29.7, 31.9, 55.4, 114.3, 118.0, 124.5, 127.2, 128.2, 128.8, 130.3, 133.9, 135.2, 135.7, 137.3, 150.6, 160.3; EI-MS (m/z): 688 $[M+1]^+$, 668 $[M-19]^+$. Anal. Calcd. for $C_{41}H_{40}BF_2N_3O_4$: C, 71.62; H, 5.86; N, 6.11%; Found: C, 71.23; H, 5.98; N, 6.32%.

3.4.3. Photophysical Studies

The absorption and emission spectra of the dyes (~10^{-6} M) in CH_2Cl_2 were recorded using a 1 cm quartz cuvette at ambient room temperature (298 ± 1 K). The fluorescence quantum yields (Φ_{fl}) of the dyes **63a-f**, **63d'**, **64** and **65** were measured relative to that of **32** and **21** respectively.

3.4.4. Electrochemical Studies

All the cyclic voltammetry experiments were done in deoxygenated CH_2Cl_2 containing TBAP (0.1 M), and a solute concentration of 1-5 × 10^{-3} M, at 25 °C. The redox potentials were standardized with ferrocene (Fc) as the internal reference and converted to SCE assuming that $E_{1/2}$ (Fc/Fc^+) = 0.38 V SCE. The error in half-wave potentials is ±10 mV. All waves were monoelectronic unless specified otherwise.

CHAPTER-4

DEVELOPMENT OF WATER-SOLUBLE BODIPYS FOR BIOLOGICAL APPLICATIONS

Chapter 4: Table of Contents

4.1. Preamble

Fluorescence spectroscopy, fluorescence imaging and fluorescence indicators are nowadays indispensable tools in various fields of modern science and medicine, including clinical diagnostics, biotechnology, molecular biology, and biochemistry. The major classes of currently used synthetic fluorophores include the cyanines, rhodamines, and oxazines. While these dye systems provide a host of functional groups that can be used for covalent attachment to various target molecules, many have limited biological utility due to poor photochemical stability, lengthy synthetic routes, poor solubility, and tendency for aggregation in aqueous media that surrounds a biomolecule.[30] Instead, the bright fluorescence, high photostability, generally low toxicity and ease of synthetic make the Bodipy-type dyes particularly promising candidates for biological imaging/sensing applications.[80] The fluorescence-based in vivo imaging has emerged as a promising real-time, non-invasive, and high-resolution technique that uses fluorescent probes to visualize normal and abnormal biological processes.[81]

Moreover, the Bodipy derivatives are amenable to modifications by attachment of ancillary residues at the appropriate positions of their cores. This can help in attenuating their strong fluorescence, thereby generating relatively long-lived triplet states, and eventually large amount of singlet oxygen ($^1O_2$) that would induce selective photo-damage in regions that are illuminated. Such an approach, known as photodynamic therapy (PDT) was the one of the foci of the present investigations. Hence the concept of PDT and in particular the application of the Bodipy compounds in PDT is briefly discussed below.

4.2. Principle of PDT

PDT is a therapeutic modality wherein nontoxic light-sensitive compounds, known as photosensitizer (PS) are selectively exposed to light, preferably in the visible or near-IR regions whereupon they become toxic to the targeted malignant and other diseased cells. Depending on the nature of the PS, its photo-excitation a specific wavelength leads to a transition of its electron from the S^0 state to the S^1 state. This is followed by an inter system crossing (ISC) of the excited electron for the favourable cases where the T^1 state is stable. Subsequently the PS can excite O_2 molecules at its ground (T^1) state to generate $^1O_2$ molecules, which, because of its higher energy can damage important bio-macromolecules. Hence the process can be used for therapy if targeted to specific cells (tumour, microbial etc.). The light used for PDT can come from a laser or other sources that can be directed through fiber optic cables (thin fibers that transmit light) to deliver light to areas inside the body. Because the excitation wavelength determines how far the light can travel into the body, and the PS is non-toxic, PDT generally show minimal side effect. Thus, PDT combines a photosensitizer (PS), its preferential localization in target tissues (like tumors), photo-excitation to generate reactive oxygen species (ROS) such as singlet oxygen ($^1O_2$) in presence of oxygen to achieve selective cell killing irreversibly. It provides a noninvasive therapeutic modality for certain types of cancers and pre-cancerous inductions,[82a-e] age-related macular degeneration and actinic keratosis, and other diseases, such as localized infections, dermatological and cardiovascular illnesses and wound healing.[83a-e] It is particularly promising in the treatment of multidrug-resistant (MDR) tumors selectivity, as both PS and light can be effectively localized to the tumor.[84a] It offers an attractive alternative or complement to conventional therapies.[84b-e]

4.3. Bodipy-based PDT Agents

Despite offering these advantages its current clinical use is restricted to a few functionalized porphyrins. However, the porphyrins are not the ideal PDT drugs due to their low extinction coefficients in the therapeutic window (650–800 nm), and low absorptivity in mammalian tissues.[85] Recognition of these disadvantages of porfimer sodium has inspired efforts to develop more effective PDT photosensitizers. Most of the Bodipy dyes have many ideal characteristics of PDT agents such as low dark toxicities, good cellular uptake, high extinction coefficients, and low quantum yields for photobleaching. These dyes can also be functionalized at different positions to enhance ISC and $^1O_2$ generation. Spin-coupling to heavy atoms is the most common of these modifications (the ‘‘heavy atom effect’’), and the one most frequently encountered is halogenation. Appropriate placing of heavy atoms on the Bodipy core promotes spin–orbit coupling, hence ISC, but not energy loss from excited states. However, Bodipys, possessing the heavy atoms, such as iodine, bromine, selenium, sulphur and certain lanthanides often show dark toxicity, as well as extended toxicity even after switching off the light. To this end, PSs containing dimeric Bodipys at an orthogonal orientation,[86a] or use of spin convertors, such as C60, in Bodipy-based dyads[86b] may help to sensitize $^1O_2$ generation, by intramolecular energy transfer (EnT). These aspects have been adequately highlighted in several excellent reviews.[87]

4.4. Studies on Bodipy-based PDT Agents

The existing limitations and future prospects, discussed above collectively provide a compelling rationale for the development of new Bodipy derivatives as PDT

photosensitizers. These provided the required impetus to undertake the present project for developing some novel and efficient Bodipy sensitizers for potential use in PDT.

4.4.1. Molecular design

In terms of molecular design, the first criteria of the fluorophore is the emission range between 700-900 nm, due to the optical sensitivity associated with the 'biological window', including minimal interference from endogenous chromophores, reduced light scattering, increased photon penetration through tissue, and low photodamage to the cells or tissues under observation.[88] For an enhanced biological effect in deeper tissues, it is imperative that the PS has a high extinction coefficient in the body's therapeutic window (650–800 nm), where typical mammalian tissues show low absorptivity. This can be conveniently achieved by a base-catalyzed condensation of the 3- or 5-methyl substituents of the Bodipys with suitable aldehydes. The resultant dyes possess longer wavelength absorption (~100 nm red-shifted) to move it to 590–600 nm with intramolecular charge transfer (ICT) characteristics.[89] Incorporation of a second styryl group would result in further red shifts in the absorption spectrum. Another factor of paramount importance is the water solubility of the PS. It should have a balance between hydrophilicity and lipophilicity, as too high lipophilicity would hamper their transport through blood vessel, while a high hydrophilicity would impede its cell membrane penetration. Earlier attempt to overcome hydrophobicity of the dye sensitizer, using micellar drug formulations have met with limited success, as the emulsifying agents often elicit anaphylactic reactions in vivo.[90] Given that the Bodipy core is hydrophobic, attachment polar neutral or ionic moieties can impart a higher amphiphilicity. For this purpose, Sengee *et al*. have designed four water soluble porphyrin derivatives as

piperazinium and imidazole salts and studied their comparative PDT activities on the human lung cancer A549 cells. Incorporation of the hydrophilic bases was found to potentiate the PDT property.[91a] With regard to the Bodipy compounds, introduction of a number of amphiphilic triethyleneglycol moieties at the *meso*-aryl and/ or 3,5-distyryl groups also improved their efficacy as PDT agents.[52] More recently, some unsymmetrical distyryl Bodipys were also converted to their amphiphilic analogues using both oligoethyleneglycol as well as 2-ethyleneglycol ammonium moieties.[91b] In another report, the combination of bromination as well as pegylation of some distyryl Bodipys was used by the same group to harness the benefit of heavy atom effect, amphiphilicity and red-shifted emission.[48b] The rationale of choosing the oligoethyleneglycol appendages are based on the fact these moieties are biocompatible, and confer cell permeability as well as tumor targeting characteristics on the photosensitizers.[92]

4.4.2. Synthesis

For the present investigation, it was envisaged that the C-3/C-5 styrylation strategy, used extensively by others,[48b,91b] as well as our group (presented in Chapter 2) would be easy to adopt to red-shift the emission wavelength of the Bodipy dyes. Hence the same strategy was adopted, as discussed below. However, the resultant dyes would be highly hydrophobic, as realized in the lasing studies of the red-Bodipys (*vide supra* Chapter 2). It was also found that appending an ethyleneglycol moiety at the B-centre of a even the mono-styryl dye **60a** did not improve its water-solubility. Hence, for the present work, attachment of a glucose unit was planned to improve the hydrophilicity. Such a strategy seemed attractive for the following reasons. Carbohydrates are known as

ligands of various cell surface lectins. Intense research have been focused to develop tumor-specific imaging probes by targeting cell membrane glycoproteins, such as galectins that play significant roles in numerous types of cancer.[93a] The galectins are abundant in tumor cells to promote tumor growth and development, angiogenesis and metastasis.[93] Hence, the proposed carbohydrate-based fluorophores may selectively target tumors. Also, carbohydrate–protein interactions are viewed as important mechanisms for many biological processes including immune response, cell proliferation, adhesion and death, cell–cell interaction and communication. Aggregation of the carbohydrates in vivo, may enhance the protein binding affinity.[94a-c]

Although the mechanism of retention of PSs by tumors is not well understood, the balance between lipophilicity and hydrophilicity is recognized as an important factor for photosensitizing efficiencies and tumor and cellular uptake. The linkages of a PS with sugar moieties are of great importance in terms of membrane interaction and specific affinity for malignant tumors. Hence, particular attention was devoted to the glycoconjugated Bodipy derivatives. It was planned to incorporate the glucose unit at the phenolic functionality present at the *meso*-postion or as a part of the C-3/C-5 styryl/distyryl moieties in the Bodipys. Thus, three Bodipy dyes shown in **4.4.2.3** were targeted. Of these, compound **72** was devoid of any additional conjugation, while compounds **74** and **76** had additional styryl moieties.

As shown in **Scheme 4.4.2.1**, the syntheses of the parent Bodipys were straightforward. Thus, kryptopyrrole **58** was condensed with the aryl aldehydes **67**/**68** using trifluoroacetic acid (TFA) as the catalyst to obtain compounds **69** and **70**. In general, CH_2Cl_2 is used as the solvent in the synthesis of Bodipys dyes, and the yields are

moderate with most of the aromatic aldehydes. During the synthesis of **70**, it was found that the reaction became sluggish to form a dark brown mixture from which the product could be isolated in poor yield. However, minor modification of the reaction conditions such as use of THF as the solvent and addition of DDQ at 0 °C improved the yield of **70**, as the reaction was clean and separation was easy. Due to the shielding effect of the C-8 aryl groups, the C-1 and C-7 methyl protons of both the compounds appeared upfield in their respective ^{1}H NMR spectra.

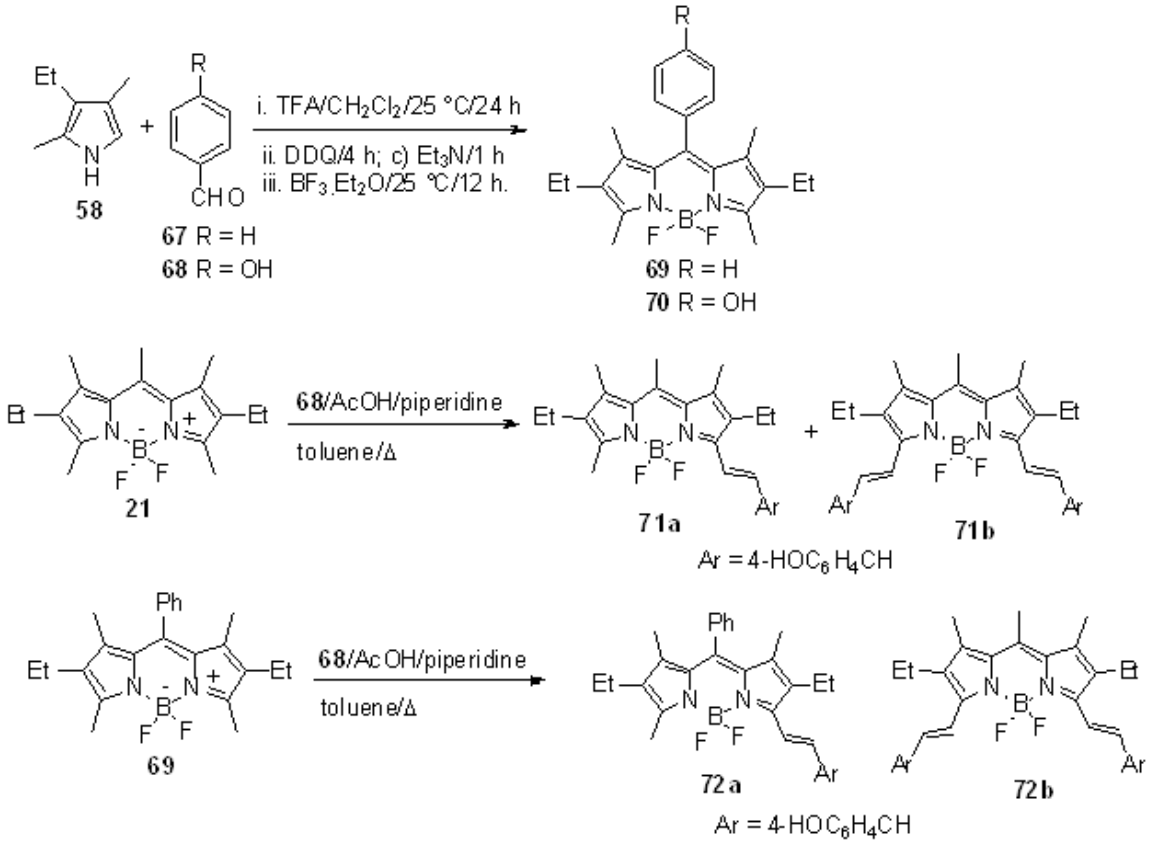

Scheme 4.4.2.1 Synthesis of the precursor Bodipys for glucosylation.

Next two types of red Bodipys *viz*. *meso*-methyl and *meso*-phenyl groups were synthesized. For this, compound **21 (**PM567**)** was subjected to condensation with the aldehyde **68** in the presence of piperidine and acetic acid. This expectedly led to the

formation of the monostyryl and distyryl derivatives **71a** and **71b** respectively. A similar condensation **69** with **68** afforded the corresponding monostyryl and distyryl derivatives **72a** and **72b** respectively. The results were consistent with that observed when the condensation was carried out between **21** and 4-methoxybenzaldehyde.

The attachment of the glucose moiety to the compounds **70**, **71a**/**71b** and **72** was achieved by the improved classical Konigs-Knorr method.[95a] The required glycosyl donor **74** was synthesized by acetylation of glucose with acetic anhydride in the presence of NaOAc to furnish glucose pentaacetate **73**. This on treatment with HBr-HAc furnished the bromide **74** via chemo-selective deacetylation of the anomeric acetyl group and bromination (**Scheme 4.4.2.2**.). After recrystallization from Et_2O/hexane and stored in the refrigerator at -18 °C.[95b-d]

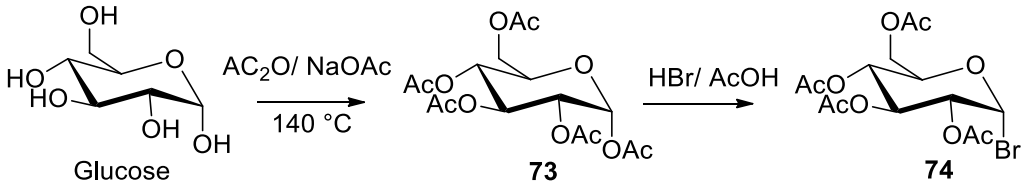

Scheme 4.4.2.2 Synthesis of the glucosylating agent.

For the glycosylation of compound **70** and **71a**, the pentaacetate **73** was used as the glycosyl donar in presence of BF_3.etherate catalyst in CH_2Cl_2. Appearance of characteristics mutiplets due to carbohydrate –CH protons between δ 3.5 to 5.5 in the ^1H NMR spectrum and four carbonyl peaks at δ 170 in the ^{13}C NMR spectrum confirmed formation of compounds **75** and **77** (**Figure 4.2.4** and **4.2.5**). However, when the same strategy was applied to glycosylate the dyes **71a** and **71b**, a very low yield of product from **71a** and complete degradation of **71b** were observed. Apparently, the reagent BF_3.etherate induced two parallel processes *viz.* glycosylation and removal of a F atom

from the Bodipys, the latter causing the partial or complete degradation dyes, depending on their nature. Fortunately, the glycosylation of **72a** and **72b** could be successfully performed by reacting them at room temperature with **74** in 1:1 $H_2O/CHCl_3$ and in the presence of K_2CO_3 as the base and Bu_4NBr as the phase transfer catalyst to afford **79** and **81** respectively. Because the glycosylation process does not change the L-configuration of the anomeric carbon of sugars,[95e] the structures of the products were assigned as shown in **Scheme 4.4.2.3**. Finally, the acetyl groups of **75**, **77**, **79** and **81** were removed by treating the products with NaOMe in MeOH to furnish the target Bodipys **76**, **78**, **80a** and **80b** respectively (**Scheme 4.4.2.3**).[95b] These water-soluble Bodipy compounds were subsequently used for the spectroscopic and PDT studies. As some representative data, the ^{1}H and ^{13}C NMR spectra of compound **76** and its precursor **75** are shown in **Figures 4.2.1.2** and **4.2.1.3**.

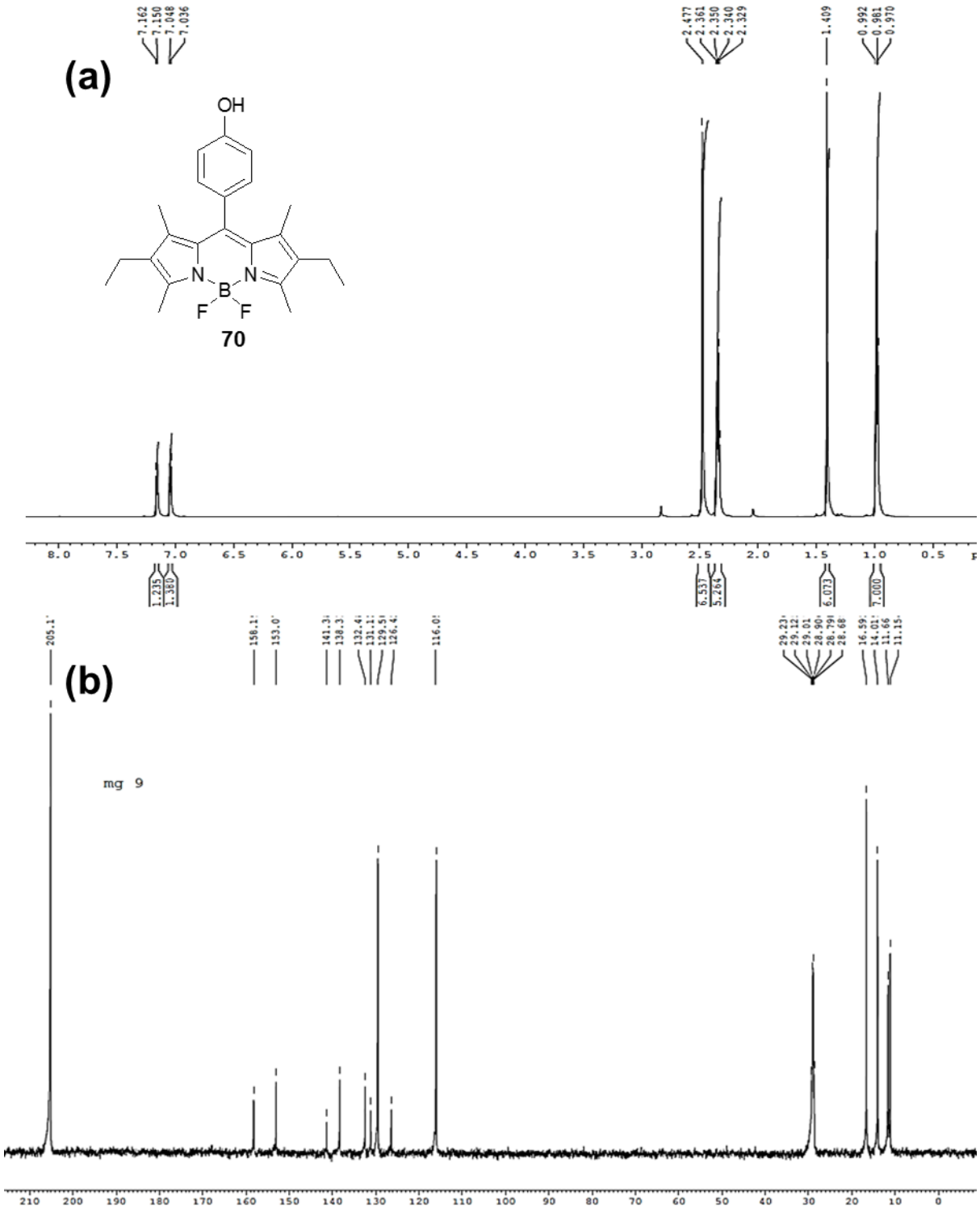

Figure 4.4.2.1 The NMR spectrum of **70** (a) ^{1}H NMR, (b) ^{13}C NMR.

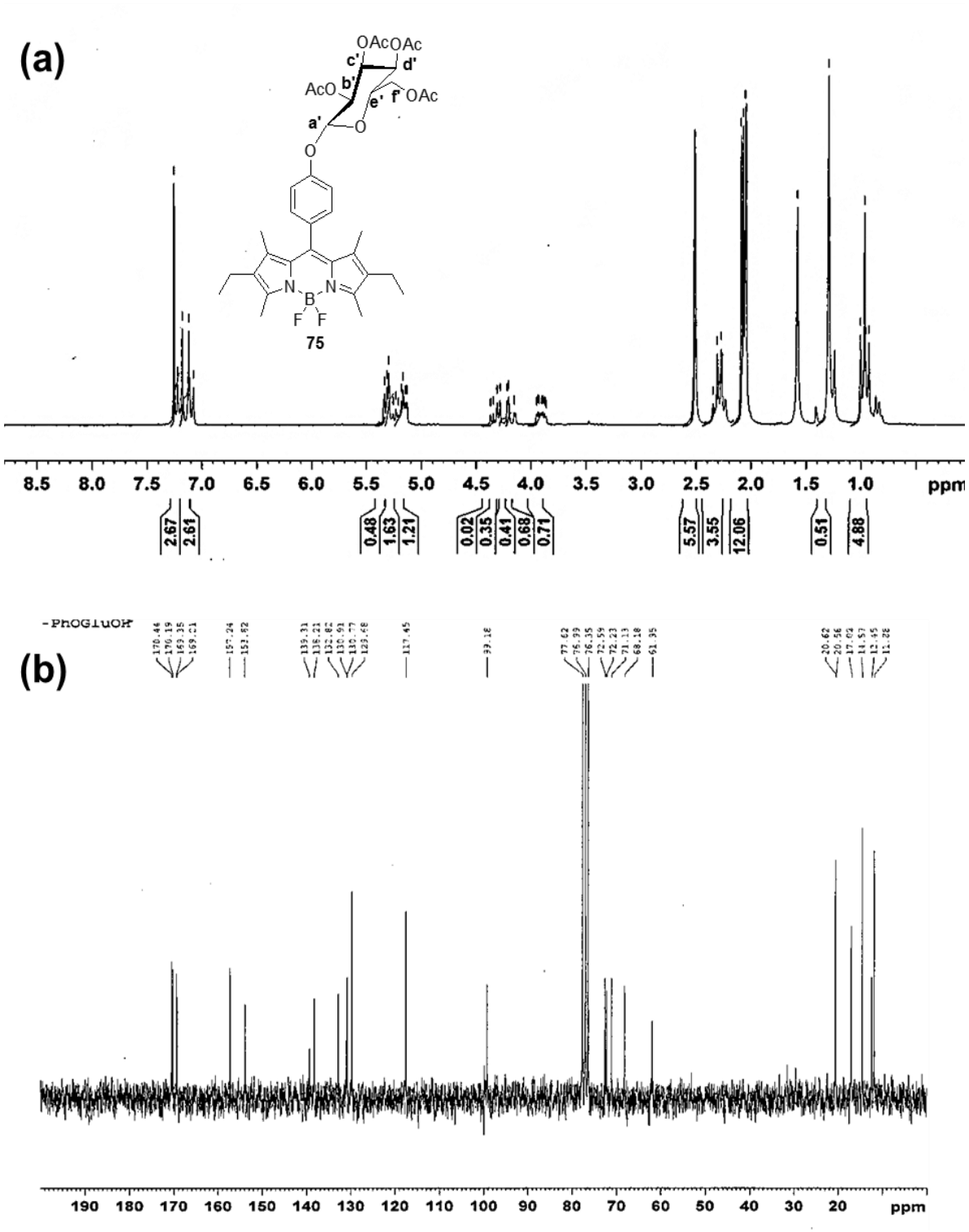

Figure 4.4.2.2 The NMR spectrum of **75** (a) ^{1}H NMR, (b) ^{13}C NMR.

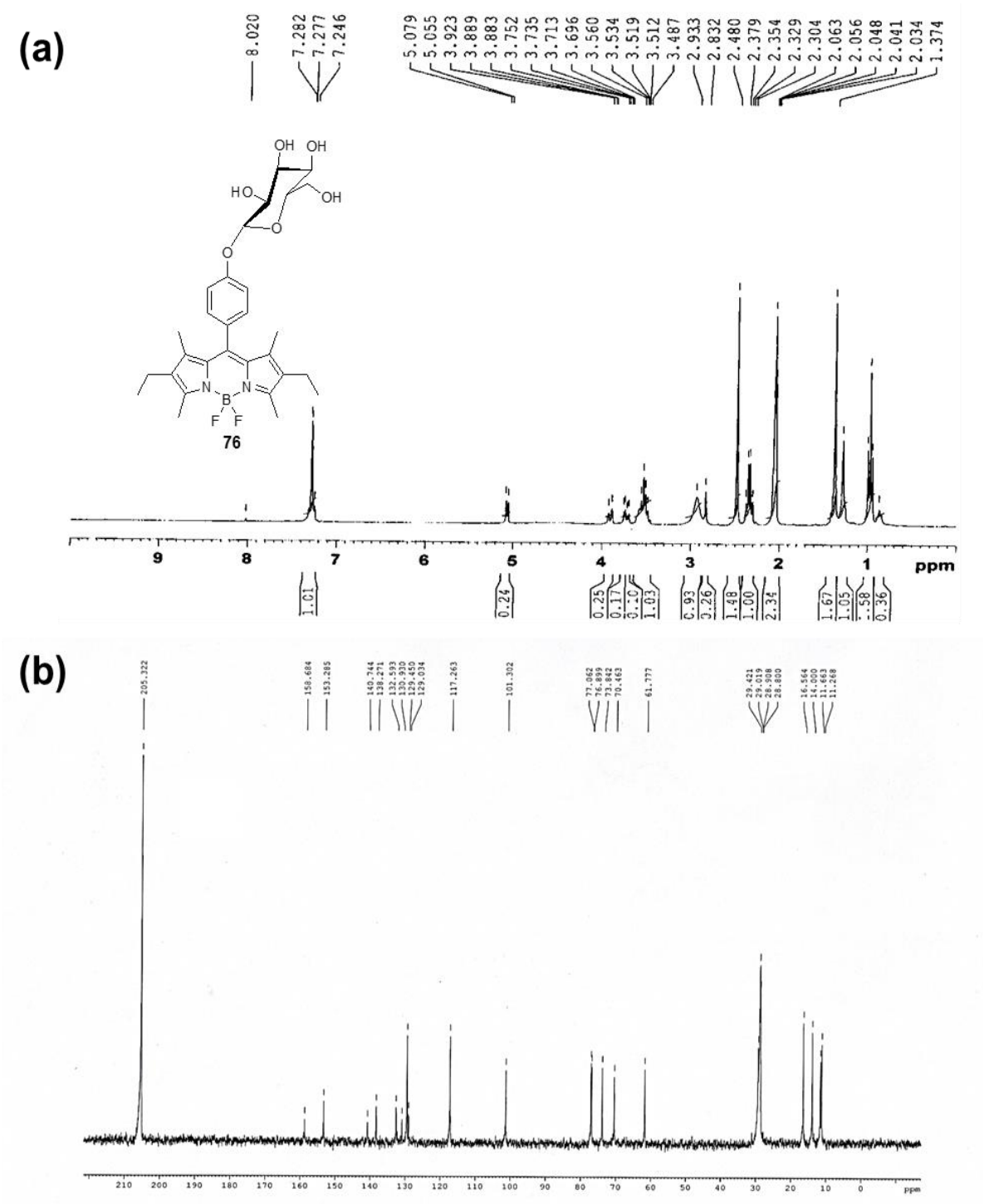

Figure 4.4.2.3 The NMR spectrum of **76** (a) ^{1}H NMR, (b) ^{13}C NMR.

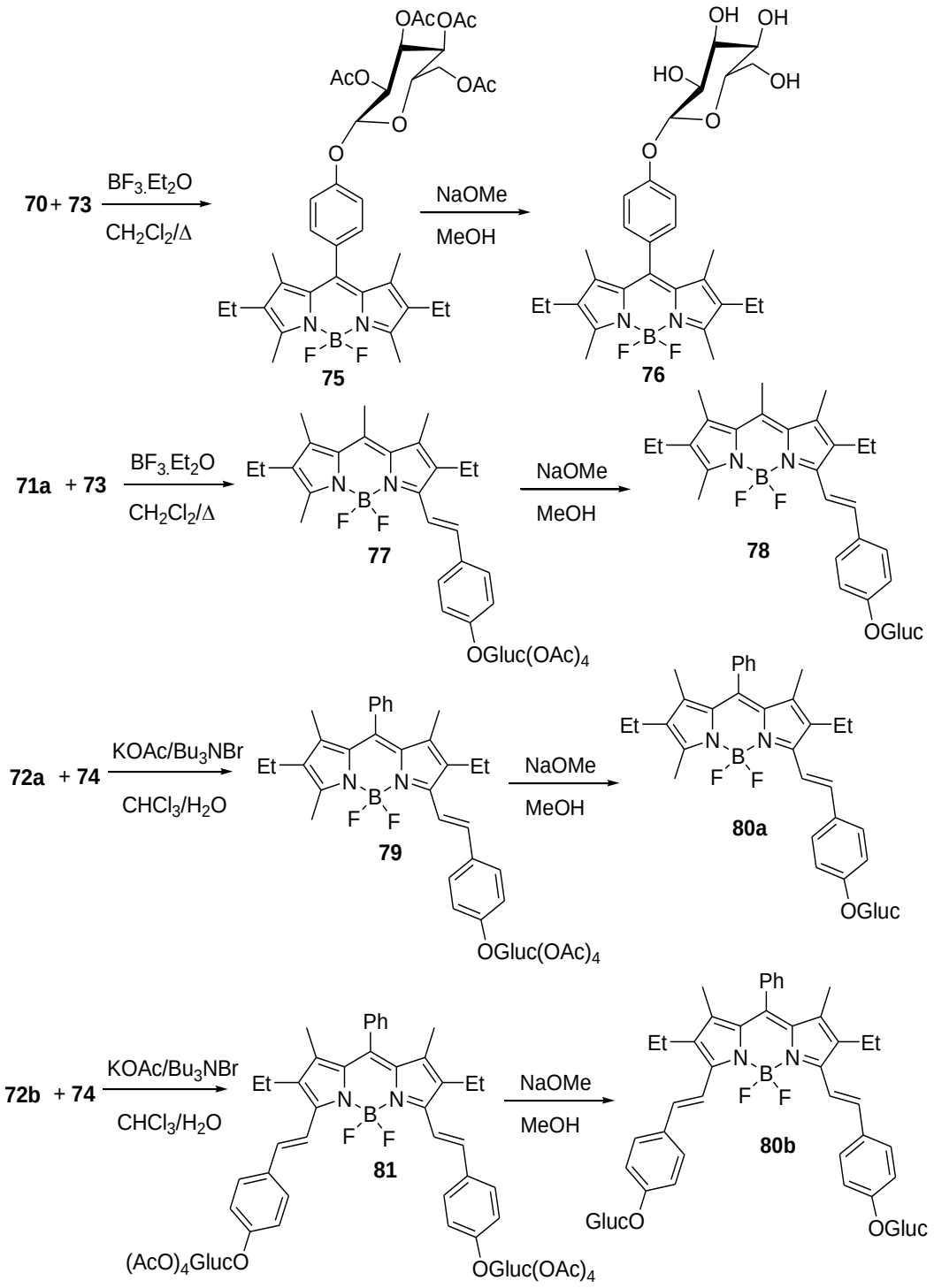

Scheme 4.4.2.3 Synthesis of the water-soluble Bodipy-dyes.

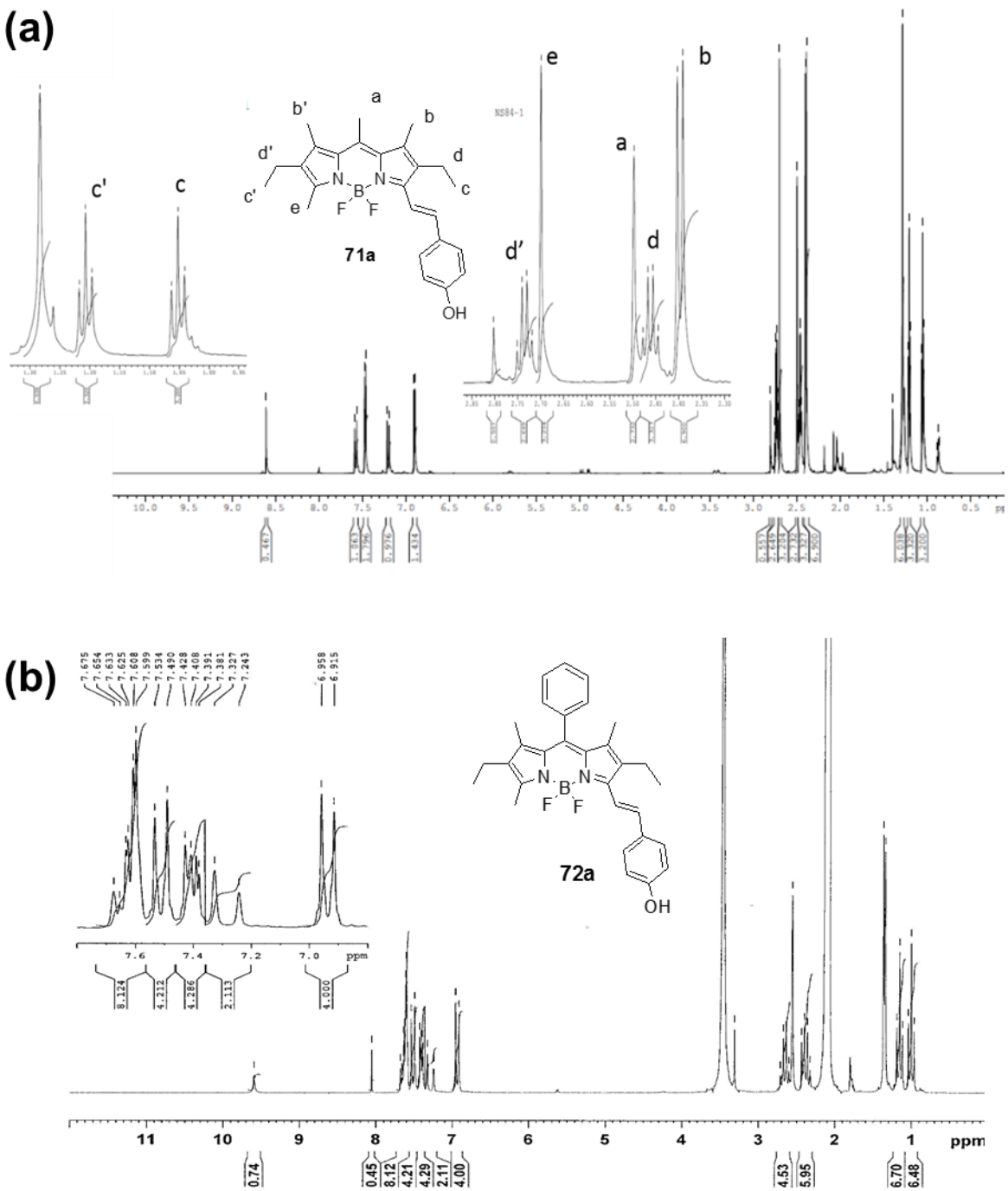

Figure 4.4.2.4 The ^{1}H NMR spectrum of compound (a) **71a**, (b) **72a**.

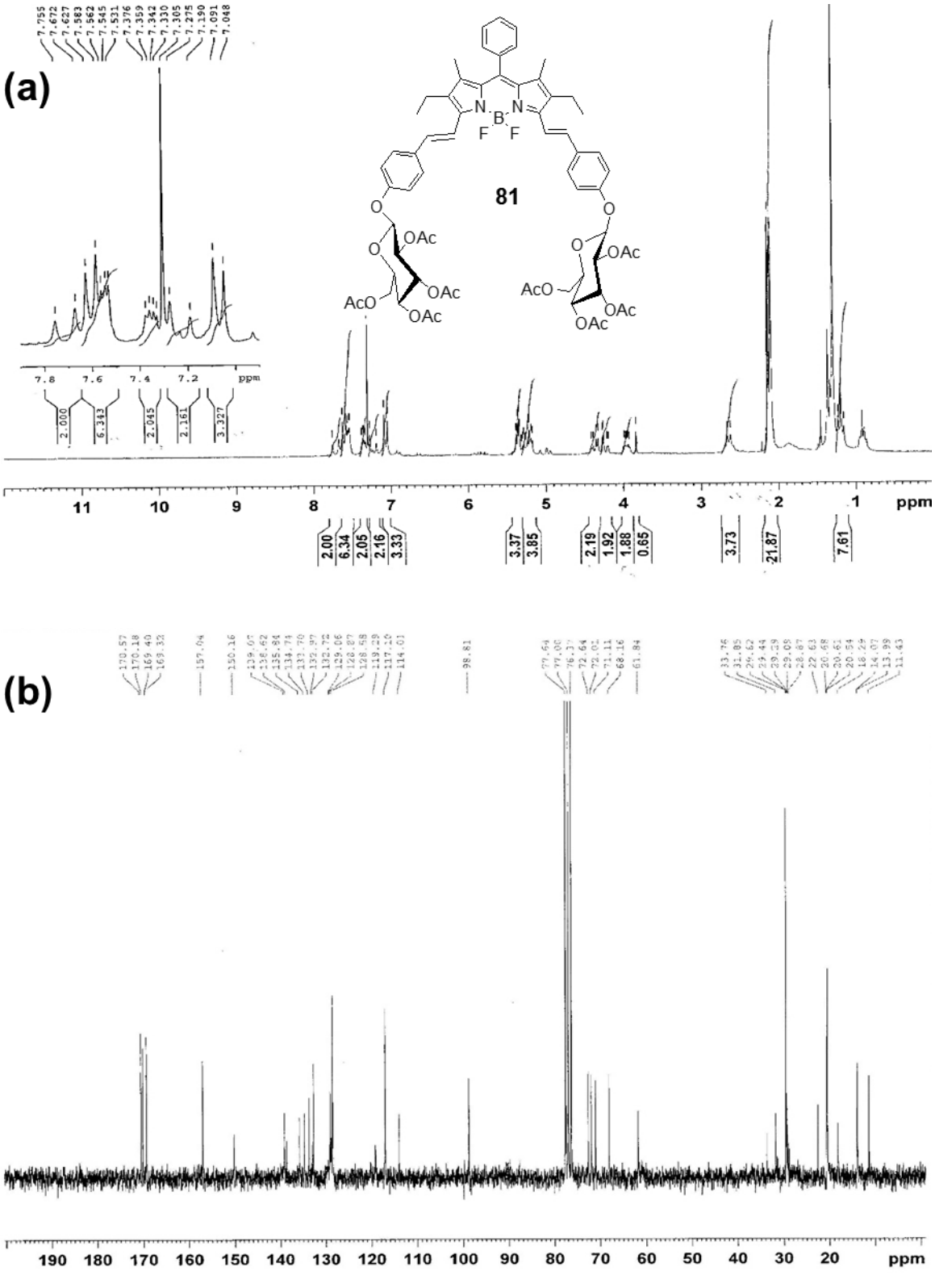

Figure 4.4.2.5 The NMR spectrum of **81** (a) ^{1}H NMR, (b) ^{13}C NMR.

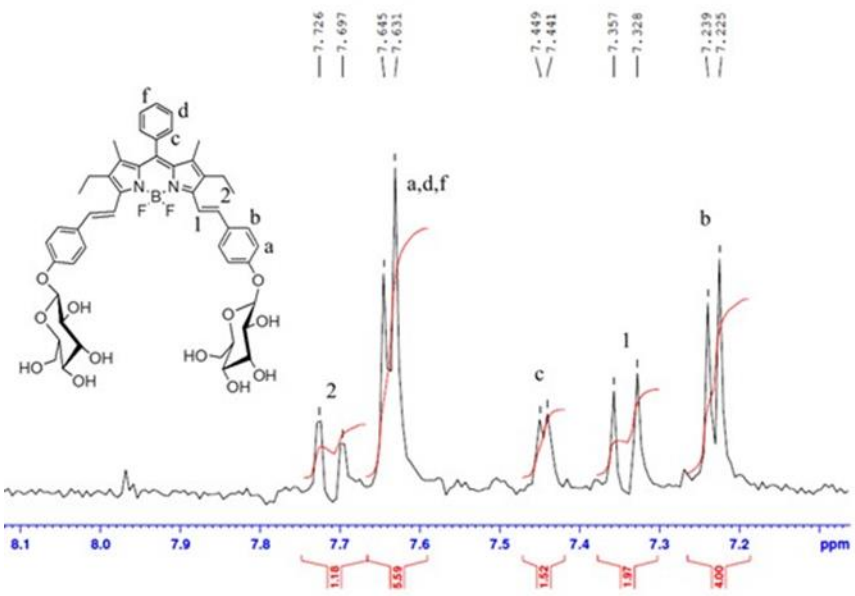

Figure 4.2.2.6 ^{1}H NMR of compound **80b** in d^{4}-methanol.

4.4.3. Photophysical characteristics

The UV/Vis absorption and fluorescence spectra of Bodipy-*O*-glycosides **76**, **78**, **80a** and **80b** in ethanol are shown in **Figures 4.4.3.1a** and **b** and the photophysical data summarized in **Table 4.4.3.1**. All these Bodipy-*O*-glycosides exhibited typical spectral characteristics of the Bodipy core dyes with narrow $S_0 \rightarrow S_1$ absorption band, a weak and broad $S_0 \rightarrow S_2$ absorption band, high molar extinction coefficients, intense fluorescence emissions and small Stokes' shifts. The absorption and emission spectra were almost mirror images of each other, indicating that the emitting species are similar to the absorbing ones. Compared to the non-styrylated Bodipy **76**, introduction of first styryl group as in **78** and **80a** induced significant bathochromic shifts in the absorption (51-63 nm) and emission maxima (50-55 nm), whereas introduction of a second styryl moiety as in **80b** caused further red-shifts (123 nm) of both absorption and emission maxima. Fluorescence quantum yields of compounds **80a** and **80b** were significantly lower due to nonradiative loss of energy via rotation around the C-Ar bonds.[96]

Table 4.4.3.1: Photophysical parameters of the dyes **76**, **79a**, **80a** and **80b** in ethanol.

Dye	λ_{abs}[a] **[nm]**	ε_{max}[b] **[10^4 $M^{-1}cm^{-1}$]**	λ_{em}[c] **[nm]**	Φ_{fl}[d]
76	523	8.3	540	0.84[e]
78	574	8.2	590	0.60
80a	586	8.0	595	0.52
80b[f]	646	9.2	665	0.50

[a]Error: ± 0.2 nm. [b]Extinction coefficients for the corresponding λ_{max}. [c]Error: ± 0.3 nm. [d]The fluorescence quantum yields of the dyes **78**, **80a** and **80b** are relative to that of the dye Rh101 (Φ_{fl} = 1 in EtOH). [e]The fluorescence quantum yields of **76** is relative to that of **21** (Φ_{fl} = 0.84 in EtOH). [f]Because of poor solubility of **80b**, its solution in EtOH was prepared by diluting its stock solution, made in DMSO with appropriate amount of EtOH.

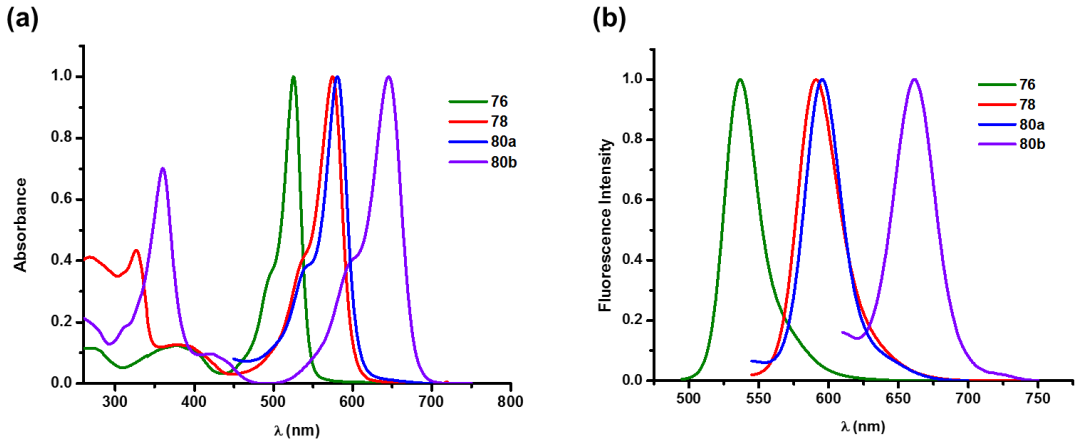

Figure 4.4.3.1. Spectral features of the water-soluble Bodipy dyes in EtOH. (a) Absorption spectra; (a) Emission spectra.

4.4.4. Aggregation behaviour

Fluorescent organic nanoparticles are of interest in materials science, particularly for biological imaging, and as delivery vehicles.[97] These materials offer the possibilities of intercalating multiple dyes of disparate optical properties into one-dimensional

heterostructures,[98a] or promoting fluorescence resonance energy transfer (FRET) for white-light emission.[98b] Further, compounds with carbohydrates as appendages are known to form organogels or hydrogels that are of potential applications in tissue engineering, and development of new materials that reversibly respond to various external stimuli.[99] A large number of glucose derivatives have been reported to form hydrogels.[100] The poor solubility of compound **80b** in most of the organic solvents except DMSO and presence of two glucose moieties in it encouraged us to probe its ability to form aggregates. For this, the UV–vis absorption and fluorescence spectra of compound **82b** (5.0 μM) in THF and EtOH as such, and with gradual addition of H_2O were recorded. The H_2O concentration was varied between 0-90%. In pure THF and EtOH, the compound showed strong and sharp absorption maxima at 648 nm and at 646 nm respectively due to the $S_0 \rightarrow S_1$ transition of the monomeric Bodipy core, and showed an emission maximum at 700 nm on excitation at 580 nm.

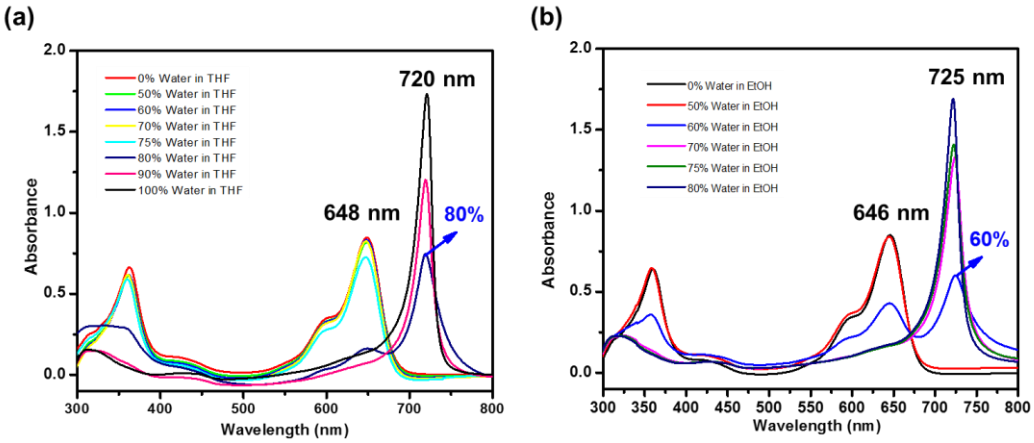

Figure 4.4.4.1. UV–vis spectra of **80b** (5.0 μM) in THF-water (a), and EtOH-water (b).

On incremental addition of H_2O, a new absorption peak at 725 nm emerged, but at a considerably higher water concentration. However, the spectra retained the typical shapes of the Bodipy chromophores, while the lower wavelength peak at 370 nm

accounted for the styryl moieties. The emergence of the new peak signified aggregation of the dye that started at 60% and 52% water in THF and EtOH respectively. The absorption peak of the parent dye completely vanished in 90% water-THF and 75% of water-EtOH media (**Figure 4.4.4.1**). Significant color changes, dramatically reduced fluorescence color and intensities were the other distinct hallmarks of water addition. The dye fluorescence completely vanished at 95% aqueous THF. These changes signify solvent-induced formation of aggregates. The lack of any isosbestic point in the absorption spectra during the aggregation process, clearly indicated non-existence of a two-state equilibrium between the monomer and aggregates.

Furthermore, the loss of the monomer peak or the rise of the aggregates peak followed a complex kinetics rather than the first or second order kinetics (data not shown), negating the possibility of a simple reaction mechanism that did not involve intermediates. Finally, it should be noted that the changes in monomer absorbance exactly paralleled changes in fluorescence intensity, but no changes were observed in the shape of the excitation spectrum, consistent with the nonfluorescent nature of the aggregate species.[101] Previously, almost quantitative formation of nonfluorescent Bodipy H dimers has been reported by molecular confinement of the dyes within a sodium silicate derived glass. No interference from higher-order aggregates or fluorescent J dimers was observed.[102] Based on the previous and present observations, it is tempting to propose initial formation H dimers of **80b** in aqueous THF and EtOH solvents that may stack to furnish the aggregates.

The aggregation process was also followed as a function of water concentration by ^{1}H NMR spectra (**Figure 4.4.4.2**). Significant upfield and downfield shifts of various

aromatic protons as well as their signatures clearly established the complex kinetics of the process.

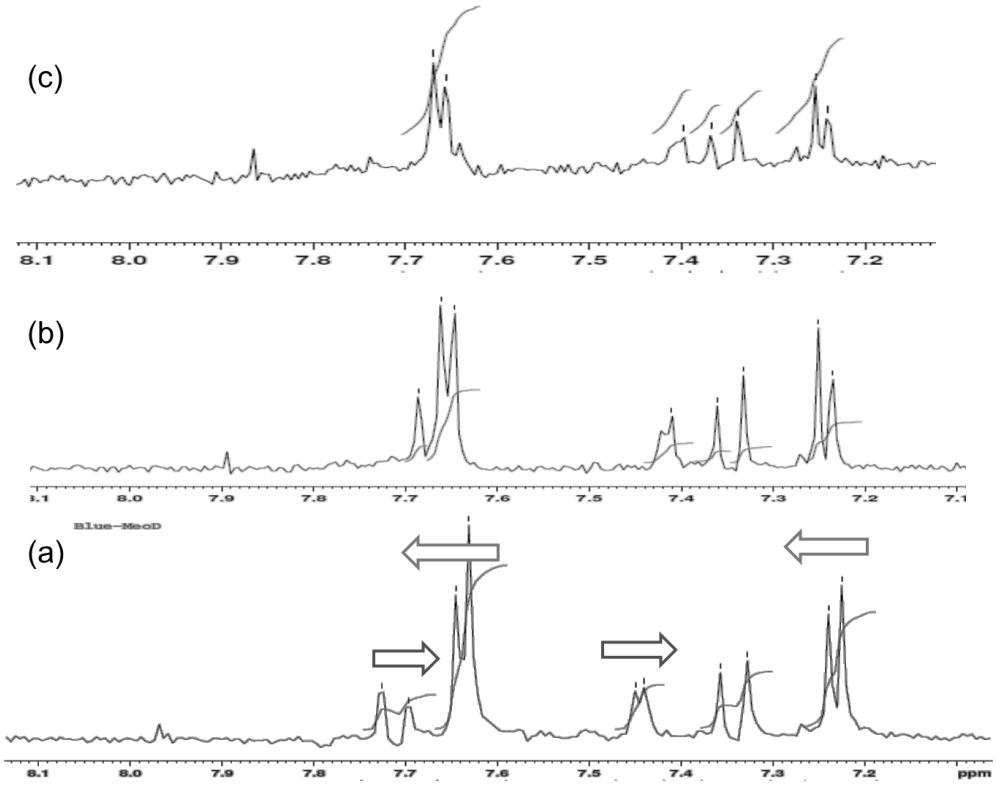

Figure 4.4.4.2 ^{1}H NMR spectra of **80b** (50 μM) in in d^4-methanol (a) 0% D_2O; (b) 20% D_2O; (c) 30% D_2O.

Final evidence for the aggregation behavior of **80b** in the mixed solvents was obtained from the dynamic light scattering (DLS) studies. In pure THF or EtOH, no correlation was observed indicating the absence of any aggregation. **Figure 4.4.4.3a** shows the intensity of the correlation function of **80b** (5 μM) in THF-water mixtures at varying water concentration. The correlation function developed as the water content reaches 70% and its amplitude increased progressively with the increase in water content from 72% to 76%. Analysis of the correlation function using the Inverse Laplace

transform software gives the size distribution of the aggregates present. **Figure 4.4.4.3.b** shows the corresponding size distribution obtained by analyzing the data of **Figure 4.4.4.3a**. The aggregates were polydisperse in nature with the size ranging from about 20 nm to 1 micron, and an intensity weighted average diameter of 260 nm. With an increase in water content, the distribution shifted to larger sizes, although the size distribution did not change much beyond 74% of water content.

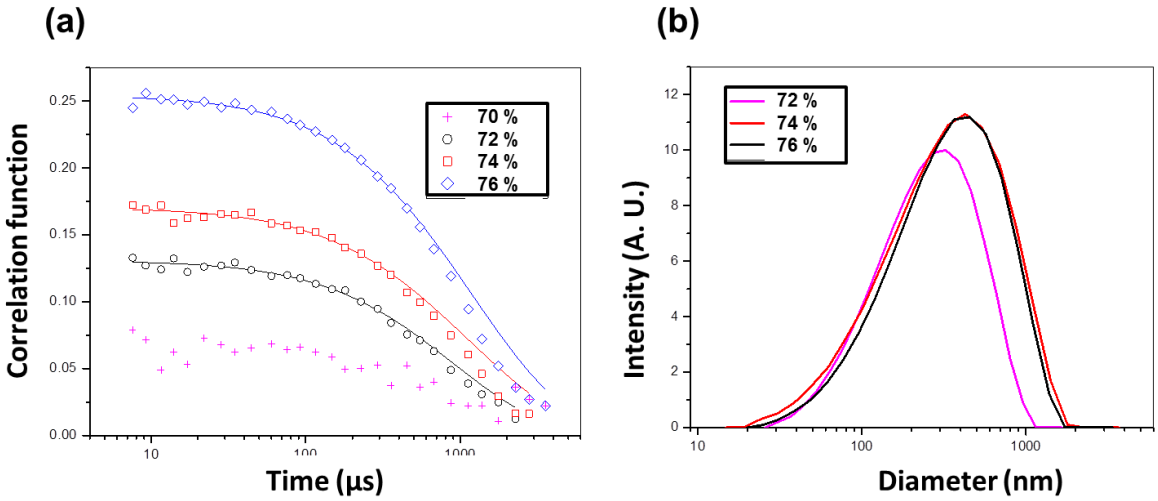

Figure 4.4.4.3. (a) The scattered intensity correlation function of **80b**-aggregates (5 µM) in THF/water mixture at different water contents. (b) Size distribution of the aggregates obtained by fitting the data in **Figure 4.4.4.3a** (solid lines indicating the fit).

The size distribution of the nanoaggregates in EtOH-water was found to vary from 100 nm to 10 micron with an intensity-weighted average diameter of 1 micron. However, there was no further growth in size of aggregates in 52% aqueous EtOH, and the aggregates were stable even after more than one month.

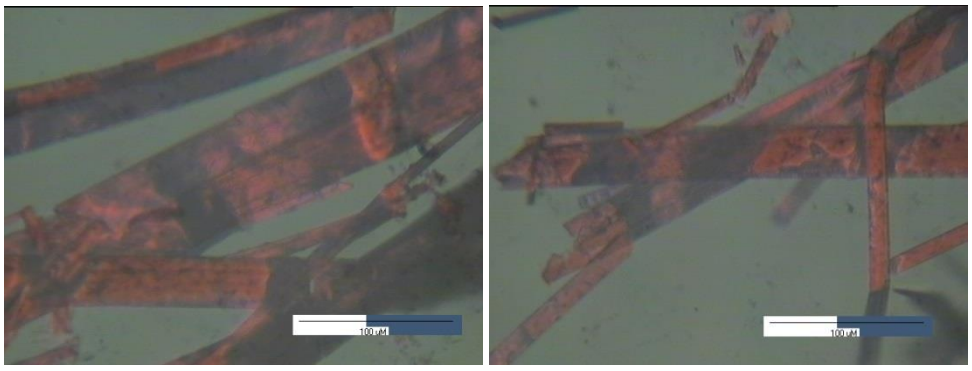

Figure 4.4.4.4. Images of self-assemblies of **80b**-aggregates, formed in THF-water system via slow evaporation, as revealed by obtained from optical microscopy.

The organogels can self-assemble into various nanoscale superstructures such as fibers, rods, ribbons, and tubes. The ability of the Bodipy derivative **80b** to undergo self-association was clearly visible in the optical microscopic images (representative images shown in **Figure 4.4.4.4**). The morphology of the aggregates, obtained on slow evaporation of the solvent appeared as solid fibrillar assemblies without any tubular structure. Possibly, hydrogen bonding between the hydroxyl groups of the sugar moiety in **80b** stabilized the aggregates and determined the overall morphologies. More ordered crystalline aggregates can be induced by reducing the water concentration in aqueous THF. The formation of the self-assembly is a spontaneous process, and takes place under non-equilibrium conditions. Noncovalent interactions give rise to the formation of superstructures, which subsequently entrain and immobilize the solvent inside the interstices of a three-dimensional network.[103] Earlier, formation of Bodipy aggregates could be synthesized by incorporating long chain trialkoxyphenyl fragments and trimethylammonium head-groups.[104] Thus, the present result of Bodipy aggregation by mere introduction of two glucose units is unique, and may be useful for soft matter chemistry.

4.4.5. DNA binding characteristics

$^1O_2$ is a highly reactive species but has a short apparent lifetime (ca. 2.0 μs) with a low apparent diffusion coefficient (4×10^6 cm^2 s), and thus a very limited sphere of activity (about 155 nm in radius) in biological systems. This implies that the PDT agents should have good binding ability toward DNA that is one of the main targets of many anticancer drugs, including the PDT agents. Hence the DNA binding properties of the dyes **76** and **78** were studied using absorption photometric technique. Compounds **76** and **78** had strong absorption bands at 522.6 nm and 573.8 nm respectively, which could be conveniently used the spectrophotometric titrations. Incremental addition of double stranded calf thymus (CT)-DNA (0–200 μM DNA base pair) to a fixed concentration of **76** (20 μM) and **78** (50 μM) led to gradual reductions in the intensities of their respective absorption maxima (**Figure 4.4.5.1**), confirming their binding with DNA. Based on the site-exclusion model,[105] the equilibrium binding constants (K) in respective cases were derived by quantitative analysis of the UV–visible data (**Figure 4.4.5.2**). The moderate K-values of were 3.4×10^4 M^{-1} and 1.8×10^4 M^{-1} for of **76** and **79a** respectively, while the linear fits in regression analysis indicated a single mode binding of them with DNA. Because the DNA-intercalators generally show higher binding constants ~10^5 - 10^7 M^{-1}, the lower K-values suggested an ionic binding. This was also evident from the lack of additional absorption peak for any new species. Earlier the well-known DNA intercalator, coralyne was reported to produce new species on binding with DNA.[106]

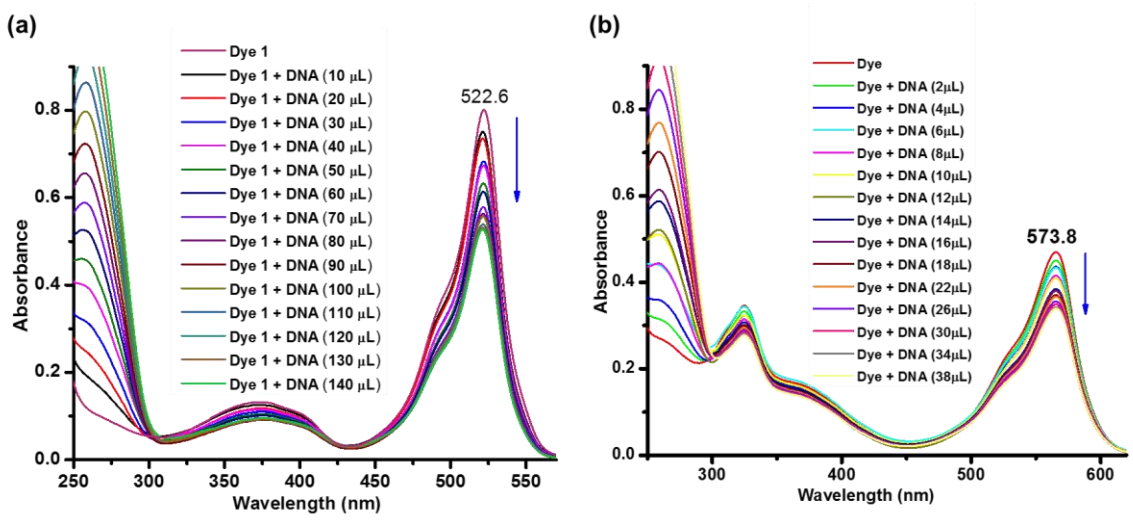

Figure 4.4.5.1 The UV–vis titration of dyes with CT-DNA. (a) dye **76** (20.4 µM); (b) dye **78** (50 µM). The experiments were carried out in phosphate buffer (5 mM, 7.4 pH) at at 25 ^{o}C. The CT DNA concentrations were varied from 9.9 to 130.8 µM for **76** and 5.3 to 110.5 µM for **78**, using 0.164 mM bp aliquots.

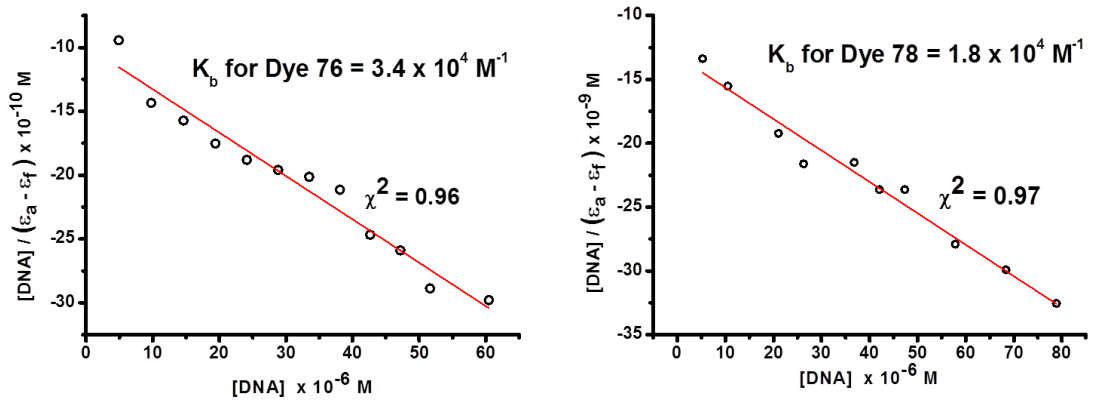

Figure 4.4.5.2 Scatchard plots of the DNA binding experiments. (a) dye **76** (20.4 µM); (b) dye **78** (50 µM).

4.4.6. PDT studies

In view of the above results, the *in vitro* photodynamic activities of the Bodipy-*O*-glycosides **76**, **78** and **80a** were assessed against the highly invasive and metastatic human lung cancer A549 cell lines. For comparison, the corresponding non-glycosylated precursors, **70**, **71a** and **72a** as well as the commercial dye PM567 **21** were included for

their cytotoxicities. In addition, the dark cytotoxicities of some of the compounds were also evaluated. The compounds used for the PDT studies are shown in **Figure 4.4.6.1**.

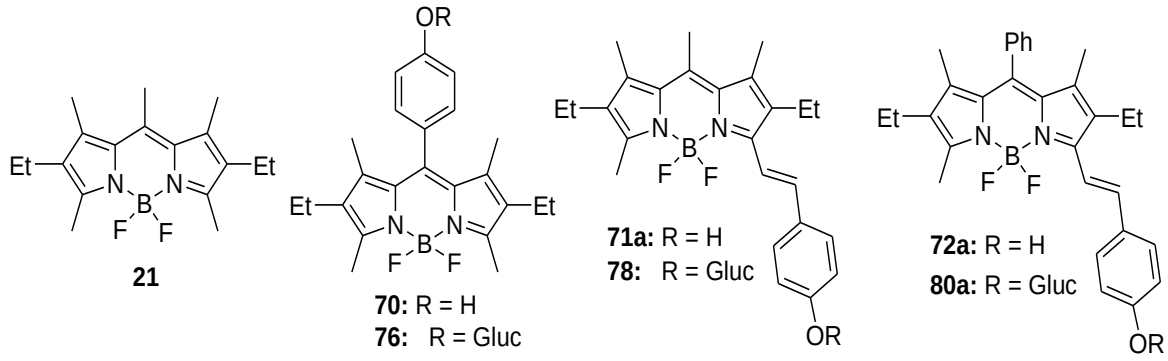

Figure 4.4.6.1 The chemical structures of the Bodipys, used for the PDT evaluation.

The studies were specifically targeted to lung cancer as it remains one of the most common cancer-related causes of death. This type of cancer typically develops over a period of many years, and its incidence and mortality rate increase gradually each year. Despite the rapid progress of surgery, radiotherapy, chemotherapy, and biotherapy, the long-term survival rate of patients with lung cancer remains poor, and new therapeutic strategies are urgently needed.[107] Fortunately its early detection can improve the prognosis significantly and increase the life span of the patients. Since early lung cancer detection is now becoming feasible, PDT may play an important role in lung cancer treatment especially at an early stage.[108] Several clinical trials have established the efficacy of PDT with superficial small tumors, while its use as a preoperative measure may reduce tumor burden and the degree of surgery for larger tumors.[109] Presently, besides evaluating the *in vitro* cytotoxicity of the designated Bodipys, their intracellular localization, and the involvement of apoptosis in their PDT property were also examined, as discussed below.

4.4.6.1. Cytotoxicity. None of the test compounds showed any toxicity to the A549 cells up to 200 μM, as revealed by the MTT results at 24 h. However, all the compounds dose-dependently reduced viabilities of the A549 cells under photo-exposure, with respect to vehicle treated controls (**Figure 4.4.6.2.**).

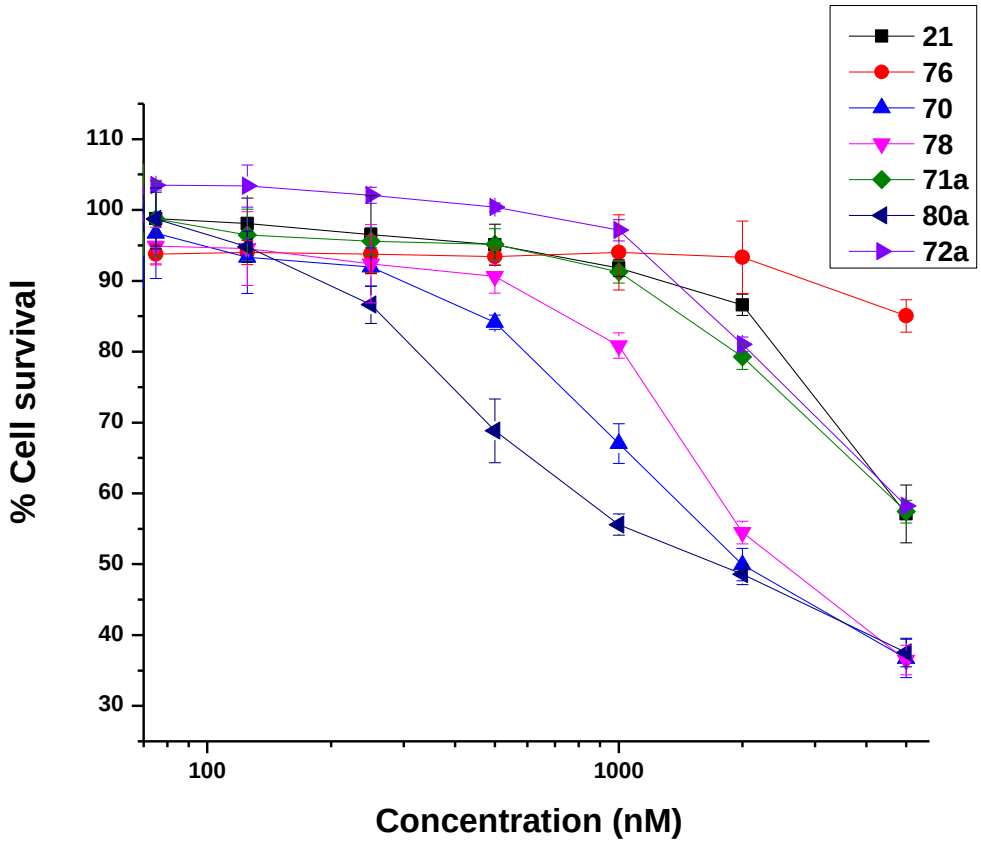

Figure 4.4.6.2 Dose-dependent photo-cytotoxicities of PM57, the parent Bodipy dyes and their *O*-glycosides against human lung cancer A549 cells. Cells (1×10^4/well), grown in 96-well plates were treated with vehicle (0.1% DMSO) or increasing concentrations of the test compounds along with photo-exposure (dose 5.5 J/cm^2). The cell viability was assessed by the MTT assay after 24 h. The results are expressed in percentage survival considering that of the vehicle-treated control cells as 100. The experiments were repeated three times with similar results. All determinations were made in four replicates, and the values are means ± S. E. M. $^{*}P<0.01$, $^{**}P<0.001$ compared to vehicle control.

Based on the MTT assay results, the growth inhibitory IC_{50} values, defined as the concentrations of the dyes required to kill 50% of the cells were calculated and are shown

in **Table 4.4.6.1**. The relative potency of the test compounds was **80a**>**70**>**78**>**71a=72a~21**>**76**. Thus, amongst those chosen, the mono- and distryryl Bodipys **78** and **80a** were more potent than their non-glycosylated precursors **71a** and **72a**. Surprisingly, however, glycosylation reduced the potency in case of the *meso*-aryl containing compounds **70** and **76**. The other interesting observation was the almost similar activity of **71a**, **72a** and **21**, suggesting that red-shifting of the emission maxima had less impact on the PDT activity of the chosen Bodipys.

Table 4.4.6.1: Comparative cytotoxicities of the chosen Bodipy dyes against A549 human lung cancer cells.[a]

Non-glycosylated Bodipys	IC_{50} (μM)	**Glycosylated Bodipys**	IC_{50} (μM)
21	6.8 ± 1.8		
70	2.1± 0.6*	**76**	> 10
71a	6.5± 2.1	**78**	2.7± 0.8**
72a	6.4± 2.0	**80a**	1.8± 0.5**

[a]The MTT data shown above was used to calculate IC_{50} values. The experiments were repeated three times with similar results. All determinations were made in four replicates, and the values are means ± S. E. M. *P<0.001 compared to the corresponding glycosylated Bodipy, **P<0.001 compared to the corresponding non-glycosylated Bodipys.

4.4.6.2. Subcellular localization. Photodynamic efficacy is principally determined by the subcellular localization of a PS.[110a] The distribution of a PS within a cell depends on its chemical nature, concentration in the culture medium and also on the incubation time.[110b] Some photosensitizers show a broad distribution, while some may localize more specifically. Hence, to explain the photocytotoxicity results, fluorescence microscopic

studies were carried out to investigate the cellular uptake and localization of these compounds. The intracellular accumulation of all the Bodipy dyes loaded on the A549 cells as displayed in the dual staining with Hoechst-33342 (nucleus specific dye) by fluorescence microscopy exhibited particular localization in the cytoplasm (**Figure 4.4.6.3.**). However, compared to the other dyes, compound **21** showed lower fluorescence, indicating its lesser cellular uptake. Also, the patchy fluorescence in the cells, stained with **21** indicated its non-uniform presence in the cytoplasm with higher accumulation near the membrane. The other dyes had uniform florescence all over the cytoplasm of the cells. The significantly less uptake of the dye **80b** was anticipated considering its tendency of aggregation in aqueous-organic media. Hence, the uptake of the acetate **79**, the less polar precursor of **80b** was checked. Surprisingly, the acetate displayed almost no cellular uptake (**Figure 4.4.6.4.**) that was even less than that of **21**. This also ascertained good hydrophilic-hydrophobic balance in the glycosylated dyes, selected for the present investigations. The non-glycosylated precursors (**70**, **71a**, **72a**, and **72b**) showed more diffused florescence compared to their respective glycosylated dyes. This may account for the poorer efficacy of the styryl-Bodipys **71a**, and **72a** compared to that of the glycosylated counterparts **78**, and **80a**.

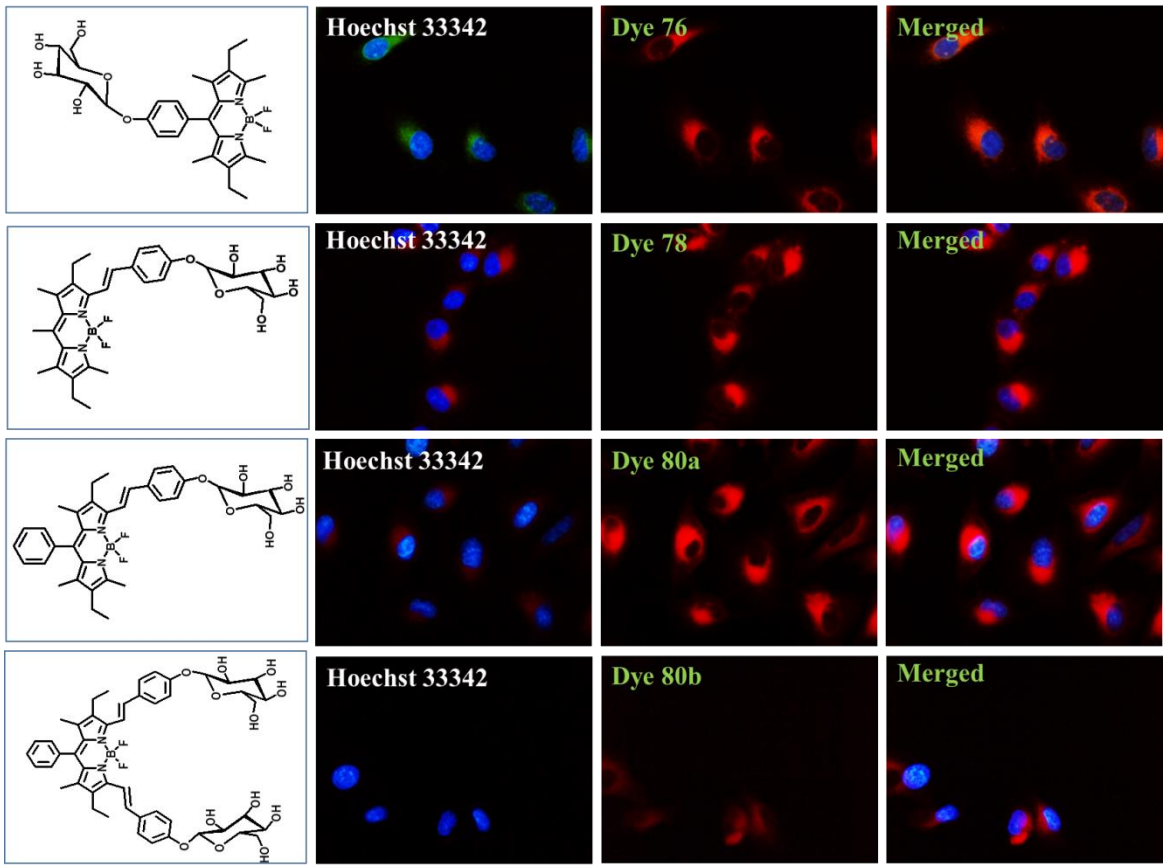

Figure 4.4.6.3 Subcellular localization of the glycosylated Bodipy dyes in A549 cells. The cells were incubated with the dyes (5 μM) and Hoechst 33342 (used as the nucleus tracer) for different periods and the images captured with a fluorescence microscope. Representative Hoechst 33342-stained, bright field and the corresponding superimposed images, captured at 1 h are shown in columns 2-4, respectively.

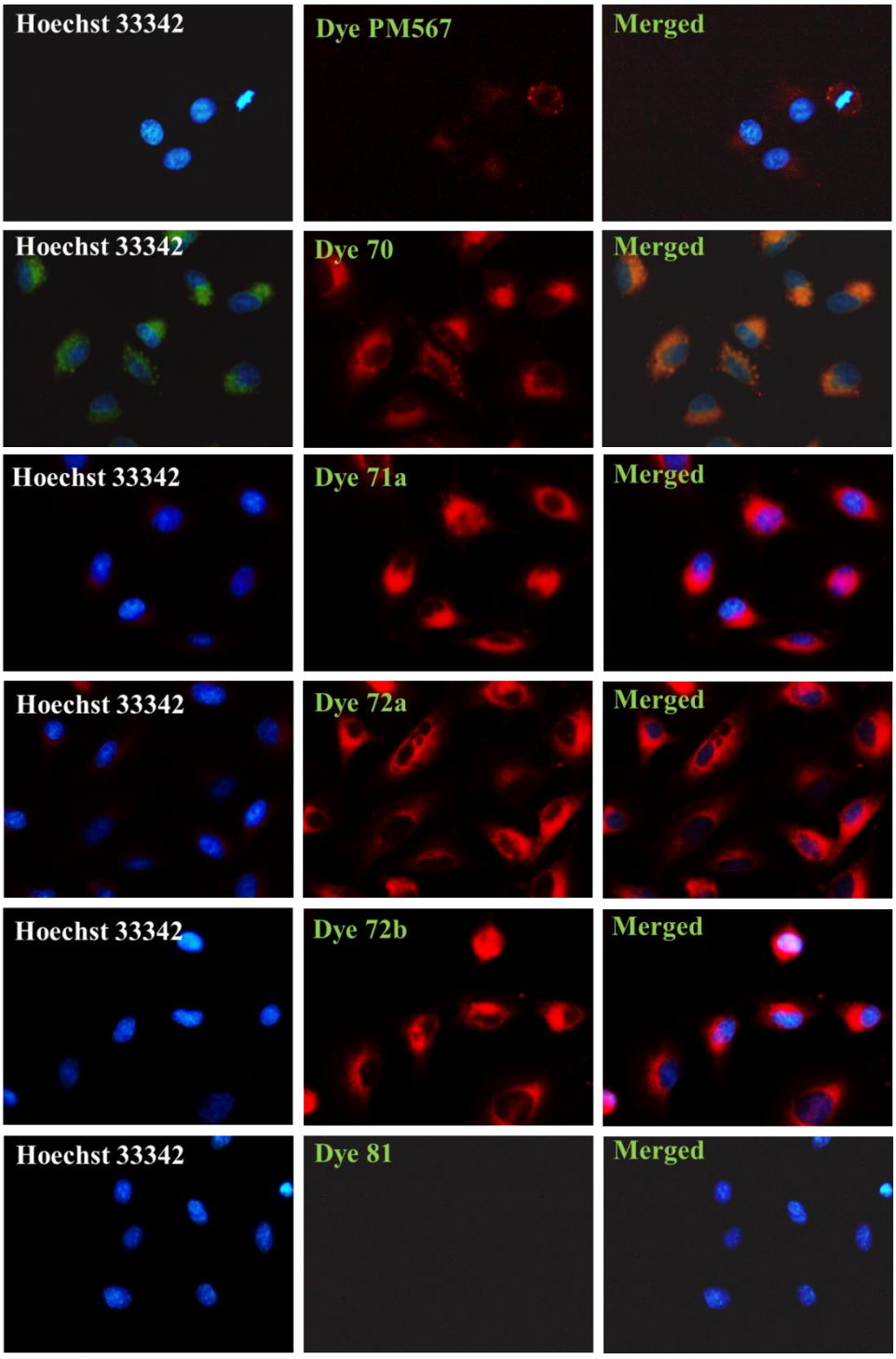

Figure 4.4.6.4 Subcellular localization of the non-glycosylated Bodipy dyes in A549 cells. The cells were incubated with the dyes (5 μM) and Hoechst 33342 (used as the nucleus tracer) for different periods and the images captured with a fluorescence microscope. Representative Hoechst 33342-stained, bright field and the corresponding superimposed images, captured at 1 h are shown in columns 2-4, respectively.

***4.4.6.3. Apoptosis induction*.** Apoptosis is an important cellular event that plays a key role in pathogeny and therapy of many diseases.[111] It is believed to be associated with caspase activation via two separate *viz.* extrinsic or cytoplasmic, and intrinsic or mitochondrial pathways. The intrinsic pathway involves perturbation of intracellular homeostasis, and is linked primarily to mitochondrial changes, directly inducing the release of cytochrome c into the cytosol and apoptosome complex formation with activation of caspase-9. The extrinsic pathway, however, is initiated by the binding of a member of the tumor necrosis-factor (TNF)-family of death-receptor ligands to their cognate receptors (TNFR or Fas). When a death stimulus triggers the pathway, the membrane-bound FasL interacts with the inactive Fas complexes and forms the death-inducing signaling complex (DISC). The DISC contains the Fas-associated death domain (FADD) and procaspase 8, which becomes autocatalytically activated, and in turn, cleaves downstream effector pro-caspase-3/-7. The effector caspases then process different substrates, leading to apoptotic cell death. Studies have demonstrated that apoptosis induction plays the most vital role in the cancer treatment.[112a] Dysregulation in apoptotic pathways has been implicated in the development and progression of malignant tumors as well as occurrence of chemoresistant phenotypes.[112b,c] In response to PDT, apoptosis has been found to be a prominent form of cell death for many cell lines in tissue culture.[112d]

In the present study, apoptosis induction by the Bodipys was confirmed by quantifying the sub G1 population in the cells, treated with different concentrations (0–50 μM) of **76** and **78** at 24 h. Although compound **80a** was slightly more potent, the vast difference in the MTT assay results of **76** and **78** was inexplicable. In particular, it was

important to confirm that the better cytotoxicty of **78** was due to apoptosis, and not necrosis. Hence, the compounds **76** and **78** were chosen for the apoptosis studies that also included parallel assays in the absence of light. The results (**Figure 4.4.6.5.**) indicated that the compounds are essentially non-toxic toward the A549 cells in darkness. However, under illumination, both the compounds increased the sub-G1 cells population concentration-dependently, compared to control, and the effects were also proportional to the illumination dose up to 80 min of photo-exposure. For an illumination time of 80 min, compound **76** (10-50 μM) increased the sub-G1 phase cell population to ~2–4.8 fold, revealing induction of a robust apoptosis. But when the illumination time was reduced to 30 min, it could induce significant apoptosis only at concentrations ≥20 μM. In comparison, compound **78** was a more effective apoptosis-inducer as it (5 μM) increased the sub-G1 phase cell population to ~3.5 and 5.2 folds, compared to control at 30 and 80 min of illumination respectively. Further, its activity reached a plateau value (4 fold) at 10 μM after 30 min of photo-exposure. A similar activity trend was also noticed when the photo-exposure time was 80 min. This confirmed that the photo-toxicity of **78** to the A549 cells was due to apoptosis without any significant necrosis.

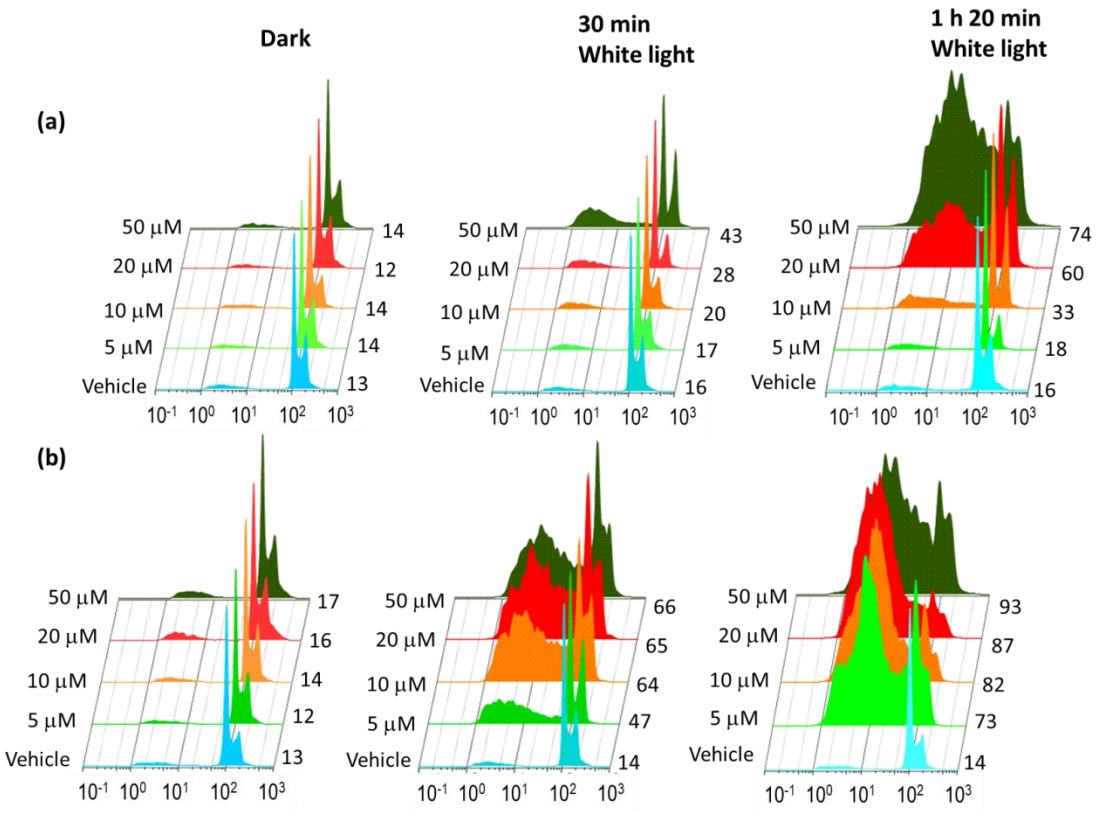

Figure 4.4.6.5 Apoptosis induction by **76** and **78** in A549 cells under dark and white light illumination, as revealed by flow cytometry. The cells were incubated with **76** and **78** (0-50 µM) for 1 h, exposed to light for 30/80 min and further incubated for 24 h. Subsequently, 20000 cells in each treatment were acquired using a flow cytometer, and the DNA content of the nuclei registered on a logarithmic scale. The Sub-G1 region (RN1) represents the percentage of cells undergoing apoptosis. The experiments were repeated three times with similar results. All determinations were made in three replicates, and the values are means ± S. E. M. ***P*<0.001 compared to vehicle control**. A representative figure is shown.

***4.4.6.4. Caspase activation*.** Several observations have indicated that compounds that localize within mitochondria or ER promote apoptosis, while activation of PS targeting either the plasma membrane or lysosomes can either delay or even block the apoptotic program prompting the cells to necrosis. [113a,b] Because, all the chosen Bodipy compounds for the present studies were accumulated in the cytoplasm, it was necessary to confirm the apoptosis induction by other methods, besides the sub-G1 accumulation. Activation

of the caspases is perhaps the most well characterized apoptotic cascade.[114a] Depending on the involvement of extrinsic or cytoplasmic pathway, the final execution of apoptosis is often mediated through caspase-8 or caspase-9 as the initiators, and caspase-3 as the effector. Assaying caspase-3 is widely used as a tool for detecting programmed cell death.[114b,c] Presently the involvement of apoptosis was further ascertained by examining the activation of the above caspases by compound **78** under photo-exposure. The compound **78** was chosen because of its better activity than **76**.

At 16 h, compound **78** (1.25 μM) stimulated (*P<0.001*) the activities of caspase-3 (~2.7 fold) and caspase-8 (~3.1 fold) without any increase in the caspase-9 activity, compared to the untreated control cells (**Figure 4.4.6.6**). Such activation of caspase-3/8 was abrogated in the presence of the respective specific caspase inhibitors (each 20 μM).

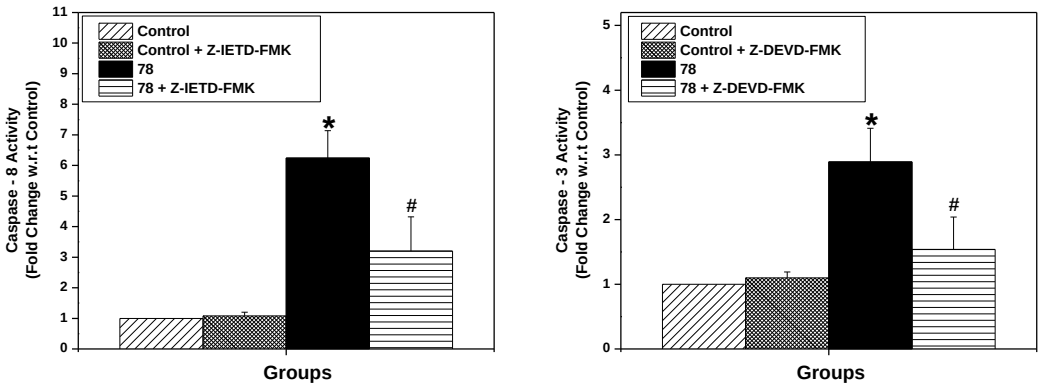

Figure 4.4.6.6 Caspase activation by **78** in A549 cells under white light illumination. The cells, as such or pre-incubated with specific caspase-3 and caspase-8 inhibitors (40 μM) for 1 h were incubated with **78** (1.25 μM) for 1 h, and exposed to light for 1 h. The caspase-3 and caspase-8 activities were assayed by ELISA after 16 h. The experiments were repeated three times with similar results. All determinations were made in three replicates, and the values are means ± S. E. M. $^{*}P$<0.001 compared to vehicle control; $^{\#}P$<0.001 compared to **78**-treatment.

For further confirmation, the effects of the specific caspase inhibitors (each 40 μM) on the cytotoxicity of compound **78** (1.25 μM) under photo-exposure for 80 min

were assessed by the MTT assay at 24 h. Pre-incubation of the A549 cells for 1 h with specific caspase-8 and caspase-3 inhibitors increased the cell viability by 76.2% (P<0.001) and 22.4% (P<0.05) respectively, compared to the only **78**-treated cells under photo-illumination (**Figure 4.4.6.7.**). However, the caspase-9 inhibitor did not show any effect on the cell survival. Pre-treatment the cells with the pan-caspase inhibitor increased the cell survival to 2.1 fold (P<0.001) compared to the cells not receiving the above inhibitor. Taken together, these suggested the involvement of the extrinsic apoptotic pathway in the photo-toxicity of **78** to the A549 cells.

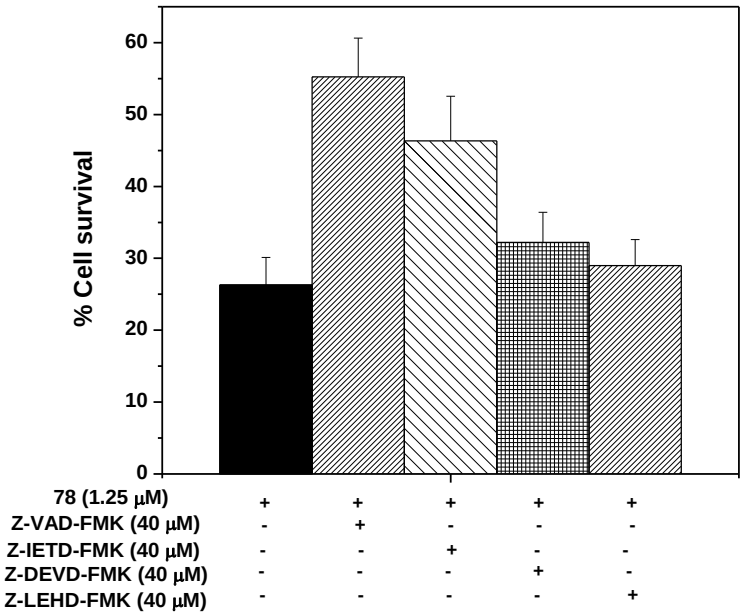

Figure 4.4.6.7 Identification of the apoptotic pathway in the photo-toxicity of **78** to the A549 cells. The cells, as such or pre-incubated with specific caspases inhibitors (each 40 μM) for 1 h were incubated with **78** (1.25 μM) for 1 h, and exposed to light for 1 h. The cell survival was assayed by the MTT reduction protocol after 24 h. The experiments were repeated three times with similar results. All determinations were made in three replicates, and the values are means ± S. E. M. $^{*}P$<0.001 compared to vehicle control.

Current evidence suggests that the most common pathway for apoptosis in PDT-treated cells involves mitochondria. Most PSs are lipophilic, and preferentially localize in

the intracellular membrane systems, particularly mitochondria. From that perspective the cytoplasmic localization of the chosen Bodipys is interesting. However, this is not unprecedented. Few PSs photosensitizers, and with limited cell types, follow other pathways, especially through caspase-8, particularly when the dominant pathway is suppressed.[113a] For example, the widely used PS, photofrin has been shown to concentrate into plasma membranes or cytoplasm upon brief incubation, and in the Golgi complex or ER upon prolonged incubation.[115a] It is possible that the Bodipys **70**, **76**, **78**, **80a** or some of them can re-localize at other subcellular locations from the primary sites of their accumulation. Such time-dependent re-localization of certain PS has been reported earlier.[115b,c] It has been reported that procaspase-3 localizes in the cytoplasm and that caspase-3 activation is initiated in the cytosol. The activated caspase-3 redistributes to the nuclear compartment to induce apoptosis.[116a,b]

4.5. Summary

Considerable efforts have been devoted to develop PSs with better tumor selectivity and higher phototherapeutic efficiency. Although the mechanism of PS retention by tumors is not well understood, the balance between lipophilicity and hydrophilicity is recognized as an important factor for photosensitizing efficiencies and tumor and cellular uptake. The linkages of PSs with sugar moieties are of great importance because the sugar increases water solubility, membrane interaction and specific affinity for malignant tumors. Factors such as lower pH and more low-density lipoprotein (LDL) receptors in malignant tissue than normal one may explain the observed cellular specificity of the PS.[117]

Keeping this in mind, in this work, a new series of Bodipy carbohydrate conjugates have been designed and synthesized by introducing glucose units to a hydroxyl phenyl subunit present at the *meso*- or C-3 styryl moieties of the Bodipy core. The styryl moieties were introduced so as to induce red shifts in the emission maxima. The in vitro biological investigations with the human lung cancer A549 cells revealed insignificant dark cytotoxicity of the synthesized dyes, despite high cell membrane permeability. As expected, two of the mono-styryl glycosylated dyes **78** and **80a** showed better potency than their respective non-glycosylated precursors **71a** and **72a**. Both **78** and **80a** induced apoptosis via the extrinsic pathway. Surprisingly, the dye **70** containing a *meso*-phenol moiety instead of any extended conjugation (lack of the C-3-styryl group) showed a similar growth inhibitory property as that of **78** and **80a**, and incorporation of a glucose unit at a *meso*-phenol unit reduced the activity drastically.

It was also demonstrated that compound **80b**, possessing the glycosylated styryl moieties at both C-3 and C-5 positions of the Bodipy core formed stable fibrillar nano-aggregates in aqueous THF and EtOH. More importantly the aggregate size could be controlled by changing the water content of the media without the need of any additional lipophilic attachment, as reported previously.[104] Taken together the good phototoxicity of the red-emissive Bodipy-*O*-glycosides **78** and **80a**, and hydrogel formation ability of **80b** make them potentially attractive materials for photodynamic therapy, and as biological imaging, and delivery vehicles respectively.

4.6. Experimental

4.6.1. General details

The general details of the synthetic methodologies and spectroscopic studies have already been discussed in Chapter-2. The chemicals used for the biological studies were: 3-(4,5-dimethylthiazol-2-yl)-2,5-diphenyltetrazolium bromide (MTT), penicillin, streptomycin, and kits of caspases-3, -8, -9 activities (all from Sigma chemicals, St. Luois, MO); Dulbecco's modified Eagle's medium (DMEM, HiMedia, Mumbai); and fetal bovine serum (FBS, Gibco Life Technologies, Carlsbad, CA); Z-DEVD-FMK (pan-caspase inhibitor), Z-VAD-FMK (caspase-8 inhibitor), Z-IETD-FMK (caspase-3 inhibitor), Z-LEHD-FMK (caspase-9 inhibitor).

4.6.2. Synthesis

2,6-Diethyl-4,4-difluoro-1,3,5,7-tetramethyl-8-phenyl-4-bora-3a,4a-diaza-s-indecene (69). As described in Chapter-2, compound **69** was synthesized using **58** (0.450 g, 3.7 mmol), **67** (0.196 g, 1.85 mmol), TFA (0.012 g, 0.10 mmol), DDQ (0.420 mg, 1.85 mmol), Et_3N (0.5 mL) and $BF_3{\cdot}Et_2O$ (0.762 mL, 4.6 mmol) in CH_2Cl_2 (10 mL). Usual work-up, followed by column chromatography (silica gel, hexane-EtOAc) furnished pure **69** as a reddish solid. Yield: 0.175 g (24.9%); orange needles (hexane); mp: 184-185 °C (lit.[118] mp: 185-186 °C); ^{1}H NMR: δ 0.97 (t, *J* = 7.6 Hz, 6H), 1.26 (s, 6H), 2.27 (q, *J* = 7.6 Hz, 4H), 2.52 (s, 6H), 7.25- 7.29 (m, 2H), 7.45-7.48 (m, 3H); ^{13}C NMR: δ 11.6, 12.5, 14.6,17.1, 128.3, 128.7, 129.0, 130.8, 132.7, 135.8, 138.4, 140.2, 153.7; MS (*m*/*z*): 380 $[M]^+$.

2,6-Diethyl-4,4-difluoro-1,3,5,7-tetramethyl-8-(4'-hydroxyphenyl)-4-bora-3a,4a-diaza-s-indecene (70). For the synthesis of **70**, compounds **58** (0.500 g, 4.07 mmol), **68** (0.226 g, 1.85 mmol), DDQ (0.420 mg, 1.85 mmol), Et_3N (1.56 mL, 11.09 mmol), $BF_3.Et_2O$ (1.39 mL, 11.09 mmol) and THF (70 mL) were used. It was purified by column

chromatography (silica gel, hexane/EtOAc). Yield: 0.350 g (23.4%); red-orange square crystals (acetone/cyclohexane); mp: 228 ^{o}C; ^{1}H NMR (700 MHz, $(CD_3)_2CO$): δ 0.98 (t, *J* = 7.7 Hz, 6H), 1.41 (s, 6H), 2.34 (q, *J* = 7.7 Hz, 4H), 2.48 (s, 6H), 7.04 (d, *J* = 8.4 Hz, 2H), 7.15 (d, *J* = 8.4 Hz, 2H), 8.71 (s, 1H); ^{13}C NMR (175 MHz, $(CD_3)_2CO$): δ 10.2, 10.6, 13.0, 15.6, 115.0, 125.4, 128.5, 130.1, 131.5, 137.3, 140.3, 152.0, 157.1; EI-MS (m/z): 396.1 $[M]^+$, 395.4 $[M-1]^+$. Anal. Calcd. for $C_{23}H_{27}BF_2N_2O$: C, 69.71; H, 6.87; N, 7.07%. Found: C, 69.42; H, 6.74; N, 7.22%.

2,6-Diethyl-4,4-difluoro-3-(4'-hydroxystyryl)-1,5,7,8-tetramethyl-4-bora-3a,4a-diaza-s-indecene 71a. As described in Chapter-2, compound **71a** was synthesized by condensing **21** (0.200 g, 0.629 mmol) with **68** (0.077 g, 0.629 mmol) in the presence of glacial acetic acid (0.3 mL) and piperidine (2.0 mL) in toluene (20 mL), followed by usual isolation. Yield: 0.080 g (30.1%); dark pink crystals (CH_2Cl_2/cyclohexane); mp: 225 ^{o}C; ^{1}H NMR (700 MHz, $(CD_3)_2CO$): δ 1.04 (t, *J* = 7.7 Hz, 3H), 1.19 (t, *J* = 7.7 Hz, 3H), 2.38 (s, 3H), 2.39 (s, 3H), 2.45 (q, *J* = 7.7 Hz, 2H), 2.49 (s, 3H), 2.69 (s, 3H), 2.72 (q, *J* = 7.7 Hz, 2H), 6.88 (d, *J* = 8.4 Hz, 2H), 7.18 (d, *J* = 16.8 Hz, 1H), 7.45 (d, *J* = 8.4 Hz, 2H), 7.56 (d, *J* = 16.8 Hz, 1H), 8.6 (s, 1H); ^{13}C NMR (125 MHz, $(CD_3)_2CO$): δ 12.7, 14.2, 14.6, 14.8, 15.2, 17.6, 18.8, 116.7, 118.3, 129.3, 130.2, 133.1, 133.5, 133.9, 135.2, 138.1, 140.9, 148.7, 153.6, 159.1; HRMS (m/z): Calcd.: 423.2419 $[M+1]^+$; Found: 423.2400 $[M+1]^+$.

2,6-Diethyl-4,4-difluoro-3-(4'-hydroxystyryl)-1,5,7-trimethyl-8-(4'-phenyl)-4-bora-3a,4a-diaza-s-indecene 72a and **2,6-Diethyl-4,4-difluoro-3,5-di(4'-hydroxystyryl)-1,7-trimethyl-8-(4'-phenyl)-4-bora-3a,4a-diaza-s-indecene 72b.** As above, condensation of **69** (0.600 g, 1.579 mmol) and **68** (0.193 g, 1.579 mmol) in the presence of glacial acetic

acid (0.9 mL) and piperidine (6.0 mL) in toluene (60 mL), followed by usual isolation give a residue, which on column chromatography (silica gel, hexane/EtOAc) furnished **72a** and **72b**.

72a: Yield: 0.160 g (20.9%); dark pink crystals (acetone/cyclohexane); mp: 228 ^{o}C; ^{1}H NMR (200 MHz, $(CD_3)_2CO$): δ 0.99 (t, *J* = 7.4 Hz, 3H), 1.13 (t, *J* = 7.4 Hz, 3H), 1.33(s, 3H), 1.34 (s, 3 H), 2.34 (q, *J* = 7.4 Hz, 2H), 2.54 (s, 3H), 2.62 (s, *J* = 7.4 Hz, 2H), 2.85 (s, 6H), 6.89 (d, *J* = 8.6 Hz, 2H), 7.22 (d, *J* = 17 Hz, 1H), 7.38-7.43 (m, 2H), 7.48 (d, *J* = 8.6 Hz, 2H), 7.58-8.00 (m, 4H); ^{13}C NMR (75 MHz, $CDCl_3$): δ 11.4, 11.7, 12.7, 14.1, 14.5, 17.1, 18.3, 24.3, 115.7, 117.5, 128.4, 128.7, 129.0, 129.9, 131.7, 132.9, 133.4, 135.2, 135.8, 138.6, 138.8, 139.2, 149.8, 154.7, 156.7; EI-MS (m/z): 483.3 $[M-1]^+$. Anal. Calcd. for $C_{30}H_{31}BF_2N_2O$: C, 74.39; H, 6.45; N, 5.78%; Found: C, 74.68; H, 6.31; N, 5.94%.

72b: Yield: 0.400 g (43.1%); dark green powder (acetone/cyclohexane); mp: >250 ^{o}C; ^{1}H NMR (300 MHz, $(CD_3)_2SO$): δ 1.09 (t, *J* = 7.2 Hz, 6H), 1.29 (s, 6H), 2.50(s, 6H), 2.57 (q, *J* = 7.4 Hz, 4H), 6.85 (d, *J* = 8.2 Hz, 4H), 7.19 (s, *J* = 17 Hz, 2H), 7.40-7.57 (m, 11H);EI-MS (m/z): 587.5 $[M-1]^+$. Anal. Calcd. for $C_{37}H_{35}BF_2N_2O_2$: C, 75.51; H, 5.99; N, 4.76%; Found: C, 75.14; H, 5.83; N, 4.87%.

Glycosylation of 70. To a mixture of **73** (0.142 g, 0.568 mmol) and **70** (0.150 g, 0.379 mmol) in CH_2Cl_2 (20 mL), $BF_3.Et_2O$ (47.6 µL, 0.379 mmol) was added and the resulting mixture refluxed for 5 h. It was brought to room temperature, washed with aqueous saturated $NaHCO_3$ (2 × 10 mL), H_2O (2 × 10 mL) and brine (10 mL), and dried. Removal of solvent in vacuo followed by column chromatography of the residue (silica gel, hexane/EtOAc) furnished **75**. Yield: 0.138 g (50.2%); orange powder

(acetone/cyclohexane); mp: 216 ^{o}C; ^{1}H NMR (200 MHz, $CDCl_3$): δ 0.97 (t, *J* = 7.6 Hz, 6H), 1.29 (s, 6H), 2.04-2.09 (m, 12H), 2.27 (q, *J* = 7.6 Hz, 4H), 2.51 (s, 6H), 3.86- 3.95 (m, 1H), 4.15-4.21 (m, 1H), 4.28-4.37 (m, 1H), 5.13-5.34 (m, 4H), 7.09 (d, *J* = 8.6 Hz, 2H), 7.19 (d, *J* = 8.6 Hz, 2H); ^{13}C NMR (50 MHz, $CDCl_3$): δ 11.9, 12.5, 14.6, 17.0, 20.5, 20.6, 62.0, 68.2, 71.1, 72.2, 72.6, 99.2, 117.5, 129.7, 130.8, 130.9, 132.8, 138.2, 139.3, 153.8, 157.2, 169.2, 169.4, 170.2, 170.4; EI-MS (m/z): 727.4 $[M+1]^+$, 725.5 $[M-1]^+$, 707.4 $[M-19]^+$. Anal. Calcd. for $C_{37}H_{45}BF_2N_2O_{10}$: C, 61.16; H, 6.24; N, 3.86%. Found: C, 60.94; H, 6.20; N, 3.50%.

Glycosylation of 71a. To a mixture of **73** (0.071 g, 0.284 mmol) and **71a** (0.80 g, 0.189 mmol) in CH_2Cl_2 (15 mL) was added $BF_3.Et_2O$ (23.8 µL, 0.189 mmol), and the resulting mixture refluxed for 3 h, brought to room temperature, washed with aqueous saturated $NaHCO_3$ (2 × 10 mL), H_2O (2 × 10 mL) and brine (10 mL), and dried. Removal of solvent in vacuo followed by column chromatography of the residue (silica gel, hexane/EtOAc) furnished **77**. Yield: 0.060 g (42.1%); dark pink powder (acetone/cyclohexane); mp: 186 ^{o}C; ^{1}H NMR (200 MHz, $CDCl_3$): *δ* 1.04 (t, *J* = 7.4 Hz, 3H), 1.20 (t, *J* = 7.4 Hz, 3H), 2.03-2.09 (m, 12H), 2.34-2.42 (m, 8H), 2.46 (s, 3H), 2.52-2.69 (m, 5H), 3.83-3.90 (m, 1H), 4.12-4.32 (m, 2H), 5.06-5.31 (m, 4H), 6.95 (d, *J* = 8.8 Hz, 2H), 7.03 (d, *J* = 16.8 Hz, 1H), 7.48-7.61 (m, 3H); ^{13}C NMR (75 MHz, $CDCl_3$): δ 13.8, 14.3, 14.6, 17.0, 18.2, 20.4, 20.5, 61.2, 61.7, 67.5, 68.2, 69.6, 70.0, 70.1, 71.9, 72.6, 91.5, 98.8, 117.0, 119.2, 128.1, 132.2, 132.4, 132.8, 133.0, 133.2, 136.2, 137.2, 139.2, 146.9, 153.7, 156.6, 169.1, 169.3, 170.0, 170.4; HRMS (m/z): Calcd.: 752.3292 $[M]^+$; Found: 752.3255 $[M]^+$.

Glycosylation of 72a and 72b. A mixture of Bu_4NBr (4 mmol) in 1:1 H_2O–$CHCl_3$ (20 mL) was stirred at 40 ^oC. A solution of **74** (0.02 mol) in $CHCl_3$ (15 mL), and another solution of **72a** or/ **72b** (0.02 mol) and K_2CO_3 (6.9 g) in water (20 mL) were simultaneously dropped into the above mixture, the reaction mixture heated to 60 ^oC and stirred vigorously for 6 h. It was brought to room temperature, washed with aqueous 5% NaOH (3 ×10 mL), H_2O (2 × 10 mL) and brine (10 mL), and dried. Removal of solvent in vacuo followed by column chromatography of the residue (silica gel, hexane/EtOAc) furnished the **79** and **81** respectively. **79:** Yield: 0.095 g (35.3%); mp: 105 ^oC; HRMS (m/z): Calcd.: 837.3346 $[M+Na]^+$; Found: 837.3309 $[M+Na]^+$.

81: Yield: 0.180 g (28.3%); mp: 218 ^oC; ^1H NMR (200 MHz, $CDCl_3$): δ 1.14 (t, *J* = 7.6 Hz, 6H), 1.34 (s, 6H), 2.04-2.09 (m, 18H), 2.57 (q, *J* = 7.4 Hz, 4H), 3.88-3.93 (m, 2H), 4.14-4.36 (m, 4H), 5.12-5.33 (m, 8H), 6.98 (d, *J* = 8.6 Hz, 4H), 7.14 (d, *J* = 17 Hz, 2H), 7.28-7.32 (m, 2H, *meso*-Ph), 7.48-7.57 (m, 7H); ^{13}C NMR (50 MHz, $CDCl_3$): δ 11.4, 13.9, 14.1, 18.3, 20.5, 20.6, 20.7, 22.6, 28.9, 29.1, 29.3, 29.4, 29.6, 31.8, 33.8, 61.8, 68.2, 71.1, 71.1, 72.0, 72.6, 98.8, 114.0, 117.1, 119.3, 128.6, 128.8, 129.0, 132.7, 133.0, 133.7, 134.7, 135.8, 138.6, 139.1, 157.0, 169.3, 169.3, 170.2, 170.6; HRMS (m/z): Calcd.: 1287.4298 $[M+K]^+$; Found: 1287.4213 $[M+K]^+$.

Deacetylation of the Bodipy-*O*-glucosides. NaOMe (0.399 mmol) was added to the solution of **77/79/81** (0.080 mmol) in MeOH (5 mL) and the resulting mixture was stirred at room temperature for 1 h. Solvent removal in vacuo followed by column chromatography (silica gel, $CHCl_3$/MeOH) of the residues furnished **78/80a/80b**. Compound **76** was prepared in a similar manner using NaOMe (0.691 mmol) and **75** (0.100 g, 0.138 mmol) in MeOH (5 mL).

Compound 76: Yield: 0.070 g (91.1%); orange powder (CH_2Cl_2/cyclohexane); mp: 166 ^oC; ^1H NMR (300 MHz, $(CD_3)_2CO$): δ 0.97 (t, *J* = 7.5 Hz, 6H), 1.37 (s, 6H), 2.33 (q, *J* = 7.5 Hz, 4H), 2.48 (s, 6H), 2.93 (broad s, 4H), 3.49-3.56 (m, 4H), 3.70-3.75 (m, 1H), 3.88-3.92 (m, 1H), 5.05-5.08 (d, *J* = 7.2 Hz, 1H), 7.24-7.28 (m, 4H); ^{13}C NMR (175 MHz, $(CD_3)_2CO$): δ 10.3, 10.7, 13.0, 15.6, 60.8, 69.5, 72.8, 75.9, 76.1, 100.3, 116.3, 128.0, 128.4, 129.9, 131.6, 137.3, 139.7, 152.3, 157.7; EI-MS (m/z): 559.4 $[M+1]^+$, 558.4 $[M]^+$. Anal. Calcd. for $C_{29}H_{37}BF_2N_2O_6$: C, 62.37; H, 6.68; N, 5.02%; Found: C, 62.63; H, 7.11; N, 4.98%.

Compound 78: Yield: 85.8%; dark pink crystals (acetone/cyclohexane); mp: 143 ^oC;^1H NMR (300 MHz, $(CD_3)_2CO$): δ 1.06 (t, *J* = 9.0 Hz, 3H), 1.21 (t, *J* = 9.0 Hz, 3H), 2.40-2.41(m, 6H), 2.42-2.51 (m, 5H), 2.71-2.76 (m, 5H), 2.85 (s, 3H), 3.46-3.49 (m, 4H), 3.72-3.76 (m, 1H), 3.88-3.93 (m, 1H), 5.01-5.04 (m, 1H), 7.10 (d, *J* = 8.6 Hz, 2H), 7.19 (d, *J* = 16.8 Hz, 1H), 7.52 (d, *J* = 8.8 Hz, 2H), 7.61 (d, *J* = 17 Hz, 1H); ^{13}C NMR (75 MHz, $(CD_3)_2CO$): δ 12.7, 14.1, 14.2, 14.6, 14.7, 14.8, 14.9, 15.2, 15.3, 17.6, 18.8, 18.9, 62.7, 71.4, 74.7, 77.9, 78.0, 101.8, 117.8, 119.5, 128.8, 128.9, 132.5, 132.7, 132.9, 133.2, 134.2, 134.4, 137.9, 138.5, 140.8, 141.2, 148.0, 154.2, 159.2; HRMS (m/z): Calcd.: 585.2948 $[M+1]^+$; Found: 585.2910 $[M+1]^+$.

Compound 80a: Yield: 0.038 g (50.4%); dark pink powder (acetone/cyclohexane); mp: 138 ^oC; ^1H NMR (200 MHz, $(CD_3)_2CO$): δ 0.99 (t, *J* = 7.6 Hz, 3H), 1.14 (t, *J* = 7.4 Hz, 3H), 1.33(s, 3H), 1.34 (s, 3 H), 2.35 (q, *J* = 7.6 Hz, 2H), 2.54 (s, 3H), 2.62 (q, *J* = 7.6 Hz, 2H), 3.44-3.87 (m, 7H), 5.01 (d, 1H), 7.11 (d, *J* = 8.0 Hz, 2H), 7.24 (d, *J* = 17.4 Hz, 1H), 7.39-7.41 (m, 2H), 7.43-7.72 (m, 6H); HRMS (m/z): Calcd.: 669.2923 $[M+Na]^+$; Found: 669.2887 $[M+Na]^+$.

Compound 80b: Yield: 0.060 g (45.6%); dark green powder (acetone/cyclohexane); mp: >250 ^{o}C; HRMS (m/z): Calcd.: 935.3714 $[M+Na]^{+}$; Found: 935.3653 $[M+Na]^{+}$.

4.6.3. Dynamic light scattering (DLS) studies

The DLS measurements were performed using a Malvern 4800 Autosizer instrument employing a diode pumped solid state laser (532 nm, vertical polarisation) and avalanche photodiode detector, at a scattering angle of 130°. The data processing was carried out by Malvern 7132 digital correlator. The scattered intensity correlation function was analyzed by the inverse Laplace transformation algorithm, CONTIN (software supplied by Malvern Instruments, UK) to extract the size distribution data.

4.6.4. Biological studies

4.6.4.1 Cell culture: The A549 cell line, procured from National Centre for Cell Science, Pune, India were cultured in DMEM medium, supplemented with 10% FBS, 100 U/mL penicillin and 100 μg/mL streptomycin. The cells were grown at 37 ^{o}C under an atmosphere of 5% CO_2.

4.6.4.2 MTT assay. Viabilities of the control cells and those treated with various concentrations of the test compounds were determined at 48 h by the MTT reduction assay.[119] Briefly, cells (1×10^4/well) grown in 96-well plates were incubated overnight at 37 ^{o}C under an atmosphere of 5% CO_2. Next day the cells were incubated with vehicle (0.1% DMSO) or various concentrations of the test compounds for 1 h. The cells were washed two times with PBS, DMEM (200 μL) added, and subsequently exposed to light (dose rate 7.76 Watt) for different time periods (0.5, 1, 2, 3, and 4 h) using a 20 W CFL lamp. Serum was added to the medium which was incubated for 24 h. The cells were washed once with PBS, MTT solution (0.5 mg/mL, 100 μL) was added to each well and kept at 37 ^{o}C for 6 h. The formazan crystals in the viable cells were solubilized with 0.01

N HCl (100 μL) containing 10% SDS and the absorbance at 550 nm read. Experiments were also carried out without the photo-exposure, wherein the assays were carried out at 48 h after addition of the compounds. For studying the Similar assays were also carried out by pre-incubating the cells with the caspases inhibitors (each 40 μM) prior to the addition of the test compound **78**.

4.6.4.3 Flow cytometry. The hypodiploid DNA content were analyzed as a marker for apoptosis by flow cytometry, after staining with PI. The cells were incubated with **76** or **78** (0-50 μM) for 1 h, washed two times with PBS, DMEM (200 μL) added, and subsequently exposed to light (dose rate 7.76 Watt) for different time periods (30 and 80 min) using a 20 W CFL lamp. Serum was added to the medium which was incubated for 24 h. The cells were washed once with cold PBS, incubated with PI (400 μg/mL) and RNAse A (200 μg/mL) in 1 mL hypotonic buffer (0.1% sodium citrate plus 0.1% Triton X-100) for 30 min at 37 ^{o}C, and analyzed with a Pertec CyFlow® Space flow cytometer using the FlowJo program. Cellular debris was excluded from analysis by raising the forward scatter threshold, and the DNA content of the nuclei was registered on a logarithmic scale. At least 2×10^4 cells of each sample were analyzed. The apoptotic nuclei appeared as broad hypodiploid DNA peaks.

4.6.4.4 Fluorescence microscopy. A549 cells seeded in 6-well plate on coverslip were loaded with the Bodipy dyes (5 μM) for varying periods (0.25, 0.5 h, 1, 2 and 3 h) at 37 ^{o}C, washed with PBS, subsequently stained with Hoechst 33342 (10 μM), washed once again with PBS, mounted with 70% glycerol, and analyzed under Axioskop II Mot plus (Zeiss) microscope (40 × optics). When overlaying blue/red images by ImageJ software, some adjustments to image stretch and tone were made to both blue and red images. This

was done only for overlay display contrast purposes so as to ensure that the blue color of the Hoechst-stained nucleus and red color of the dye are both visible.

4.6.4.3 Caspase activity assay. The assays were performed with a caspase-3 colorimetric kit or caspase-8 and caspase-9 fluorimetric kits according to the manufacturer's protocol. Briefly, cells (1×10^6/well), seeded in 90 mm plate were incubated with **78** (1.25 μM) for 1 h followed by 1 h photo-illumination, and the individual caspase activities were assayed at 16 h. These assays were based on spectrophotometric detection of the chromatophore, pNA after cleavage from the respective labeled substrates by the caspases. The untreated but photo-exposed cells served as the control. For the caspase inhibition studies, the cells were pre-incubated with the inhibitory peptides, Z-VAD-FMK, Z-IETD-FMK, Z-LEHD-FMK (each 40 μM), prior to the other treatments.

CHAPTER-5

FORMULATION OF BODIPY-SI-BASED MOLECULAR ELECTRONICS DEVICES

Chapter 5: Table of Contents

5.1. Preamble

Silicon microelectronics, playing a dominant role in almost every sphere of our life, *viz.* automobiles, home appliances, telecommunications, medical and scientific equipments etc, has undergone relentless miniaturization during the last few decades. This has increased the speed and memory of computational devices. Now it is being anticipated that due to several physical as well as economic factors, the Si technology will face the scaling limits in very near future.[120] Factors such as (i) unacceptable power dissipation, (ii) change in the Si band structure, (iii) difficulty in uniform doping of Si, (iv) limitation of lithographic techniques, and (v) exponential increase in financial investment would restrict attaining the sizes of the transistors to ≤ 20 nm.

This has given birth to the concept of information processing at the molecular-scale (molecular electronics) as a promising alternative for the nano-electronics of the future.[121] It is viewed as a technology wherein integrated circuitry (IC) will be constructed from component molecules acting as capacitors, resistors, logic gateways, memory registers, *etc*, joined by molecular wires. In molecular electronic devices, organic molecules are sandwiched between conducting electrodes. Supramolecular assembly of organic molecules on solid substrates is a powerful `bottom-up' approach for the fabrication of devices for molecular-scale electronics. This is generally achieved by forming Langmuir-Blodgett (LB) films,[122a] or self-assembly of monolayers of organic molecules on solid substrates (SAM) via metal/molecules/metal (MMM) junction.[122b] However, chemically-grafted organic molecules on semiconductors like Si is most promising for this purpose because the surface potential of Si can be easily tailored to develop improved hybrid molecular devices.[122c] The p-n junction threshold voltage for rectification can be adjusted by changing the electronic nature of the organic π group molecules, instead of the classical method of doping.

Si-hybrid nanoelectronics. In the third approach, termed as Si-hybrid nanoelectronics, organic molecules exhibiting various functionalities, such as, dielectric, diode, memory and transistor are deposited to Si, so that the nanoscale electronic functionality of molecules can be utilized in Si-based microelectronics. The advantage of the molecule-on-Si hybrid concept is that the inputs available from an already existing powerful Si-based IC industry can be effectively used for the development of integrated hybrid devices. Thus, nonlinear charge transport in functional molecules grafted to Si has become a fundamental area of research in the development of various components for hybrid nanoelectronics *e. g*. molecular diodes, resonant tunnel diodes, memory devices, transistors etc.[120]

Organic molecules in molecular electronics. Organic molecules are made up of mainly covalent bonds which are formed either by linear (σ bonds) or lateral overlap (π bonds) of the atomic orbitals. Electrons in σ bonds lye between two nuclei and are highly localized, whereas the electron density in π bonds is delocalized. In terms of molecular orbital theory, when two atomic orbitals overlap they form one bonding orbital (lower in energy than that of atomic orbitals) and one antibonding orbital (higher in energy than that of atomic orbitals). These molecular orbitals (MO's) are filled up by Pauli's exclusion principle. The energy difference between highest occupied molecular orbital (HOMO) and lowest unoccupied molecular orbital (LUMO) is related to the band gap of the molecule. The HOMO-LUMO gap for the σ bonds is ~8 eV, whereas for the conjugated molecules this gap is in reduced to 2-5 eV. Therefore, under applied electric field, σ bonded molecules are expected to exhibit no charge transport, and may act as dielectrics in hybrid nanoelectronics. On the other hand, presence of extended electronic wave functions in the conjugated (π bonded) molecules is suitable as semiconducting channels in the hybrid devices. In these devices, highly doped Si (resistivity < 0.001 Ωcm) is used as substrate for organic

monolayer deposition so that it also acts as an electrode. The counter electrodes can be formed using techniques such as liquid Hg-drop, thermally evaporated Au/Al pads, CP-AFM/ STM tip or carbon nanotubes. Using this type of assemblies, various devices such as, a) molecular dielectrics using alkyl-chains,[123a] b) molecular diodes using σ–π molecules,[123b] c) resonant tunnel diode or RTD using σ–π– σ molecules[123c] etc. have been constructed. Here, the alkyl-chains of different lengths, and conjugated molecules were used as σ and π components respectively.

It is well-established that covalent attachment of the organic molecules onto Si-surfaces produces reproducible and robust hybrid nanoelectronics, suitable for device applications. Previously, σ–π systems grafted on Si through an alkyl spacer (σ) have shown current rectification behavior.[124] The rectification property has been attributed to a resonant transport between the Si conduction band (CB) and the HOMO of the π group. The Fermi level pinning at the metal/π-group interface plays a key role in the electrical behavior of these molecular rectifying junctions. Molecules, showing rectification behaviour with high rectification ratio (RR) is very useful for making diodes.

The negative differential resistance (NDR) behaviour (*i. e*., an initial rise in current and its subsequent sharp drop even with progressively augmented voltage, as opposed to Ohm's law) with high peak to valley ratio (PVR) has drawn significant attention because of its potential application in realization of logic devices and memory circuits,[125a-c] and is found in a variety of molecular devices.[125] The NDR behavior should be accompanied by hysteresis although in many cases it is observed without hysteresis.[126] Several mechanisms such as charge transfer-induced change of the charge state, and chemical/conformational changes under finite bias have been proposed to explain NDR phenomenon.[127] Recent theoretical studies showed that the origin of

NDR with hysteresis is associated with the polarization response, *i. e.*, combined effects of charging and conformational change.[128]

5.2. Concept of Si-BODIPY Devices

In principle, organic molecules with suitable redox properties such as high band gaps and ionization energies, and matching HOMO/LUMOs with the Fermi level of the electrodes are suitable for molecular electronics applications. To this end, a large number of electron-rich organic molecules such as the polyaromatic hydrocarbons, porphyrinoids etc. have been extensively used to construct Si-hybrid nanoelectronics. Rectification effect of several organic n-type molecules deposited on Si has been demonstrated previously.[129] Nevertheless, developing devices that are environmentally stable, and show high-mobility and easy processability remains a specific challenge in this area. In particular, the performance and stability of organic n-type materials have significantly lagged behind their p-type counterparts.

The Bodipy class of compounds has rich redox chemistry with excellent reversibility both during oxidation and reduction. As discussed in section 1.5.2., the redox chemistry of the Bodipy derivatives depends on the type of substitution in the dipyrromethene core.[130a] When the dyes are completely substituted with alkyl or other groups, the radical ions are highly stable. But in absence of any substitutions, especially at the 2-, 6-, and meso-positions, highly reactive radical ions are generated, which can undergo dimerization or other reactions.[130b] The properties can be tuned by varying different substituents on the dye chromophore. Till so far, the Bodipy compounds have been used extensively for various photo-voltaic applications such as OLEDs, solar cell etc. The reversible redox property of Bodipy dyes, their robustness under ambient conditions and chemical tenability is very attractive for their use in molecular electronics which still remains unprecedented. Presently, the rectification property of some tailor-made Si-grafted

Bodipy monolayers, and their tuning to elicit NDR response by forming bi-layers with another Bodipy molecule is presented, and the electronic behaviors explained by theoretical calculations. These are sequentially presented below.

5.2.1. Molecular design

Given the importance of molecular bridges in nano-devices, design of the organic molecule is crucial in attaining the present objectives. The molecular design was conceived keeping in mind that the energy gap (ΔE) between the energy states (LUMO/HOMO) of the molecular bridges and the Fermi levels of the donor and acceptor units control the electron-transfer rate and current flow.[131] For constructing devices for current rectification, the required σ–π systems were synthesized using the *O*-alkenylated analogs of the Bodipy **70**. It was envisaged that the π–moiety (Bodipy core) and the σ–moieties (alkyl chains) will acts as a quantum well and the tunnel barriers respectively. For the σ–moieties, a C_5- and a C_{11}-alkenyl chains were chosen, because that would assist in subsequent fabrication of their monolayers on the highly-doped Si (111)-surface due to enhanced solubility and increased spacer lengths. Further, the alkenyl group can be used for electro-grafting the monolayers on Si surface.

Previous theoretical studies predicted that the molecules having redox properties and bias-induced conformational changes are potential candidates for NDR effect with hysteresis.[128] However, it is difficult to change the conformation of a molecule that is chemically bonded, using a bias. But it will be easier in case of a bi-layer formed by physical interaction. Hence, such a bi-layer strategy was explored for making NDR devices which is currently lacking in literature.

5.2.2. Synthesis

The commercially available aldehyde **68** was subjected to a base-catalyzed alkylation of with 1-bromohexane and 1-bromoundec-10-ene to furnish the aldehydes **82a** and **82b** respectively. The aldehydes were individually subjected to a TFA-catalyzed condensation with kryptopyrrole (**58**), and the resultant dipyrromethanes were subjected to oxidation with DDQ, followed by complexation with BF_3 in the presence of Et_3N as the base (**Scheme 5.2.2.1**) to afford the compounds **83a** and **83b** respectively. These compounds are also designated as BODIPY-C5 and BODIPY-C11, and characterized by the ^1H and ^{13}C NMR spectra (**Figure 5.2.2.1** and **Figure 5.2.2.2**). The major differences in the spectra of these compounds were the additional ^1H NMR singlet at δ 1.32 (12H) and the up-field ^{13}C NMR resonances for the longer chain alkyl moiety of **83b**.

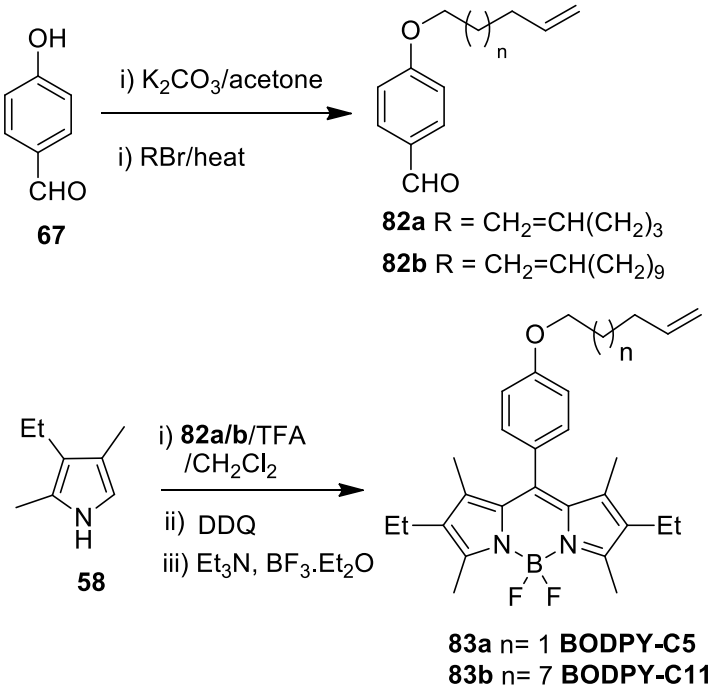

Scheme 5.2.2.1 Syntheses of the Bodipys **83a** and **83b**.

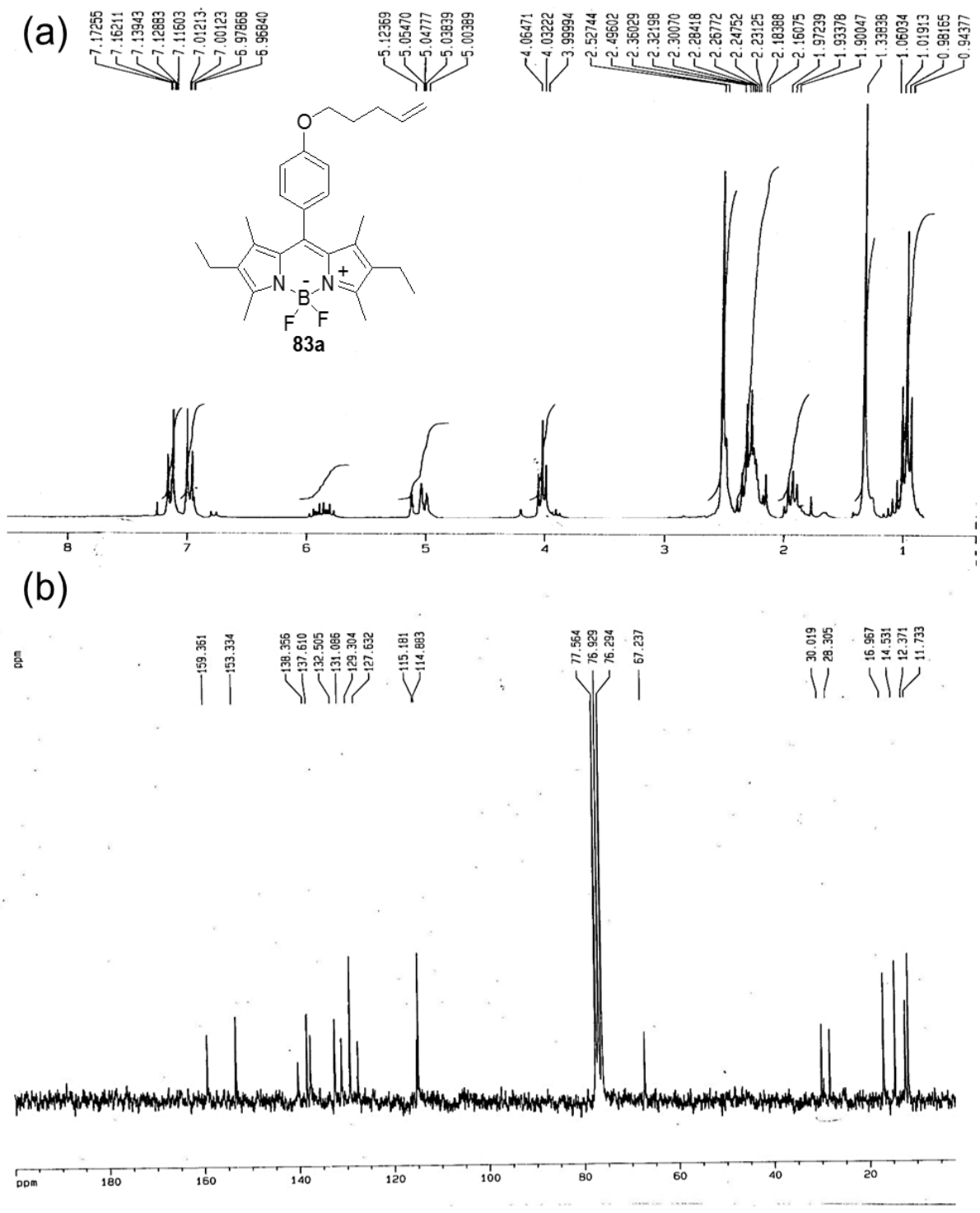

Figure 5.2.2.1 The NMR spectrum of **83a** (a) ^{1}H NMR, (b) ^{13}C NMR.

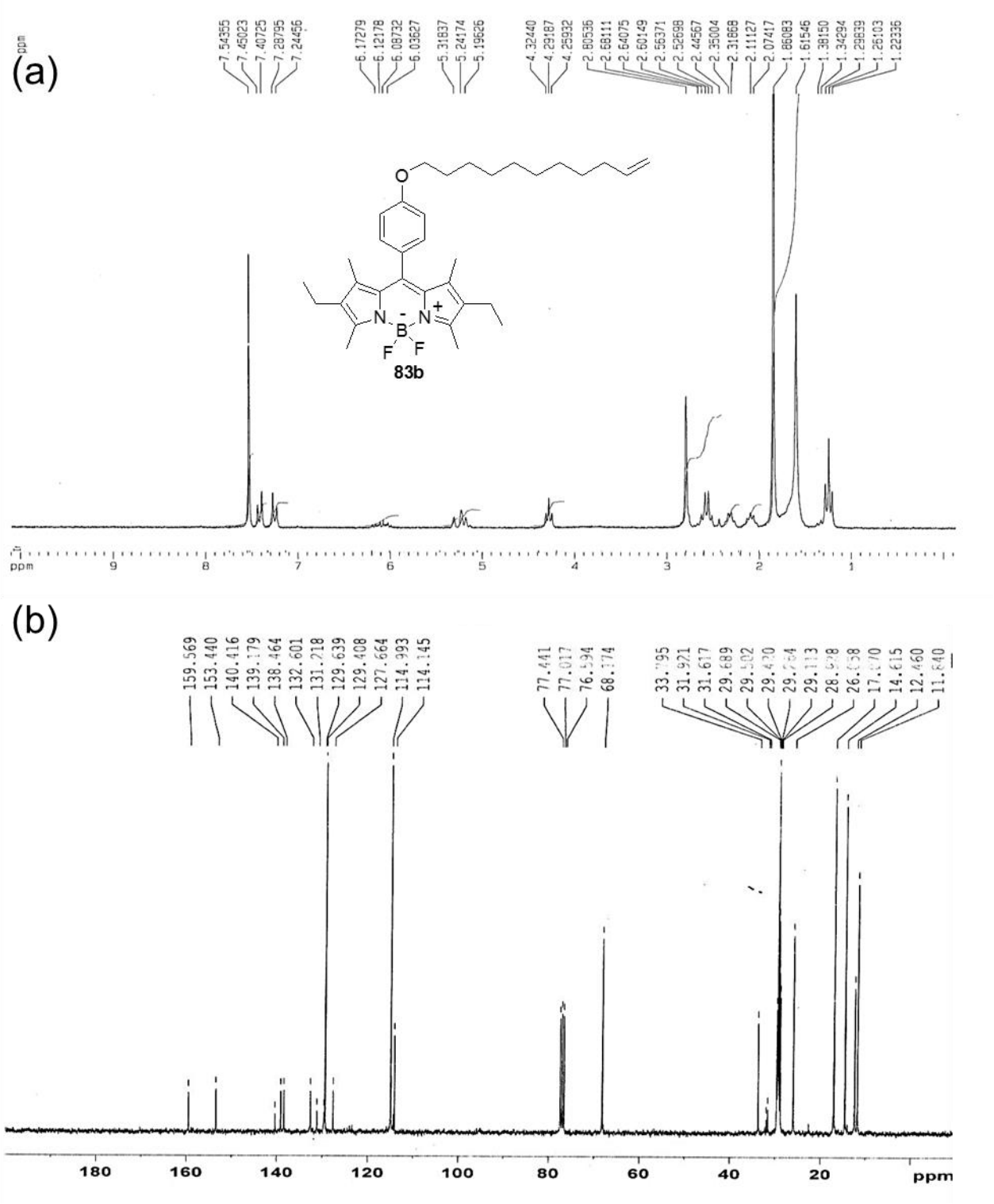

Figure 5.2.2.2 The NMR spectrum of **83b** (a) ^{1}H NMR, (b) ^{13}C NMR.

5.2.3. Preparation of the Si(n^{++})-Bodipys assemblies

***Monolayers formation by electro-grafting*.** Physisorption of organic molecules as Pockels-Langmuir (PL) films or by vapor-phase deposition on electrodes is often used to fabricate hybrid organic electronic devices. However, ordering of PL films are usually achievable with amphiphilic molecules only, restricting the molecular design. On the other hand, the vapor-phase deposition method usually results in poor deposition yield, disordered packing and random orientations. Further, the physisorbed molecules often move to seek a lower energetic state on the surface, or in response to an applied electric field. Instead, covalent linking of organic molecules to metal/semiconductor surfaces provides a better alternative.[132] Extensive work using Au electrodes revealed them to be thermally unstable.[133a,b] On the other hand, grafting of alkyl silanes monolayers on SiO_2 surface involves multi-steps protocol requiring stringent reactions conditions (optimized temperature and anhydrous conditions), besides the need to synthesize many of the alkyl silanes separately.[123b,133c] Instead, cathodic electrografting of organic molecules having a cleavable group that reacts with H-terminated Si offers the advantage assessing the deposition process by *in situ* measuring the redox peak of the electrografting reaction. The known cleavable electroactive group includes vinyl (C=C), ethynyl (C≡C), halide (Cl, Br, I), tetraalkylammonium salt, diazonium salt and silane.[133d] Hence, we followed electro-grafting for an easy attachment of the porphyrins on Si (111) surface through the strong Si-C bond (Si-C ~76 kcal mol^{-1}).

Thus, the molecules **83a** and **83b** were separately electrografted to H-terminated Si(n^{++}) surface through their respective terminal alkene groups.[134] The electrografting mechanism (**Figure 5.2.3.1**) is based on formation of Si-radicals on application of negative potential, which reacts with C=C group of the molecules to form Si–C bond.[133d] The electrochemical deposition

was carried by cyclic voltammetry (CV) using the Si-H wafers as the working electrode (WE), Pt as the counter electrode (CE) and Ag/AgCl as the reference electrode (RE).

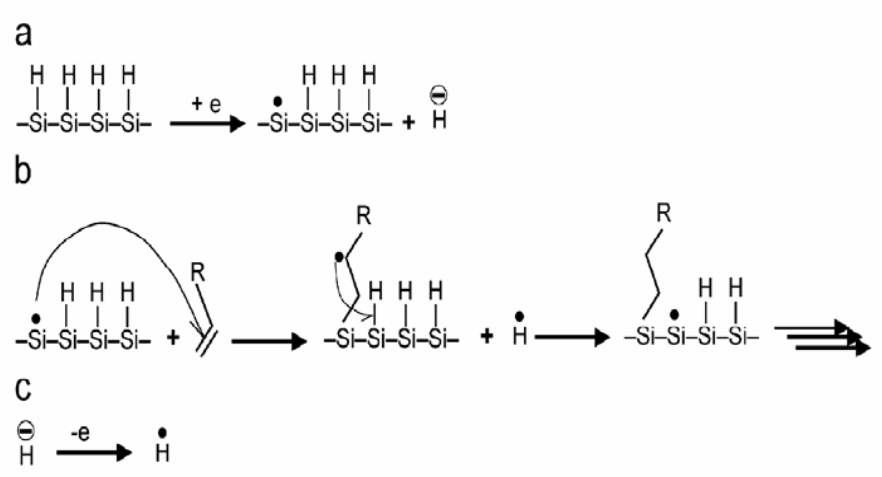

Figure 5.2.3.1 Schematic of the electrografting process on Si via Si–C bond formation.

Typical CV scans recorded using **83a** and **83b** (**Figure 5.2.3.2**) revealed appearance of an irreversible oxidation peak at -0.25 V. As the number of scans increased, the peak diminished owing to the non-availability of nucleophilic Si atoms at the surface and, eventually vanishes for 50^{th} scan. This confirmed the completion of multilayers deposition (AFM image, *vide infra*). At higher scans, formation of multilayers was evident by AFM analysis (data not shown). The irreversible CV peak indicated an irreversible reaction (i. e. the cleavage of vinyl-group) is associated with the electron transfer. No peak at -0.25V appeared when the CV was run using the TBAP solution alone.

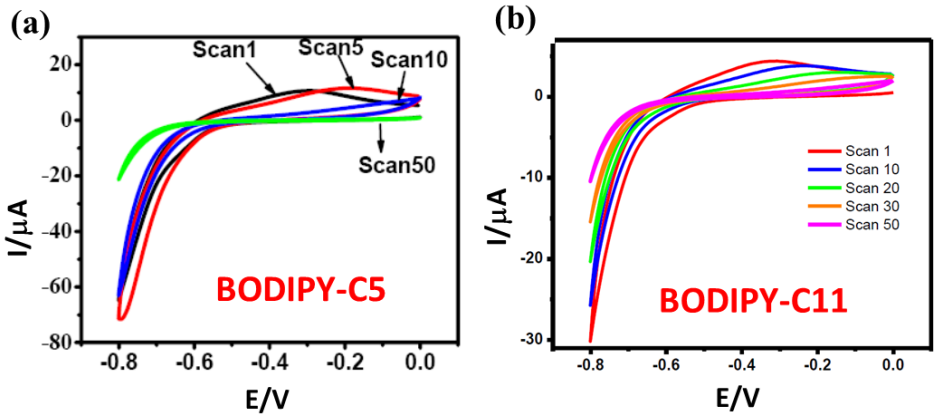

Figure 5.2.3.2 Cyclic voltammograms (CVs) indicating electrografting of Bodipy compounds on H-terminated Si(n^{++}) substrates. (a) compound **83a**; (b) compound **83b**.

Bilayers formation by self- assembly. For the bi-layer formation, compound **21** was chosen with the presumption that the planar molecule may easily intercalate onto Si-grafted monolayers of **83a** and **83b** by the self-assembly.[135] This 2nd layer was formed by dipping the mono-layered Si wafers into a CH_2Cl_2 solution of **21** for 24 h. The film thickness did not increase by dipping the monolayers in the solution of **21** for several days, as well as increasing the concentration of **21**. The bilayers are represented as **21**:**83a**/Si(n^{++}) and **21**:**83b**/Si(n^{++}) respectively.

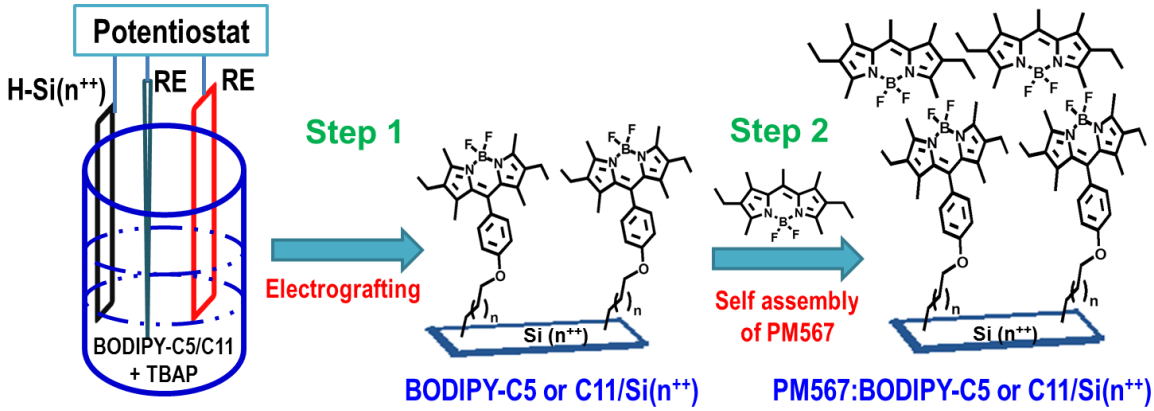

Figure 5.2.3.3 Schematics of the bilayer formation process. Step 1: Electrografting of monolayers of **83a** or **83b** on H-Si(n^{++}); Step 2: Intercalation of **21** into the monolayers.

5.2.4. Characterization of modified surfaces

The mono and bilayers were characterized by several techniques, such as, electrochemical characterization, contact angle measurements, ellipsometry, secondary ion mass-spectrometry (SIMS), atomic force microscopy (AFM) and X-ray reflectivity (XRR). Amongst these, SIMS is used for chemical analysis as well as for identifying the alignment of the molecules on the Si substrate. The thickness of the organic layers can be determined using ellipsometry, XRR, and SIMS depth profile. Contact angle measurements provide information on the surface groups of the grafted organic layer. The ordering of the monolayer can be also be assessed by imaging the surface morphology using AFM.

Electrochemical characterization. The fast scan (100V/s) CVs were recorded for **83a**/Si(n^{++}) and bilayer **21**:**83a**/Si(n^{++}) as the WE (surface area = 0.25 cm^2) and 0.1 M TBAP as electrolyte with a Pt counter-electrode and an Ag/AgCl reference electrode (**Figure 5.2.4.1.a**). For the monolayer, a single peak was observed at 0.77 V. The bilayer CV showed two closely spaced oxidation peaks at 0.73 V and 0.83 V, indicating that the bilayer undergoes a double oxidation. Similarly for the monolayer of **83b**/Si(n^{++}) a single peak at 0.89 V was observed in the CV. But, in this case, even the bilayer CV showed only a single flattened peak at 0.94V, which may be due of two closed and unresolvable peaks.

The molecular densities of the monolayers and bilayers, determined by fast scan (10 V/s) CVs are shown in **Figure 5.2.4.1**. The net charge transferred during the oxidation process, calculated from the area under the oxidation peak were 7.92×10^{-7} C and 1.83×10^{-6} C respectively for **83a** and **83b**. These amounted to surface coverages of 4.12×10^{11} and 1.69×10^{12} molecules /cm^2 respectively for **83a** and **83b**. The surface coverages increased to 8.43×10^{11} and 3.16×10^{12} molecules /cm^2 respectively for the bilayers **21**:**83a**/Si(n^{++}) and

21:**83a**/Si(n^{++}) respectively. Thus, the mono- and bilayers of **83b** were more compact with more (~ 4 times) surface coverage, compared to that of **83a**. So, the numbers of BODIPY molecules almost get doubled after self-assembly, implying the 1:1 interaction between compound **21** and compound **83a**/**83b**.[136]

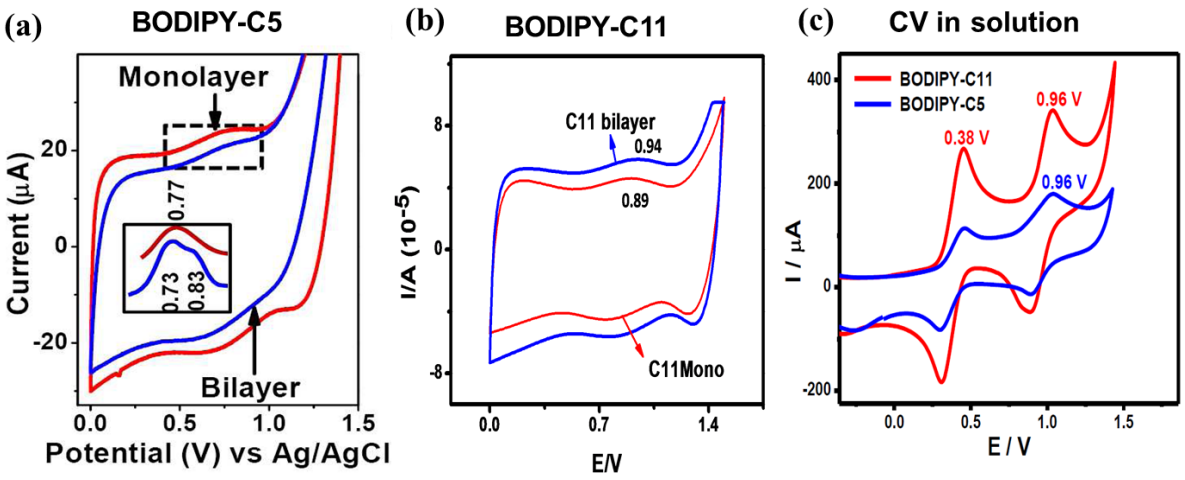

Figure 5.2.4.1 Typical fast scan CVs (scan rate 100V/s) of the mono- and bilayers. (a) **83a**/Si(n^{++}) and **21**:**83a**/Si(n^{++}); (b) **83b**/Si(n^{++}) and **21**:**83b**/Si(n^{++}); (c) CV of compounds **83a** and **83b** recorded in CH_2Cl_2 at 25 ^oC using 0.1 M Bu_4NClO_4 (TBAP) as the supporting electrolyte and ferrocene (Fc) as internal reference at +0.38V.

Contact angle measurements. The contact angle measurement is a valuable tool to investigate the surface polarity and orientation of the attached molecules at a surface.[137a] The contact angles of deionized water in case of Si wafers, grafted with **83a** and **83b** were 52.7^o and 53.7^o respectively, and on bilayer formation these increased to 56.0^o and 60.7^o respectively, whereas for the cleaned, ungrafted Si wafer it was 84^o. Thus, in both the cases, the bilayers were more hydrophobic compared to their respective monolayers. However, the observed contact angles were much less than the reported values (97-108) of the methyl terminated alkyl chains.[124b,137b,c] This suggested interaction of the water molecule with the Bodipys, possibly through their pyrrole rings, which is possible only when the molecules are tilted.

To understand the orientation of molecule **21** in the bilayers, the Owens and Wendt method was used to determine the total surface energy and its resolution into polar and dispersive components, wherein the total solid surface tension γ was assumed to be of the general form as shown in equation (1)

$$l + \cos\theta = 2\sqrt{\gamma_s^d}\,(\sqrt{\gamma_l^d}/\gamma_l) + 2\sqrt{\gamma_s^p}\,(\sqrt{\gamma_l^p}/\gamma_l) \quad \ldots\ldots (1)$$

In this equation, the subscripts, *s* and *l* refer to the solid and liquid surface tension respectively; the superscripts, d and p coincide with dispersive and polar components of total surface tension, where sum of these two values are equal to the total surface tension. In order to resolve the $\sqrt{\gamma_s^d}$ and $\sqrt{\gamma_s^p}$, the contact angles were measured independently using two different liquids (water and diiodomethane) whose surface tension components are known (**Table 5.2.4.1**). All samples showed high surface energies with no significant difference in the dispersive components (**Table 5.2.4.2**). However, compared to the monolayers of compounds **83a** and **83b**, their respective bilayers showed a decrease in the polar components, indicating their hydrophobicity. These results clearly indicated that the fluorine atoms of the Bodipys are less exposed to the space.

Table 5.2.4.1: The surface tension components of H_2O and CH_2I_2 at 20 ^oC

Liquid	**Surface tension (mN/m)**		
	γ_l	γ_l^d	γ_l^p
Water	68.9	18.6	50.3
Diiodomethane	49.7	48.0	1.7

Table 5.2.4.2: Surface energy of modified Si surfaces

Sample	Surface energy (mJ/m^2)		
	Total Energy	Polar component	Dispersive component
BODIPY –C5 Monolayer	55.1	15.7	39.4
BODIPY –C5 Bilayer	53.9	14.7	39.2
BODIPY –C11 Monolayer	56.1	15.1	41.0
BODIPY –C11 Bilayer	52.7	13.3	39.4

Atomic force microscopy (AFM) and ellipsometry. The AFM images (**Figure 5.2.4.2**) revealed that each of the mono- and bi-layers had granular surface morphology with an average grain size of 8 and 14 nm, respectively. The AFM analyses revealed that the mono- and bilayers of **83b** were more organized, compact and uniform with lesser number of voids and hillocks than those **83a**. The numbers of voids were less in the bilayers compared to the respective monolayers.

Measurement of the layer thicknesses is essential to determine if it is a monolayer or a multilayer. For a monolayer, its orientation on the surface can also be determined by comparing the experimental results and the theoretical lengths of the molecules. Amongst the methods, used for measuring the thicknesses of Si-grafted layers, presently ellipsometry and XRR technique were used. The ellipsometry data revealed the average thicknesses of respective monlayers as ~ 1.3 ± 0.2 nm in case of **83a** and 2.2 ± 0.2 nm with **83b**, while the corresponding theoretically calculated (using Molkel software) values were 1.3 nm and 2.25 nm. The thicknesses of the bilayers from **83a** and **83b** were 2.1±0.2 nm (theoretical: 2.0 nm), and 3.1±0.2 nm (theoretical: 2.95 nm) respectively. The thickness values, determined by ellipsometry also revealed doubling of the BODIPY molecules in almost 1:1 ratio after self-assembly in the bilayers, which is in

accord with the fast scan CV results. These data are also consistent with the AFM analyses, both revealing more compact monolayers with **83b** than **83a**.

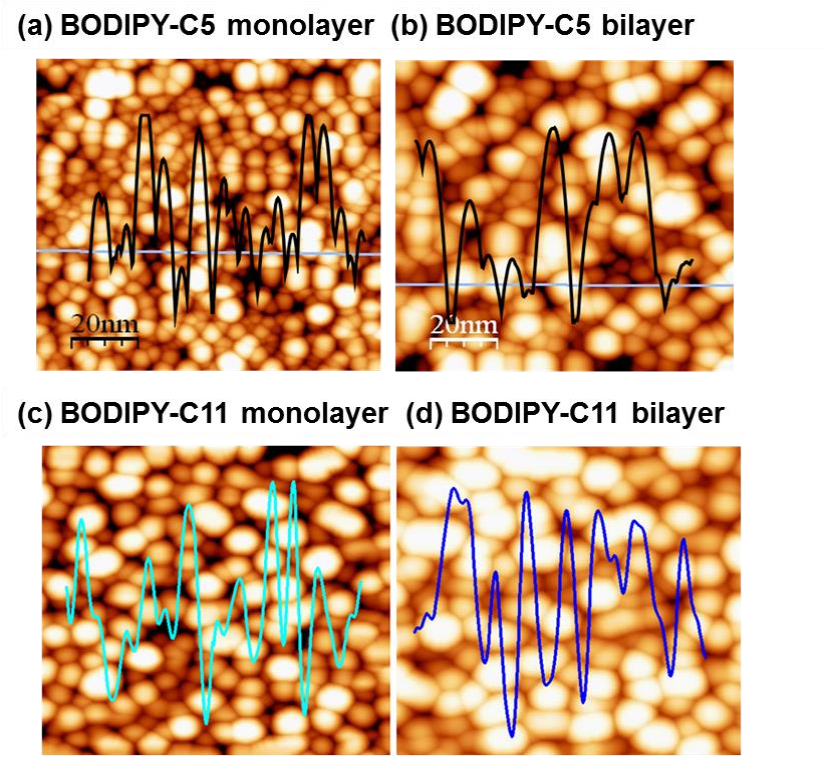

Figure 5.2.4.2 The non-contact atomic force microscope images recorded for (a) **83a**/Si(n^{++}) monolayer; (b) **21**:**83a**/Si(n^{++}) bilayer; (c) **83b**/Si(n^{++}) monolayer; (d) **21**:**83b**/Si(n^{++}) bilayer, respectively.

XRR analyses. XRR is a non-destructive and non-contact technique for determination of thickness between 2-200 nm with a precision of about 1-3 Å. In addition, this technique is also employed to determine the density and roughness of films and multilayers. X-rays have a refractive index in solids which is fractionally smaller than unity, so if one approaches a surface at a sufficient grazing angle, total external reflection can be achieved below some critical angle (few tenths of a degree). For an angle of incidence greater than critical angle, the beam penetrates the film and interference between X-ray amplitudes reflected from surface and interfaces of a layered sample gives rise to a complex reflectivity pattern. This principle is

effectively utilized in the sensitive XRR technique wherein detailed analysis of this XRR data yields information about electron density profile as a function of depth, layer thickness and surface/interface roughness, regardless of the amorphous or crystalline nature of the sample.

The experimental data are fitted with a theoretical model of depth-dependent scattering length density (SLD), ρ that gives information about the composition and density gradient in a layered structure. Thus, the depth profile of electron SLD from XRR data (ρ^x) can be obtained. Scattering length densities in XRR are related to the atomic number densities in a system. The SLD values of different layers are calculated from the following equation (2):

$$\rho^x(z) = r_e \sum_i N_i(z)(Z_i + f_i') \quad \text{.....(2)}$$

where $\rho^x(z)$ is the depth (z) dependent scattering length density (in units of $Å^{-2}$) for x-rays. Z_i and f_i' are the charge number and real anomalous dispersion factor respectively of the i^{th} element, r_e (= 2.818 fm) is the classical electron radius and N_i are the corresponding depth-dependent number densities per unit volume of the components. The accuracy with which these parameters can be determined is typically of the order of a few nm or better, making it very useful for the study of ultrathin organic layers.[138]

Since compound **83a** with a small alkyl chain of less electron density formed less compact organic layers, we focused only on the monolayer **83b**/Si(n^{++}) and the bilayer **21**:**83b**/Si(n^{++}), and confirmed the films thicknesses using X-ray reflectivity (XRR) technique in specular mode. A specular geometry reflectivity measurement as a function of the incident angle provided a number of information *viz.* refractive index depth profiles, electron/mass density profiles along the normal axis direction, total and/or individual layer thicknesses, and interface roughnesses. Suitable model fitting of the reflectivity profiles confirmed formation of BODIPY-C11 monolayers and bilayers at the Si substrate (**Figure 5.2.4.3**). For the bilayer **21**:**83b**/Si(n^{++}),

the XRR data were modeled as arising from two layers of organic material, deposited on Si base. From the plot of SLD *vs* interface distance, the thicknesses for monolayer and bilayer were calculatd a 2.40 ± 0.02 nm and 3.1 ± 0.02 nm respectively. The roughness values for the monolayer of were higher than that of the bilayer of (BODIPY-C11).

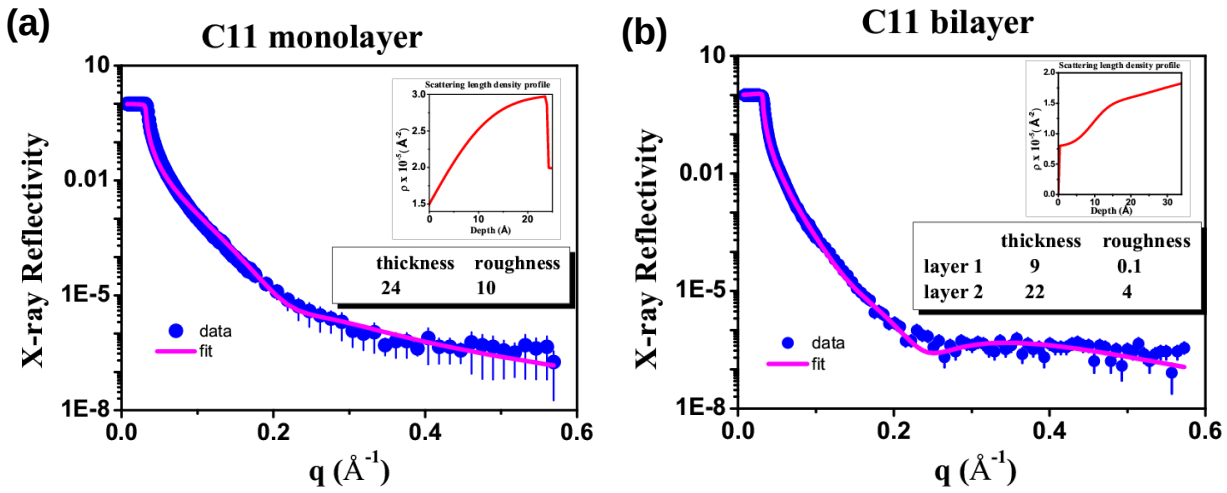

Figure 5.2.4.3 XRR plots of the BODIPY-C11 systems (a) **83b**/Si(n^{++}) monolayer; (b) **21**:**83b**/Si(n^{++}) bilayer. (inset: SLD plots).

Secondary ion mass-spectrometry (SIMS).

SIMS is most sensitive of all the commonly-employed surface analytical techniques, as it can detect impurities on a surface layer at < 1 ppm concentration, and in bulk at ~1 ppb concentrations, in favorable cases. In SIMS the surface of the sample is subjected to bombardment by high energy ions, ejecting (or *sputtering*) of both neutral and charged (+/-) species including atoms, clusters of atoms and molecular fragments from the surface. The ions are extracted from the sample region, and subjected to energy-filtering before they are mass analyzed by a quadruple or more often by a time-of-flight (TOF) mass analyzer, the latter providing substantially higher sensitivity and mass resolution, and a much greater mass range (albeit at a higher cost). In general, TOF analyzers are preferred for static SIMS, whilst

quadruple and magnetic sector analyzers are preferred for dynamic SIMS. Presently, the SIMS data of the monolayer of **83a** showed peaks at m/z 325, 281 and 191 amu due to the Bodipy fragments (**Figure 5.2.4.4a**). Similar results were obtained with the **83b** monolayer (data not shown). The SIMS data of the bilayer **21**:**83b**/Si(n^{++}) showed an additional mass peak at m/z 317 amu, accounting for the $[M-1]^+$ peak for compound **21** along with the peaks due to the Bodipy fragments (**Figure 5.2.4.4b**). The SIMS data of the **21**:**83a**/Si(n^{++}) were also similar (data not shown). Nevertheless, the SIMS data confirmed deposition of their respective layers on the Si wafers.

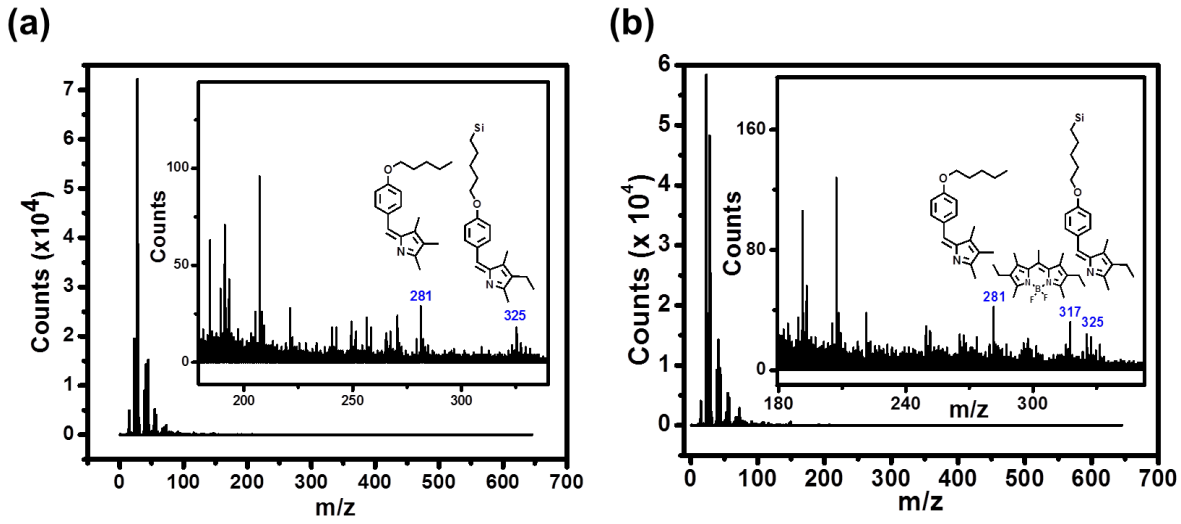

Figure 5.2.4.4 TOF-SIMS of positive secondary ions desorbed from monolayer and bilayer by mono-isotopic ^{69}Ga projectile. (a) **83a**/Si(n^{++}) monolayer; (b) **21**:**83b**/Si(n^{++}) bilayer. (insets: enlarged plots.)

Since the SIMS mass fragmentation pattern did not provide much information about the orientation of the bilayers, the SIMS depth profile of the bilayer **21**:**83b**/Si(n^{++}) was studied. The SIMS depth profile (**Figure 5.2.4.5.a**) revealed the thickness for the bilayer **21**:**83b**/Si(n^{++}) as ~3 nm, which was in good agreement with the XRR data. Further, the magnified SIMS data (**Figure 5.2.4.5.b**) of the monolayer **83b**/Si(n^{++}) and the bilayer **21**:**83b**/Si(n^{++}) showed fragmented

boron species B_{10} and B_{11} of the Bodipys, and as expected, the number of boron atoms in the bi-layer was nearly double that of the mono-layer.

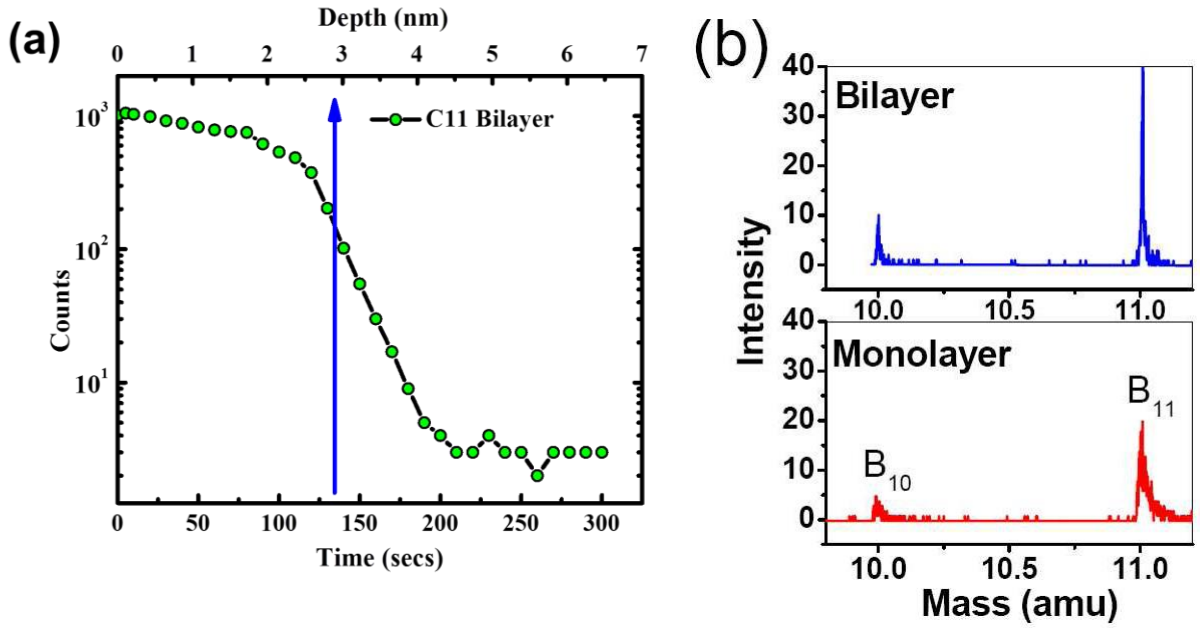

Figure 5.2.4.5 (a) SIMS depth profile of bilayer of **83b**, (b) SIMS spectra: B_{10} and B_{11} peaks for compound **83b**.

5.2.5. J-V characteristics

To measure the *J*–*V* characteristics, a metal/molecule/Si (n++) structure was completed by using a tiny drop of liquid mercury of diameter ~500 μm as the counter electrode as illustrated in **Figure 5.2.5.1a/b (insets)**. The area in contact with the grafted monolayer was 0.018 mm^2. Typical current voltage (*J*-*V*) curves of undeposited Si (111) wafers are shown in **Figure 5.2.5.2a**. Compared to that, the *J*-*V* curves (**Figure 5.2.5.1a** and **5.2.5.1b** respectively) of the mono-layers **83a**/Si(n^{++}) and **83b**/Si(n^{++}) exhibited current rectification behavior in the forward bias, as per the hypothesis, proposed earlier in this chapter. The rectification ratio (RR) – defined as a ratio of current densities at ±1.5 V (in absolute value) ($RR = | J_{-1.5V} | / J_{1.5V}$) was found to be 37 for **83a**/Si(n^{++}) and 500 in case of **83b**/Si(n^{++}) monolayer. The RR values,

measured for 42 samples for the former varied in the range of 30-70, while for the latter the variation was 100-500. With **83a**/Si(n^{++}), a larger number (20) of devices showed RR between 60-70. However, with **83a**/Si(n^{++}), 15 out of 28 devices showed RR > 300 and 9 devices had RR between 100-300. The detailed statistics of the devices are presented in **Table 5.2.5.1**.

Table 5.2.5.1: Statistics of the current rectification by the monolayers

Compound	No. of samples	No. of devices in each sample	Total no. of devices	No. of devices showing Rectification Ratio					
				0-30	**30-60**	**60-70**	**50-100**	**100-300**	**300-500**
83a	6	7	42	6	16	20	--	--	--
83b	4	7	28	--	--	--	4	9	15

The significantly increased RR value increased for the **83b**/Si(n^{++}) monolayers may be due to their compact packing. Further, comparison of the results in **Figures 5.2.5.1a-c** revealed that the current rectification behavior is exclusively due to the Bodipy molecules. The *J*–*V*s of these diodes also exhibited hysteresis, which could be due to formation of electric dipole under high applied electric field, as reported previously by others.[139]

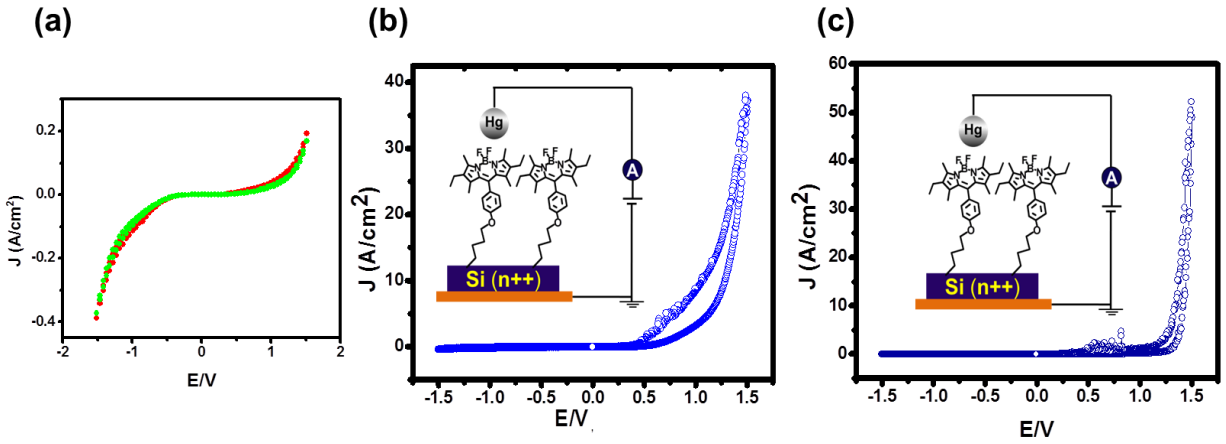

Figure 5.2.5.1 Room temperature *J-V* characteristic recorded for monolayers by scanning the bias in the sequence -1.5 V → 0 V → +1.5 V→ 0 V → -1.5 V at a scan speed of 5 mV/s. (a) un-deposited Si surface; (b) compound **83a**; (c) compound **83b**. Insets: schematic of the device structures.

On the other hand, for a positive bias applied to the Hg-electrode, the bi-layers exhibited strong NDR effects concomitant with pronounced hysteresis(**Figure 5.2.5.2a/b**). The devise structure is schematically shown in **Figure 5.2.5.2c**. The PVR value measured, for 80 samples varied between 10 and 1000. The percentages of devices attaining the maximum PVR (1000) were 3.1 and 8.3 by the bilayers **21**:**83a**/Si(n^{++}) and **21**:**83b**/Si(n^{++})respectively. Expectedly the devices made from the more compact **21**:**83b**/Si(n^{++}) bilayers showed better attribues such as (i) less failure (no NDR behaviour): 25% vs 31%; and (ii) PVR 1-10: 20.8% vs 27.7%; PVR 100-500: 12.5% vs 4.6%. The comparative PVR values are represented in the form of π-charts in **Figure 5.2.5.3**. It may be noted that NDR is obtained only in the first bias scan and in the subsequent scans NDR disappeared and the current remained low. However, if the electrodes are short-circuited, the neutral state is regained and hence the NDR effect reappears. Among the previous reported hybrid nanoelectronics with NDR property,[126] only in one case the PVR as high as ours but the NDR effect was observed at low temperature (60 K).[126a-c]

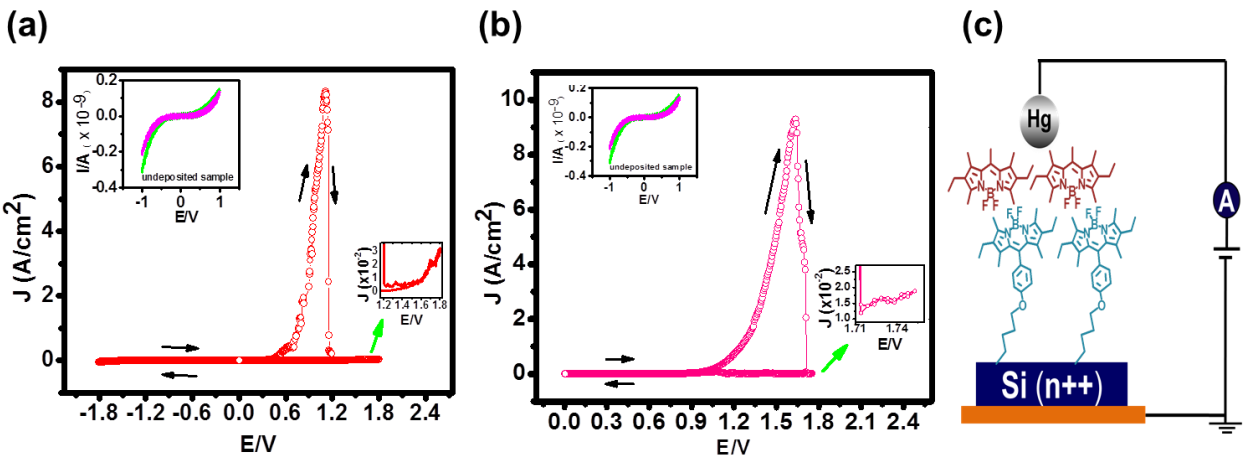

Figure 5.2.5.2 Room temperature *J-V* characteristics for the bilayers, recorded by scanning the bias in the sequence -1.8 V → 0 V → +1.8 V→ 0 V → -1.8 V at a scan speed was 5 mV/s. (a) **21**:**83a**/Si(n^{++}); (b) **21**:**83b**/Si(n^{++}); (c) schematic of the devices employed for the measurements.

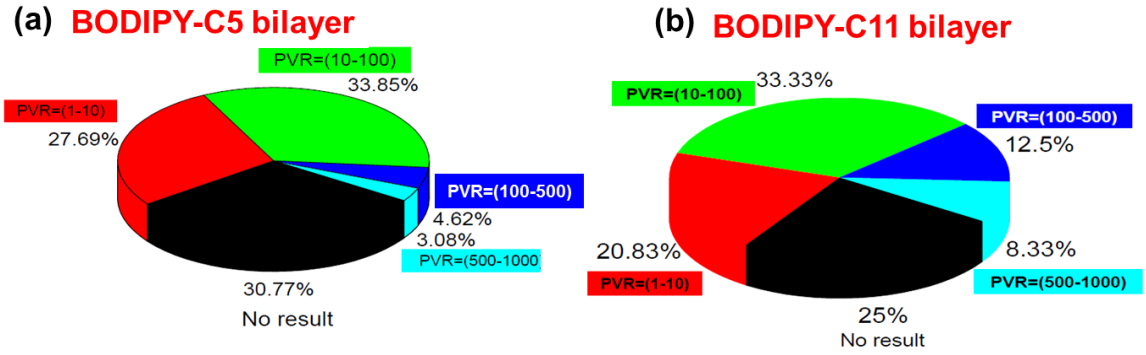

Figure 5.2.5.3 Comparative PVR values of NDR in bilayers (a) **21**:**83a**/Si(n^{++}); (b) **21**:**83b**/Si(n^{++})

5.2.6. Theoretical explanation

In order to gain an insight into the rectification and NDR behaviors of the respective mon- and bi-layers, the HOMO and LUMO energies of BODIPY-C5 (or **83a**) and PM567:BODIPY-C5 (or **21:83a**) molecules were calculated using MO theory, as implemented in GAMESS software.[140] The geometries and total energies of the molecules were optimized under the density functional theory using the linear combination of atomic orbital (LCAO) approach. A standard 6-31G+(d,p) basis set was employed for this purpose. The exchange correlation energy

was calculated using B3LYP functional, which consists of Hartree-Fock exchange, Becke's exchange and Lee-Yang-Parr correlation functional.[141] Consistent with experimental the CV data (**Figure 5.2.4.1.a**), the theoretical calculation also predicted a single oxidation state of **83a**, and two oxidation states for the **21:83a** bi-layer. The double oxidation by the bilayer is expected as it has two Bodipy layers. The theoretically calculated spatial orientation of HOMO's of neutral **21:83a**, and after its I^{st} and II^{nd} oxidations are shown in **Figure 5.2.5.1.a**).

The HOMO of the BODIPY-C5 (or **83a**) lies on the Bodipy moiety in both neutral and oxidized state. Thus, the rectification behavior of the monolayer *i. e.*, Hg/ **83a** /Si(n^{++}) is due to the resonant tunneling through the HOMO of the Bodipy moiety (π group) of compound **83a**.[141] Due to the lack any major conformational Changes after its oxidation, no NDR was observed with the monolayer of **83a**. In case of the bi-layer, the HOMO lies on both the Bodipy moieties in the neutral state. After the I^{st} oxidation, it still remains on the Bodipy moieties, but with a slight conformational change. However, after II^{nd} oxidation, there is a huge conformational change, because the HOMO largely shifts to the alkyl-chain. This could be attributed to slippage or rotation at Bodipy interface, which is likely as the bi-layer is formed by weak interaction.

The schematic energy level diagram of Hg/ **21:83a**/Si(n^{++}), obtained using the theoretically estimated values of HOMO and LUMO energies is shown in **Figure 5.2.6.1.b**. For the neutral state, the theoretical calculations show doubly degenerate HOMO (-5.26, -5.27eV) and LUMO (-2.67, -2.01 eV) energy levels, indicating that the bi-layered Bodipys can undergo double oxidation. At zero bias *i. e.*, V = 0, the degenerate HOMO and LUMO levels of **21:83a** are off-resonance with the Fermi level of the Hg electrodes. For an applied positive bias (V>0), a rise in current in the *J-V* curve (see **Figure 5.2.5.2.a** and **b**) is attributed to non-resonant tunneling. However, for bias >0.7 V, there is a sharp current rise due to the alignment of the

Fermi level of Hg with the HOMO energy levels, inducing a resonant tunneling. Since the molecule undergoes a first oxidation, without any major changes in the configuration, the current keeps rising sharply with the bias. However, at still higher bias, the molecule undergoes second oxidation leading to a large conformational change. Consequently, the HOMO and LUMO levels are shifted and become off-resonance to the Fermi level of Hg. As a result, the current drops sharply as it now can pass only though the direct tunneling process, and therefore, results in the NDR effect. The current always remains low in the subsequent *J*-*V* cycles, indicating that the conformational changes achieved after second oxidation are quite stable. However, if the electrodes are short-circuited, the neutral state of **21:83a** is regained, and the NDR effect reappears. For the negative bias on Hg electrode *i. e.* $V < 0$, the current remains low as a very high bias is required to obtain a resonance between the Hg Fermi level and LUMO of the molecule. Moreover, the molecule does not undergo any reduction, and therefore, no additional features other than non-resonant tunneling current, appears in the negative bias.

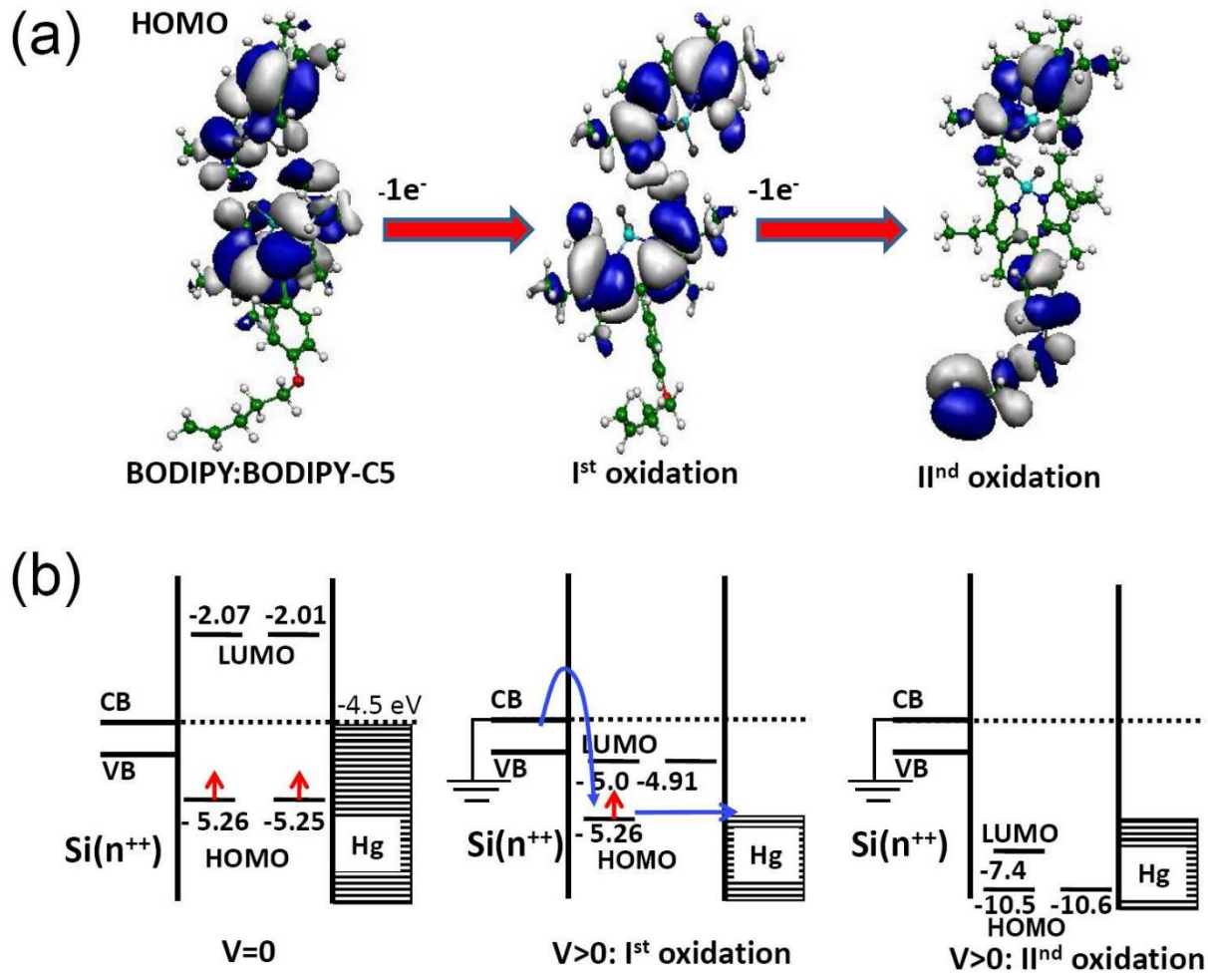

Figure 5.2.5.1 (a) Theoretically calculated geometries of HOMO of **21:83a** under different oxidation states. (b) Schematic representation of the energy level diagrams for Hg/ **21:83a**/Si(n^{++}) device at different applied bias.

5.3. Summary

In conclusion, we have measured the charge transport properties of some tailor-made Bodipy monolayers and bilayers, grafted on Si (111) surfaces. Room temperature current rectification in the monolayer and NDR effect in the bilayer with PVR values upto 1000 were have demonstrated. The studies showed that the NDR associated with hysteresis is due to resonant tunneling through molecular orbital, and bias-induced conformational changes in the

molecules. The results presented here will clearly pave the way for design and development of new molecular devices suitable for molecules-on-Si hybrid nanoelectronics.

5.4. Experimental

5.4.1. General methods

The general details of the synthetic methodologies and spectroscopic studies have already been discussed in Chapter-2. The monolayers were characterized in terms of thickness, using an ellipsometer (Sentech: model SE400adv); surface morphology by AFM imaging (Multiview 4000, Nanonics), de-ionized water contact angle (Data Physics System, model: OCA20), and molecular mass by SIMS (BARC make, Kore's Technology software). The current voltage characteristics were recorded in a dark box using a potentiostat/galvanostat system (model: Autolab PGSTAT 30).

5.4.2. Synthesis of Bodipys

4-(4'-penentenyloxy)benzaldehyde (82a) and 4-(10'-undecenyloxy)benzaldehyde (82b).

A mixture of **68** (4.0 g, 32.7 mmol), 1-bromopentene (39.3 mmol) or 1-bromo-10-undecene (39.3 mmol), K_2CO_3 (5.52 g, 40 mmol) and Bu_4NI (10 mol%) in acetone (100 mL) was refluxed. After completion of the reaction (*cf*. TLC ~ 16 h) the mixture was filtered, concentrated in vacuum, the residue taken in Et_2O (40 mL) and washed with H_2O (2 × 10 mL) and brine (1 × 20 mL), dried and concentrated in vacuo. The residue was purified by column chromatography (silica gel, 5% EtOAc/hexane) to give pure **82a** (5.7 g, 91%) and **82b** (8.1 g, 91%).

Compound 82a: Viscous liquid; IR : 3019, 1687 cm^{-1}; ^1H NMR: δ 1.28-1.42 (m, 2H), 2.32 (t, *J* = 6.8 Hz, 2H), 4.01 (t, *J* = 6.2 Hz, 2H), 6.97 (d, *J* = 9.5 Hz, 2H), 7.80 (d, *J* = 9.5 Hz, 2H), 9.85 (s, 1H); ^{13}C NMR : δ 13.6, 22.2, 25.3, 28.7, 31.2, 68.1, 114.4, 129.6, 131.5, 163.9, 190.1; Anal.

Calcd. for $C_{12}H_{14}O_2$: C, 75.76; H, 7.42%. Found: C, 75.44; H, 7.16%.

Compound 82b: viscous liquid; IR: 3019, 2856, 1687 cm^{-1}; ^1H NMR : δ 1.38 (m, 12H), 1.82 (m, 2H), 2.05 (m, 2H), 4.04 (t, *J* = 6.0 Hz, 2H), 4.98 (t, *J* = 10.0 Hz, 2H), 5.79 (m, 1H), 6.99 (d, *J* = 8.0 Hz, 2H), 7.83 (d, *J* = 8.0 Hz, 2H), 9.88 (s, 1H); ^{13}C NMR : δ 25.9, 28.9, 29.0, 29.3, 29.4, 33.7, 68.4, 114.8, 129.9, 131.9, 139.1, 164.3, 190.6; MSMS (m/z): 275.1 (100) $[M+H]^+$ amu; Anal. Calcd. for $C_{18}H_{26}O_2$: C, 78.79; H, 9.55%. Found: C, 79.02; H 9.55%.

BODIPY-C5 (83a) and BODIPY-C11 (83b).

As described in Chapter-2, compound **83a** was synthesized using **58** (1.00 g, 8.1 mmol), **82a** (0.70 g, 3.7 mmol), TFA (1 drop), DDQ (0.84 g, 3.7 mmol), Et_3N (3.1 mL) and $BF_3{\cdot}Et_2O$ (2.8 mL, 22.2 mmol) in CH_2Cl_2 (10 mL). Usual work-up, followed by column chromatography (silica gel, hexane-EtOAc) furnished pure **83a**.

For the synthesis of **83b**, compounds **58** (1.00 g, 8.1 mmol), **82b** (0.99 g, 3.7 mmol), TFA (1 drop), DDQ (0.84 g, 3.7 mmol), Et_3N (3.1 mL, 22.2 mmol), $BF_3.Et_2O$ (2.8 mL, 22.2 mmol) and CH_2Cl_2 (30 mL) were used.

83a: Yield: 0.24 g (13.7%); red square shaped crystals (CH_2Cl_2/cyclohexane); mp: 177-178 ^oC; IR: 2964, 2880, 1608, 1643 cm^{-1}; ^1H NMR: δ 0.98 (t, *J* = 7.6 Hz, 6H), 1.34 (s, 6H), 1.93 (t, *J* = 7.7 Hz, 2H), 2.16–2.36 (m, 6H), 2.53 (s, 6H), 4.03 (t, *J* = 6.5 Hz, 2H), 5.00–5.12 (m, 2H), 5.89-5.99 (m, 1H), 7.01 (d, *J* = 6.7 Hz, 2H), 7.13 (d, *J* = 6.7 Hz, 2H); ^{13}C NMR: δ 11.7, 12.4, 14.5, 17.0, 28.3, 30.0, 67.2, 114.9, 115.2, 127.6, 129.3, 131.1, 132.5, 137.5, 138.4, 140.3, 153.3, 159.4; EI-MS (*m/z*): 464.0 $[M]^+$. Anal. Calcd. for $C_{28}H_{35}BF_2N_2O$: C, 72.42; H, 7.60; N, 6.03%. Found: C, 71.95; H, 7.91; N, 6.28%.

83b: Yield: 0.36g (17.8%); mp: 160 °C; IR: 2964, 2880, 1608, 1643 cm^{-1}; ^1H NMR: δ 1.02 (t, *J* = 7.6 Hz, 6H), 1.32 (s, 12H), 1.57 (s, 6H), 1.78 (p, *J* = 6.4 Hz, 2H), 2.02 (q, *J* = 7.8 Hz, 2H),

2.30 (q, *J* = 7.6 Hz, 2H), 2.51 (s, 6H), 4.00 (t, *J* = 6.4 Hz, 2H), 4.90-5.03 (m, 2H), 5.75-5.88 (m, 1H), 6.95 (d, *J* = 8.7 Hz, 2H),7.11 (d, *J* = 8.7 Hz, 2H); ^{13}C NMR: δ 11.8, 12.5, 14.6, 17.1, 26.0, 28.9, 29.1, 29.3, 29.4, 29.5, 29.7, 31.6, 31.9, 33.8, 68.2, 114.1, 115.0,127.7, 129.4, 129.6,131.2, 132.6, 138.5, 139.2, 140.4, 153.4, 159.6; EI-MS (*m/z*): 548.3 $[M]^+$. Anal. Calcd. for $C_{34}H_{47}BF_2N_2O$: C, 74.44; H, 8.64; N, 5.11%. Found: C, 74.48; H, 8.48; N, 5.12%.

5.4.3. Preparation of the Si(n^{++})-Bodipys hybrids

The Si (111, resistivity $<10^{-3}$ Ωcm) wafers were cleaned by heating them in 4:1 (v/v) of conc. H_2SO_4: 30% H_2O_2 (piranha) for 10 min at 80 ^oC. *Piranha is exceedingly dangerous and should be kept away from organic materials and treated with care*. The wafers were removed, washed with excess H_2O, and immersed successively in a de-aerated (purged with high pure Ar for 30 min) 40% aqueous NH_4F for 10 min, and in 2% aqueous HF for 2 min. The wafers were further washed with deionized H_2O for 1 min, dried under a stream of N_2 and immediately taken into the electrochemical cell for electro-grafting.

The electro-grafting of organic molecules to Si surface was carried out using a three-electrode electrochemical setup, as shown schematically in **Figure 5.2.3.3**. The H-terminated Si on which the molecules are to be grafted was used as the WE, while a Pt wire served as the CE. A pseudo RE was prepared by depositing AgCl layer over Ag by the galvanostatic method. For this, a constant current (1mA) between Ag wire and Pt electrode in 1 M HCl was maintained for 15 min. The AgCl-coated Ag wire was washed thoroughly with de-ionized water to remove the acid, and dried. This was standardized with respect to the redox potential of ferrocene, and used for the experiments. The electro-grafting was carried out using CV using a solution containing 1:1(v/v) of 0.1 M TBAP as the supporting electrolyte and compounds **83a** or **83b** (1 mM) in dry CH_2Cl_2. The potential was scanned from –0.8 V to 0 V at a scan rate of 0.05 V/s for number of

scans. Control experiments were also carried out using TBAP solution alone to ensure no deposition of TBAP on Si. After electrografting, the WEs were sonicated in CH_2Cl_2, acetone and methanol for 10 min each to remove the physisorbed molecules and obtain monolayered Si-hybrids.

For the deposition of the bilayers, the Si-hybrid monolayers were dipped into a 1 µM solution of **21** in dry CH_2Cl_2 for 24h under inert atmosphere. The resultant self-assembled materials were sonicated in dichloromethane, acetone and methanol for 10 min as above to obtain the required materials. Additional similar experiments were also carried out by dipping the WEs in the 1 µM solution of **21** for 7 days, and also using a 3 µM solution of **21** to ensure uniform bilayer deposition.

5.4.4. Characterization of Bodipy monolayers and bilayers

The thicknesses of the deposited layers were measured by ellipsometry. The AFM images, used for characterizing the surface morphology were analyzed by WXSM software.

Contact angle measurements. Millipore-Q water (conductivity 0.05 $\mu S.cm^{-1}$) was used for contact angle studies. Dynamic contact angle analysis by wetting angle measurements was carried out to investigate the change in surface energy of samples and to investigate the kinetics. The measurement of contact angles of the sample was carried out by sessile drop technique using an image analysis software. A liquid droplet (1.5- 2.5 µL) was allowed to fall on the samples to be studied from a software-controlled syringe.

SIMS analyses. The SIMS was recorded using a TOF-SIMS instrument, consisting of a 25 KeV fine focusing primary Liquid metal Ion gun (Mono-isotopic ^{69}Ga) that can focus ion beams to a spot size as small as 250 nm with current density of ~ 0.03 mA/cm^2. The primary ion beam was pulsed at high potential (+ 2000 VDC) at a rate of 10 kHz with a pulse width of approximately

10 – 15 ns. A modified Wiley-Mclaren type Reflectron produces a uniform electrostatic field over a length of 415 mm. The secondary ions, generated from the impact of primary ions were accelerated and extracted (with a small delay) from the sample surface using a unique ion optical lens that employs large acceptance and a small energetic distribution. After passing through a flight tube, the extracted secondary ions with slightly varying kinetic energies were reflected and time focused onto a microchannel plate detector, operated in the ion counting mode with the help of a specially designed gridless reflectron (Model : R500, Kore Technology, UK). A fast pre-amplifier with a rise-time of <500 ps was used to detect and amplify the ion signals before being counted by a P7887 (Fast ComTec, Germany) Multi-scaler with a timing resolution of about 300 ps. Three ion pumps were utilized to ensure an ultimate low background pressure of $< 1 \times 10^{-9}$ mbar in both the analysis chamber and the flight tube. The signals, detected by the microchannel plate detector were amplified and coupled to a high-speed time to digital converter to generate the time spectrum which was directly converted into a mass spectrum using the following relation: $m = \left(\frac{t - t_0}{C_b}\right)^2$, where t - is the arrival time of the ions, t_0 and C_b are constants with values 1.105 and 5.00 respectively, depending on the geometrical parameters of the flight tube and the extraction optics. By rastering the primary ion beam over the sample surface, and detecting the secondary ions corresponding to each raster point, a chemical image of the sample surface was generated. The TOF-SIMS had a mass resolving power > 10,000, with a mass range of about 1500 amu and a dynamic range > 4 (4 orders of magnitude between the smallest peak and the largest peak). A low energy electron flood gun was used to neutralize charging of the insulating samples. A load lock chamber connected to the analysis chamber was used for loading samples from atmosphere which ensured that the analysis chamber was never exposed to

atmospheric contaminations. For the depth profiling studies, an Ar ion etch gun at 500 eV was interlaced with the primary liquid metal ion gun to etch sample surfaces. The depth profiles were obtained by alternating between sputter cycles and data acquisition cycles.

XRR analyses. The XRR mesaurements for the structural depth profiles were carried out in specular mode with a laboratory X-ray source using Cu Kα. The calculation of optical reflectivity of the X-rays in this case was based on recursive formalism for stratified media.[142] The SLD profiles were produced as a function of depth in the sample by independently fitting the experimental reflectivity data from the XRR measurements through a theoretical model as a series of layers. Detailed significant information for the layers and the interfaces were gathered in terms of three characteristic parameters: thickness of the layers, interface roughness and scattering length density as a function of depth. Errors of the parameters gained from the fits were found to be within the range of 5–10%.

5.4.5. Measurement of current-voltage characteristics

To measure current–voltage (J–V) characteristics, a metal/monolayer or bilayer/ Si(n^{++}) structure was completed by using a very small drop of liquid mercury as a counter electrode. The *J–V* was recorded at room temperature by scanning the bias in the sequence -1.8 V → 0 V → +1.8 V→ 0 V → -1.8 V at a scan speed was 5 mV/s in a dark box using HP4140 (pA meter–dc voltage source).

5.4.6. Theoretical computation

We have theoretically calculated the highest occupied molecular orbital (HOMO) and lowest unoccupied molecular orbital (LUMO) energies for neutral, and at different oxidation state of BODIPY-C5 and \BODIPY:BODIPY-C5 molecules respectively. The geometries and total energies of molecules were optimized using the density functional theory with linear

combination of atomic orbital (LCAO) approach using General Atomic and Molecular Electronic Structure System (GAMESS). A standard 6-31G+(d,p) basis set was employed for this purpose. The exchange correlation energy was calculated using B3LYP functional. This function uses part of Hartree-Fock exchange and Becke's exchange functional, and the Lee-Yang-Parr correlation functional. For the computation, PC and two supercomputers, namely, Ameya and Ajeya were used. Ameya is 128-proceesor ANUPUM supercomputer built on 64 dual Xeon servers (2.4GHz) as compute node, interconnected by a high-speed (300 MBps) communication network. The 512-processors ANUPAM-ameya supercomputer is built using 256 dual Xeon servers as a compute node. Each server is based on dual Xeon, 3.6 GHz processors. The inter-communication network is a Gigabit Ethernet with a node-to-node communication speed of 1 Gbps. The performance of ANUPAM-ameya is 1.73 Teraflops. The open source Linux operating system was used on each parallel processing node in these two supercomputers.

Summary

Summary

The major objectives of the present investigation was to develop some Bodipy-based functional materials for various applications such as photostable laser dyes, Bodipy based organoelectronic materials and water soluble Bodipys for biological applications. This warranted synthetic modifications of the Bodipy core, available commercially or synthesized in-house so as to impart the desirable attributes to the newly developed molecules/assemblies. To this end, various sites of the Bodipy cores *viz*. different positions of the dipyrrole moieties and/ or the *meso*-position were innovatively used for introduction of different functional groups. Finally, the efficacy of the protocols in designing new molecules and the potential functional uses were investigated. The achievements are highlighted below.

I. For improving the photostability, two new congeners of the commercially available Bodipy dye PM567 were rationally designed and synthesised by replacing the F atoms at the boron centre with a polyethyleneglycol (PEG) derivative as such and in conjunction with introduction of an electron-rich bulky aryl group at the *meso*-position. Both these dyes showed increased photostability than PM567, without compromising the lasing efficiency. In fact, the lasing performance of the dye containing substitutions both at the *meso*-site and the B-centre was marginally better than that of PM567. The results of the theoretical calculations and pulse radiolysis studies explained that the designated substitutions reduced the $^1O_2$ generation capacity of the dyes and their reaction rates with $^1O_2$, enhancing the lifetimes of these dyes under lasing conditions.

II. *meso*-Functionalization of the Bodipy core provides functionally rich new molecules with unaltered photophysical properties, which may be important for various applications. Using a novel concept of steric-strain release that can override the acidity factor of per-methylated

Bodipys, a new regioselective strategy for Knovenagel condensation at the *meso*-methyl site was developed starting from PM597 and PM567 molecules. The reaction proceeded exclusively at the *meso*-position with all the aldehydes when sterically more crowded PM597 was used. For the less crowded compound PM567, exclusive regioselectivity was observed with aryl aldehydes, containing electon-withdrawing groups. This strategy provided easy access to several Bodipy derivatives, which are otherwise not amenable easily.

III. Given that water-soluble Bodipys, preferably with red-shifted emission are useful for biolabeling and as PDT agents, several new Bodipy-*O*-glycosides were synthesized by incorporating the glucose unit at *meso*-phenol or C-3/C-5 hydrostyryl moieties. All the compounds showed impressive good photo-toxicity to the human lung cancer A549 cells, without any dark toxicity due to their accumulation in cytoplasm. These compounds induced cellular apoptosis via the extrinsic pathway, and are potential PDT agents. Interestingly, the C-3 and C-5 diglycoside of dihydrostyryl Bodipy formed nano-hydrogel in aqueous EtOH and THF, and their size could be controlled by varying the water concentration.

IV. In a radically different approach, a Bodipy-based σ–π monolayer, grafted on Si was constructed that showed good current rectification due to a resonant transport between the Si conduction band and the HOMO of the π group. The σ–π system was synthesized by attaching some alkenyl moieties at the *meso*-phenol group of a Bodipy. While the Bodipy served as the π-system, the alkenyl group was used both for electro-grafting on Si-surfaces and also as the σ-system. More importantly, self-assembly of the Bodipy, PM567 on the monolayer led to another type of device showing NDR behavior with good PVR (10-1000) with hysteresis. Such systems may be useful for constructing memory devices.

References

1. Loudet, A.; Burgess, K. *Chem. Rev.* **2007**, *107*, 4891–4932.

2. (a) Haughland, R. P.; Kang, H. C.; US Patent US4774339, Sep. 27, **1988**; (b) Monsma, F. J.; Barton, A. C.; Kang, H. C.; Brassard, D. L.; Haughland, R. P.; Sibley, D. R. *J. Neurochem.* **1989**, *52*, 1641–1644; (c) Karolin, J.; Johansson, L. B.-A.; Strandberg, L.; Ny, T. *J. Am. Chem. Soc.* **1994**, *116*, 7801–7806; (d) Haugland, R. P. *Handbook of Fluorescent Probes and Research Chemicals*, 6th ed.; Molecular Probes: Eugene, OR, **1996**; (e) Wagner, R. W.; Lindsey, J. S. *Pure Appl. Chem.* **1996**, *68*, 1373–1380; (f) Metzker, M. L. WO Patent WO/2003/066812, **2003**.

3. (a) Pavlopoulos, T.; Boyer, J. H.; Shah, M.; Thangaraj, K.; Soong, M. L. *Appl. Optics* **1990**, *29*, 3885-3886; (b) Pavlopoulos, T.; Boyer, J. H.; Thangaraj, K.; Sathyamoorthi, G.; Shah, M. P.; Soong, M. L. *Appl. Optics* **1992**, *31*, 7089–7094; (c) Guggenheimer, S. C.; Boyer, J. H.; Thangaraj, K.; Shah, M. P.; Soong, M. L. Pavlopoulos, T. *Appl. Optics* **1992**, *32*, 3942–3943; (d) Shah, M.; Thangraj, K.; Soong, M. L.; Wolford, L.; Boyer, J. H.; Politzer, I. R.; Pavlopoulos, T. G. *Heteroat. Chem.* **1990**, *1*, 389–399; (e) Boyer, J. H.; Haag, A. M.; Satyamoorthi, G.; Soong, M. L.; Thangaraj, K.; Pavlopoulos, T. *Heteroat. Chem.* **1993**, *4*, 39–49.

4. Wang, Y. W.; Descalzo, A. B.; Shen, Z.; You, X. Z.; Rurack, K. *Chemistry* **2010**, *16*, 2887–2903.

5. Dixon, H. B. F.; Cornish-Bowden, A.; Liebecq, C.; Loening, K. L.; Moss, G. P.; Reedijk, J.; Velick, S. F.; Venetianer, P.; Vliegenthart, J. F. G. *Pure Appl. Chem.* **1987**, *59*, 779–832.

6. (a) Yogo, T.; Urano, Y.; Ishitsuka, Y.; Maniwa, F.; Nagano, T. *J. Am. Chem. Soc.* **2005**, *127*, 12162–12163; (b) Rurack, K.; Kollmannsberger, M.; Daub, J. *New J. Chem.* **2001**, *25*, 289–292.

7. Galletta, M.; Campagna, S.; Quesada, M.; Ulrich, G.; Ziessel, R. *Chem. Commun.* **2005**, 4222–4224.

8. Treibs, A.; Kreuzer, F.-H. *Justus Liebigs Annalen der Chemie* **1968**, *718*, 208–223.

9. (a) Li, Z.; Mintzer, E.; Bittman, R. *J. Org. Chem.* **2006**, *71*, 1718–1721; (b) Burghart, A.; Kim.; H.; Welch, M. B.; Thoresen, L. H.; Reibenspies, J.; Burgess, K. *J. Org. Chem.* **1999**, *64*, 7813–7819.

10. (a) Nicolaou, K. C.; Claremon, D. A.; Papahatjis, D. P. *Tetrahedron Lett.* **1981**, *22*, 4647–4650; (b) Tahtaoui, C.; Thomas, C.; Rohmer, F.; Klotz, P.; Duportail, G.; Mely, Y.; Bonnet, D.; Hibert, M. *J. Org. Chem.* **2007**, *72*, 269–272.

11. Li, L.; Han, J.; Nguyen, B.; Burgess, K. *J. Org. Chem.* **2008**, *73*, 1963–1970.

12. Jiao, L.; Yu, C.; Li, J.; Wang, Z.; Wu, M.; Hao, E. *J. Org. Chem.* **2009**, *74*, 7525–7528.

13. Li, M.; Wang, H.; Zhang, X.; Zhang, H. S. *Spectrochim. Acta, Part A* **2004**, *60*, 987–993.

14. Zhang, X.; Zhang, H. S. *Spectrochim. Acta, Part A* **2005**, *61*, 1045–1049.

15. (a) Qi, X.; Jun, E. J.; Xu, L.; Kim, S. J.; Hong, J. S. J.; Yoon, Y. J.; Yoon, J. *J. Org. Chem.* **2006**, *71*, 2881–2884; (b) Bricks, J. L.; Kovalchuk, A.; Trieflinger, C.; Nofz, M.; Bueschel, M.; Tolmachev, A. I.; Daub, J.; Rurack, K. *J. Am. Chem. Soc.* **2005**, *127*, 13522–13529.

16. Werner, T.; Huber, C.; Heinl, S.; Kollmannsberger, M.; Daub, J.; Wolfbeis, O. S. *Fresenius J. Anal. Chem.* **1997**, *359*, 150–154.

17. (a) DiCesare, N.; Lakowicz, J. R. *Tetrahedron Lett.* **2001**, *42*, 9105–9108; (b) Li, J. S.; Wang, H.; Huang, K. J.; Zhang, H. S. *Anal. Chim. Acta* **2006**, *575*, 255–261.

18. Loudet, A.; Bandichhor, R.; Wu, L.; Burgess, K. *Tetrahedron* **2008**, *64*, 3642–3654.

19. Ulrich, G.; Ziessel, R.; Harriman, A. *Angew. Chem. Int. Ed.* **2008**, *47*, 1184–1201.

20. Coskun, A.; Yilmaz, M. D.; Akkaya, E. U. *Org. Lett.* **2007**, *9*, 607–609.

21. Wories, H. J.; Koek, J. H.; Lodder, G.; Lugtenburg, J.; Fokkens, R.; Driessen, O.; Mohn, G. R. *Recueil des Travaux Chimiques des Pays-Bas* **1985**, *104*, 288–291.

22. Pavlopoulos, T. G.; Boyer, J. H.; Shah, M.; Thangaraj, K.; Soong, M.-L., *Appl. Opt.* **1990**, *29*, 3885–3886.**3a**

23. (a) Cakmak, Y.; Akkaya, E. U. *Org. lett.* **2009**, *11*, 85–88; (b) Thivierge, C.; Loudet, A.; Burgess, K. *Macromolecules* **2011**, *44*, 4012–4015; (c) Chase, D. T.; Young, B. S.; Haley, M. M. *J. Org. Chem.* **2011**, *76*, 4043–4051; (d) Lee, J.-I.; Klaerner, G.; Davey, M. H.; Miller, R. D. *Synthetic Metals* **1999**, *102*, 1087–1088.

24. (a) Saki, N.; Dinc, T.; Akkaya, E. U. *Tetrahedron* **2006**, *62*, 2721–2725; (b) Sathyamoorthi, G.; Wolford, L. T.; Haag, A. M.; Boyer, J. H. *Heteroat. Chem.* **1994**, *5*, 245–249.

25. (a) Buyukcakir, O.; Bozdemir, O. A.; Kolemen, S.; Erbas, S.; Akkaya, E. U. *Org. Lett.*, **2009**, *11*, 4644–4647; (b) Kostereli, Z.; Ozdemir, T.; Buyukcakir, O.; Akkaya, E. U. *Org. Lett.* **2012**, *14*, 3636-3639.

26. Rohand, T.; Baruah, M.; Qin, W.; Boens, N.; Dehaen, W. *Chem. Commun.* **2006**, 266–268.

27. (a) Baruah, M.; Qin, W.; Vallee, R. A. L.; Beljonne, D.; Rohand, T.; Dehaen, W.; Boens, N. *Org. Lett.* **2005**, *7*, 4377–4380; (b) Thoresen, L. H.; Kim, H.; Welch, M. B.; Burghart, A.; Burgess, K. *Synlett* **1998**, 1276–1278.

28. (a) Murase, S.; Tominaga, T.; Kohama, A. Eur. Pat. 1253151 A, **2002**; (b) Ulrich, G.; Goze, C.; Guardigli, M.; Roda, A.; Ziessel, R. *Angew. Chem.* **2005**, *117*, 3760–3764; (c) Ulrich, G.; Goze, C.; Guardigli, M.; Roda, A.; Ziessel, R. *Angew. Chem. Int. Ed.* **2005**, *44*, 3694–3698; (d) Goze, C.; Ulrich, G.; Mallon, L. J.; Allen, B. D.; Harriman, A.; Ziessel, R. *J. Am. Chem. Soc.* **2006**, *128*, 10231–10239; (e) Goze, C.; Ulrich, G.; Ziessel, R. *J. Org. Chem.* **2007**, *72*, 313–322; (f) Goze, C.; Ulrich, G.; Ziessel, R. *Org. Lett.* **2006**, *8*, 4445–4448.

29. Harriman, A.; Izzet, G.; Ziessel, R. *J. Am. Chem. Soc.* **2006,** *128*, 10868–10875.

30. Boens, N.; Leen, V.; Dehaen, W. *Chem. Soc. Rev.* **2012,** *41*, 1130–1172.

31. Hu, R.; Lager, E.; Aguilar-Aguilar, A.; Liu, J.; Lam, J. W. Y.; Sung, H. H. Y.; Williams, I. D.; Zhong, Y.; Wong, K. S.; Pea-Cabrera, E.; Tang, B. Z. *J. Phys. Chem. C* **2009**, *113*, 15845–15853.

32. Holmquist, H. E.; Benson, R. E. *J. Am. Chem. Soc.* **1962**, *84*, 4720–4722.

33. (a) Dost, Z.; Atilgan, S.; Akkaya, E. U.; *Tetrahedron* **2006**, *62*, 8484–8488; (b) Yu, Y.-H.; Descalzo, A. B.; Shen, Z.; RLhr, H.; Liu, Q.; Wang, Y.-W.; Spieles, M.; Li, Y.-Z.; Rurack, K.; You, X.-Z. *Chem. Asian J.* **2006**, *1*, 176–187.

34. Lai, R. Y.; Bard, A. J. *J. Phys. Chem. B* **2003**, *107*, 5036–5042.

35. Sartin, M. M.; Camerel, F.; Ziessel R.; Bard, A. J. *J. Phys. Chem. C* **2008**, *112*, 10833–10841.

36. Waltman, R. J.; Bargon, J.; Diaz, A. F. *J. Phys. Chem.* **1983**, *87*, 1459–1463.

37. (a) Ricardo, D.; Lucia, B. S.; Angel, C.; Inmaculada, G. M.; Roberto, S.; Alberto, U. A. *Appl. Opt.* **2003**, *42*, 1029–1035; (b) Pavlopoulos, T. G.; Shah, M.; Boyer, J. H. *Opt. Commun.* **1989**, *70*, 425–427.

38. (a) O'Neil, M. P. *Opt. Lett.* **1993**, *18*, 37–38; (b) Pavlopoulos, T.; Boyer, J. H. *Proc. SPIE- Int. Soc. Opt. Eng.* **1994**, *2115*, 231–239.

39. (a) Wan, C.-W.; Burghart, A.; Chen, J.; BergstrLm, F.; Johansson, L. B.-A.; Wolford, M. F.; Kim, T. G.; Topp, M. R.; Hochstrasser, R. M.; Burgess, K. *Chem. Eur. J.* **2003**, *9*, 4430–4431; (b) Ziessel, R.; Goze, C.; Ulrich, G.; Ceìsario, M.; Retailleau, P.; Harriman, A.; Rostron, J. P. *Chem. Eur. J.* **2005**, *11*, 7366–7378.

40. Chen, J.; Burghart, A.; Derecskei-Kovacs, A.; Burgess, K. *J. Org. Chem.* **2000**, *65*, 2900–2906.

41. (a) Assor, Y.; Burshtein, Z.; Rosenwaks, S. *Appl. Opt.* **1998**, *37*, 4914-4920; (b) Ray, A. K.; Kundu, S.; Sasikumar, S.; Rao, C. S.; Mula, S.; Sinha, S.; Dasgupta, K. *Appl. Phys. B* **2007**, *87*, 483–488.

42. (a) Rahn, M. D.; King, T. A. *Appl. Opt.* **1995**, *34*, 8260–8271; (b) Jones, G. H.; Klueva, O.; Kumar, S.; Pacheco, D. *Solid State Lasers SPIE* **2001**, *24*, 4267–4271.

43. (a) Costela, A.; Garcia-Moreno, L.; Sastre, R. *Chem. Phys.* **2003**, *5*, 4745–4763; (b) Ray, A. K.; Kumar, S.; Mayekar, N. V.; Sinha, S.; Kundu, S.; Chattopadhyay, S.; Dasgupta, K. *Appl. Opt.* **2005**, *44*, 7814–7822; (c) Turro, N. J. *Modern Molecular Photochemistry*; University Science Books: CA, **1991**; p 588; (d) Arbeloa, F. L.; Prieto, J. B.; Arbeloa, I. L.; Costela, A.; Garcia-Moreno, I.; Gomez, C.; Amat-Guerri, F.; Liras, M.; Sastre, R. *Photochem. Photobiol.* **2003**, *78*, 30–36.

44. Qin, W.; Baruah, M.; Van der Auweraer, M.; De Schryver, F.; Bones, N. *J. Phys. Chem. A.* **2005**, *109*, 7371–7384.

45. Jiao, L.; Yu, C.; Uppal, T.; Liu, M.; Li, Y.; Zhou, Y.; Hao, E.; Hu, X.; Vicente, M. G. H., *Org. Biomol. Chem.* **2010**, *8*, 2517–2519.

46. (a) Ehrenschwender, T.; Wagenknecht, H. A. *J. Org. Chem.* **2011**, *76*, 2301–2304; (b) Gießler, K.; Griesser, H.; Göhringer, D.; Sabirov, T.; Richert, C. *Eur. J. Org. Chem.* **2010**, *19*, 3611–3620; (c) Kálai, T.; Hideg, K., *Tetrahedron* **2006**, *62*, 10352–10360.

47. Namkung, W.; Padmawar, P.; Mills, A. D.; Verkman, A. S. *J. Am. Chem. Soc*. **2008**, *130*, 7794–7795.

48. (a) Byrne, A. T.; O'Connor, A. E.; Hall, M.; Murtagh, J.; O'Neill, K.; Curran, K. M.; Mongrain, K.; Rousseau, J. A.; Lecomte, R.; McGee, S.; Callanan, J. J.; O'Shea, D. F.; Gallagher, W. M. *British journal of cancer* **2009**, *101*, 1565–1573; (b) He, H.; Lo, P.-C.; Yeung, S.-L.; Fong, W.-P.; Ng, D. K. P. *J. Med. Chem.* **2011**, *54*, 3097–3102; (c) Gorman, A.; Killoran, J.; O'Shea, C.; Kenna, T.; Gallagher, W. M.; O'Shea, D. F. *J. Am. Chem. Soc*. **2004**, *126*, 10619–10631; (d) Niu, S. L.; Massif, C.; Ulrich, G.; Ziessel, R.; Renard, P. Y.; Romieu, A. *Org. Biomol. Chem.* **2011**, *9*, 66–69.

49. Awuah, S. G.; You Y. *RSC Advances* **2012**, *2*, 11169–11183.

50. (a) Chandra, A. K.; Turro, N. J.; Lyons A. L.; Stone, P. *J. Am. Chem. Soc*. **1978**, *100*, 4964–4968; (b) Koziar, J. C.; Cowan, D. O. *Acc. Chem. Res*. **1978**, *11*, 334–341; (c) Mcglynn, S. P.; Sunseri, R.; Christod, N. *J. Chem. Phys*. **1962**, *37*, 1818–1824; (d) Mcglynn, S. P.; Daigre, G. W.; Christodoyleas, N.; Reynolds, M. J. *J. Phys. Chem*. **1962**, *66*, 2499–2505.

51. (a) Yuster, P.; Weissman, S. I. *J. Chem. Phys.* **1949**, *17*, 1182–1188; (b) Mcclure, D. S. *J. Chem. Phys*. **1949**, *17*, 665–666; (c) Mcclure, D. S. *J. Chem. Phys*. **1949**, 17, 905–913.

52. Atilgan, S.; Ekmekci, Z.; Dogan, A. L.; Guc, D.; Akkaya, E. U. *Chem. Commun*. **2006**, 4398–4400.

53. (a) Rousseau, T.; Cravino, A.; Bura, T.; Ulrich, G.; Ziessel, R.; Roncali, J. *Chem. Commun.* **2009**, 1673–1675; (b) Rousseau, T.; Cravino, A.; Bura, T.; Ulrich, G.; Ziessel, R.; Roncali, J. *J. Mater. Chem.* **2009**, *19*, 2298–2300; (c) Rousseau, T.; Cravino, A.; Ripaud, E.; Leriche, P.; Rihn, S.; De Nicola, A.; Ziessel, R.; Roncali, J.

Chem. Commun. **2010**, 5082–5084; (d) Roncali, J. *Acc. Chem. Res.* **2009**, *42*, 1719–1730.

54. Kim B.; Ma, B.; Donuru, V. R.; Liu, H.; Fréchet, J. M. *Chem Commun*. **2010**, *46*, 4148–4150.

55. Popere, B. C.; Della Pelle, A. M.; Thayumanavan, S. *Macromolecules* **2011**, *44*, 4767–4776.

56. (a) Jones II, G.; Kumar, S.; Klueva, O.; Pacheco, D. *J. Phys. Chem. A* **2003**, *107*, 8429–8434; (b) Jagtap, K. K.; Maity, D. K.; Ray, A. K.; Dasgupta, K.; Ghosh, S. K. *Appl Phys B* **2011**, *103*, 917–924.

57. (a) Ulrich, G.; Goeb, S.; Nicola, A. De; Retailleau, P.; Ziessel, R. *Synlett* **2007**, 1517–1520; (B) Bonardi, L.; Ulrich, G.; Ziessel, R. *Org. Lett*. **2008**, *10*, 2183–2186.

58. Mula, S.; Ulrich, G.; Ziessel, R. *Tetetrahedron Lett*. **2009**, *50*, 6383–6388.

59. (a) Kee, H. L.; Kirmaier, C.; Yu, L.; Thamyongkit, P.; Youngblood, W. J.; Calder, M. E.; Ramos, L.; Noll, B. C.; Bocian, D. F.; Scheidt, W. R.; Birge, R. R.; Lindsey, J. S.; Holten, D. *J. Phys. Chem. B* **2005**, *109*, 20433–20443; (b) Chaudhuri, T. Mula, S.; Chattopadhyay, S.; Banerjee, M. *Spectrochimica Acta A* **2010**, *75*, 739–744.

60. (a) Susdorf, T.; Alvarez, M.; Holzer, W.; Penzkofer, A.; Amat-Guerri, F.; Liras, M.; Costela, A.; Garcia-Moreno, I.; Sastre, R. *Chem. Phys*. **2005**, *312*, 151–158; (b) Susdorf, T.; Del Agua, D.; Tyagi, A.; Penzkofer, A.; Garcia, O.; Sastre, R.; Costela, A.; Garcia-Moreno, I. *Appl. Phys. B* **2007**, *86*, 537–545; (c) Tyagi, A.; Del Agua, D.; Penzkofer, A.; Garcia, O.; Sastre, R.; Costela, A.; Garcia-Moreno, I. *Chem. Phys*. **2007**, *342*, 201–214.

61. Mula, S.; Elliott, K.; Harriman, A.; Ziessel, R. *J. Phys. Chem. A* **2010**, *114*, 10515–10522.

62. (a) Kim, H.; Burghart, A.; Welch, M.B.; Reibenspies, J.; Burgess, K. *Chem. Commun.* **1999**, *18*, 1889–1890; (b) Chen, J.; Reibenspies, J.; Derecskei-Kovacs, A.; Burgess, K. *Chem. Commun.* **1999**, *24*, 2501–2502.

63. (a) Rurack, K.; Kollmannsberger, M.; Daub, J. *Angew. Chem. Int. Ed.* **2001**, *40*, 385–387; (b) Zhao, W.; Carreira, E.M. *Angew. Chem. Int. Ed.* **2005**, *44*, 1677–1679.

64. Shrout, D. P.; Lightner, D. A. *Synthesis* **1990**, 1062–1065.

65. (a) Guha, S. N.; Moorthy, P. N.; Kishore, K.; Naik, D. B.; Rao, K. N. *Proc. Indian Acad. Sci. (Chem. Sci.)* **1987**, *99*, 261–271; (b) Buxton, G. V.; Stuart, C. R. *J. Chem. Soc. Faraday Trans*. **1995**, *91*, 279–281.

66. Schmidt, M. W.; Baldridge, K. K.; Boatz, J. A.; Elbert, S. T.; Gordon, M. S.; Jensen, J. H.; Koseki, S.; Matsunaga, N.; Nguyen, K. A.; Su, S. J.; Windus, T. L.; Dupuis, M.; Montgomery, J. A. *J. Comput. Chem*. **1993**, *14*, 1347–1363.

67. (a) Ziessel, R.; Ulrich, G.; Harriman, A. *New J. Chem.* **2007**, *31*, 496–501; (b) Ulrich, G.; Ziessel, R.; Harriman, A. *Angew. Chem. Int. Ed.* **2008**, *47*, 1184–1201; (c) Erten-Ela, S.; Yilmaz, D.; Icli, B.; Dede, Y.; Icli, S.; Akkaya, E. U. *Org. Lett.* **2008**, *10*, 3299–3302; (d) Oleynik, P.; Ishihara, Y.; Cosa, G. *J. Am. Chem. Soc*. **2007**, *129*, 1842–1843; (e) Kumaresan, D.; Thummel, R. P.; Bura, T.; Ulrich, G.; Ziessel, R. *Chem. Eur. J.* **2009**, *15*, 6335–6339.

68. (a) Rohand, T.; Qin, W.; Boens, N.; Dehaen, W. *Eur. J. Org. Chem.* **2006**, 4658–4663; (b) Han, J. Y.; Gonzales, O.; Aguilar-Aguilar, A.; Pena-Cabrera, E.; Burgess, K. *Org. Biomol. Chem.* **2009**, *7*, 34–36.

69. Kim, T.-I.; Park, S.; Choi, Y.; Kim, Y. *Chem. Asian J*. **2011**, *6*, 1358–1361.

70. Peña-Cabrera, E.; Aguilar-Aguilar, A.; González-Domínguez, M.; Lager, E.; Zamudio-Vázquez, R.; Villanueva-García, F. *Org. Lett.* **2007**, *9*, 3985–3988.

71. (a) Lee, H. Y.; Bae, B. R.; Park, J. C.; Song, H.; Han, W. S.; Jung, J. H. *Angew. Chem. Int. Ed.* **2009**, *48*, 1239–1243; (b) Guliyev, R.; Coskun, A.; Akkaya, E. U. *J. Am. Chem. Soc.* **2009**, *131*, 9007–9013; (c) Yuan, M.; Zhou, W.; Liu, X.; Zhu, M.; Li, J.; Yin, X.; Zheng, H.; Zuo, Z.; Ouyang, C.; Liu, H.; Li, Y.; Zhu, D. *J. Org. Chem.* **2008**, *73*, 5008–5014; (d) Liu, J.-Y.; Ermilov, E. A.; Roder, B. *Chem. Commun.* **2009**, 1517–1519.

72. Bura, T.; Retailleau, P.; Ulrich, G.; Ziessel, R. *J. Org. Chem.* **2011**, *76*, 1109–1117.

73. Arbeloa, F. L.; Banuelos, J.; Martinez, V.; Arbeloa, T.; Arbeloa, I. L. *Int. Rev. Phys. Chem.* **2005**, *24*, 339–374.

74. (a) Shivran, N.; Mula, S.; Ghanty, T. K.; Chattopadhyay, S. *Org. Lett.*, **2011**, *13*, 5870–5873; (b) Costela, A.; García-Moreno, I.; Pintado-Sierra, M.; Amat-Guerri, F.; Sastre, R.; Liras, M.; Arbeloa, F. L.; Prieto, J. B.; Arbeloa, I. L. *J. Phys. Chem. A* **2009**, *113*, 8118–8124.

75. Prieto, J, B.; Arbeloa, F. L.; Martínez, V. M.; López, T. A.; Arbeloa, I. L. *J. Phys. Chem. A* **2004**, *108*, 5503–5508.

76. Costela, A.; García-Moreno, I.; Pintado-Sierra, M.; Amat-Guerri, F.; Lirasc, M.; Sastre, R.; Arbeloae, F. L.; Prietoe, J. B.; Arbeloae, I. L. *J. Photochem. Photobiol. A: Chem.* **2008**, *198*, 192–199.

77. Third International Symposium on Functional Dyes (Cowan, D. O. Eds.). *Pure Appl. Chem*. **1996**, *68*, 1355-1478.

78. (a) Wohrle, D.; Meissner, D. *Adv. Muter.* **1991**, *3*, 129-138; (b) Law, K.-Y. *Chem. Rev.* **1993**. *93*, 449-486; (c) Krasowitskii, B. M. *Organic Luminescent Materials*, VCH, Weinheim; 1988.

79. Vos de Wal, E.; Pardoen, J. A.; van Knoeveringe, J. A.; Lugtenburg, J. *Red. Trav. Chim. Pqyi-Bus* **1977**, *96*. 306-309; (b) Karolin, J.; Johansson, L. B.-A.; Strandberg,

L; Ny, T. *J. Am. Chem. Soc.* **1994**, *l6,*7801-7806; (c) Wagner, R. W.; Lindsey, J. *J. Am. Chem. Soc.* **1996**, *118,* 3996-3997.

80. (a) Boens, N.; Leen, V.; Dehaen, W. *Chem. Soc. Rev*. **2012**, *41*, 1130–1172; (b) Olivier, J.-H.; Barbera, J.; Bahaidarah, E.; Harriman, A.; Ziessel, R. *J. Am. Chem. Soc*. **2012**, *134*, 6100–6103.

81. (a) Kelloff, G. J.; Krohn, K. A.; Larson, S. M.; Weissleder, R.; Mankoff, D. A.; Hoffman, J. M.; Link, J. M.; Guyton, K. Z.; Eckelman, W. C.; Scher, H. I.; O'Shaughnessy, J.; Cheson, B. D.; Sigman, C. C.; Tatum, J. L.; Mills, G. Q.; Sullivan, D. C.;Woodcock, J. *Clin. Cancer Res*. **2005**, *11*, 7967–7985; (b) He, X.; Wang, K.; Cheng, Z. *Nanomed. Nanobiotechnol*. **2010**, *2*, 349–366; (c) Rao, J.; Dragulescu-Andrasi, A.; Yao, H. *Curr. Opin. Biotechnol*. **2007**, *18*, 17–25.

82. (a) Bonnet, R. Chemical Aspects of Photodynamic Therapy; Gordon and Breach Science: Amsterdam, 2000; (b) Dougherty, T. J. *J. Clin. Laser Med. Surg*. **2002**, *20*, 3–7; (c) Dolmans, D. E.; Fukumura, D.; Jain, R. K. *Nat. Rev. Cancer* **2003**, *3*, 380–387; (d) Juzeniene, A.; Peng, Q.; Moan, J. *Photochem. Photobiol. Sci*. **2007**, *6*, 1234–1245; (e) MacCormack, M. A. *Semin. Cutaneous Med. Surg*. **2008**, *27*, 52–62.

83. (a) Kossodo, S.; LaMuraglia, G. M. *Am. J. Cardiovasc. Drugs* **2001**, *1*, 15–21; (b) Jori G. *J. Environ. Pathol. Toxicol. Oncol*. **2006**, *25*, 505–519; (c) Tandon, Y. K.; Yang, M. F.; Baron, E. D. *Photodermatol. Photoimmunol. Photomed*. **2008**, *24*, 222–230; (c) Cruess, A. F.; Zlateva, G.; Pleil, A. M.; Wirostko, B. *Acta Ophthalmol*. **2009**, *87*, 118–132; (d) Babilas, P.; Schreml, S.; Landthaler, M.; Szeimies, R. M. *Photodermatol, Photoimmunol. Photomed*. **2010**, *26*, 118–132; (e) Garrier, J.; Bezdetnaya, L.; Barlier, C.; Grafe, S.; Guillemin, F.; D'Hallewin, M. A. *Photodiagn. Photodyn. Ther*. **2011**, *8*, 321–327.

84. (a) Capella, M. A. M.; Capella, L. S. J. *J. Biomed. Sci*. **2003**, *10*, 361–366; (b) Brown, S. B.; Brown, E. A.; Walker, I. *Lancet Oncol*. **2004**, *5*, 497–508; (c) Allison, R. R.; Downie, G. H.; Cuenca, R.; Hu, X. H.; Childs, C. J.; Sibata, C. H. *Photodiagnosis Photodyn. Ther*. **2004**, *1*, 27–42; (d) Sharman, W. M.; van Lier, J. E.; Allen, C. M. *Adv. Drug Deliv. Rev*. **2004**, *56*, 53–76; (e) Hasan, T.; Ortel, B.; Solban, N.; Pogue, B. W. Photodynamic therapy of cancer. In: (Kufe, D.; Bast, R.; Hait, W.; Hong, W. K.; Pollock, R. E.; Weichselbaurm, R. R. *et al*., Eds.) Cancer Medicine, 7th ed. Hamilton, Ontario, Canada: BC Decker, Inc.; 2006. p. 537–48.

85. (a) Bonnet, R.; Martinez, G. *Tetrahedron* **2001**, *57*, 9513–9547; (b) O'Connor, A. E.; Gallagher, W. M.; Byrne, A. T. *Photochem. Photobiol*. **2009**; *85*, 1053–1074.

86. (a) Pang, W.; Zhang, X.-F.; Zhou, J.; Yu, C.; Haoa, E.; Jiao, L. *Chem. Commun*. **2012**, *48*, 4956–4958.; (b) Erbas, S.; Gorgulu, A.; Kocakusakogullaric, M.; Akkaya, E. U. *Chem. Commun*. **2009**, 4956–4958.

87. (a) Kamkaew, A.; Lim, S. H.; Lee, H. B.; Kiew, L. V.; Chung, L. Y.; Burgess K. *Chem. Soc. Rev*. **2013**, *42*, 77–88; (b) Awuah, S. G.; You, Y. *RSC Adv*. **2012**, *2*, 11169–11183.

88. Adams, K. E.; Ke, S.; Kwon, S.; Liang, F.; Fan, Z.; Hirschi, K.; Mawad, M. E.; Barry, M. A.; Sevick-Muraca, E. M. *J. Biomed. Opt*. **2007**, *12*, 024017–024018; (b) Luo, S.; Zhang, E.; Su, Y.; Cheng, T.; Shi, C. *Biomaterials* **2011**, *32*, 7127–7138.

89. (a) Coskun, A.; Deniz, E.; Akkaya, E. U. *Org. Lett*. **2005**, *7*, 5187–5189; (b) Rurack, K.; Kollmannsberger, M.; Daub, J. *Angew. Chem., Int. Ed*. **2001**, *40*, 385–387; (c) Coskun, A.; Akkaya, E. U. *Tetrahedron Lett*. **2004**, *45*, 4947–4949.

90. (a) Dye, D.; Watkins, J. *Br. Med. J*. **1980**, *280*, 1353–1353; (b) Michaud, L. B. *Ann. Pharmacother*. **1997**, *31*, 1402–1404.

91. (a) Sengee, G.-I.; Badraa, N.; Lee, W.-k.; Shim, Y. K. *Bull. Korean Chem. Soc*. **2008**, 29, 2505–2508; (b) He, H.; Lo, P.-C.; Yeung, S.-L.; Fong, W.-P.; Ng, D. K. P. *Chem. Commun*. **2011**, *47* 4748–4750.

92. (a) Hamblin, M. R.; Miller, J. L.; Rizvi, I.; Ortel, B.; Maytin, E. V.; Hasan, T. *Cancer Res*. **2002**, *61*, 7155–7162; (b) Sahoo, S. K.; Sawa, T.; Fang, J.; Tanaka, S.; Miyamoto, Y.; Akaike, T.; Maeda, H. *Bioconj. Chem*. **2002**, *13*, 1031–1038.

93. (a) Leffler, H.; Carlsson, S.; Hedlund, M.; Qian, Y.; Poirier, F. *Glycoconj. J*. **2004**, *19*, 433–440; (b) van Scherpenzeel, M.; Moret, E. E.; Ballell, L.; Liskamp, R. M. J.; Nilsson, U. J.; Leffler, H.; Pieters, R. J. *ChemBioChem* **2009**, *10*, 1724–1733.

94. (a) Yang, Q.; Hu, M. X.; Dai, Z. W.; Tian, J.; Xu, Z. K. *Langmuir* **2006**, *22*, 9345–9349; (b) Lee, Y. C.; Townsend, R. R.; Hardy, M. R.; Lonngren, J.; Arnarp, J.; Haraldsson, M.; Lonn, H. *J. Biol. Chem*. 1983, *258*, 199–202; (c) Lee, Y. C. *FASEB J*. **1992**, *6*, 3193–3200.

95. (a) Six, L.; Rueβ, K. -P.; Liefänder, M. *Tetrahedron Lett*. **1983**, *24*, 1229–1232; (b) Zemplën, G.; Gerecs, A.; Hadäcsy, I. *Ber*. **1936**, *69B*, 1827–1829; (c) Redemann, C., E.; Niemann, C. *Org. Synth.* **1942**, *22*, 314–319; (d) Maillard, P.; Guerquin-Kern, J. L.; Huel, C.; Momenteau, M. *J. Org. Chem.* **1993**, *58*, 2774–2780. (e) Casy, A. F. PMR Spectroscopy in Medicinal and Biological Chemistry, Academic Press, London, 1971, pp. 330–384.

96. Rettig, W. *Angew. Chem.* **1986**, *98*, 969–986.

97. (a) Landfester, K.; Montenegro, R.; Scherf, U.; Güntner, R.; Asawapirom, U.; Patil, S.; Neher, D.; Kietzke, T. *Adv. Mater*. **2002**, *14*, 651–655; (b) Elemans, J. A. A.; van Hameren, R.; Nolte, R. J. M.; Rowan, A. E. *Adv. Mater*. **2006**, *18*, 1251–1266; (c) Kaeser, A.; Schenning, A. P. H. J. *Adv. Mater*. **2010**, *22*, 2985–2997; (d) Liong, M.; Angelos, S.; Choi, E.; Patel, K.; Stoddart, J. F.; Zink, J. I. *J. Mater. Chem*. **2009**, *19*,

6251–6257; (e) Mulder, W. J. M.; Strijkers, G. J.; van Tilborg, G. A. F.; Cormode, D. P.; Fayad, Z. A.; Nicolay, K. *Acc. Chem. Res*. **2009**, *42*, 904–914.

98. (a) Lei, Y.; Liao, Q.; Fu, H.; Yao, J. *J. Am. Chem. Soc*. **2010**, *132*, 1742–1743; (b) Vijayakumar, C.; Sugiyasu, K.; Takeuchi, M. *Chem. Sci*. **2011**, *2*, 291–294.

99. Bao, C.; Lu, R.; Jin, M.; Xue, P.; Tan, C.; Zhao, Y.; Liu, G. *Carbohydr. Res*. **2004**, *339*, 1311–1316.

100. Friggeri, A.; Gronwald, O.; van Bommel, K. J. C.; Shinkai, S.; Reinhoudt, D. N. *J. Am. Chem. Soc.* **2002**, *124*, 10754–10758; (b) Gronwald, O.; Sakurai, K.; Luboradzki, R.; Kimura, T.; Shinkai, S. *Carbohydr. Res*. **2001**, *331*, 307–318; (c) Jung, J. H.; Amaike, M.; Nakashima, K.; Shinkai, S. *J. Chem. Soc., Perkin Trans. 2* **2001**, 1938–1943; (d) Kobayashi, H.; Friggeri, A.; Koumoto, K.; Amaike, M.; Shinkai, S.; Reinhoudt, D. N. *Org. Lett*. **2002**, *4*, 1423–1426; (e) Yoza, K.; Amanokura, N.; Ono, Y.; Akao, T.; Shinmori, H.; Takeuchi, M.; Shinkai, S.; Reinboudt, D. N. *Chem. Eur. J*. **1999**, *5*, 2722–2729.

101. Bergstrom, F.; Mikhalyov, I.; Hagglof, P.; Wortmann, R.; Ny, T.; Johansson, L. B.-A. *J. Am. Chem. Soc.* **2002**, *124*, 196–204.

102. Tleugabulova, D.; Zhang, Z.; Brennan, J. D. *J. Phys. Chem. B* **2002,** *106*, 13133–13138.

103. (a) Wang, R.; Geiger, C.; Chen, L.; Swanson, B.; Whitten, D. G. *J. Am. Chem. Soc*. **2000**, *122*, 2399–2400; (b) Gieger, C.; Stanescu, M.; Chen, L.; Whitten, D. G. *Langmuir* **1999**, *15*, 2241–2245.

104. Olivier, J.-H.; Widmaier, J.; Ziessel, R. *Chem. Eur. J*. **2011**, *17*, 11709–11714.

105. McGhee, J. D.; von Hippel, P. H. *J. Mol. Biol*. **1974**, *86*, 469–489.

106. Wilson, W. D.; Gough, A. N.; Doyle, J. J. *J. Med. Chem*. **1976**, *19*, 1261–1263.

107. Jemal, A.; Clegg, L. X.; Ward E. Ries, L. A.; Wu, X.; Jamison, P. M.; Wingo, P. A.; Howe, H. L.; Anderson, R. N.; Edwards, B. K. *Cancer* **2004**, *101*, 3–27; (b) Kamangar, F.; Dores, G. M.; Anderson, W. F. *J. Clin. Oncol*. **2006**, *24*, 2137–2150.

108. Ding, X.; Xu, Q.; Liu, F.; Zhou, P.; Gu, Y.; Zeng, J.; An, J.; Dai, W.; Li, X. *Cancer Lett*. **2004**, *216*, 43–54; (b) Kato, H.; Usuda, J.; Okunaka, T.; Furukawa, K.; Honda, H.; Sakaniwa, N.; Suga, Y.; Hirata, T.; Ohtani, K.; Inoue, T.; Maehara, S.; Kubota, M.; Yamada, K.; Tsuitsui, H. *Lasers Surg. Med*. **2006**, *38*, 371–375.

109. Lam S. *Semin Oncol*. **1994**, *21(6 Suppl 15)*, 15–19.

110. Buytaert, E.; Callewaert, G.; Hendrickx, N.; Scorrano, L.; Hartmann, D.; Missiaen, L.; Vandenheede, J. R.; Heirman, I.; Grooten, J.; Agostinis, P. *FASEB J*. **2006**, *20*, 756–758; (b) Pogue, B. W.; Ortel, B.; Chen, N.; Redmond, R. W.; Hasan, T. *Cancer Res*. **2001**, *61*, 717–724.

111. (a) Nagata, S. *Cell* **1997**, *88*:355–365; Ashkenazi, A.; Dixit, V. M. *Science* **1998**, *281*, 1305–1308; (c) Decker, P.; Isenberg, D.; Muller, S. *J. Biol. Chem*. **2000**, *275*, 9043–9043.

112. (a) Evan, G. I.; Vousden, K. H. *Nature* **2001**, *411*, 342–343; (b) Arends, M. J.; Wyllie, A. H. *Int. Rev. Exp. Pathol*. **1991**, *32*, 223–254; (c) Hickman, J. A. *Eur. J. Cancer* **1996**, *32*, 921–926; (d) Agarwal, M. L.; Clay, M. E.; Harvey, E. J.; Evans, H. H.; Antunez, A. R.; Oleinick, N. L. *Cancer Res*. **1991**, *51*, 5993–5996.

113. (a) Oleinick, N. L.; Morris, R. L.; Belichenko, I. *Photochem. Photobiol. Sci.* **2002**, *1*, 1–21; (b) Gryshuk, A. L.; Chen, Y.; Potter, W.; Ohulchansky, T.; Oseroff, A.; Pandey, R. K. *J. Med. Chem*. **2006**, *49*, 1874–1881.

114. (a) Liu, X.; Kim, C. N.; Yang, J.; Jemmerson, R.; Wang, X. *Cell* **1996**, *86*, 147–157; (b) Luo, K. Q.; Yu, V. C.; Pu, Y.; Chang, D. C. *Biochem. Biophys. Res. Commun*.

2001; *283*, 1054–1060; (c) Ferri, K. F.; Kroemer, G. *Nature Cell Biol*. **2001**, *3*, 255–263.

115. (a) Hsieh, Y.J.; Wu, C.C.; Chang, C.J.; Yu, J.S. *J. Cell. Physiol.* **2003**, *194*, 363–375; (b) Kessel, D. *Photochem. Photobiol. Sci.* **2002**, *1*, 837–840; (c) Marchal, S.; Francois, A.; Dumas, D.; Guillemin, F.; Bezdetnaya, L. *Br. J. Cancer* **2007**, *96*, 944–951.

116. (a) Mahitosh, M.; Liana, M.; Rakesh, K. *Biochem. Biophys. Res. Commun*. **1999**, *260*, 775–780; (b) Kiwamu, T.; Takeharu, N.; Atsushi, M.; Masayuki, M. *J. Cell Biol*. **2003**, *160*, 235–243.

117. (a) Bellnier, D. A.; Ho, Y. K.; Pandey, R. K. *J. Photochem. Photobiol*. **1989**, *50*, 221–228; (b) Castano, A. P.; Demidova, T. N.; Hamblin, M. R. *Photodiag. Photodyn. Ther*. **2004**, *1*, 279–293; (c) Kostenich, G. A.; Zhuravkin, I. N.; Zhavrid, E. A. *J. Photochem. Photobiol. B: Biol*. **1994**, *22*, 211–217; (d) Castano, A. P.; Demidova, T. N.; Hamblin, M. R. *Photodiag. Photodyn. Ther*. **2005**, *2*, 91–106.

118. Gabe, Y.; Urano, Y.; Kikuchi, K.; Kojima, H.; Nagano, T. *J. Am. Chem. Soc*. **2004**, *126*, 3357-3367.

119. Mosmann, T. *J. Immunol. Meth*. 1983, *65*, 55–63.

120. (a) International Technology Roadmap for Semiconductors (IRTS), 2007 http://www.itrs.net/reports.html; (b) Sze, S. M. Semiconductor Devices: Physics and Technology, John Wiley & Sons, New York, 2002.

121. Vuillaume, D. C. R. *Phys*. **2008**, *9*, 78–94.

122. (a) Ulman, A. An introduction to ultrathin organic flms: From Langmuir-Blodgett to self-assembly, Academic Press, Boston, 1991; (b) Schreiber, F. *Prog. Surf. Sci.* **2000**, *65*, 151–256; (c) Joachim, C.; Gimzewski, J. K.; Aviram, A. *Nature* **2000**, *408*, 541–548.

123. (a) Mann, B.; Kuhn, H. *J. Appl. Phys*. **1971**, *42*, 4398–4405; (b) Lenfant, S.; Krzeminski, C.; Delerue, C.; Allan, G.; Vuillaume, D. *Nano Lett*. **2003**, *3*, 741–746; (c) Rakshit, T.; Liang, G.-C.; Ghosh, A.W.; Datta, S. *Nano Lett.* **2004**, *4*, 1803–1807.

124. (a) Salomon, A.; Cahen, D.; Lindsay, S. M.; Tomfohr, J.; Engelkes, V. B.; Frisbie, C. D. *Adv. Mater*. **2003**, *15*, 1881–1890; (b) Aswal, D. K.; Lenfant, S.; Guerini, D.; Yakhmi, J. V.; Vuillaume, D. *Anal. Chim. Acta* **2006**, *568*, 84–108 ; (c) Vuillaume, D.; Lenfant, S.; Guerini, D.; Delerue, C.; Petit, C.; Salace, G. *Pramana J. Phys.* **2006**, *1*, 17–32.

125. (a) Chen, J.; Reed, M. A.; Rawlett, A. M.; Tour, J. M. *Science* 1999, *286*, 1550–1552; (b) Chen, J.; Wang, W.; Reed, M. A.; Rawlett, A. M.D.; Price, W.; Tour, J. M. *Appl. Phys. Lett*. **2000**, *77*, 1224–1226; (c) Mirkin, C.A.; Ratner, M.A. *Annu. Rev. Phys. Chem.***1992**, *43*, 719–754; (d) Liu, Z.; Yasseri, A. A.; Lindsey, J. S.; Bocian, D. F. *Science* **2003**, *302*, 1543–1545; (e) Seabaugh, C.; Kuo, Y.C.; Yuan, H.T. *IEEE Electron Dev. Lett*. **1992**, *13*, 479–481; (f) Chow, D. H.; Dunlap, H. L.; Williamson III, W.; Enquist, S.; Gilbert, B. K.; Subramaniam, S.; Lei, P.-M.; Bernstein, G. H. *IEEE Electron Dev. Lett*. **1996**, *17*, 69–71; (g) Donhauser, Z. J.; Mantooth, B. A.; Kelly, K. F.; Bumm, L. A.; Monnell, J. D.; Stapleton, J. J.; Price, D. W.; Rawlett, A. M.; Allara, D. L.; Tour, J. M.; Weiss, P. S. *Science* **2001**, *292*, 2303–2307; (h) Inokawa, H.; Fujiwara, A.; Takahashi, Y. *Appl. Phys. Lett*. **2001**,*79*, 3618–3620.

126. (a) Chen, J.; Reed, M. A.; Rawlett, A. M.; Tour, J. M. *Science* **1999**, *286*, 1550–1552; (b) Chen, J.; Wang, W.; Reed, M. A.; Rawlett, A. M.; Price, D. W.; Tour, J. M. *Appl. Phys. Lett*. **2000**, *77*, 1224–1226; (c) Donhauser, Z. J.; Mantooth, B. A.; Kelly, K. F.; Bumm, L. A.; Monnell, J. D.; Stapleton, J. J.; Price, D. W.; Rawlett, A. M.; Allara, D. L.; Tour, J. M.; Weiss, P. S. *Science* **2001**, *292*, 2303–2307; (d)

Pitters, J. L.; Wolkow, R. A. *Nano Lett*. **2006**, *6*, 390–397; (e) Guisinger, N. P.; Greene, M. E.; Basu, R.; Baluch, A. S.; Hersam, M. C. *Nano Lett.* **2004**, *4*, 55–59; (f) Selzer, Y.; Salomom, A.; Ghabboun, J.; Cahen, D. *Angew. Chem. Int. Ed.* **2002**, *41*, 827–830; (g) Salomon, A.; Arad-Yellin, R.; Shanzer, A.; Karton, A.; Cahen, D. *J. Am. Chem. Soc.* **2004**, *126*, 11648–11657.

127. (a) Lyo, I. -W.; Avouris, Ph. *Science* **1989**, *245*, 1369–1371; (b) Bedrossian, P.; Chen, D. M.; Mortensen, K.; Golovchenko, J. A. *Nature* **1989**, *342*, 258–260; (c) Seminario, J. M.; Zacarias, A. G.; Tour, J. M. *J. Am. Chem. Soc.* **2000**, *122*, 3015–3020; (d) Emberly, E. G.; Kirczenow, G. *Phys. Rev. B* **2001**, *64*, 125318 pp.1-5; (e) Karzazi, Y.; Cornil, J.; Bre´das, J. L. *J. Am. Chem. Soc.* **2001**, *123*, 10076–10084; (f) Karzazi, Y.; Cornil, J.; Bre´das, J. L. *Nanotechnology* **2003**, *14*, 165–171.

128. Galperin, M; Ratner, M.A.; Nitzan, A. *Nano Lett.* **2005**, *5*, 125–130.

129. (a) Martiny, A.; Sambles, J. R. *Nanotech.* **1996**, *7*, 401–405; (b) Brady, A. C.; Hodder, B.; Martin, A. S.; Sambles, J. R.; Ewels, C. P.; Jones, R.; Briddon, P. R.; Musa, A. M.; Panetta, C. A.; Mattern, D. L. *J. Mater. Chem*. **1999**, *9*, 2271–2275; (c) Chen, J.; Wang, W.; Reed, M. A.; Rawlett, A. M.; Price, D. W.; Tour, J. M. *Appl. Phys. Lett*. **2000**, *77*, 1224–1226; (d) Lenfant, S.; Krzeminski, C.; Delerue, C.; Allan, G.; Vuillaume, D. *Nano Lett*. **2003**, *3*, 741–746.

130. (a) Lai, R. Y.; Bard, A. J.; *J. Phys. Chem. B*, **2003**, *107*, 5036–5042; (b) Nepomnyashchii, A. B.; Bröring, M.; Ahrens, J.; Krüger, R.; Bard, A. J. *J. Phys. Chem. C* **2010**, *114*, 14453–14460.

131. (a) Newton, M. D. *Chem. Rev.* **1991**, *91*, 767–792; (b) Salomon, A.; Yellin, R. A.; Shanzer, A.; Karton, A.; Cahen, D. *J. Am. Chem*. Soc. **2004**, *126*, 11648–11657.

132. Buriak, J. M. *Chem. Rev.* **2002**, *102*, 1271–1308.

133. (a) Tulevski, G. S.; Myers, M. B.; Hybertsen, M. S.; Steigerwald, M. L.; Nuckolls, C. *Science* **2005**, *309*, 591–594; (b) Toher, C.; Sanvito, S. *Phys. Rev. Lett*. **2007**, *99*, 056801-1–056801-4; (c) Chen, J.; Wang, W.; Reed, M. A.; Rawlett, A. M.; Price, D. W.; Tour, J. M. *Appl. Phys. Lett*. **2000**, *77*, 1224–1226; (d) Aswal, D. K.; Koiry, S. P.; Jousseleme, B.; Palacin, S.; Yakhmi, J. V. *Physica E* **2009**, *41*, 325–344.

134. (a) Brett, C. M. A.; Brett, A. M. O. Electrochemistry: Principles, methods and applications, Oxford University Press, Oxford, Great Britain, **1994**; (b) Bagolsky, V.S. Fundamentals of Electrochemistry, Wiley Interscience, New Jersey, **2006**.

135. Bonardi, L.; Kanaan, H.; Camerel, F.; Jolinat, P.; Retailleau, P.; Ziessel R. *Adv. Funct. Mater.* **2008**, *18*, 401–413.

136. Koiry, S. P.; Aswal, D. K.; Chauhan, A. K.; Saxena, V.; Nayak, S. K.; Gupta, S. K.; Yakhmi, J. V. *Chem. Phys. Lett.* **2008**, *453*, 68–72.

137. (a) Carter, F. L.; Siatkowski, R. E.; Wohltjen, H. (Eds.) Molecular Electronic Devices: Proc. 3rd Int. Symp. on Molecular Electronic Devices, North-Holland, New York, **1989**; (b) Kluth, G. J.; Sung, M. M.; Maboudian, R. *Langmuir* **1997**, *13*, 3775–3780; (c) Lenfant, S. Ph. D. Thesis, Organic self-assembled monolayers for molecular diodes, 2001. *University of Science and Technology, Lille, France.*

138. Wei Xia, Britt A. Minch, Michael D. Carducci; Neal R. Armstrong, *Langmuir* **2004**, **20**, 7998–8005.

139. Metzger, R. M.; Baldwin, J. W.; Shumate, W. J.; Peterson, I. R.; Mani, P.; Mankey, G. J.; Morris, T.; Szulczewski, G.; Bosi, S. ; Prato, M.; Comito, A.; Rubin, Y. *J. Phys. Chem. B* **2003**, *107*, 1021–1027.

140. (a) Schmidt, W.; Baldridge, K. K.; Boatz, J. A.; Elbert, S. T.; Gordon, M. S.; Jensen, J. H.; Koseki, S.; Matsunaga, N.; Nguyen, K. A.; Su, J. S. ; Windus, T. L.; Dupuis, M.; Montgomery, J. A. *J. Comput. Chem.* **1993**, *14*, 1347–1363; (b) Francl, M. M.;

Petro, W. J.; Hehre, W. J.; Binkley, J. S.; Gordon, M. S.; DeFrees, D. J.; Pople, J. A. *J. Chem. Phys.* **1982**, *77*, 3654–3665; (c) Hariharan, P. C.; Pople, J. A. *Theor. Chim. Acta.* **1973**, *28*, 213–222; (d) Becke, A.D. *Phys. Rev A,* **1988**, *38*, 3098–3100; (e) Lee, A.; Yang, W.; Parr, R. G. *Phys. Rev. B* **1988**, *37*, 785–789.

141. Lenfant, S.; Krzeminski, C.; Delerue, C.; Allan, G.; Vuillaume, D. *Nano Lett.* **2003**, *3*, 741–746.

142. Parratt, L. G. *Phys. Rev.* **1954**, *95*, 359–369.

List of Publication

Journal papers

1. K. K. Jagtap,[#] Neelam Shivran,[#] S. Mula,[#] D. B. Naik, S. K. Sarkar, T. Mukherjee, D. K. Maity and A. K. Ray Change of Boron Substitution Improves the Lasing Performance of Bodipy Dyes: A Mechanistic Rationalisation *Chem. Eur. J.* **2013**, *19*, 702-708. Equal contribution[#]

2. Vibha Saxena, P. Veerender, S.P. Koiry, A.K. Chauhan, D.K. Aswal, S. Mula, Neelam Shivran, S. Chattopadhyay and S.K. Gupta Borondipyrromethane (BODIPY) as Sensitizer for Dye sensitized solar cell. Proc. *Am. Inst. Phys.* **2012**, *1451*, 272-274. (Indian Vacuum Society Symposium on Thin Films: Science and Technology).

3. Neelam Shivran, S. Mula, T.K Ghanty and S. Chattopadhyay Steric Strain Driven Bodipy Functionalization *Synfacts* **2012**, *8*, 0036.

4. Neelam Shivran, S. Mula, T.K Ghanty and S. Chattopadhyay Steric Strain Driven Bodipy Functionalization *Org. Lett.* **2011**, *13*, 5870-5873. (***Highlighted in Synfacts***).

5. V. Saxena, S.P. Koiry, P. Veerender, Vasundhara, D.K. Aswal, S.K. Gupta, Neelam Shivran, S. Mula, S. Chattopadhyay, J.V. Yakhmi A simple photoelectrochemical cell using Fe^{+++}/Fe^{++} (aq) as redox couple. Proc. *Am. Inst. Phys.* **2010**, *1313*, 400-402. (International Conference on Physics of Emerging Functional Materials (PEFM-2010)).

6. Neelam Shivran, M. Tyagi, P. Gupta, S. Mula, S. Chattopadhyay Synthesis and photodynamic activity of some glucose-conjugated BODIPY dyes (*J. Med. Chem.* communicated)

Conference papers

1. **Shivran Neelam**, Tyagi M., Mula S., Chattopadhyay S. A new tool for PDT: BODIPY-O-Glycosides. Sao Paulo Advanced School on Bio-organic Chemistry, Araraquara, **Brazil**, 30th June - 5th July, 2013, abstract no: OS-18.

2. **Shivran Neelam**, Mula S., S. P. Koiry, D.K.Aswal and Chattopadhyay S. Demonstration of Negative Differential Resistence (NDR) Behavior in Supramolecular Assembly of BODIPY Derivatives. Proc. 21st IUPAC International Conference on Physical Organic Chemistry (**ICPOC-21**), Durham, Royal Society of Chemistry, **United Kingdom**, September 9-13, 2012, abstract no: P-103.

3. **Shivran Neelam**, Mula S. and Chattopadhyay S. Synthesis and Photophysical Characterization of Bodipy Glycosides. Proc. 4th Interdisciplinary Symposium on Materials Chemistry (**ISMC-2012**), BARC, India, Dec. 11-15, 2012, abstract no: L-12

4. **Shivran Neelam**, Mula S., Jagtap K.K., Ray A.K. and Chattopadhyay S. Formulation of a Photo-stable Red-shifted BODIPY Laser Dye. Proc. DAE-BRNS 11th Biennial Trombay Symposium on Radiation & Photochemistry (**TSRP-2012**), BARC, India, Jan 4-7, 2012, abstract no: PC-126.

5. **Shivran Neelam**, Mula S., Jagtap K.K., Ray A.K., Dasgupta K. and Chattopadhyay S. Rational design of a new photostablepyrromethene laser dye. Proc. National Symposium on Radiation and Photochemistry (**NSRP-2011**), Jodhpur, India, March 10-12, 2011, abstract no: PC-83.

6. Saxena V., Koiry S.P., Veerender P., Vasundhara, Aswal D.K., Gupta S.K., **Shivran Neelam**, Mula S., Chattopadhyay S., Yakhmi J.V. A simple photoelectrochemical cell using Fe^{+++}/Fe^{++} (aq) as redox couple. INTERNATIONAL CONFERENCE ON PHYSICS OF EMERGING FUNCTIONAL MATERIALS (**PEFM-2010**). Proc. *Am. Inst. Phys.* 2010, *1313*, 400-402.

7. **Shivran Neelam**, Mula S., Koiry S.P., Aswal D.K. and Chattopadhyay S. Self-assembled BODIPY-bilayered silicon wafers with NDR property. Proc. DAE-BRNS 3rd International Symposium on Materials Chemistry (**ISMC-2010**), Mumbai, India, December 7-11, 2010, abstract no: D-14.

8. Jagtap K.K., Mula S., **Shivran Neelam**, Ray A.K. and Chattopadhyay S. BODIPY dye with improved photostablility and lasing efficiency. Proc. DAE-BRNS 10th Biennial Trombay Symposium on Radiation & Photochemistry (**TSRP-2010**), Lonawala, India, September 14-17, 2010, abstract no: PC-082.

9. Mula S., Jagtap K.K., **Shivran Neelam**, Ray A.K., Dasgupta K. and Chattopadhyay S. Rational Design of a new photostablepyrromethene (PM) laser dye. Proc. Ninth DAE-BRNS National Laser Symposium (**NLS-09**), BARC, Mumbai, India, January 13-16, 2010, abstract no: CP-33.